# The influence of oceanic ozone uptake on volatile organic compound production and air–sea exchange

**Daniel P. Phillips**

School of Environmental Sciences,
University of East Anglia

In collaboration with

Plymouth Marine Laboratory

**January 2022**

Page left intentionally blank

**Abstract**

This thesis focuses on the influence of oceanic ozone uptake on volatile organic compound (VOC) production, with the intention to reduce uncertainties in the ocean sink of ozone and source/sink of VOCs.

In the first data chapter, eddy covariance measurements of the air–sea fluxes of acetone, acetaldehyde and dimethylsulfide from a coastal observatory in the south-west UK are presented. Acetaldehyde and acetone show clear atmospheric deposition from both an open-water sector and a terrestrially influenced marine sector, while dimethylsulfide shows oceanic emission. Measured bulk fluxes agree reasonably well and are used to derive air–sea transfer velocities. Measured fluxes are compared to global flux estimates.

In the second data chapter, production yield measurements of acetaldehyde, acetone and isoprene from the ozone oxidation of seawater (containing marine dissolved organic matter, DOM) are presented from coastal seawater (south-west UK) over spring, summer and autumn. Experiments with phytoplankton culture and fatty acids provide evidence for a biological DOM precursor. Scaling the laboratory production yield data to the global ocean showed these reactions contribute a significant production of isoprene, which may account for the long-standing discrepancy between the top-down and bottom-up estimates of oceanic isoprene sources. The production of acetaldehyde and acetone were relatively less important from a global budget perspective.

In the third data chapter, measurements of the relative ozone loss to seawater in the Atlantic Ocean are presented. Measurements of iodide concentration and experiments with iodide standards are used to determine the contribution of iodide and DOM to surface ozone loss and results suggest near-equal contributions from these two reactant pools. Depth measurements suggest latitudinal variability due to the Antarctic waters. A coastal time series of ozone loss and VOC production is used to draw further conclusions about the linkage between ocean ozone uptake and the resultant VOC source.

**Table of Contents**

## Table of Figures

# Table of Tables

**Acknowledgements**

Firstly, I would like to thank my supervisors for their support over the last four-ish years. Thank you for conceiving my project. A special thank you goes to Ming and Frankie who were always so supportive and available to help. Ming, I am incredibly grateful for your wisdom, knowledge, motivation and friendship. Your criticism was always very constructive and helpful which enabled me to better my research. Your interest and motivation also guided me towards many valuable and exciting experiences.

I appreciate the researchers and staff at Plymouth Marine Laboratory who helped to make the laboratory my second home for four years. Thank you to Professor Thomas Bell for leading our group, maintaining the laboratory and helping with all things SOLAS. Thanks to the crew of the RV *Plymouth Quest* for the seawater samples.

Thank you to the officers and crew of RRS *Discovery* and the scientists of AMT-29 who made my first time at sea such an enjoyable and interesting experience. Thank you to Dr Giorgio Dall'Olmo for being a great supportive PSO and for organising our last-minute flight home. Shout out to Graham Stringfellow and Claudia Johnson for teaching me about the Navy and ships, and to Ophélie Meuriot for helping spark a revolution. Down with Neptune!

I cannot put into words how grateful I am to my fellow students, my friends, my PhD family. You guys were my rock to getting to the end. Paul Hackett, thank you for dragging me along to the PhD open day and being a good friend. So much of my 18 to 26 life revolves around you, from ChemSoc (I still remember flaming blue), to PhD and all things DnD. Charel Wohl, thank you for putting up with me hogging the PTR and for finding all the leaks. How many pints is it now? Daniel Ford, thank you for your Python powers and Matlab magic and also for the aftersun on that very hot equator crossing. Frances Perry, thank you for maintaining the Perry corner; a cornerstone at the very heart of PML. Maybe we are related, we'll never know. Zara Botterell, thank you for mothering me on nights out in Cambridge. Shall we go for a Nando's?

To Oskar Slocki, your continued friendship from college has supported me whilst living together, being 100's of miles apart and finally somewhat together again. I look forward to more travelling in Europe, finishing all the games we *say* we'll finish and getting to the end of the MCU.

Finally, mum, you may not have always understood what I did at university but you were always incredibly supportive and helpful in so many ways I have now lost count. Thank you.

# Chapter 1 – Background

## 1.1. Summary

Large uncertainty still exists in the role the ocean plays as a source or sink for volatile organic compound (VOC) budgets in the atmosphere (Fischer et al., 2012), largely due to competing and poorly quantified processes that control VOC cycling near the air-sea interface. This thesis aims to further our understanding of whether tropospheric ozone ($O_3$) provides a significant pathway for VOC production from the oxidation of marine dissolved organic matter (DOM) near the sea surface, and to investigate the importance of marine DOM towards the oceanic deposition of ozone.

VOC are trace low molecular mass organic species present in the atmosphere and oceans, which play an important role in mediating atmospheric reactions (e.g. quenching radicals, controlling greenhouse gas lifetimes) and cycling carbon in the biosphere (Goldstein and Galbally, 2007). VOC sources include terrestrial plant and biological marine activity, the oxidation of primary organic aerosols (POA) and marine DOM, the combustion of biomass and fossil fuels, and industrial solvent evaporation and chemical production. VOC sinks include atmospheric reactions with radicals and/or ultraviolet (UV) radiation and physical deposition to the earth's surface.

$O_3$, the triatomic allotrope of molecular oxygen ($O_2$), is a powerful oxidant and important atmospheric trace gas which contributes to the oxidative capacity of the atmosphere. Typical tropospheric $O_3$ concentration is 10–60 ppbv (Reeves et al., 2002; Gaudel et al., 2018), but can range from 1 ppbv in an unpolluted rural environment to 100 ppbv in heavily polluted regions (Thompson, 1992) due to variable sources/sinks. Tropospheric $O_3$ sources include oxidative reactions of hydrocarbons, photochemical processes, transport from the stratosphere and anthropogenic production. Tropospheric $O_3$ sinks include atmospheric reaction, photochemical destruction and deposition to the earth's surface.

DOM is a complex mixture of high molecular mass organic species ubiquitous in the marine environment, important for carbon cycling in the biosphere (Benner, 2002; Ogawa and Tanoue, 2003; Shimotori et al., 2016). DOM sources are riverine outflows from the terrestrial environment (refractory DOM; e.g. humic substances) and in situ biological activity (labile DOM; e.g. carbohydrates, fatty acids). DOM sinks are photochemical surface reactions (all DOM) and biological activity (labile DOM). Labile DOM can be produced and/or consumed via marine organisms, giving it a short lifetime within the ocean (~ hours or days), while refractory DOM cannot be consumed, leading to a far longer lifetime (~ years).

## 1.2.  Volatile organic compounds

### 1.2.1.  Chemical characteristics

VOCs have a wide range of chemical functionality, including carbonyls (ketones and aldehydes), organic acids (alcohols and carboxylic acids), nitriles, aromatics, aliphatics (Zhao and Zhang, 2004) and organosulphurs (Charlson et al., 1987). EU legislation (Directive 2004/42/CE) restricts VOCs to organic compounds with "an initial boiling point less than 250° C", which effectively limits their potential molecular mass to below 200 g mol$^{-1}$. Within the environment VOC concentrations vary temporally and spatially, depending on the proximity and magnitude of sources and sinks; rural sites generally contain a higher concentration of biogenic VOCs (e.g. terpenes, such as isoprene), compared to urban sites which typically contain more anthropogenic VOCs (e.g. aromatics, like benzene). As an example, Valach (2015) measured kerbside London and above-canopy Amazon rainforest VOC mixing ratios of biogenic isoprene (0.25 and 3.0 ppbv respectively) and anthropogenic benzene (0.29 ppb and undetectable respectively).

Thousands of volatile compounds have been measured and catalogued (Heald et al., 2008), however, in this thesis the focus will be on acetaldehyde, acetone, dimethylsulfide (DMS) and isoprene due to their relatively high concentrations in the remote marine atmosphere (Heald et al., 2008) and their importance within marine and atmospheric chemistry processes (Lewis et al., 2005). Acetaldehyde and acetone have the systematic names propanal and propanone, respectively, as per the International Union of Pure and Applied Chemistry (IUPAC), however, their traditional names will be used here. Furthermore, for the context of this work, methane ($CH_4$) will be excluded from the definition of VOC because of its long atmospheric lifetime (~10 yr; Heald et al., 2008) and high mixing ratio (~1.75 ppm; Dlugokencky et al., 2003); thus VOC will be used in place of 'non-$CH_4$ volatile organic compound'.

Little is known about the health risks of VOC at their generally low atmospheric mixing ratio; however, some research has shown the potential benefits of naturally abundant VOC as physiological antioxidative molecules (i.e. DMS; Guan et al., 2017) and overactive gene inhibition molecules (Moore, 2015). At significantly higher concentrated levels, such as those found in urban or industrial applications (i.e. cleaning products, solvents), VOCs are known to irritate the respiratory system and eyes (aldehydes), induce haematological problems (oxides) and cause cancer (aromatics) (Kampa and Castanas, 2008).

VOCs do not directly contribute to the climate as greenhouse gases, because of their weak adsorption of key infrared (IR) radiation frequencies, however indirectly affect the atmospheric lifetimes or abundances of radiatively active gases (i.e. water vapour ($H_2O$), carbon dioxide ($CO_2$), $O_3$ etc.) through direct or indirect chemical reactions. The radiatively active gases themselves vary the temperature and radiative balance of the atmosphere (i.e. radiative forcing; discussed later in Section 1.4.1) (Wigley et al., 2002).

### 1.2.2.   VOC budgets

### 1.2.2.1.   Natural VOC sources

Biogenic VOCs are released by terrestrial plants (~1150 Tg yr$^{-1}$; IPCC, 2001), with the main chemical groups emitted being terpenes, alcohols and aldehydes (Kesselmeier and Staudt, 1999). Isoprene is the dominant global biogenic VOC (~600 Tg yr$^{-1}$), of which ~90 % arises from plant foliage (Guenther et al., 2006). Lesser biogenic VOC include acetone (32–44 Tg yr$^{-1}$; Fischer et al., 2012; Guenther et al., 2012) and acetaldehyde (~23 Tg yr$^{-1}$; Millet et al., 2010; Guenther et al., 2012). Oxidative reactions of organic compounds, such as the atmospheric oxidation of POA or photooxidation at the sea surface, are also a source of some VOC. Millet et al. (2010) predicted that ~60 % of global acetaldehyde production (~128 Tg yr$^{-1}$) occurs from atmospheric oxidation of ethanol, isoprene and unknown aliphatic hydrocarbons.

The main source of acetaldehyde and acetone in seawater is the photochemical degradation of chromophoric dissolved organic material (CDOM) (Zhou and Mopper, 1997; De Bruyn et al., 2011; Zhu and Kieber, 2018) accounting for ~100 and ~70 % of seawater concentration in the Atlantic Ocean respectively (Dixon et al., 2013). The short marine lifetime of acetaldehyde (de Bruyn et al., 2013, 2017; Dixon et al., 2013), due to the rapid biological consumption, is typically coupled with an estimate of its production rate to predict the seawater concentration (Millet et al., 2010; Wang et al., 2019). Beale et al. (2013) showed that surface acetone concentrations in the North Atlantic Ocean did correlate with bacterial production, although not primary production, highlighting the importance of marine activity on the production of precursor DOM. Furthermore, elevated seawater acetone concentrations in the summer compared to the winter have been shown to be due to increased short-wave solar radiation (Beale et al., 2015). Attempts to estimate seawater acetone concentrations are thus more difficult, because of the more dynamic seawater sinks, and require advanced machine learning (Wang et al., 2020a). Further smaller marine sources of acetaldehyde and acetone include the production by marine organisms (i.e. phytoplankton and bacteria) as a by-product of carbon metabolism (Dixon et al., 2013; Halsey et al., 2017). Acetone is an intermediate in the metabolism of propane (Dixon et al., 2014), however, it can be further converted to acetaldehyde, acetic acid or ultimately pyruvic acid.

In the ocean, isoprene is mainly produced from phytoplankton with the emission to the atmosphere uncertain (0.2–1.9 Tg yr$^{-1}$; Broadgate et al., 1997; Arnold et al., 2009; Gantt et al., 2009; Booge et al., 2016) because of the variability in production by phytoplankton functional type and the measurement thereof. Seawater isoprene concentration is mainly estimated from chlorophyll *a* concentration (Milne et al., 1995; Broadgate et al., 1997; Hackenberg et al., 2017) typically using a complete chemical model, an empirical regression of remotely sensed in situ variables (i.e. chlorophyll *a* concentration, sea surface temperature (SST)) or the direct scaling of laboratory measurements (Palmer and Shaw, 2005; Booge et al., 2016; Rodríguez-Ros et al., 2020). The ocean isoprene production is considerably lower than the terrestrial production, suggesting that coastal atmospheric isoprene chemistry should be dominated by terrestrial

transport. This is however unknown considering a limited number of direct flux measurements exist near the coast.

DMS is the most abundant volatile sulfur compound in marine atmosphere and is a product of the metabolism of dimethylsulfoniopropionate (DMSP), a compound predominantly produced by phytoplankton, via algal or bacterial enzymic lysis (Kiene et al., 2000; Liss et al., 2014). Many studies have attempted to estimate the ocean emission of DMS and due to the primary dominant source and the unidirectional sea-to-air transfer (supersaturation), most estimates have been close to direct measurements (20.1–28.1 Tg yr$^{-1}$; Lana et al., 2011; Wang et al., 2020b).

Of particular interest in this thesis is the oxidation of DOM in the upper water column. Kieber et al. (1990) first showed seawater irradiated with sunlight produced low molecular mass carbonyl compounds (i.e. formaldehyde (IUPAC name: methanal) and acetaldehyde) and concluded that humic-type materials (high molecular mass chromophoric compounds) were the main oceanic precursor. More recently Zhou et al. (2014) showed that when $O_3$ was passed over a calm organic-rich seawater sample, volatile carbonyl compounds were produced, which highlights the potential for competing oxidative reactions at the sea surface. The seawater reactions of $O_3$ and DOM that produce VOC are discussed in more detail later in Section 1.5.2.6.

### 1.2.2.2. Anthropogenic VOC sources

Although global biogenic VOC sources significantly outweigh anthropogenic VOC sources (order of magnitude lower, ~100 Tg yr$^{-1}$), anthropogenic VOC can still represent a large contribution to atmospheric carbon. Biomass fires, which can sometimes also be natural, account for the majority (Crutzen and Andreae, 1990), producing acetone (~26 Tg yr$^{-1}$; Fischer et al., 2012) and acetaldehyde (~3 Tg yr$^{-1}$; Millet et al., 2010). In comparison, fossil fuel combustion accounts for significantly less anthropogenic VOC production, producing hydrocarbons, acetaldehyde (~2 Tg yr$^{-1}$; Millet et al., 2010) and aromatics (i.e. benzene and toluene). Other anthropogenic VOC sources are chemical production and solvent evaporation. Although important, especially in a high-density urban environment where anthropogenic VOC can outweigh natural production, this thesis is primarily interested in natural sources of VOC.

### 1.2.2.3. VOC sinks

Oxidative atmospheric reactions are the main sink of VOC, providing a typical lifetime of 1–12 days (Atkinson and Arey, 2003; Lewis et al., 2005), with the end fate being full oxidation to $CO_2$. Gas-phase alkanes only react with the hydroxyl radical (OH), and nitrate radical ($NO_3$) to a lesser extent, but not $O_3$. Both radicals initiate reactions with VOC by hydrogen atom abstraction to leave an alkyl radical, which subsequently reacts with $O_2$ to produce an alkylperoxy radical ($RO_2$) (Atkinson and Arey, 2003);

$$R + OH \rightarrow R' + H_2O \qquad\qquad \text{R1a}$$

$$R' + O_2 \rightarrow R'O_2 \qquad\qquad \text{R1b}$$
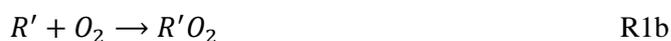
where $R$ and $R'$ represent an organic species without and with removed hydrogen respectively. All alkanes undergo this initial OH pathway to produce $RO_2$, however, the $RO_2$ species can

undergo a multitude of possible pathways with nitrogen oxides ($NO_X$ = NO and $NO_2$), hydroperoxyl radicals ($HO_2$) and other $RO_2$. Unique products are formed in most cases with an inert quenching species M (e.g. $N_2$) (Atkinson and Arey, 2003), which acts to remove excess energy, for example;

$$RO_2 + NO \rightarrow RO + NO_2 \qquad\qquad\qquad\qquad \text{R2a}$$
$$RO_2 + NO + M \rightarrow RONO_2 + M \qquad\qquad\qquad \text{R2b}$$

Through these reactions (Reaction R2b), acetone and acetaldehyde can sequester $NO_X$ as peroxyacyl nitrates (Singh et al., 1995) which leads to the long-distance transport of $NO_X$. As saturated species, acetaldehyde, acetone and DMS behave similarly to alkanes. On the other hand, gas-phase alkenes react with OH, $NO_3$ and $O_3$. All three radicals initiate reactions by addition to the unsaturated bonds, however via different pathways (Atkinson and Arey, 2003). The additional rapid reactions that are possible with unsaturated species and OH explain the significantly increased destruction kinetics (i.e. short lifetime) of atmospheric isoprene.

Physical deposition to the earth's surface (land and oceans) accounts for a small but important step for biosphere carbon cycling. Beale et al. (2013) extrapolated flux measurements of oxygenated VOC in the North Atlantic Ocean to present global ocean fluxes of acetaldehyde (~-17 Tg yr$^{-1}$) and acetone (~-4 Tg yr$^{-1}$) and further showed the consumption of acetaldehyde in the North Atlantic Ocean was 0.3–1 nM hr$^{-1}$, supporting the sink. Global models show there is a net consumption of seawater acetone in the temperate and cold zones, which causes the ocean to act as an atmospheric sink, contrarily, in the tropics and sub-tropics, net seawater production and an atmospheric source are observed (Wang et al., 2020a). On the other hand, the net production of acetaldehyde is nearly always estimated (Wang et al., 2019). The predominant loss process of acetaldehyde and acetone in the ocean is bacterial consumption (Dixon et al., 2013, 2014) with typical lifetimes <1 d and 5–55 d respectively (Dixon et al., 2013; de Bruyn et al., 2017). Acetone can be consumed via heterotrophic bacteria and further converted to acetaldehyde before further consumption (Dixon et al., 2014). Other minor ocean loss processes of VOC include direct seawater photolysis and venting to the atmosphere (for supersaturated VOC).

For seawater isoprene, the predominant loss process is venting to the atmosphere (Booge et al., 2018), and a minor loss is bacterial consumption, leading to a seawater lifetime of 7–10 d (Palmer and Shaw, 2005; Booge et al., 2018).

### 1.2.3. Evidence of missing sources

### 1.2.3.1. HO reactivity

A recent study identified missing OH reactivity in the marine boundary layer (MBL) (~0.7 s$^{-1}$ below 1 km) that is likely connected to a missing oceanic VOC source (Thames et al., 2020). Correlations are shown between the missing reactivity and DMS, SST, acetaldehyde and chlorophyll *a* which implies the missing source likely originates in the ocean. Although the correlation with acetaldehyde is weak, this may be because acetaldehyde has multiple complex sources that contribute to the MBL (e.g. atmospheric VOC oxidation, ocean biological and/or

photochemical production) that are equal in magnitude or higher than the missing source; thus difficulty arises in identifying specific source correlation. Furthermore, the weak correlation with chlorophyll *a* may represent co-dependence between biological activity and the ocean DOM pool.

The additional mixing ratio of gas *X* required to explain the missing reactivity can be calculated (Thames et al., 2020);

$$C_X = \frac{mOHr}{k_{X+OH}} \frac{10^9}{M}$$ 1

where m*HO*r represents the missing OH reactivity, $k_{X+OH}$ represents the reaction rate constant and *M* represents the molecule density of air. Assuming a rate constant of $1.5 \times 10^{-11}$, $1.7 \times 10^{-13}$ and $1.0 \times 10^{-10}$ cm$^3$ molec.$^{-1}$ s$^{-1}$ for acetaldehyde, acetone and isoprene, respectively (Atkinson and Arey, 2003), and an air molecule concentration of $2.5 \times 10^{19}$ molec. cm$^{-3}$, the calculated required additional mixing ratios of the three VOCs are ~1.9, ~165, ~0.3 ppbv respectively.

The more reactive isoprene requires the lowest additional atmospheric mixing ratio and thus would seem the most likely contender, especially since Thames et al. (2020) show a correlation between the missing source and formaldehyde which is a product of isoprene–OH oxidation (Wolfe et al., 2016). However, an additional atmospheric isoprene mixing ratio of 0.3 ppbv, with only the ocean as a source, would require an extortionately high air–sea flux of ~138 μmol m$^{-2}$ d$^{-1}$. Acetone was calculated to have an extortionately high mixing ratio that has never been modelled or observed in the environment, while acetaldehyde was calculated to have a mixing ratio that is unseen in the remote ocean. With this considered, these three VOCs are unlikely responsible for the missing OH source on their own. Zhou et al. (2014) also showed the formation of glyoxal (IUPAC name: ethanedial), butanone and pentanone from heterogeneous oxidation of the surface microlayer (SML), which require additional mixing ratios of ~2.5, ~22.9 and ~8.7 ppbv respectively.

### 1.2.3.2. Global modelling and VOC budgets

Bottom-up budget methods involve the scaling up, to regional or global values, of localised sources and sinks. For example, field measurements of biomass burning at select tropical sites and extrapolation to the entire tropics (Crutzen and Andreae, 1990). On the other hand, top-down budget methods involve the modelling of environmental fluxes required to explain observed atmospheric mixing ratios, normally using global chemistry transport models via remote measurements, knowing the other sources and sinks. For example, remote measurements of glyoxal over the Pacific and modelling an expected flux from the ocean (Myriokefalitakis et al., 2008).

Theoretically, both methods should agree on a budget value, however, this sometimes does not happen due to incorrectly understood (or missing) sources and sinks. Top-down estimates of surface fluxes exceeding the bottom-up estimates would suggest a net missing source. Arnold et al. (2009) used laboratory measurements of isoprene production from different phytoplankton communities (i.e cyanobacteria, diatoms etc.) and remote measurements of phytoplankton

community abundance to model a global bottom-up budget of ~0.31 Tg yr$^{-1}$. In comparison, by reducing the difference between modelled and observed isoprene flux values, a top-down budget of ~1.9 Tg yr$^{-1}$ was produced. The approximate factor of 6 difference highlights the literature discrepancies of VOC budgets from the ocean.

Methods for global isoprene air–sea flux estimates use: (1) a model that balances biological production, biological/chemical destruction and physical emission (Palmer and Shaw, 2005; Booge et al., 2016), (2) empirical regression of in situ variables (Rodríguez-Ros et al., 2020), or (3) the direct scaling of laboratory measurements (Arnold et al., 2009) to first calculate seawater concentration. The balance models only use biological production and Booge et al. (2016) showed that their model underestimated seawater isoprene concentrations by a factor of 1.7±1.2, which was likely due to not including surface microlayer production (i.e. heterogeneous or photochemical). Booge et al. (2016) concluded isoprene air–sea fluxes would need to be more than an order of magnitude higher than predicted from seawater concentration alone to match atmospheric mixing ratios in the Indian and Eastern Pacific Oceans; the additional sea-to-air flux needed was 2.08±1.33 and 2.04±1.00 µmol m$^{-2}$ d$^{-1}$ respectively. When the measurements were binned into day or night, the difference could be explained by reduced photochemical (direct or indirect) sinks at night resulting in increased atmospheric concentration. The flux difference was strongly dependent on atmospheric concentration simply because the top-down estimates were greater than the bottom-up estimates (order of magnitude) and the estimate for top-down flux was dependent on concentration;

$$C_a = \frac{F\tau}{h} \qquad\qquad 2$$

where $F$ represents total flux, $\tau$ represents atmospheric lifetime and $h$ represents MBL height. The results suggested no apparent photochemical isoprene production, whether direct photochemical reactions with seawater organics or light-induced biological effects, which was further evident with no observation of a diurnal cycle in surface seawater concentration (Booge pers. comm.). Positive near-surface gradients between 5–10 m and 30 cm have been observed recently in the Canadian Arctic Archipelago (Wohl et al., 2022). Booge et al. (2016) measured seawater isoprene from a depth of ~6 m, thus their estimates do not account for any near-surface gradients which would increase the bottom-up flux estimates and reduce the difference with the top-down estimates.

Wang et al. (2019) estimated the global oceans are a net source of acetaldehyde, however, a 50 % enhancement to the model's predicted seawater concentrations was necessary to explain observed remote tropospheric mixing ratios. No correlation was shown to the oceans, other than the enhanced seawater concentration, therefore organic aerosol (OA) or unaccounted gas-phase precursors were assumed. With the photolysis and ozonolysis of OA included (see Wang et al. (2019) supplement), the North Atlantic Ocean bulk flux became zero (near equilibrium with the atmosphere, similar to estimates by Beale et al. (2015)) and a strong sink respectively. The

inclusion of additional heterogeneous oxidation of organics at the sea surface (Zhou et al., 2014) would decrease the diffusive emission required further.

While not a key compound in this thesis, Myriokefalitakis et al. (2008) adapted the chemical model TM4 to quantify glyoxal distribution and illustrated a missing ~20 Tg yr$^{-1}$ source over the ocean compared to remote measurements. Sinreich et al. (2010) later measured atmospheric glyoxal in the remote pacific ocean and similarly could not find a certain source. Direct photooxidation of DOM was ruled out, along with VOC precursor production and terrestrial source transport, however, an indirect link with surface DOM was noted as possible. Glyoxal has recently been shown to be produced through multiple mechanisms from the heterogeneous oxidation of the SML (Zhou et al., 2014), which further implied other VOC could also be produced via similar mechanisms in the remote ocean.

## 1.3. Dissolved organic matter

### 1.3.1. Carbon in the ocean

Organic material in the ocean can be split into a series of sub-contained categories (Figure 1) with the largest and fully encompassing category being total organic matter (TOM). TOM can be split into DOM and particulate organic matter (POM; shown in Figure 1 as undissolved organic matter); the operational definition that splits DOM and POM is the material that can and cannot pass through a 0.45–1 µm filter (Sharp, 1973; Hedges, 2002; Davis et al., 2019).
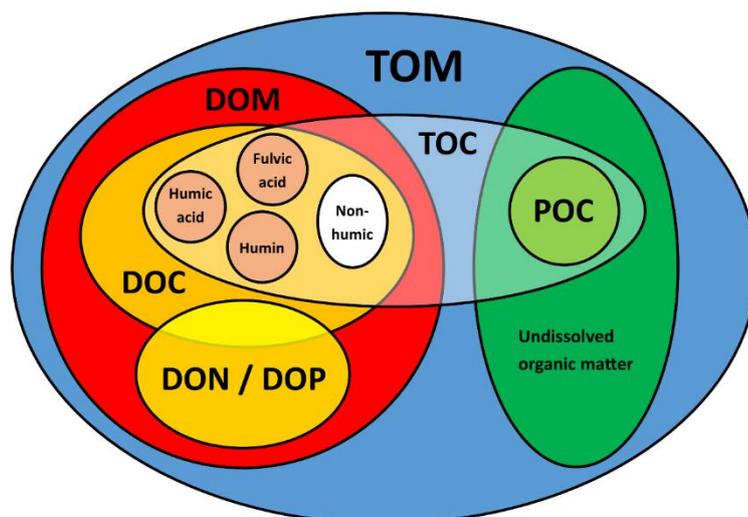


**Figure 1: Representation of the various forms of organic matter found in natural waters and how each is categorised by others. Total organic matter (TOM), total organic carbon (TOC), dissolved organic matter (DOM), dissolved organic carbon (DOC), particulate organic carbon (POC), dissolved organic nitrogen (DON), and dissolved organic phosphorus (DOP) are represented. DOC is further broken down into its humic and non-humic material components. Figure reproduced from Pagano et al. (2014).**

DOM is the larger of the two main categories and accounts for 660–700 Pg ($10^{15}$ g) of carbon storage in the ocean (Siegenthaler and Sarmiento, 1993; Hansell et al., 2009); the distribution is ~7, ~21 and ~72 % in the surface ocean (<200 m), 200–1000 m, >1000 m respectively (Hansell et al., 2009). The main source of DOM in the open ocean is extracellular release, grazer-mediated release or excretion, bacterial or viral cell lysis, solubilisation of POM, and bacterial transformation and release (Meon and Kirchman, 2001; Carlson, 2002; Davis et al., 2019). The

main sinks of DOM are biological consumption, photochemical destruction and absorption to particles (Carlson, 2002).

POM is the smaller of the two main TOM categories (<0.1–10 %; Sharp, 1973; Thurman, 1985) and is a mixture of approximate millimetre marine biomass (i.e. assorted plankton and bacteria) and insoluble organic material. The predominant source of POM is phytoplankton growth through photosynthesis (Bodineau et al., 1999; Davis et al., 2019). POM is lost to a variety of biological, physical and chemical processes (Lee et al., 2004) and in the surface ocean, a simple but large sink is the literal sinking of suspended POM.

### 1.3.2.   Chemical characteristics of DOM

Dissolved organic carbon (DOC), dissolved organic nitrogen (DON) and dissolved organic phosphorous (DOP) are sub-categories of DOM that are defined by the absence of nitrogen and phosphorous, containing nitrogen and containing phosphorous, respectively. Typical concentrations of DOC in the surface ocean are 40–90 µM (Hansell et al., 2009; Romera-Castillo et al., 2016) and the contribution of DOC, DON and DOP to DOM are ~93, ~7 and ~0.3 % respectively (Benner, 2002); thus is it common for the DOC and DOM terms to be used interchangeably.

To this day, the chemical composition of DOM remains largely unclassified as individual molecules but can be summarised by overall chemical functionality. The main components of marine DOM are thought to be proteins (25−50 %), lipids (5−25 %) and carbohydrates (up to 40 %) (Carpenter and Nightingale, 2015).

The highly biologically active compounds, which include free amino acids, sugars and organic acids, turn over on a short timescale (minutes to days) and are referred to as labile DOM (Ogawa and Tanoue, 2003). Due to the rapid turnover of labile DOM, the contribution to total DOM is <6 % (Carlson, 2002). Compounds that are less biologically active but can still be lost to bacterial oxidation (timescale of months to years) are referred to as semi-labile DOM while compounds that are not biologically active (timescale of >100 yr) are referred to as refractory DOM (Ogawa and Tanoue, 2003). Refractory DOM is formed when labile/semi-labile DOM is not remineralised and biotic and/or abiotic processes alter the DOM so that it cannot be biologically consumed (Meon and Kirchman, 2001; Hansell, 2013).

Humic acids (soluble <2 pH, >1500 g mol$^{-1}$), fulvic acids (soluble any pH, 600–1000 g mol$^{-1}$), and humins (insoluble any pH) are humic-type substances and defined components of DOC, which account for only a small fraction (≤2.4 %) of DOC in the ocean (Malcolm, 1990; Opsahl and Benner, 1997; McDonald et al., 2004). Closer to the terrestrial environment (i.e. rivers, estuaries and coastal seas), the concentration of humic-type substances is much higher.

## 1.4. Ozone

### 1.4.1. Importance of ozone

$O_3$ is a powerful atmospheric oxidant which contributes to the atmosphere's oxidative capacity. Since the mid-1800s, the atmospheric concentration of $O_3$ has risen sharply from ~20 ppbv (Vingarzan, 2004) to ~40 ppbv (Reeves et al., 2002; Gaudel et al., 2018) because of increased localised anthropogenic emissions of $O_3$ precursor compounds. The IPCC's third annual report suggests $O_3$ precursor compounds will continue to rise during the 21st century, especially anthropogenic $NO_X$ and VOC, leading to higher ground level concentrations (Griggs and Noguer, 2002b).

Stratospheric $O_3$ importantly protects the biosphere by absorbing solar UV (UV-b, 230–320 nm; Hartley, 1881) and significantly reducing the intensity at ground level; this absorption is responsible in part for stratospheric temperature (Wallace and Hobbs, 2006) due to emittance in lower energy IR. $O_3$ in the lower stratosphere is concentrated approximately 20–30 km above sea level in the $O_3$ layer, with the bulk concentration kept reasonably constant due to the cyclic nature of the photolysis reactions of $O_2$ and $O_3$ (Reeves et al., 2002; Monks, 2005) commonly referred to as the Chapman cycle (net of Reactions R3a–f given as R3g);

$$O_2 + h\nu \longrightarrow 2O(^1D) \qquad\qquad \text{R3a}$$

$$O(^1D) + O_2 \longrightarrow O_3 \qquad\qquad \text{R3b}$$

$$O_3 + h\nu \longrightarrow O_2 + O(^1D) \qquad\qquad \text{R3c}$$

$$O_2 + O(^1D) + M \longrightarrow O_3 + M \qquad\qquad \text{R3d}$$

$$O_3 + O(^1D) \longrightarrow 2O_2 \qquad\qquad \text{R3e}$$

$$2O(^1D) \longrightarrow O_2 \qquad\qquad \text{R3f}$$

$$\boldsymbol{O_2 + h\nu \rightleftharpoons O_3} \qquad\qquad \text{R3g}$$
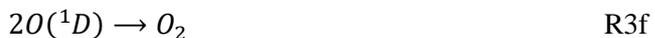
Tropospheric $O_3$, depending on its location in the troposphere, can be seen as a benefit or a problem. In the upper troposphere (~15 km), $O_3$ acts as a greenhouse gas by absorbing IR radiation released from the earth's surface and radiating a fraction back to the earth. The difference between incoming solar radiation and outgoing reflected radiation controls the radiative balance of the atmosphere, which affects atmospheric temperature (Shine, 2001). $O_3$ does not contribute to the greenhouse effect as much as other greenhouse gases (i.e. $H_2O$, $CO_2$, $CH_4$ etc.), however, is important due to its high reactivity (i.e destroying or producing other greenhouse gases) and contribution to moving the atmosphere out of radiative balance equilibrium (radiative forcing). The contribution of $O_3$ is dependent on temporal and spatial effects (e.g. vertical distribution) to balance heating/cooling effects (Wang et al., 1995; Shine, 2001). For example, of the expected 2.4 W m$^{-2}$ radiative forcing driven since pre-industrial times, $O_3$ is expected to account for ~15 % compared to ~60 % from $CO_2$ (Shine and Forster, 1999). Increasing anthropogenic $O_3$ precursor species have significantly increased $O_3$ total column concentrations (Reader et al., 2013), and as shown by Wigley et al. (2002) who used the IPCC 100 yr forecast of $NO_X$, carbon monoxide (CO) and VOC, a positive forcing (warming) is modelled for expected future precursor abundances.

In the lower surface-level troposphere $O_3$ acts as a pollutant through the production of photochemical smog in the presence of elevated levels of precursor pollution (Li et al., 2022). Anthropogenic activities within urban environments emit high levels of $NO_X$ (e.g. fossil fuel combustion), which undergoes photochemical reactions to produce significant amounts of $O_3$ as a regional pollutant. The same cyclic hydrocarbon oxidation reactions subsequently produce significantly more oxidised hydrocarbons, SOAs and particulate matter within the local environment of the $NO_X$ source; together these species produce the smog. Furthermore, as a pollutant and an oxidant, $O_3$ is harmful to human and animal respiratory tracts (Cohen et al., 2017; Kazemiparkouhi et al., 2020) and causes widespread damage to crops and vegetation (Murphy et al., 1999; Young, 1999). In the year 2015, exposure to ambient concentrations of $O_3$ was predicted to have caused ~250000 deaths (Cohen et al., 2017). Crop loss occurs through a range of biological impacts (e.g. reductions in chlorophyll content and photosynthesis) and importantly affects yield quantity and quality with the potential for global yield loss of up to 11 % globally (Emberson, 2020).

### 1.4.2.   Ozone budgets

### 1.4.2.1.   Ozone sources

Oxidative reactions of hydrocarbons (VOC + $CH_4$) in the troposphere account for ~85 % of all $O_3$ sources (~5000 Tg $O_3$ $yr^{-1}$; Stevenson et al., 2006). These reactions vary the yield of $O_3$ depending on the ratio of $NO_X$, the abundance of OH and the presence of UV and are described in detail by Monks et al. (2015) and Archibald et al. (2020). $NO_X$ and OH can appear as naturally occurring compounds, with $NO_X$ coming from soils, lightning strikes and downward transport of nitric oxide (NO) from the stratosphere (Vingarzan, 2004) and OH from the photochemical reactions of $O_3$ and $H_2O$ (Whalley et al., 2010; Monks et al., 2015), hence the non-zero $O_3$ background concentrations in the 19th century (Vingarzan, 2004). More recently, elevated concentrations of NO from anthropogenic sources have led to large increases in $O_3$ concentration (Shine, 2001; Griggs and Noguer, 2002b; Fusco and Logan, 2003).

To start the production, OH reacts with organic species (i.e. VOC) and $O_2$ to produce an oxygenated organic species (organic peroxy radicals, $RO_2$) and $H_2O$;

$$R + OH \longrightarrow ROH \qquad \text{R4a}$$

$$ROH + O_2 \longrightarrow R'O_2 + H_2O \qquad \text{R4b}$$

The organic peroxy radicals produced through Reactions R4a–b can react with NO and $O_2$ to produce another oxygenated species (RO), $NO_2$ and $HO_2$;

$$R'O_2 + NO \longrightarrow R'O + NO_2 \qquad \text{R5a}$$

$$R'O + O_2 \longrightarrow R''O + HO_2 \qquad \text{R5b}$$

If $R$ was $CH_4$, formaldehyde would be the final product of Reactions R4a–b and R5a–b ($R''O$, with loss of two hydrogen) (Reeves et al., 2002). $O_3$ is produced when the $NO_2$ undergoes photolysis, in the presence of $O_2$, to produce NO;

$$NO_2 + h\nu + O_2 \longrightarrow NO + O_3 \qquad \text{R6a}$$

$$NO + HO_2 \longrightarrow NO_2 + HO \qquad \text{R6b}$$
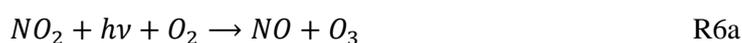
The cyclic nature of $NO_X$ and $HO_X$ in Reactions R4–R6, fueled by UV and organic species or CO, leads to the efficient production of $O_3$ when the $NO_2/NO$ ratio is high (Monks et al., 2015). The highest concentrations of $NO_X$ and OH occur in the lower troposphere, closest to high polluting urban sites and large bodies of water, respectively, because of the large sources (Monks et al., 2015). Direct photochemical production from $O_2$ is negligible in the troposphere, due to the strong UV absorption in the stratosphere. Transport from the stratosphere (600–1000 Tg $O_3$ yr$^{-1}$; Ganzeveld et al., 2009; Reader et al., 2013) accounts for a small but significant amount of $O_3$ in the troposphere and is enhanced by convective rain activity (Yoo et al., 2014).

### 1.4.2.2.  Ozone sinks

$O_3$ is a precursor to OH, which provides the majority of the oxidizing capacity of the lower atmosphere and thus acts as the main sink for many atmospheric trace gases (i.e. pollutants and greenhouse gases) (Wallace and Hobbs, 2006); as VOC are a limiting reagent in the middle-upper troposphere, they are scrubbed efficiently. $O_3$ undergoes photolysis to produce $O(^1D)$ which reacts with $H_2O$ to produce two OH radicals;

$$O(^1D) + H_2O \longrightarrow 2OH \qquad \text{R7}$$

This sink is most important in the tropical humid lower troposphere (Monks et al., 2015). Direct photochemical destruction is a minor sink of tropospheric $O_3$ because the stratosphere absorbs most of the required UV.

Dry deposition of $O_3$ to the ocean accounts for approximately a third of the global $O_3$ deposition (100–600 Tg $O_3$ yr$^{-1}$; Ganzeveld et al., 2009; Hardacre et al., 2015; Luhar et al., 2018; Pound et al., 2020), nearly equal to downwards stratospheric–tropospheric transport. The rate of oceanic $O_3$ deposition, the deposition velocity ($v_d$), is affected by physical and chemical parameters at or around the SML (Fairall et al., 2007). Considerable uncertainty exists in the parameterisation of ocean surface $O_3$ $v_d$ due to a lack of understanding of the physical drivers and also the chemical reactivity of dissolved compounds. This physical enhancement of atmosphere–ocean gas exchange and the chemical enhancement of $O_3$ $v_d$ are discussed later in Section 1.5.2.

### 1.5.  Gas exchange

Gas exchange is an important concept in oceanography that explores the transfer of gases, measured as a flux (a quantity per area per time), between the atmosphere and the ocean. The sign convention for flux direction often changes between literature publications depending on the interests of the literature concerning atmospheric or marine budgets. In this thesis, positive (+) fluxes discuss sea-to-air transfer (i.e. gain to the atmosphere). Two methods for measuring air–sea fluxes are commonly used; the eddy covariance (EC) method and the two-layer (TL) method.

### 1.5.1. Air–sea flux measurement techniques

### 1.5.1.1. Eddy covariance method

The EC technique is the most direct method for gas flux measurements, which measures the effect of vertically mixing atmospheric eddies on gas concentration to extrapolate a vertical flux (Tanner and Thurtell, 1969; Guenther and Hills, 1998). Realistically, the technique can be used to calculate the vertical flux of any variable that is influenced by eddies (e.g. heat and momentum fluxes; Tanner and Thurtell, 1969), however, for this thesis, the focus is on trace gases.

Vertical mixing of a gas in a turbulent flow can be expressed by:

$$F = \overline{\rho_a w x} \qquad\qquad 3$$

where $\rho_a$ represents air density, $w$ represents vertical wind velocity, $x$ represents the gas mixing ratio and the overbar represents temporal averaging (Burba, 2013). Equation 3 can be expanded to include deviations from the mean with Reynolds decomposition (where primes represent fluctuations from the mean) and then simplified by two important assumptions of the EC technique, (1) density fluctuations ($\rho_a'$) are negligible and (2) mean vertical flow/transport ($\overline{\rho_a}\,\overline{w}\,\overline{x}$) is negligible. Further removal of terms with an average deviation of the average leads to a single remaining term used to calculate vertical EC fluxes (Burba, 2013);

$$F \approx \rho_a \overline{w' x'} \qquad\qquad 4$$

The EC method principally relies on rapid measurements of $w'$ and $x'$, normally on the order of ~10 Hz, to capture the influence of small ~5 Hz eddies. Difficulties in designing and constructing sensitive fast-response instrumentation have limited the deployment of EC measurements around the globe (Lenschow et al., 1982; Lenschow and Hicks, 1989).

### 1.5.1.2. Two layer model and method

In the TL technique, the air-sea interface is described as two thin diffusive layers, either side of the interface, sandwiched between the bulk turbulent bodies of the atmosphere and underlying ocean (Liss and Slater, 1974; Wanninkhof et al., 2009); this approximation considers the turbulent bodies to be thoroughly mixed and homogeneous in concentration. Measurements of the concentration difference across the interface and parameterisations of the transfer velocity from turbulent wind motion are used to predict a gas flux (Liss and Slater, 1974; Johnson, 2010);

$$F = -K_a(C_a - HC_w) = -K_w(C_a/H - C_w) \qquad\qquad 5a$$

$$K_a = \left(\frac{1}{k_a} + \frac{H}{k_w}\right)^{-1} \qquad\qquad 5b$$

$$K_w = \left(\frac{1}{k_w} + \frac{1}{Hk_a}\right)^{-1} \qquad\qquad 5c$$

where $K_a$ and $K_w$ represent total exchange velocities with respect to air and water phases, $C_a$ and $C_w$ represent gas concentrations in the bulk atmosphere and water, $k_a$ and $k_w$ represent exchange velocities in the air and water phases and $H$ represents Henry's air-over-water solubility. Two equal expressions are derived because different gasses are limited by airside transfer (high solubility), waterside transfer (low solubility) or a combination of the two (Yang et al., 2016b).

The most commonly used $k_w$ and $k_a$ parameterisations are that of Nightingale et al. (2000) and Duce et al. (1991) respectively;

$$k_w = \left(0.222 U_{10}{}^2 + 0.333 U_{10}\right) \left(\frac{S_{C_w}}{600}\right)^{-0.5} \qquad 6$$

$$k_a = \frac{U_{10}}{770 + 45\ MW^{1/3}} \qquad 7$$

where $U_{10}$ represents the wind speed at 10 m above the water surface, $S_{C_w}$ represents the waterside Schmidt number (ratio of kinematic viscosity in water and molecular diffusivity of the gas in water) and $MW$ represents the molecular weight of the gas. $S_{C_w}$ is used to normalise the parameterisations for environmental changes in gas diffusivity (i.e. water temperature).

More recently, the coupled ocean–atmosphere response experiment (COARE) model has provided theoretical parameterisations (Fairall et al., 2007, 2011; Edson et al., 2013) which have been used extensively in recent measurements (e.g. Yang et al., 2013a, 2014b; Bell et al., 2017). The equations of the COARE models are significantly more advanced than previous parameterisations and are out of the scope of this Introduction.

Instead of semi-empirical parameterisations between wind speed and gas transfer velocity ($k_w$ and $k_a$), the TL model can also be represented as gas resistances. This is most useful for reactive gases (i.e. O$_3$) that are lost upon contact with seawater. For reactive gases, $C_a \gg H C_w$ thus Equation 5a can be simplified to $F = v_d C_a$. $v_d$ can be calculated (Chang et al., 2004);

$$v_d = \frac{1}{R_T} = \frac{1}{R_1 + R_2 + R_3} \qquad 8a$$

$$R_1 = \frac{1}{\kappa u_*} \ln\left(\frac{z}{z_0}\right) \qquad 8b$$

$$R_2 = \frac{5}{u_*} S_{C_a}{}^{2/3} \qquad 8c$$

$$R_3 = \frac{H}{\sqrt{\lambda D}} \qquad 8d$$

where $R_1$ represents aerodynamic resistance, $R_2$ represents gas-phase film resistance, $R_3$ represents aqueous-phase film resistance, $\kappa$ represents the von Karman constant, $u_*$ represents friction velocity, $z$ represents wind measurement height, $z_0$ represents the aerodynamic roughness length, $S_{C_a}$ represents airside Schmidt number, $\lambda$ represents chemical reactivity (product of concentration and second-order reaction kinetic) and $D$ represents gas diffusivity (Garland et al., 1980; Chang et al., 2004; Carpenter et al., 2013). $R_1$ and $R_2$ describe the transport of a gas to the ocean surface, while $R_3$ describes the loss of that gas due to aqueous reactions. $R_3$ is the dominant resistance in O$_3$ deposition with $R_T$ contributions of 93–97 % (Lenschow et al., 1982; Kawa and Pearson, 1989).

### 1.5.2.  Enhancement of gas exchange

### 1.5.2.1.  Physical enhancement of gas exchange

The combination and rearrangement of Equations 4 and 5a ($\rho_a \overline{w'x'} = -K_a(C_a - HC_w)$) allows for the estimation of $K_a$. Measurements have shown wind speed is the dominant enhancement factor for $K_a$ because of the breakdown of diffusive layers caused by higher surface wind stress (Jähne and Hauecker, 1998). The vast majority of research has been on relatively insoluble gases (waterside controlled, i.e. $CO_2$, DMS) and has mainly shown a quadratic, cubic or similar wind speed dependence (Liss and Merlivat, 1986; Watson et al., 1991; Wanninkhof, 1992; Nightingale et al., 2000). Limited measurements exist of the windspeed dependence at high wind speed, in part because of difficulty in gaining open ocean measurements in high winds or storms. Some measurements up to 25 m s$^{-1}$ exist for $CO_2$, DMS, acetone and methanol, gases with variable solubilities, and show good agreement with the COARE model (Yang et al., 2014a; Blomquist et al., 2017).

Many parameterisations attempt to incorporate the effects of breaking waves and bubble-mediated transfer at high wind speed, however, this is sensitive to the specific solubility of the gas used. Using simultaneous $CO_2$ and DMS EC measurements, Bell et al. (2013, 2017) showed bubble-mediated gas transfer is important for $CO_2$ but less important for DMS above the threshold for wave-breaking, and also the wind speed dependence is of similar form to predicting whitecap areal extent from wind speed.

Other physical controls on gas exchange include seawater/air temperature which varies the $S_{C_w}$. The $S_{C_w}$ is the ratio of seawater kinematic viscosity and molecular diffusivity of the gas in seawater; as temperature increases, seawater kinematic viscosity decreases and gas diffusivity increases which subsequently both act to increase $S_{C_w}$.

### 1.5.2.2.  Organics at the air–sea interface

The SML comprises the top 10–100 μm of ocean water and has significantly altered conditions compared to the underlying bulk ocean water. Organic material in the SML has been shown to both increase and decrease gas transfer (Fairall et al., 2007; Calleja et al., 2008; Pereira et al., 2018; Yang et al., 2021). Surface active species (surfactants) concentrate in the SML by either being naturally hydrophobic and/or being scavenged by rising air bubbles in the top few metres of the surface ocean (Wurl et al., 2011; Cunliffe et al., 2013). Typical concentration enhancement of organics, compared to the bulk water below the surface, is approximately 1–2.5 (Wurl et al., 2011; Sabbaghzadeh et al., 2017) however has strong spatial variability in part due to the sources and characteristics of the organic material.

Donaldson and George (2012) show four categories of the effect of surfactants on gas exchange; prohibiting transport to the surface (Figure 2a), prohibiting solution at the surface (either by limiting soluting species reaching the gas (Figure 2b) or concentrating the gas within the film itself (Figure 2c)) or direct reaction between the gas and organic substrate (Figure 2d). Note, while Figure 2 shows a gas crossing the interface from the airside, the same effects apply

to a gas from the waterside for Figure 2a and Figure 2c. Most research has been conducted on the suppression of gas transfer due to surfactants (Calleja et al., 2008; Pereira et al., 2018; Yang et al., 2021). Surface organics have been shown to suppress the gas transfer of relatively inert gases (i.e. $CO_2$) at wind speed <5 m s$^{-1}$ (Calleja et al., 2008; Yang et al., 2021) which is thought to be due to surfactants dampening waves and turbulence (McKenna and McGillis, 2004). Yang et al. (2021) show the largest suppression in the Southern Ocean (~50 %) was <5 m s$^{-1}$, which was reduced to ~30 % and no suppression at ~7 and >11 m s$^{-1}$ respectively. At high wind speed, the organic surface layer surface tension breaks down, leading to less suppression and higher transfer. Natural surfactant concentration and SML enrichment both linearly decrease $CO_2$ $K_a$ by up to 32 % in the Atlantic Ocean (Pereira et al., 2018) and up to 44 % in the coastal North Sea (Pereira et al., 2016). Artificial surfactants (oleyl alcohol) suppress DMS and $SF_6$/$^3$He $K_a$ by up to 39 and 55 % respectively (Salter et al., 2011).
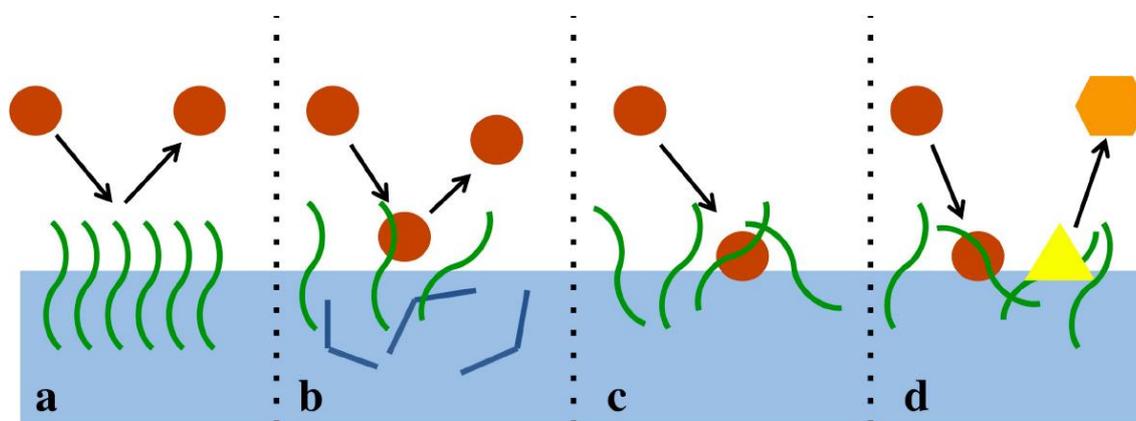


**Figure 2: Proposed model for the effects of surfactants on gas transfer and chemical processes in the surface microlayer. The coating may (a) prevent interfacial transport of, (b) prevent surface hydrolysis of, (c) concentrate, or (d) react with the gas phase species of interest (red circles). Graphic from Moore (2014), which was originally adapted from Donaldson and George (2012).**

Organic compounds prohibiting hydrolysis of a gas at the surface, by limiting soluting species reaching the gas are important for acidic and basic gases (Clifford et al., 2007; Ardura and Donaldson, 2009) and, by themselves acting as the solvent shell are important for water-insoluble gases (Donaldson and Vaida, 2006, and ref. within).

### 1.5.2.3.  Chemical enhancement of ozone deposition

For gases with a permanent air–sea flux due to a negligible water concentration (i.e. $O_3$), $K_a$ is modified to $v_d$ (Section 1.5.1.2), where $v_d$ encompasses the solubility and waterside mechanisms. Chang et al. (2004) showed $O_3$ $v_d$ was constant (~0.018 cm s$^{-1}$) below 4 m s$^{-1}$ wind speed and increased by a factor of 2 when wind speed increased to 10 m s$^{-1}$; the non-zero velocity with negligible wind speed implied other competing chemical (i.e. halides, organics) and physical (i.e. solubility, diffusion) parameters. The large range of current literature $O_3$ $v_d$ is due to poorly quantified heterogeneous chemical SML conditions (Chang et al., 2004).

Chloride (Cl$^-$), bromide (Br$^-$) and iodide (I$^-$) are halide species present throughout the ocean that are known to rapidly react with $O_3$. I$^-$ has the largest second-order rate (Garland et al., 1980), an ocean concentration of 10–400 µM (Chance et al., 2014), and is important to $O_3$ $v_d$ at low

wind speed (Chang et al., 2004). Although Cl⁻ and Br⁻ have higher seawater concentrations than I⁻, their second-order rate with $O_3$ is much lower (Garland et al., 1980), thus their overall reactivity ($\lambda = C_i k_i$) is much lower than I⁻. Table 1 highlights the expected reactivity ranges of known aqueous $O_3$ destroying species.

**Table 1: Expected concentrations and ozone reactivity for known seawater constituents. References are as follows; (a) (Garland et al., 1980), (b) (Garland et al., 1980), (c) (Flury and Papritz, 1993), (d) (Chance et al., 2014; Sherwen et al., 2019), (e) (Garland et al., 1980; Liu et al., 2001; Moreno et al., 2018), (f) (Bodineau et al., 1999; Romera-Castillo et al., 2010; Chen, 2017), (g) (Coleman et al., 2010; Sarwar et al., 2016), (h) (Wang et al., 2020b), (i) (Gershenzon et al., 2001), (j) (McClain, 2009) and (k) (Clifford et al., 2008). * rate measurements of $O_3$–DOC reactions are bulk estimations and not direct measurements.**

| Species | Concentration range | Reaction rate, $10^7 \times k$ (M⁻¹ s⁻¹) | Ozone reactivity, $\lambda$ (s⁻¹) |
|---|---|---|---|
| Chloride | ~0.55 mM[a] | $3.2 \times 10^{-10}$ [b] | ~0.002 |
| Bromide | 0.8–0.9 mM[c] | $3 \times 10^{-5}$ [b] | 0.2–0.3 |
| Iodide | 10–200 nM[d] | 120–200[e] | 12–400 |
| DOC | 30–200 μM[f] | 0.34–0.40[g] * | 102–800 |
| DMS | 0.1–10 nM[h] | 86[i] | 0.09–9 |
| Chlorophyll $a$ | 0.01–10 nM[j] | 6[k] | 0.0006–0.6 |

Table 1 clearly identifies organic compounds as being highly reactive with $O_3$, potentially outcompeting I⁻ by a factor of 2 under some conditions. This was first shown by Martino et al. (2012) who compared the contribution of NOM (natural organic material, Suwannee River standard) and I⁻ on $O_3$ $v_d$ and arrived at the conclusion that I⁻ and NOM are equally important. Martino et al. (2012) however highlighted that the Suwannee River NOM is considerably more unsaturated than marine DOM, therefore their result could be an overestimation compared to the real ocean due to the significantly faster atmospheric reactions of $O_3$ and unsaturated species (Atkinson and Arey, 2003). Clifford et al. (2008) hypothesised that marine chlorophyll $a$ may also contribute to $O_3$ deposition at low wind speed; experiments showed that chlorophyll $a$ enhanced $v_d$ by a factor of 3, using atmospherically relevant $O_3$ concentrations. Whether or not the chlorophyll $a$ prepared by Clifford et al. (2008), via solvent extraction of leaves, can be compared to in situ seawater concentrations is debatable considering healthy phytoplankton should not emit much chlorophyll $a$. Reeser et al. (2009) showed the photochemical properties of chlorophyll $a$ in an illuminated SML produced highly reactive radicals that enhanced waterside $O_3$ destruction reactions.

### 1.5.2.4.   Langmuir-Hinshelwood and Eley-Rideal mechanisms

Gaseous $O_3$ and DOM either undergo reactions at the air–sea interface or in the aqueous phase. Literature over the last two decades has shown surface reactions of $O_3$ and aqueous organics species follow a Langmuir–Hinshelwood mechanism (Mmereki et al., 2004; Raja and Valsaraj, 2005; Kahan et al., 2006; Clifford et al., 2008) where the two species react after adsorbing onto an interface following a Langmuir isotherm (Langmuir, 1916, 1922a);

$$A_g + S \rightarrow A_s \qquad\qquad \text{R8a}$$

$$B_{aq} + S \rightarrow B_s \qquad\qquad \text{R6b}$$

$$A_s + B_s \rightarrow C_s \qquad\qquad \text{R6c}$$

For this thesis, species A represents gas-phase $O_3$ and species B represents aqueous phase organic material/DOM. The reactions (Reaction R8a–c) for the two species can be modelled as;

$$\frac{dC_{C,\text{surf}}}{dt} = k_{\text{surf}}C_{A,\text{surf}}C_{B,\text{surf}} \tag{9a}$$

$$C_{A,\text{surf}} = \frac{N_{\text{surf}}^{\text{max}}R_A C_{A,\text{bulk}}}{1 + R_A C_{A,\text{bulk}} + R_B C_{B,\text{bulk}}} \tag{9b}$$

$$C_{B,\text{surf}} = \frac{N_{\text{surf}}^{\text{max}}R_B C_{B,\text{bulk}}}{1 + R_A C_{A,\text{bulk}} + R_B C_{B,\text{bulk}}} \tag{9c}$$

where $C_{X,Y}$ represents the concentration of X in phase Y, $k_{\text{surf}}$ represents the surface bimolecular rate constant ($O_3$ + DOM), $N_{\text{surf}}^{\text{max}}$ represents the total surface binding sites and $R_X$ represents the adsorption:desorption ratio of surface equilibrium constants for X (Reeser and Donaldson, 2011; Prins, 2018). Equations 9b–c describe Langmuir isotherms for the surface concentration of a bulk species (Langmuir, 1916).

A bimolecular Langmuir–Hinshelwood mechanism proceeds fastest when both reagents have a high surface concentration and share an approximately equal proportion of $N_{\text{surf}}^{\text{max}}$. When both species have very low absorption to the interface, Equations 9a–c simplify to Equation 10 (reaction is second-order) (Prins, 2018);

$$\frac{dC_{C,\text{surf}}}{dt} = k_{\text{surf}}N_{\text{surf}}^{\text{max}2}R_A C_{A,\text{bulk}}R_B C_{B,\text{bulk}} \tag{10}$$

In the scenario where species B (i.e. aqueous organics) has a significantly lower absorption than species A (i.e. gaseous $O_3$) but species A has a low bulk concentration, Equations 9a–c also simplify to Equation 10. On the other hand, if species A has high surface concentration with respect to species B, Equations 9a–c simplifies to Equation 11 (reaction is zeroth-order, i.e. species A inhibits the reaction);

$$\frac{dC_{C,\text{surf}}}{dt} = k_{\text{surf}}N_{\text{surf}}^{\text{max}2}\frac{R_B C_{B,\text{bulk}}}{R_A C_{A,\text{bulk}}} \tag{11}$$

A potentially competing but less accepted reaction is the Eley–Rideal mechanism where the gaseous reagent does not absorb to the interface but reacts with aqueous material extending into the gas phase (hydrophobic end of amphipathic molecules, i.e. lipids, fatty acids) (Langmuir, 1922b, 1922a);

$$B_{aq} + S \longrightarrow B_s \tag{R9a}$$

$$A_g + B_s \longrightarrow C \tag{R7b}$$

The reactions (Reactions R9a–b) for two species can be modelled as;

$$\frac{dC_C}{dt} = k_{\text{surf}}C_{A,bulk}C_{B,surf} \tag{12a}$$

$$C_{B,\text{surf}} = \frac{N_{\text{surf}}^{\text{max}}R_B C_{B,\text{bulk}}}{1 + R_B C_{B,\text{bulk}}} \tag{12b}$$

A bimolecular Eley–Rideal mechanism proceeds fastest when species A is concentrated in the airside diffusive layer (reactions always first-order concerning species A) and species B has a high surface concentration. If the surface concentration of species B is low, Equations 12a–b

simplify to Equation 13. On the other hand, if the surface concentration of species B is high, Equations 12a–b simplify to Equation 14;

$$\frac{dC_C}{dt} = k_{surf} N_{surf}^{max} C_{A,bulk} R_B C_{B,bulk} \qquad\qquad 13$$

$$\frac{dC_C}{dt} = k_{surf} N_{surf}^{max} C_{A,bulk} \qquad\qquad 14$$

### 1.5.2.5. Combined surface and aqueous reactions

$O_3$ undergoes quick reaction with DOM in and/or at the SML and the location of the reaction depends on the surface concentration of DOM and thus whether a Langmuir–Hinshelwood or Eley–Rideal mechanism occurs. If $O_3$ can diffuse through the interface into the aqueous phase, aqueous reactions will occur alongside surface reactions. Moreno et al. (2018) studied $O_3$–I⁻ reactions to calculate how many collisions of $O_3$ and a solution lead to a reaction (γ) which can be used to calculate $v_d$; $v_d = 0.25\gamma c$, where c represents $O_3$ thermal velocity (Clifford et al., 2008). The following equation incorporates surface and aqueous reactions and may be suitable for $O_3$–organic reactions;

$$\gamma = \left(\frac{1}{\alpha_s} + \left(\left(\alpha_s \frac{k_{sol}}{k_d} + \frac{1}{\Gamma_{rxn}}\right)^{-1} + \Gamma_{surf\,rxn}\right)^{-1}\right)^{-1} \qquad\qquad 15$$

where γ represents total uptake, $\alpha_s$ represents the surface accommodation coefficient (ratio of collisions that equal adsorption to total collisions), $k_{sol}$ and $k_d$ represent the rate of $O_3$ surface solvation and desorption, respectively, and $\Gamma_{surf\,rxn}$ and $\Gamma_{rxn}$ represent the conductance of the surface and aqueous reactions respectively (Moreno et al., 2018).

### 1.5.2.6. Ozone and DOM reactions

$O_3$ undergoes quick reaction with DOM in and/or at the SML to produce VOC and other organic compounds, which can either release into the atmosphere or mix into the bulk layer. The majority of the literature has focused on the reactions of $O_3$ and fatty acids (e.g. Eliason et al., 2003; Katrib et al., 2004; Thornberry and Abbatt, 2004; Zahardis et al., 2005; King et al., 2009; Zhou et al., 2014; Schneider et al., 2019) as proxies for DOM in tropospheric OA or the SML. The work by Zhou et al. (2014) was in part the genesis for this thesis.

Zhou et al. (2014) importantly identified the production of volatile carbonyl (ketones and aldehydes) compounds from the heterogeneous oxidation of oceanic and coastal SML samples. $O_3$ exposure of the oceanic and coastal samples produced $C_2$–$C_5$ monocarbonyl gases (i.e. acetaldehyde, acetone) that increased and remained steady across multiple repeats, indicating that the DOM precursors were being replenished at the air–water interface. $C_4$–$C_6$ unsaturated hydrocarbon fragments (i.e. $C_4H_9^+$, $C_5H_9^+$) were only produced from the coastal SML samples and did not equally increase upon secondary $O_3$ exposure which suggested the DOM precursors were of lower concentration and rapidly consumed upon first exposure. Prompted by the results of Zhou et al. (2014), work by Chen (2017) showed the effect of light, temperature and DOM addition on the heterogeneous production rate of VOC via reaction with $O_3$, and found that

acetaldehyde, acetone and isoprene were significant products. Ambient light was found to have no significant effect, temperature produced the interesting result of a minimum VOC production/emission rate at 15 °C and DOM addition was shown to affect the production rate of VOC differently depending on the source.

Zhou et al. (2014) also identified the production of glyoxal from the ozonolysis of artificial SML monolayers and, importantly, a mechanism of production could be established. Lininoic acid was oxidised by the addition of $O_3$ to the carbon double bond ($C_9$ 30–50 or $C_{12}$ 50–70 % yield) forming a primary ozonide which decomposed into n-hexanal ($C_9$) or 3-nonenal ($C_{12}$) and other aqueous products. The n-hexanal and 3-nonenal products underwent further carbon double bond ozonolysis which either produced glyoxal or malondialdehyde (MDA, IUPCA name: propanedial). Produced MDA was further oxidised to form glyoxal. This source may resolve the glyoxal budget discrepancies in the remote open ocean, especially considering the indirect link with surface DOM (Myriokefalitakis et al., 2008; Sinreich et al., 2010). It is the aliphatic hydrocarbon end of lininoic acid that produces the volatile glyoxal and MDA; thus any suitable organic compound with long aliphatic ends (a carbon double bond with an 8 or 11 carbon chain specifically required here) can be a source of glyoxal and MDA.

It is clear some carbon leaves the seawater as volatile compounds, however, as described above, some carbon remains as an aqueous product either as soluble or insoluble DOM. This was shown by King et al. (2009) who studied reactions of air–water monolayer oleic acid and gas-phase $O_3$ and identified that during ozonolysis, half the surface film disappeared. This suggested that at least two species were produced, one of which remained on the surface (likely nonanoic acid) and one which either diffused into the bulk water (likely nonanedioic acid) or transferred into the gas phase. With the seawater DOM cleaving into volatile and aqueous components, the reactions of $O_3$ and DOM likely influence seawater DOM chemistry and retention time in the surface ocean.

While not of direct marine significance, the treatment of TOC in riverine petrochemical wastewater by $O_3$ has been shown to increase the concentration of hydrophilic neutral and acid compounds and decrease all other TOC components (Fu et al., 2019). The TOC concentration in the water was largely similar before and after $O_3$ addition which suggested that $O_3$ alone does not significantly mineralise TOC. For the hydrophilic fractions and the hydrophobic base fractions, the reactions of $O_3$ caused an increase in low molecular weight TOC. Hydrophobic NOM has also been shown as the principal component for $O_3$ attack (Cho et al., 2003).

## 1.6. Aims and objectives

Current VOC literature clearly identifies a discrepancy between estimations of the top-down and bottom-up budgets from the MBL distant from terrestrial sources. One of the most important VOCs, isoprene, has an estimated missing source of ~1.6 Tg yr$^{-1}$ compared to ~0.3 Tg yr$^{-1}$ production by phytoplankton (Arnold et al., 2009). A limited number of direct ocean

measurements, coupled with a potentially incomplete understanding of all the chemical sources of VOC at the ocean surface leads to considerable uncertainty.

Due to the limited number of direct ocean measurements, and the subsequent uncertainly in the main two sources (biological metabolism of organic material and direct photochemical reactions DOM) and the newly uncovered source (direct reactions of atmospheric $O_3$ and DOM), each VOC source could solve the budget discrepancy if they have been scaled incorrectly so far.

This thesis attempts to combine field measurements and laboratory experiments to calculate the significance of the production of three VOC (acetaldehyde, acetone and isoprene) from the oxidation reactions that occur at the sea surface ($O_3 + DOM \rightarrow VOC$), compared to the air-sea flux of VOCs.

The main aims of the project were:

1. Quantify realistic VOC flux and concentration values through undertaking field measurements at a coastal atmospheric observatory.

2. Quantify VOC production yields through laboratory measurements of the oxidation of seawater by $O_3$.

3. Scale the laboratory VOC yield measurements to evaluate the significance towards global atmospheric budgets.

4. Quantify the variability in the chemical uptake of $O_3$ by seawater and determine the importance of DOM.
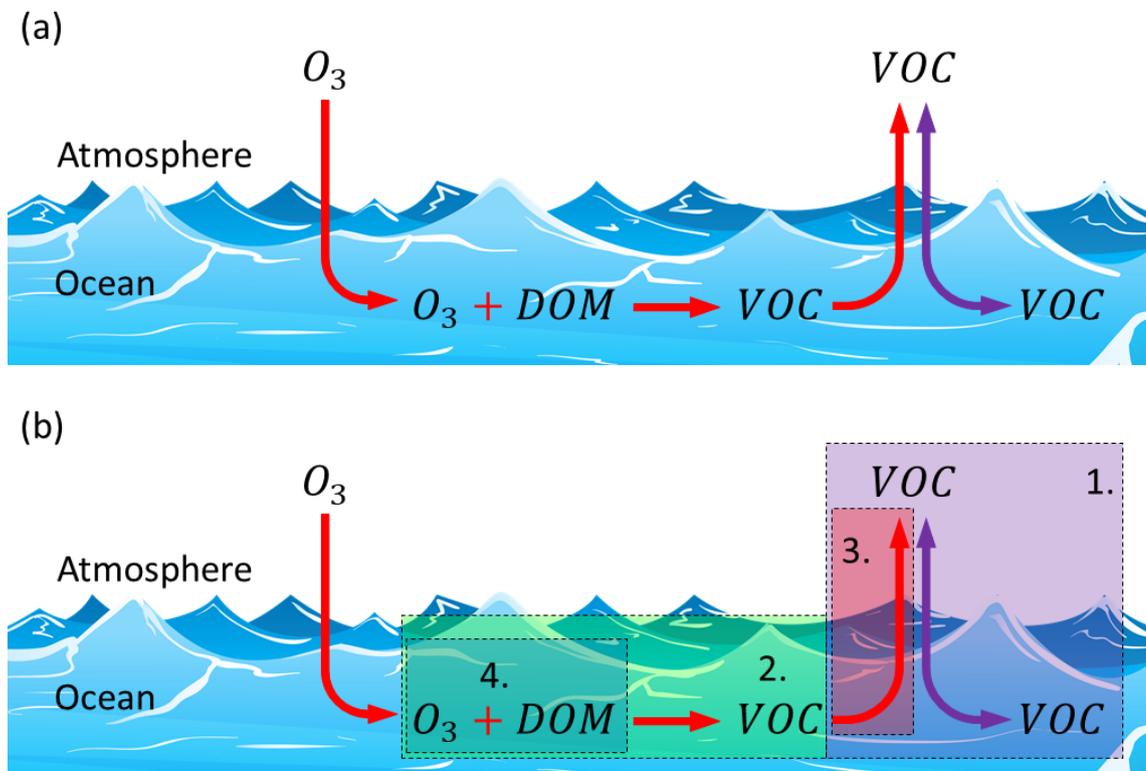


**Figure 3: A schematic of some of the main research themes of the thesis (red arrows), including the breakdown by project aim (numbered coloured boxes) in the lower figure.**

# Chapter 2 – The air–sea exchange of acetone, acetaldehyde, DMS and isoprene at a UK coastal site

This chapter has been published in *Atmospheric Chemistry and Physics* with the following citation: Phillips, D. P., Hopkins, F. E., Bell, T. G., Liss, P. S., Nightingale, P. D., Reeves, C. E., Wohl, C., and Yang, M.: Air–sea exchange of acetone, acetaldehyde, DMS and isoprene at a UK coastal site, Atmos. Chem. Phys., 21, 10111–10132, https://doi.org/10.5194/acp-21-10111-2021, 2021. A few changes have been made to the format for the thesis, which includes the incorporation of the paper appendices into the main text, the addition of the penultimate paragraph in Section 2.3.3 (discussion on the potential of interfacial $O_3$–DOM reactions resulting in EC and TL method disagreement) for discussion in the subsequent Chapters, and also some minor phrasing corrections suggested by doctoral examiners. Where possible, please reference Phillips et al. (2021) and not the thesis chapter.

## 2.1.  Introduction

VOCs are ubiquitous in the atmosphere and play an important role in atmospheric chemistry and carbon cycling in the biosphere (Heald et al., 2008). Many VOCs can influence the oxidative capacity of the atmosphere by acting as a source or sink of atmospheric $O_3$ and OH radicals (Atkinson, 2000; Lewis et al., 2005), thereby influencing local air quality. The lower volatility oxidation products, produced from reactions of some VOCs with atmospheric oxidants, can condense into particulates and form cloud condensation nuclei (CCN) (Charlson et al., 1987; Blando and Turpin, 2000; Henze and Seinfeld, 2006), affecting the Earth's radiative forcing and climate.

The terrestrial environment is the largest source of VOCs to the atmosphere with the emission dominated by isoprene from plant foliage (Guenther et al., 2006). Terrestrial biological processes also produce carbonyls including ketones and aldehydes in varying amounts (Kesselmeier and Staudt, 1999). Large uncertainties exist concerning the role that the ocean plays as a net source or sink of these gases (Broadgate et al., 1997; Arnold et al., 2009; Millet et al., 2010; Fischer et al., 2012; Wang et al., 2019). This is due to poorly quantified air–sea fluxes as well as uncertainties in the biogeochemical and physical processes that control them.

Acetone and acetaldehyde are carbonyl-based VOCs that have been shown to make up to ~57 % of the carbon mass of all non-$CH_4$ organic carbon compounds in remote marine air over the North Atlantic Ocean (Lewis et al., 2005). These VOCs have been detected in the surface ocean at concentrations of up to tens of nanomolar (nM) (Zhou and Mopper, 1997; Williams et al., 2004), with known oceanic sources including the photochemical degradation of DOM in bulk seawater (Kieber et al., 1990; Zhou and Mopper, 1997; Zhu and Kieber, 2018) and possibly autotrophic/heterotrophic biological processes (Halsey et al., 2017; Schlundt et al., 2017). The

heterogeneous oxidation of DOM at the sea surface has recently been identified as a source of carbonyl-containing VOCs (Zhou et al., 2014; Ciuraru et al., 2015b); however, the significance of this is currently unknown.

DMS is a biogenic sulfur-containing VOC that constitutes the majority of the organic sulfur in the atmosphere (Andreae et al., 1985). It is produced in the surface ocean from the degradation of the algal osmolyte DMSP (Kiene et al., 2000) and subsequently emitted into the atmosphere. DMS is often the dominant source of sulfur in the marine atmosphere (Yang et al., 2011b), and the oxidation products of DMS can act as CCN (Charlson et al., 1987; Veres et al., 2020).

Isoprene is an unsaturated terpene-based VOC that is produced in the ocean by a broad range of phytoplankton as a secondary metabolic product (Moore et al., 1994; Shaw et al., 2003; Exton et al., 2013; Booge et al., 2016; Dani and Loreto, 2017). Oceanic sources of isoprene are important for the remote marine atmosphere (Lewis et al., 2001; Arnold et al., 2009; Booge et al., 2016) because transport from terrestrial sources is negligible due to isoprene's very short atmospheric lifetime (~30 min; Carslaw et al., 2000).

The main oceanic sink of most carbonyl VOCs is biological metabolism at varying rates (Dixon et al., 2014; Royer et al., 2016; Halsey et al., 2017). Surface seawater concentrations of acetone and acetaldehyde tend not to be very sensitive towards their air–sea fluxes (Beale et al., 2015). Emission to the atmosphere is generally considered to be a small loss for seawater DMS (Yang et al., 2013b) but a much larger loss relatively for seawater isoprene (Booge et al., 2018).

There have been very few direct measurements of air–sea VOC fluxes with the EC technique (e.g. Marandino et al., 2005; Yang et al., 2013c, 2014b; Kim et al., 2017). More often, the fluxes are estimated with the bulk method using air and sea concentrations in a TL model (e.g. Baker et al., 2000; Beale et al., 2013; Wohl et al., 2020). Most studies focus on open ocean air–sea exchange, while air–sea VOC flux measurements from the coast are essentially non-existent (EC or bulk). Compared to the open ocean, the coastal waters tend to be very dynamic biogeochemically (Borges et al., 2005; Bauer et al., 2013) and physically. For example, riverine runoffs carry nutrients and organic carbon into the coastal seas, which could stimulate intense biological cycling (Cloern et al., 2014). Furthermore, compared to the remote marine atmosphere, coastal air is affected by terrestrial emissions.

The air–sea gas transfer velocity can be derived by equating the EC flux with the bulk TL flux (e.g. Blomquist et al., 2010; Bell et al., 2013; Yang et al., 2013a, 2014a). Limited studies have been undertaken to identify whether open-ocean-derived parameterisations of the transfer velocity apply to coastal systems (Borges et al., 2004; Yang et al., 2019a). Turbulent processes (i.e. wave-breaking, tidal currents, bottom-driven turbulence) are expected to behave differently in these environments (Upstill-Goddard, 2006), with potential impacts on gas exchange.

In this chapter, the air–sea fluxes of acetone, acetaldehyde and DMS are determined using the EC technique at a coastal observatory in the south-west UK. Seawater concentrations measured from a marine station 6 km offshore are used to compute the TL fluxes of these VOCs as well as

the TL flux of isoprene. Comparisons are made between the coastal flux measurements and previous observations of open ocean fluxes as well as global model estimates. From the EC fluxes and air and sea concentrations, the gas transfer velocities of DMS, acetone and acetaldehyde are derived and compared to previous observations from the open ocean.

## 2.2. Method

### 2.2.1. Location

The Penlee Point Atmospheric Observatory (PPAO) is a long-term monitoring station and a part of the Western Channel Observatory (WCO; westernchannelobservatory.org.uk/data [WCO data]) on the south-west (SW) coast of the UK (50.318° N, -4.189° E). Measurements were made between 05/04/18 and 03/05/18. The suitability of the observatory for direct air–sea exchange measurements (momentum, heat, greenhouse gases, sea spray aerosols, $O_3$) has been discussed in detail before (Yang et al., 2016a, 2016c, 2019a, 2019b; Loades et al., 2020). The PPAO is located on an exposed headland that observes two distinct wind sectors representative of different air–sea exchange regimes. The SW open-water sector (depth of ~20 m within the flux footprint) faces the western English Channel and North Atlantic Ocean. The north-east (NE) Plymouth Sound sector (fetch-limited with a depth of ~10 m) is influenced by estuarine output from the rivers Tamar and Plym (Uncles et al., 2015) as well as natural terrestrial and anthropogenic atmospheric emissions. The theoretical extent of the flux footprint at the PPAO has been discussed previously (Yang et al., 2019a; Loades et al., 2020).
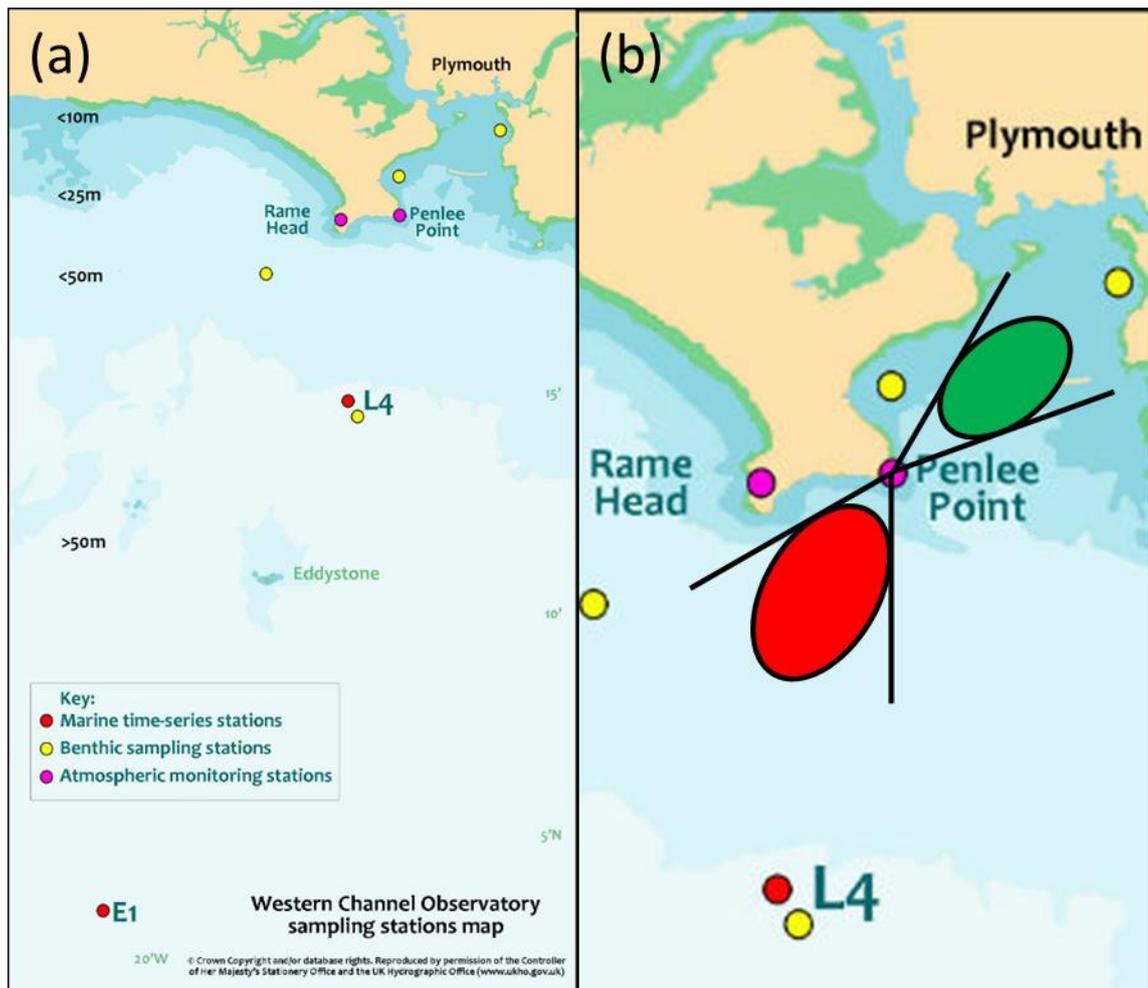
**Figure 4: Map of key sampling locations in the Western Channel Observatory. Panel (b) shows the estimated flux footprint for the two wind sectors; 30–70° N and 180–240° N with the size relative to the measured windspeed. Reproduced with permission from the UKHO and the Keeper of Public Records. ©** *Crown Copyright 2021.*

### 2.2.2.   Set-up and measurements

The EC system here principally consists of a proton-transfer-reaction mass spectrometer (PTR-MS, Ionicon Analytik high-sensitivity PTR-quadrupole-MS) and a sonic anemometer (Gill Windmaster Pro). The measurement set-up closely followed previous PPAO flux campaigns (Yang et al., 2016a, 2016d), with a few adaptations made to accommodate the PTR-MS requirements. A simple gas flow diagram is shown in Figure 5.
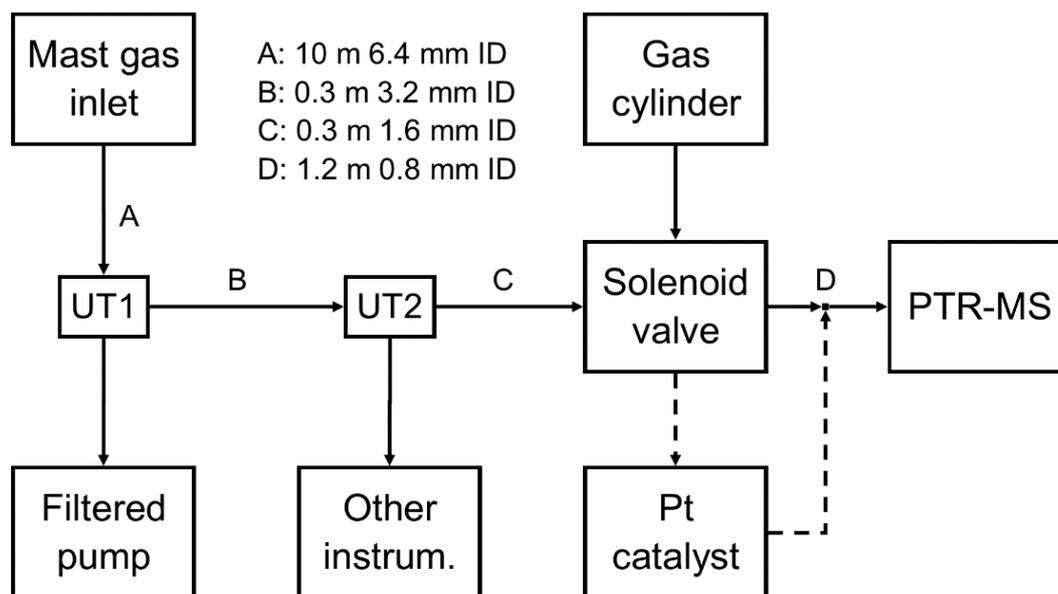
**Figure 5: Schematic of the tubing set-up used to draw an atmospheric sample to the gas instrument (PTR-MS). Dashed lines represent the set-up of the platinum catalyst before the synthetic gas blank was added. UT represents union-tee; a three-way static connection.**

The sonic anemometer was mounted on a mast ~19 m above mean sea level and run at 10 Hz. The air inlet consisted of a downwards-facing 90 ° union, mounted 30 cm below the anemometer, connected via a 10 m tube to a union tee upstream of the air pump (UT1). All PPAO air sampling instruments (including the PTR-MS) subsampled ambient air from this union tee. A dry pump (Gast 1023 series) was used to draw ambient air into the observatory. The total flow rate was ~13.5 L min$^{-1}$, as calculated from the continuously monitored flow of the pump (Bronkhurst EL-FLOW series) and the sum of independent flows of connected instruments. All unions and tubing before UT1 were 6.4 mm internal diameter (ID).

Downstream of UT1 (i.e. closer to the instruments) was a 0.3 m, 3.2 mm ID tube and union tee (UT2), which split the sample air between the PTR-MS and other equipment (see Loades et al. (2020) for simultaneous PPAO $O_3$ fluxes). Downstream of UT2 (i.e. closer to the PTR-MS) was a 0.3 m, 1.6 mm ID tube, which connected through a solenoid valve (Takasago Electric, Inc. MLV-3T-1/8NG) to the 1.2 m, 0.8 mm ID PTR-MS inlet tubing. All tubing, unions and fittings between the mast inlet and PTR-MS inlet were made from perfluoroalkoxy (PFA), while the solenoid valve was polytetrafluoroethylene (PTFE) and the PTR-MS inlet was polyetheretherketone (heated to 80 °C to limit surface adsorption).

VOC concentrations were quantified using the PTR-MS technique (see Lindinger et al. (1998) for a detailed measurement description). The PTR-MS uses a hollow cathode discharge to produce hydronium ions ($H_3O^+$), starting with a saturated $H_2O$ vapour from a low pressure pure water reservoir, which protonate analytes and allow them to be filtered by mass inside a mass spectrometer;

$$R + H_3O^+ \rightarrow RH^+ + H_2O \qquad\qquad\qquad R10$$

where $R$ represents a VOC or analyte.

The advantages of the PTR-MS technique, in contrast to the historic gas chromatography (GC)-MS technique, are higher temporal resolution (De Gouw and Warneke, 2007), limited molecular fragmentation (Lindinger et al., 1998) and continuous online measurement. The disadvantages are limited compound measurement, potential isobaric interferences and occasionally lower limits of detection. Complete $H_3O^+$ ionisation only occurs when analytes have a proton affinity greater than $H_2O$ (165.2 kcal mol$^{-1}$; Lindinger et al., 1998); some VOC (e.g. $CH_4$, formaldehyde) therefore cannot be measured using $H_3O^+$. Note that PTR-MS measurements are not limited to just using $H_3O^+$ as a reagent ion; additional ions following the $XH^+$ scheme, such as $NH_4^+$ and $CH_5^+$, can offer a route of lower energy exchange when protonating the analyte leading to lower molecular fragmentation (Blake et al., 2009). Furthermore, different reagent ions can show unique proton affinities for structural isomers, allowing for the selective measurement of isomer mixtures (Blake et al., 2009). Other forms of chemical ionisation mass spectrometry, which work on a very similar principle to PTR-MS, can operate with $O_2^+$ and $Kr^+$, which have a higher ionisation potential than $H_3O^+$ and thus can ionise and quantify more compounds (Sulzer et al., 2012), or $NO^+$ ions which have the same selective isomer advantage described above (Koss et al., 2016). See Rogerson (2016) for the use of $NO^+$ with the PTR-MS used here.

A potential trade-off for PTR-MS measurements using $H_3O^+$ ions is the influence voltage has on the stability of the signal. Under typical drift chapter conditions, $H_3O^+$ will combine with excess $H_2O$ to create hydrated clusters;

$$H_3O^+ + nH_2O \rightarrow H_3O^+(H_2O)_n \qquad\qquad \text{R11}$$
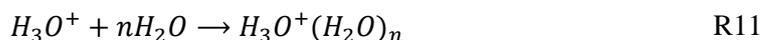
These clusters have different reaction kinetics with VOCs, which can affect the instrumental sensitivity, and thus are ultimately undesired. Increasing the drift voltage leads to a lower cluster formation because the higher energy cluster product, from higher energy $H_3O^+$ colliding with $H_2O$ or other clusters, is unstable. On the other hand, the higher energy $H_3O^+$ and VOC can cause unintentional reactions which destroy/fragment VOC and subsequently reduce signal strength. Hydrated clusters are normally only an issue with humid gas samples (e.g. measuring marine atmosphere) and the unintentional reactions usually only occur for unstable branched VOC (i.e. isoprene), thus under dry usage, this is not a problem.

For this experiment, the PTR-MS was set to multiple ion detection mode, where the quadrupole cycles between and holds desired masses for a selected dwell time, with four VOCs of interest: acetaldehyde, acetone, DMS and isoprene (initially at $m/z$ 45, 59, 63 and 69 respectively). Previous experiments (Schwarz et al., 2009) and our laboratory tests (Wohl et al., 2019) show that substantial isoprene fragmentation occurs at the voltage used in these measurements (690 V, 166 Td; see Appendix C for the calculation of Td). Importantly, the $m/z$ 41 fragment ion was shown to provide a larger and more stable signal than that of the isoprene parent ion ($m/z$ 69). As a result, a week into the campaign the monitoring of isoprene was changed to $m/z$ 41. The calibration (see Section 2.2.4) and thus calculation of the isoprene mixing ratio accounted for the fragmentation and the change in ion monitored. The quadrupole mass dwell

time was set to 50 ms for $H_3O^+$ and 100 ms for each VOC. In total, the full ion cycle was just over 450 ms, which resulted in a sampling frequency of 2.2 Hz. Dwell time for each VOC was a compromise between measurement frequency and instrument noise. The PTR-MS parameters are listed in Table 2, which largely follows from Yang et al. (2013c). A high drift voltage was used to limit the formation of hydrated clusters caused by the high humidity of marine air (Reaction R11), however, increased voltage also caused a greater degree of isoprene fragmentation (Schwarz et al., 2009; Wohl et al., 2019). Isoprene fragmentation was corrected using gas-phase calibration. Data from the sonic anemometer, flow meter and PTR-MS were all recorded on the same computer to avoid desynchronisation.

**Table 2: PTR-MS method used for measurements.**

| Parameter | Value |
|---|---|
| Drift chamber pressure (mBar) | 2.3 |
| Drift chamber voltage (V) | 690 |
| Drift chamber temperature (°C) | 80 |
| $H_2O$ mass flow (mL min$^{-1}$) | 5 |
| Source/proportional valve (%) | 49 |
| Inlet flow rate (mL min$^{-1}$) | 150 |
| Inlet temperature (°C) | 80 |

A solenoid valve, controlled from the PTR-MS, was used to automate routine hourly blanking for the VOC measurements (first 5 min of each hour). At the beginning of the campaign, sample gas (ambient air) was diverted through a platinum catalyst (heated to 450 °C) to produce VOC-free air (full oxidation to $CO_2$; Yang and Fleming, 2019). However, the use of the catalyst caused overheating within the PPAO building and was replaced with an activated charcoal filter, which unfortunately proved to be inefficient at removing VOCs. The charcoal filter was replaced with compressed clean air (BOC synthetic air) towards the end of the campaign (27/04/18–03/05/18), which yielded the most consistent blanks. Post-campaign experiments showed that the acetaldehyde background when measuring dry, $CO_2$-free compressed air was lower than measuring moist atmospheric air scrubbed by the catalyst by about 0.33 ppbv (Wohl et al., 2020). This difference was due to the different levels of $CO_2$ (accounting for ~0.3 ppbv) and to a lesser extent water vapour (accounting for ~0.03 ppbv) between the compressed air and ambient air, qualitatively consistent with previous works (Warneke et al., 2003; Schwarz et al., 2009). The calculation of the atmospheric acetaldehyde mixing ratio accounted for these sensitivities. Overall, the determination of the VOC backgrounds was more uncertain during this campaign than in previous measurements (Yang et al., 2013c), however, this is not expected to significantly influence the EC fluxes since the air concentrations were detrended during the flux calculation (see Section 2.2.3).

### 2.2.3. Eddy covariance flux calculation

EC gas fluxes are determined from the correlation between rapid changes (at least a few Hz) in vertical wind velocity and the gas mixing ratio using Equation 4. Air density was computed using the PPAO air temperature, pressure and humidity data (Gill Instruments Metpak Pro). Wind measurements were linearly interpolated from 10 Hz to match the VOC measurement frequency.

A double wind rotation (Tanner and Thurtell, 1969; Hyson et al., 1977) was applied to each 10 min segment of wind data ($u$ and $v$ = horizontal, $w$ = vertical), such that $u$ became the wind speed ($U$) in the mean wind direction and $v$ and $w$ each averaged zero. This was done to minimise the effect of flow distortion caused by the headland to achieve the stationary requirements of the EC technique (assumption 2, Section 1.5.1.1)

A lag time of approximately 3.5 s between wind and PTR-MS measurements was calculated from the dimensions of the tubing and flow rate. The lag time was further determined hourly using a lag correlation analysis between $w$ and $x$ over a window of +10 s. Acetone had the strongest flux signal of the four VOCs measured and was used to determine the lag time. Note the PTR-MS data output had a single timestamp for all four measured masses, even though each mass was measured sequentially (~100 ms). No attempt was made to calculate lag time with the specific timestamp of the acetone mass because the possible increase in accuracy was far smaller than the accuracy of either PTR-MS or wind instrument. Lag-adjusted PTR-MS data were used to calculate fluxes in 10 min segments, the sampling interval chosen as the best compromise between maintaining sufficient flux signal-to-noise ratio and satisfying the stationarity criteria in this dynamic region (Yang et al., 2016a, 2016c, 2019a, 2019b).

The sampling frequency of the PTR-MS is relatively low (2.2 Hz), and the instrument's response time determined from laboratory tests is just under 0.5 s. The computed fluxes were corrected for high-frequency signal loss due to (1) sampling at 2.2 Hz, and thus missing the flux above the Nyquist frequency of 1.1 Hz, and (2) attenuation due to the tubing, using a combined $U$ dependent attenuation factor (mean=1.09, max=1.18). This signal attenuation was estimated from the instrument's response time following the approach of Yang et al. (2013a). Table 3 shows the quality control criteria used to filter 10 min flux data segments, developed from EC measurements of $CO_2$ and $CH_4$ fluxes at the PPAO (Yang et al., 2016a). Standard deviation in wind direction was used to ensure fairly constant wind direction and minimise the influence from areas outside the specified NE and SW wind sectors. The remaining controls check for the stationary criteria required for EC measurements, remove periods with obvious flow distortion or remove periods with substantial rain influence on the sonic anemometer.

**Table 3: Flux segment quality control criteria.**

| Parameter | Value |
|---|---|
| Wind direction, $\sigma$ (°) | < 10 |
| Momentum flux (kg m$^{-2}$ s$^{-1}$) | < 0 |
| Tilt angle (°) | < 15 |
| $\sigma_w/u_*$ | 1.2 < x < 1.9 |
| $\sigma_U^2/U$ (m s$^{-1}$) | < 0.35 |

The 10 min flux segments that met the quality control criteria were averaged into 1 h or 3 h fluxes, which reduces random noise by a factor of $\sim\sqrt{6}$ and $\sim\sqrt{18}$, respectively. Over the entire duration of the campaign, 61 % of the data were discarded, mainly due to inappropriate wind directions (i.e. from land) or large variability in wind direction (more common at low wind speed). Diurnal variability was apparent in the open-water wind sector data (SW winds) concerning the

number of acceptable flux segments. About twice as many flux segments passed quality control in the daylight hours compared to at night, which is likely due to a diurnal sea-breeze effect. When EC fluxes were averaged across 5 weeks of measurements, no difference was observed per hour of the day. No diurnal cycle could be seen in the Plymouth Sound wind sector data (NE winds), likely in part due to the limited data size.

Random uncertainty in the EC flux depends on variability (instrument noise + ambient variability) in the VOC measurement and the wind measurement. Precision (or random error) in the EC technique can be approximated as the standard deviation of 'null' fluxes (i.e. covariance data with a lag time between vertical wind and concentration measurements that is much greater than the integral timescale; Spirig et al., 2005). Fluxes are resolvable when they are higher than 3 times the measurement noise, which can be a problem for PTR-MS flux measurements due to the traditionally noisy signal on short time scales (noisy in this experiment due to the short mass dwell times and low VOC concentrations). An artificial lag time of 300 s was chosen for this calculation here. The 3 times standard deviation was calculated from hourly averages over a 5 h window of stable open-water wind speed and direction as 10.1, 6.8, 4.7 and 4.7 $\mu$mol m$^{-2}$ d$^{-1}$, for acetaldehyde, acetone, DMS and isoprene respectively. LOD estimates here are 140–250% of the LOD from a previous deployment of this PTR-MS at sea (Yang et al., 2014b), mainly due to the greater ambient variability in VOC mixing ratio at this coastal environment. Hourly data were averaged to 3 h intervals to reduce random error by a factor of $\sqrt{3}$; thus the 3 h LOD are 5.8, 4.0, 2.7 and 2.7 $\mu$mol m$^{-2}$ d$^{-1}$, for acetaldehyde, acetone, DMS and isoprene respectively.

Co-spectra of acetone and DMS averaged over all quality-controlled periods are shown in Figure 6 for both the open-water and Plymouth Sound wind sectors. Here the areas between the co-spectral curves and zero represent the magnitudes of the fluxes. Theoretical co-spectral fits constrained by the actual wind speed and measurement height (Kaimal et al., 1972) suggest that the measured co-spectral shapes were reasonable. The Kaimal fits also showed the high-frequency flux loss (>~1 Hz) was small, consistent with the estimated high frequency signal loss correction. Acetaldehyde and isoprene are not shown here because the bidirectionality in acetaldehyde flux and the low isoprene flux magnitude (Section 2.3.1) cause very noisy co-spectra.
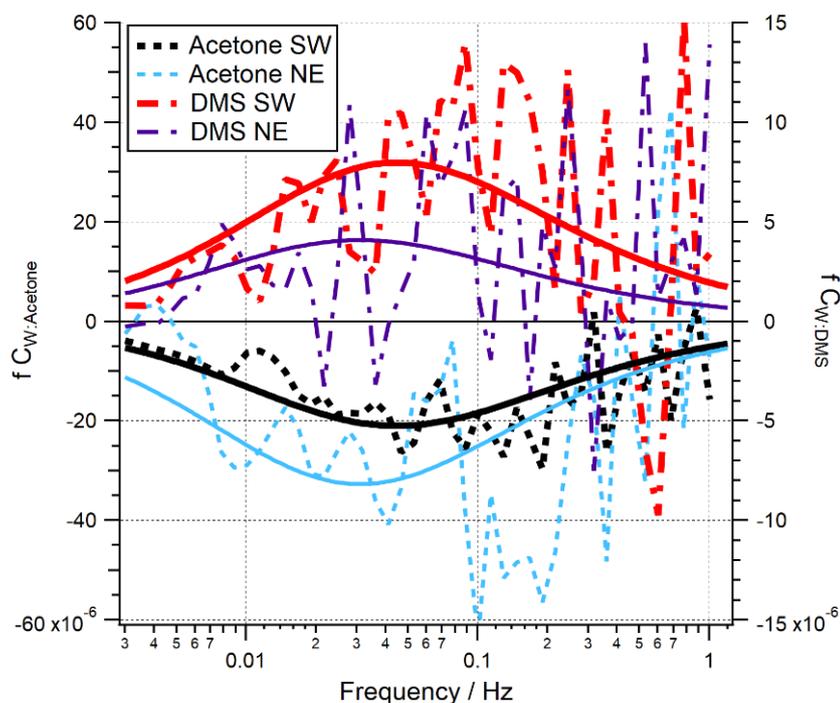
**Figure 6: Mean flux co-spectra for acetone and DMS in the SW and NE wind sectors. Dashed/broken lines represent PPAO observations. Solid lines represent the idealised spectral fits (Kaimal et al., 1972), where measurement height and wind speed are specified according to the measurement conditions.**

### 2.2.4. Seawater measurements and two-layer flux calculation

Discrete seawater samples were collected from the L4 marine time series station (50.250° N, -4.217° E) of the WCO, which is ~6 km S–SW of the PPAO headland (Figure 4). The near-surface VOC concentrations are presumed to be similar between L4 and the PPAO open-water flux footprint despite the outflow from the Tamar estuary that hugs the PPAO headland (Uncles et al., 2015); this assumption is revisited in Section 2.3.3. Seawater acetaldehyde, acetone, DMS and isoprene concentrations were determined using a segmented flow coil equilibrator (SFCE) coupled to the PTR-MS before and after the PPAO campaign (following Wohl et al. (2019)). Additional seawater DMS concentration measurements were made weekly at L4 using GC (following Hopkins and Archer (2014)) for the Mar–May 2018 period.

Atmospheric VOC mixing ratios from PPAO were blank-corrected using the synthetic gas cylinder measurements (27/04/18 onwards; Section 2.2.2), accounting for the humidity dependence in the background of DMS (mean correction of 0.22 and 0.12 ppbv, for SW and NE air respectively, estimated from Wohl et al. (2019)) and the $CO_2$ plus humidity dependences in the background of acetaldehyde (constant correction of 0.33 ppbv estimated from data from Wohl et al. (2020)). There is greater confidence in the measured atmospheric VOC mixing ratios after switching to synthetic air for the blank measurement, thus the EC fluxes and the TL bulk fluxes were compared over this period (27/04/18–03/05/18) only. Gas-phase calibrations of the PTR-MS (using a certified gas standard, Apel-Riemer Environmental Inc.) before and after the deployment were averaged and applied to both the atmospheric and seawater VOC data.

Surface saturation values of DMS and acetaldehyde were calculated using the recommended solubility from the literature (Burkholder et al., 2015; Sander, 2015) as a function of temperature and adjusted for salinity (Johnson, 2010). Recent calibrations at environmentally relevant concentrations in seawater suggest that acetone is less soluble than previously thought (Wohl et al., 2020); thus the acetone air-over-water solubility recommended by Burkholder et al. (2015) was divided by 1.4 as recommended by Wohl et al. (2020).

The calculation of the bulk TL fluxes requires the use of wind speed dependent gas transfer velocity parameterisations. The measured $U$ at the PPAO was corrected for flow acceleration due to the headland using results from a comparison with a wind sensor on the L4 buoy (Yang et al., 2019a). This scaled $U$ from 19 m (height of the PPAO mast) to 4.9 m (height of L4 wind sensor) and also removed the effect of wind acceleration from the sloped PPAO headland. The corrected winds were then scaled to 10 m;

$$U_{10} = U_{4.9} \frac{\ln\left(\frac{10}{z_0}\right)}{\ln\left(\frac{4.9}{z_0}\right)} \qquad 16$$

where $z_0$ was calculated from $U$ using the COAREG 3.5 model (Edson et al., 2013). Overall, the mean correction factor was 0.93 (min=0.79 and max=1.39) for the two wind sectors. The relationship between the corrected $U_{10}$ and friction velocity ($u_*$) from the EC wind data shows reasonable agreement with the COAREG 3.5 model as well as with Mackay and Yeun (1983) (Figure 7), which validate these wind corrections. $u_*$ is calculated as follows:

$$u_* = ((\overline{u'w'})^2 + (\overline{v'w'})^2)^{0.25} \qquad 17$$
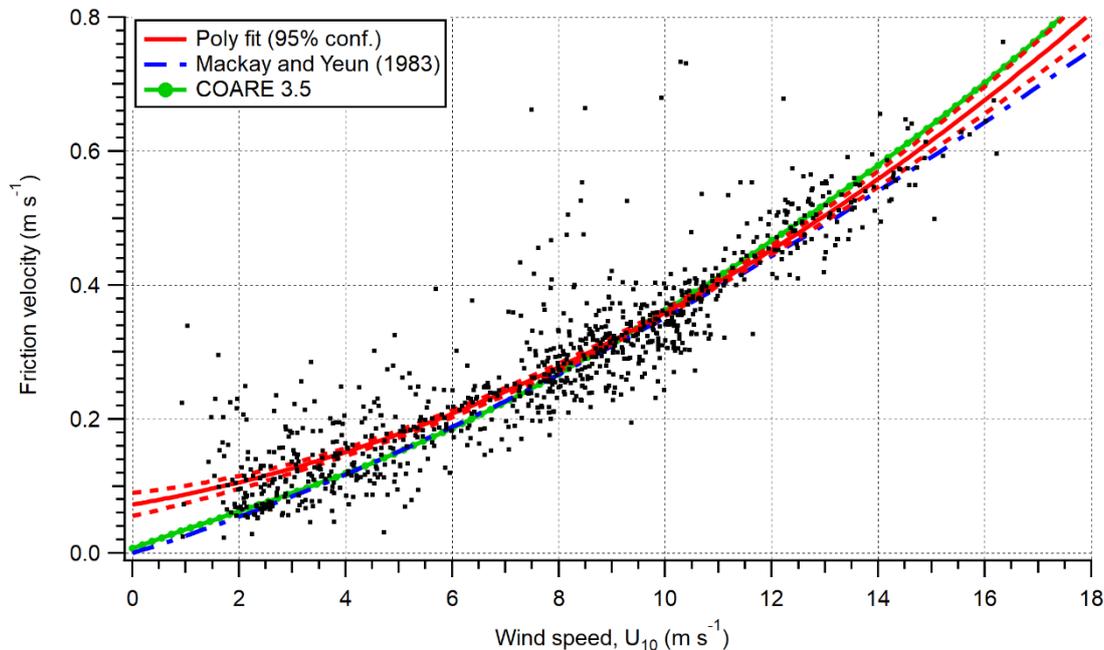


**Figure 7: Comparison of measured friction velocity to wind speed (corrected to 10 m height). Data were filtered to remove the influence of rain. The theoretical fits of Mackay and Yeun (1983) and the COAREG 3.5 model (Edson et al., 2013) are also shown.**

Bulk fluxes were calculated following Liss and Slater (1974) and Johnson (2010) using Equations 5a and 5b. Note that total waterside transfer velocity ($K_w$), more commonly used for

waterside controlled gases such as DMS and isoprene, is equal to $HK_a$. $k_a$ was calculated from the COAREG 3.5 model (Edson et al., 2013), which can be approximated as $k_a \approx -0.32884U_{10}^3 + 27.428U_{10}^2 + 34.936U_{10} + 553.71$. The VOCs targeted here span only a small range in diffusivity in air and are thus assumed to have the same $k_a$ for simplicity (Yang et al., 2014a, 2016b). $k_w$ for acetone, acetaldehyde and DMS was calculated using the fit from Yang et al. (2011a); this was an average of DMS observations from five cruises: $k_w \approx \left(-0.00797U_{10}^3 + 0.208U_{10}^2 + 0.484U_{10}\right)(S_{Cw}/660)^{-0.5}$. $k_w$ for isoprene was calculated using the fit from Nightingale et al. (2000) (Equation 6). At a $U_{10}$ of 10 m s$^{-1}$, the Nightingale et al. (2000) parametrisation would overestimate DMS $k_w$ by ~37 % because bubble-mediated gas exchange is less important for the moderately soluble DMS (Bell et al., 2017; Blomquist et al., 2017). The $S_{C_w}$ number for all gases was computed following Johnson (2010) at the ambient temperature and salinity; Table 4 shows the solubility and solubility temperature dependence (Burkholder et al., 2015) and molar volume data (Johnson, 2010) used in the calculations of salinity-dependent $H$ and $S_{Cw}$. In the diffusion coefficient calculation, the original association factor of solvent (2.6) was used as recommended by Saltzman et al. (1993) for DMS.

**Table 4: Freshwater solubility ($H^{cp}$), solubility temperature dependence ($\frac{d\ln(H^{cp})}{d(1/T)}$) and molar volume ($V_b$) used in calculations of seawater solubility and Schmidt number at ambient temperature and salinity. $H^{cp}$ and $d\ln(H^{cp})/d(1/T)$ for freshwater are updated from Sander (2015) and Burkholder et al. (2015).**

| Compound | $H^{cp}$ (mol L$^{-1}$ atm$^{-1}$) | $\frac{d\ln(H^{cp})}{d(1/T)}$ (K) | $V_b$ (cm$^3$ mol$^{-1}$) |
|---|---|---|---|
| Acetaldehyde | 13.4 | 5775 | 56 |
| Acetone | 29.0 | 5170 | 77.6 |
| DMS | 0.541 | 3520 | 77 |
| Isoprene | 0.0345 | 4400 | 105 |

During the period with satisfactory hourly blanking (27/04/18–03/05/18), the mean ($\pm\sigma$) L4 water temperature and salinity were 10.6±0.8 °C and 34.9±0.1 PSU. These were taken from the surface measurement of a weekly CTD profile collected on the RV *Plymouth Quest*. Mean atmospheric pressure was 1006±4 mB, $U_{10}$ was 9.93±3.76 m s$^{-1}$ and friction velocity (also from EC) was 0.364±0.166 m s$^{-1}$. Table 5 shows the available VOC concentration data just before, during and after the campaign. Simultaneous measurements and calculated fluxes were made using concentration data from as close as possible to the period with satisfactory blanking (*).

**Table 5: Seawater concentrations of VOCs at the L4 marine station at 2 m depth. * denotes concentration used for two-layer calculation.**

| Date | VOC surface concentration (nM) | | | | Measurement method |
|---|---|---|---|---|---|
| | Acetaldehyde | Acetone | DMS | Isoprene | |
| 26/03/18 | 8.09* | 3.93* | 1.11 | 0.09* | SFCE-PTRMS |
| 10/04/18 | - | - | 2.56 | - | GC |
| 19/04/18 | - | - | 10.34 | - | GC |
| 23/04/18 | - | - | 3.03* | - | GC |
| 30/04/18 | - | - | 4.13* | - | GC |
| 21/05/18 | - | - | 10.69 | - | GC |
| 30/05/18 | 6.16* | 6.71* | 4.99 | 0.10* | SFCE-PTRMS |

## 2.3.   Results and Discussion

### 2.3.1.   EC fluxes for the open-water and Plymouth Sound wind sectors

Flux measurements were made between 05/04/18 and 03/05/18. During this period, winds arrived from the open-water wind sector (180–240° N) 30 % of the time and from the Plymouth Sound sector (30–70° N) 8 % of the time. The wind directions defining these two marine flux sectors were re-established compared to previous PPAO studies after raising the mast height by ~1 m at the beginning of this campaign. Figure 8 shows the double wind rotation tilt angle correction and drag coefficient ($C_D$) for 10 min segments of wind data averaged into wind direction bins. $C_D$ is calculated as follows:

$$C_D = (u_*/U)^2 \hspace{4cm} 18$$

The 10 min data were filtered ($U$>3 m s$^{-1}$) to reduce the influence of the flux footprint overlapping with the narrow strip of land upwind under low wind speed conditions (Yang et al., 2019a). The majority of winds had a positive tilt angle due to the rotation of ocean (horizontal) winds hitting the headland. However, winds from 260–360° N were negatively angled due to the raised headland behind the observatory. The 30–70° N and 180–240° N zones exhibit a small, positive tilt angle and a low drag coefficient, as might be expected for the open ocean (Kara et al., 2007; Edson et al., 2013), thus are defined as the two air–water exchange sectors.
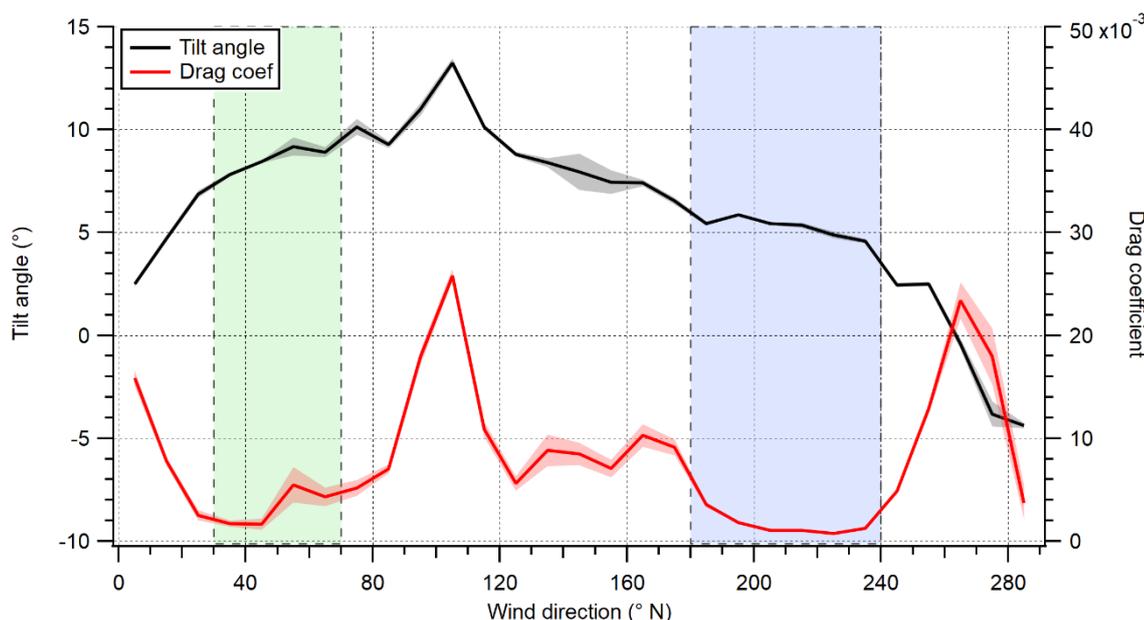


**Figure 8: Vertical tilt angle correction (tilt of horizontal plane) applied to approaching winds and drag coefficient (> 3 m s$^{-1}$), averaged into 10° wind direction bins. The shaded region on lines is 1 standard error. The green and blue boxes represent the NE and SW wind sectors respectively.**

A time series of VOC fluxes (3 h average) is shown in Figure 9. While acetone and DMS had clear unidirectional fluxes (deposition and emission respectively), acetaldehyde showed bidirectional fluxes throughout the campaign. EC fluxes of acetone, acetaldehyde, DMS and isoprene from the two marine wind sectors averaged over the entire campaign are summarised in Table 6, with positive fluxes representing net sea-to-air emission.
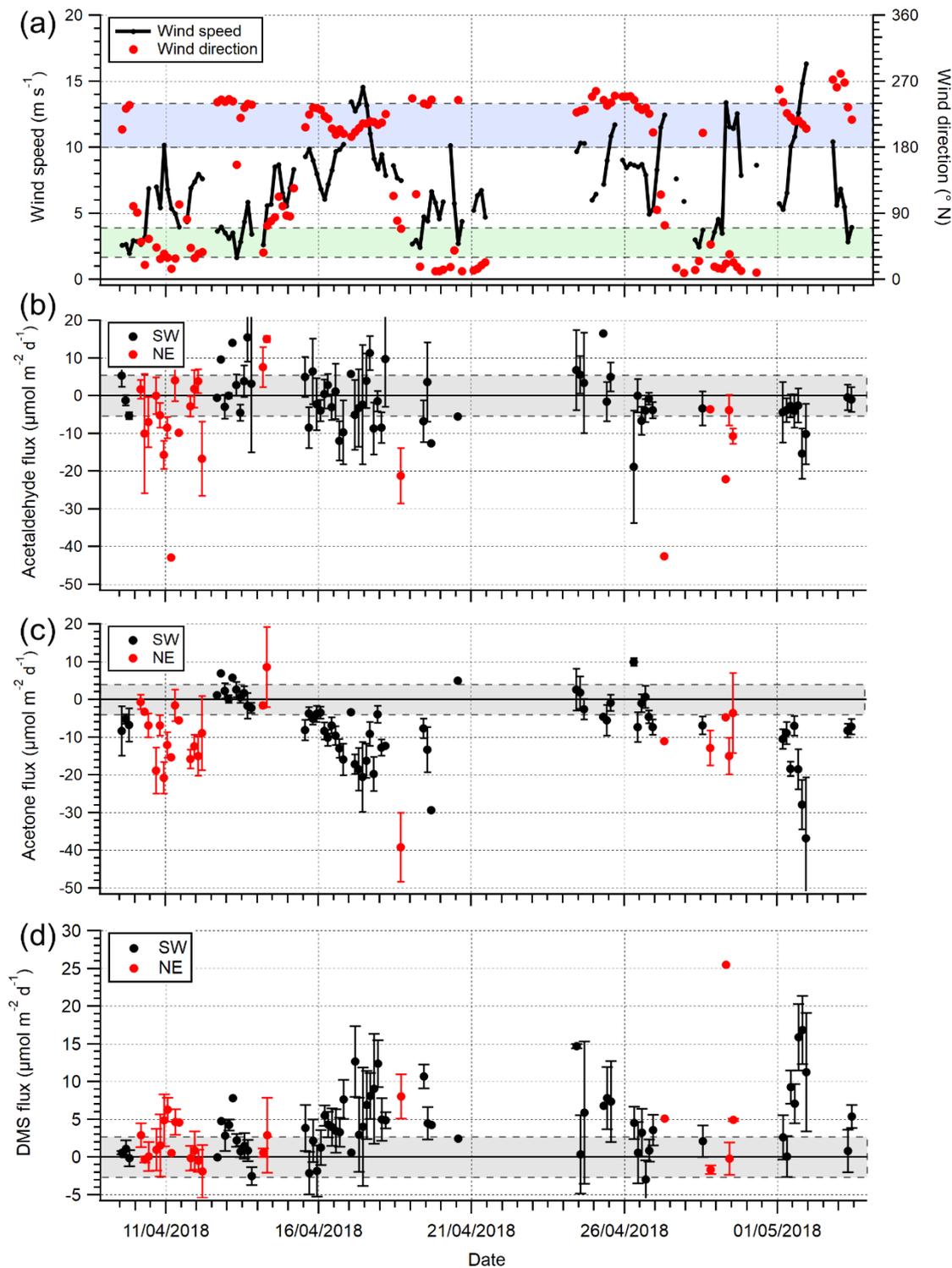
**Figure 9: Time series of 3 h averages of (a) wind speed ($U_{10}$) and wind direction, (b) acetaldehyde flux, (c) acetone flux and (d) DMS fluxes for the open-water (180–240° N) and Plymouth Sound (30–70° N) wind sectors that met quality control criteria. Error bars are 1 standard error. The blue and green shaded zone in panel (a) represent the two wind sectors. The grey shaded zones in panels (b)–(d) represent limits of detection for 3 h averages, 5.8, 4.0 and 2.7 µmol m$^{-2}$ d$^{-1}$ for acetaldehyde, acetone and DMS respectively.**

**Table 6: Eddy covariance flux measurements over the entire campaign. Errors indicate standard errors with n=135 and n=40 bins (1 h averages) for the open-water and Plymouth Sound sectors respectively. Also included are the quartiles (qrt).**

| VOC | Open water ($\mu$mol m$^{-2}$ d$^{-1}$) | | | | Plymouth Sound ($\mu$mol m$^{-2}$ d$^{-1}$) | | | |
|---|---|---|---|---|---|---|---|---|
| | 25 % qrt. | Median | Mean | 75 % qrt. | 25 % qrt. | Median | Mean | 75 % qrt. |
| Acetald. | -7.44 | -1.23 | -1.55±1.14 | 4.93 | -10.86 | -4.45 | -4.45±1.73 | 1.84 |
| Acetone | -12.15 | -6.27 | -8.01±0.77 | -2.19 | -17.52 | -9.47 | -12.93±1.37 | -2.19 |
| DMS | 0.79 | 4.05 | 4.67±0.56 | 8.26 | -0.96 | 1.16 | 1.75±0.80 | 4.80 |
| Isoprene | -3.54 | 0.60 | 1.71±0.73 | 5.82 | -8.84 | -0.24 | -1.95±1.65 | 3.56 |

For the open-water sector, acetone and DMS fluxes had relative standard errors ($\sigma_{\bar{x}}$) <12 % (from 1 h bins), which are confidently represented by the measurements in the mean thanks to the robust signal-to-noise ratio. Acetaldehyde had a much greater relative $\sigma_{\bar{x}}$ (74 %) because the fluxes often changed in direction and were smaller in magnitude (closer to the limits of detection, LOD); acetaldehyde $\sigma_{\bar{x}}$ is lowered to 51 % when the 573 10 min flux segments are instead averaged over the campaign. The isoprene flux was not resolvable with the EC method using our PTR-MS due to the low signal-to-noise ratio. The only direct measurement of isoprene flux from the sea (Kim et al. (2017) in the North Atlantic Ocean) used a chemical ionisation mass spectrometer that is significantly more sensitive than the PTR-MS here.

Overall, 68, 33, 62 and 35 % of 3 h averages of acetone, acetaldehyde, DMS and isoprene fluxes, respectively, were above the LOD (DMS and isoprene had the additional condition of a positive flux above LOD) for the open-water sector. The estimation of LOD is shown in Section 2.2.3.

The greater air-to-sea deposition fluxes of acetone and acetaldehyde in the Plymouth Sound sector, compared to the open-water sector, were likely driven by the higher gas mixing ratios in terrestrially influenced air. Distributions of the atmospheric acetone mixing ratio from the two wind sectors are shown in Figure 10b–c. Seawater concentrations of acetone and acetaldehyde within the Plymouth Sound flux footprint were not measured, and thus no comment can be given on the quantitative effect of riverine outflow on the dissolved VOC concentrations. The weaker sea-to-air flux of DMS in the Plymouth Sound sector compared to the open-water sector was likely due to a combination of low DMS water concentrations associated with freshwater outflow (Uncles et al., 2015) and lower wind speed (Figure 10a) that results in reduced gas transfer velocity ($k_w$; Nightingale et al., 2000; Yang et al., 2011a).
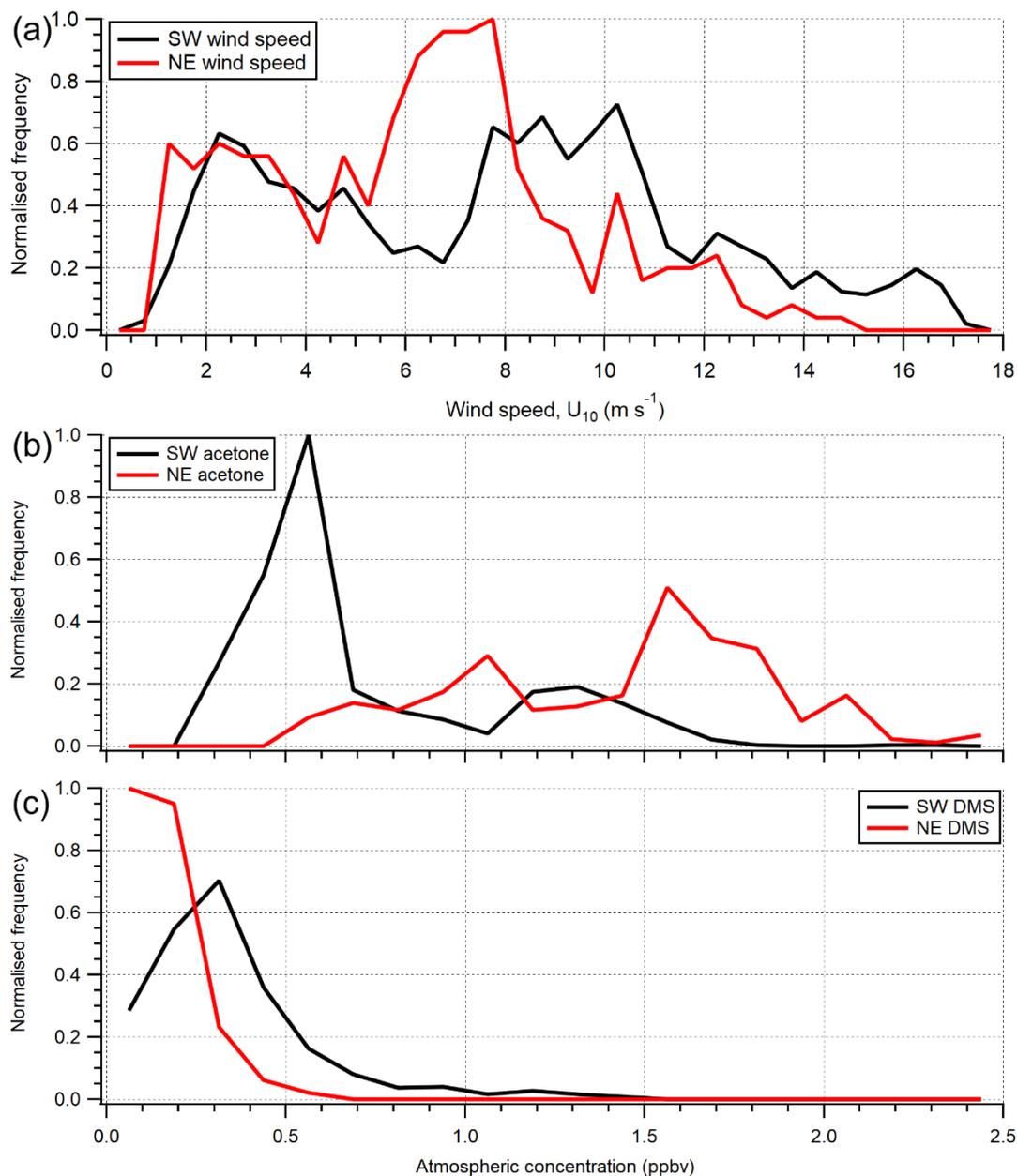
**Figure 10: Histogram of (a) wind speed ($U_{10}$) and (b) acetone and (c) DMS atmospheric gas-phase mixing ratio over the entire campaign. Histograms are normalised for probability density separately and then to the same relative maximum occurrence. The gas mixing ratio calculations here use extrapolated blanks, which introduce some uncertainty; however, the two wind sectors can still be compared.**

### 2.3.2.  Seawater concentration and atmospheric mixing ratios of VOCs

The seawater concentrations of acetone, acetaldehyde and DMS measured around the campaign (Table 5) are broadly similar ($\leq$48 % difference) to previous measurements in the western English Channel (Archer et al., 2009; Beale et al., 2015), a highly variable and seasonal environment. No seawater measurements of isoprene have been published in this region, so comparisons are made to previous observations from the eastern North Atlantic (~0.02 nM; Broadgate et al., 2004; Hackenberg et al., 2017), which are ~79 % lower than measurements here. The eastern North Atlantic measurements were conducted in Sep–Oct, thus likely representing a period of lower isoprene productivity. An annual study in the North Sea found the highest

isoprene seawater concentrations in May (~0.06 nM; Broadgate et al., 1997), which were closer to L4 measurements here but still lower (~41 %).

The mean atmospheric mixing ratios of acetone and acetaldehyde from the open-water sector (0.82±0.16 and 0.51±0.07 ppbv respectively, Table 7) are greater than previous measurements around the sample site, possibly in part due to measurements here occurring mainly over 1 d (1st May 2018; see Figure 14 later for time series); thus a multi-day average was not possible. Remote marine Atlantic Ocean measurements from the ATom-4 campaign (Apr–May 2018), within 0.5 km of the sea surface and at latitudes of 40–60° N, observed 0.31±0.01 ppbv acetone (±$\sigma$) and 0.15±0.04 ppbv acetaldehyde (Wofsy et al., 2018). A better agreement was seen with shipboard measurements between 40 and 50° N in the eastern North Atlantic Ocean (Yang et al., 2014b) and coastal measurements at the Mace Head Observatory (Lewis et al., 2005) with mean acetone mixing ratios of ~0.65 and 0.50 ppbv, respectively, and acetaldehyde mixing ratios of ~0.16 and 0.44 ppbv, respectively. Finally, rooftop measurements at PML (~350 m north of the Plymouth Sound, ~6 km NE of the PPAO, and affected by local ship/port activities) showed night-time atmospheric mixing ratios of ~0.4 and ~0.1 ppbv, respectively for acetone and acetaldehyde (Yang et al., 2013c). A summary of these concentrations, in coordinate form, can be found in Figure 11. The atmospheric carbonyl measurements at the PPAO from this day might not represent purely oceanic conditions even though the wind was from the open-water sector. HYSPLIT (Stein et al., 2015; Rolph et al., 2017) backward trajectories suggest that the air mass sampled on 1st May 2018 made contact with land (mainland UK) ~24–48 h before arriving at the PPAO (Figure 12). Lewis et al. (2005) show that similar air-mass trajectories over the UK and continental Europe contained high acetone levels (max=~1.67 ppbv).

**Table 7: Saturations and two-layer bulk fluxes of VOCs in open-water (SW) and Plymouth Sound (NE) water (27/04/18–03/05/18) along with the eddy covariance measurements for this period. Units for fluxes are µmol m$^{-2}$ d$^{-1}$. Errors for water concentration and air mixing ratio (measurement) and saturation (propagation) indicate one standard deviation. Errors for flux indicate one standard error.**

| VOC | Water conc. (nM) | Air mixing ratio (ppbv) | Open-water Satur. (%) | TL flux | EC flux | Plymouth Sound Air mixing ratio (ppbv) | EC flux |
|---|---|---|---|---|---|---|---|
| Acetald. | 7.1±1.4 | 0.51±0.07 | 44±6 | -6.76±0.59 | -3.94±1.23 | 0.75±0.04 | -7.32±2.86 |
| Acetone | 5.3±2.0 | 0.82±0.16 | 15±3 | -18.98±2.24 | -14.93±2.09 | 1.09±0.09 | -8.21±4.00 |
| DMS | 3.6±0.8 | 0.20±0.09 | 1434±569 | 9.41±1.03 | 9.61±1.55 | 0.015±0.006 | 2.55±2.36 |
| Isoprene | 0.09±0.01 | 0.18±0.05 | 971±221 | 0.30±0.05 | 1.65±1.89 | 0.28±0.03 | 9.27±3.01 |
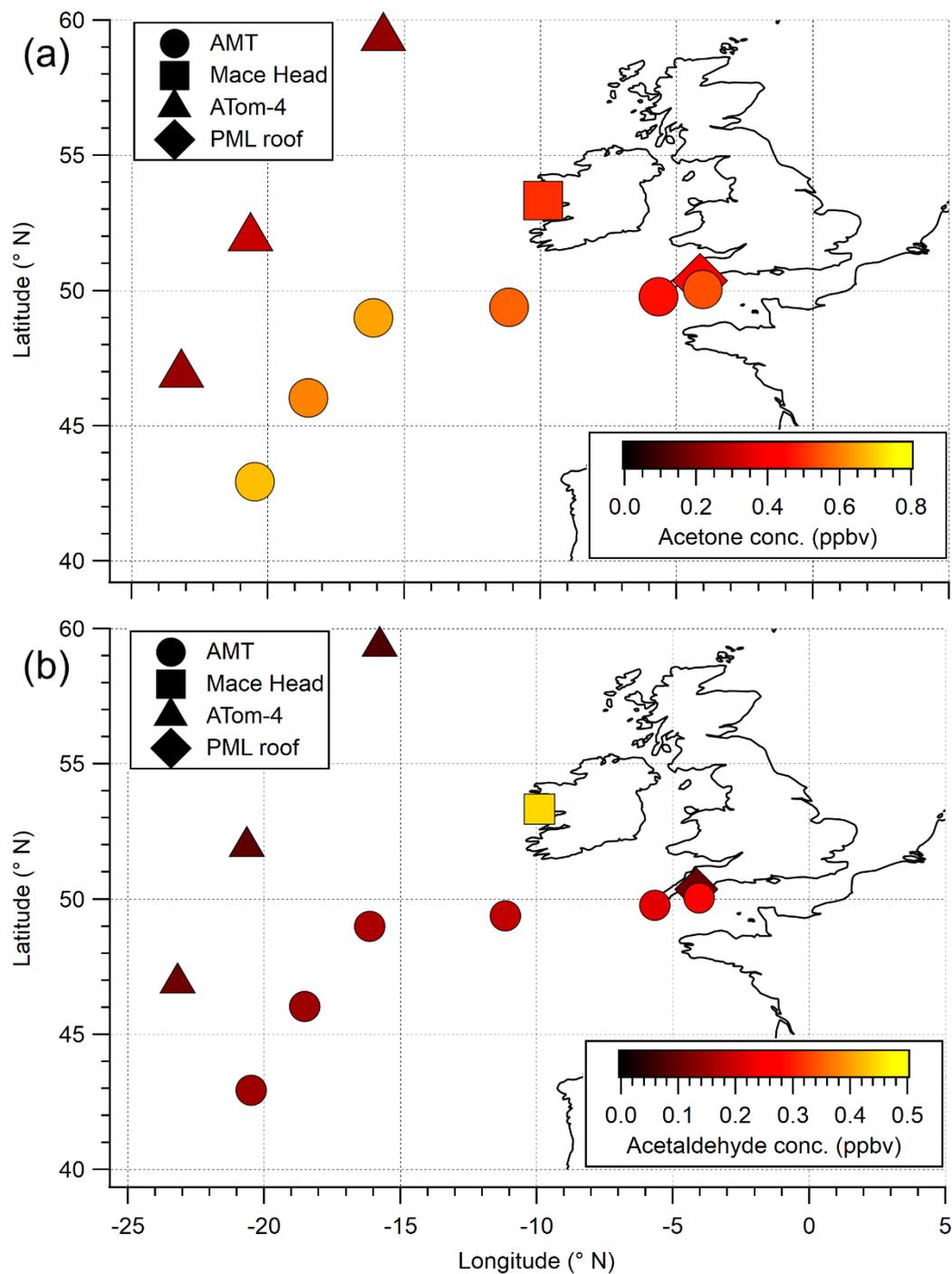
**Figure 11: Location summary of atmospheric a) acetone and b) acetaldehyde mixing ratios discussed in Section 2.3.2 of the main text.**
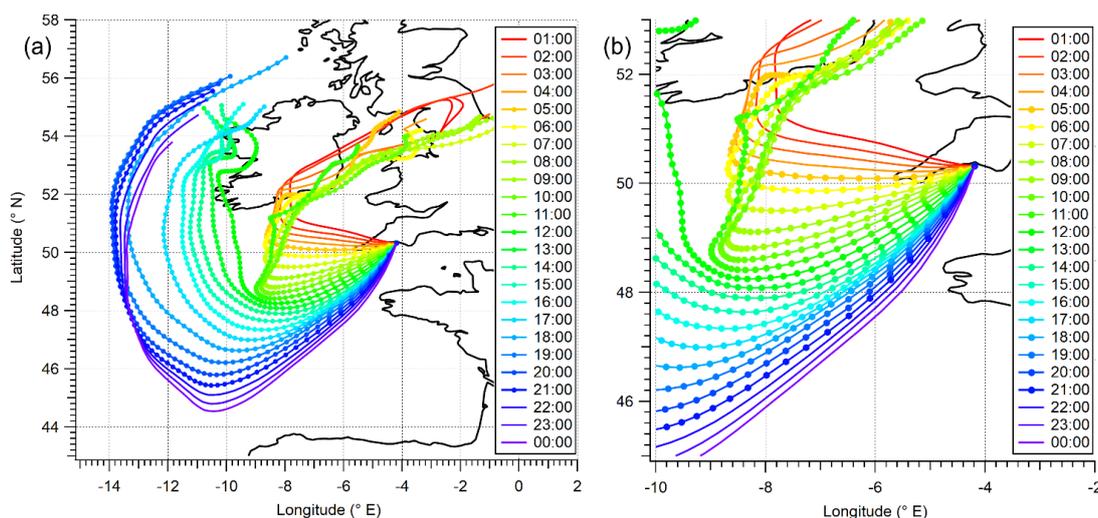
**Figure 12: a) full and b) partial wind trajectories (72 h length) for a day (01/05/18) of near-constant SW winds. Circles represent 1 h travel distances. Lines without circles correspond to periods removed by the quality control filtering for EC fluxes. The legend represents the hour of the day the trajectory arrived at the observatory.**

The mean DMS mixing ratio (0.20±0.09 ppbv, Table 7) is in agreement with shipboard measurements in the eastern North Atlantic Ocean in Jun or Jul (0.16±0.14 and 0.12±0.08 ppbv, with and without a phytoplankton bloom, respectively; Huebert et al., 2010) and the western North Atlantic Ocean in March (~0.13±0.04; Quinn et al., 2019). The mean isoprene mixing ratio (0.18±0.05 ppbv) is higher than observations in autumn from the western North (0.035±0.025 ppbv; Kim et al., 2017) and eastern North (0.0044±0.0083 ppbv; Hackenberg et al., 2017) Atlantic Ocean. The PPAO isoprene mixing ratio is more similar to measurements at the Mace Head Observatory (Carslaw et al., 2000), which further implies some influence from terrestrial land sources at the PPAO site. Note that the TL air–sea isoprene flux is almost purely governed by its seawater concentration where it is grossly supersaturated; the flux is insensitive to the elevated atmospheric mixing ratio.

### 2.3.3. Comparison of EC and TL fluxes and derivation of gas transfer velocities

Here the EC fluxes of acetone, acetaldehyde and DMS from the open-water sector are compared with fluxes computed with the TL model (using concurrent atmospheric mixing ratios from the PPAO and linearly interpolated seawater concentrations from L4). This is to assess two assumptions in the TL flux calculation: (1) that gas transfer velocity parameterisations from deeper water (i.e. the open ocean or shelf seas) apply to this shallower coastal environment, and (2) seawater VOC concentrations in the PPAO flux footprint and at the L4 station are similar.

Acetone and acetaldehyde were both undersaturated in seawater in the open-water sector (Table 7), while DMS and isoprene were both supersaturated. The mean TL fluxes of acetone, acetaldehyde, DMS and isoprene (n=20) are provided in Table 7 with corresponding EC measurements from the open-water wind sector for the last week of the campaign (27/04/18–03/05/18). For this short period with satisfactory VOC blanking, the open-water EC fluxes were fairly large in part because of a 17 % higher mean $U$ compared to the rest of the campaign.

Figure 13 compares the VOC EC and TL fluxes for the open-water sector (not including isoprene), and Figure 14 shows the same data as a time series. Acetone, acetaldehyde and DMS fluxes exhibit reasonable agreement between the EC and TL methods, with both covarying with wind speed. The data points furthest from the 1:1 line in Figure 13 are hourly averages with $\leq 2$ 10 min flux segments, suggesting that the discrepancy is mainly due to random noise in the flux measurement. There was no attempt to calculate TL fluxes for the Plymouth Sound sector due to a lack of concurrent seawater measurements and limited EC measurements for comparison.
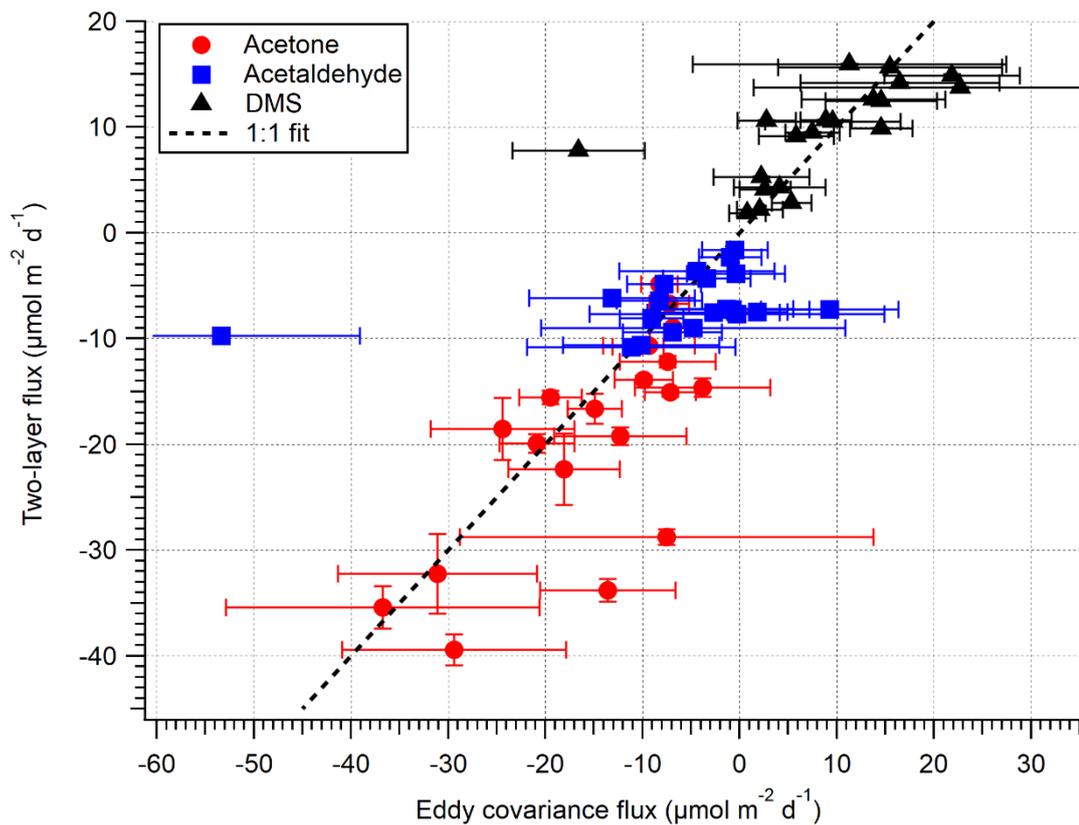


**Figure 13: A comparison between EC and bulk TL fluxes (hourly) for the open-water sector during the dates 27/04/18–03/05/18. The error on EC measurements is $1\sigma_{\bar{x}}$, whilst the error on TL is the propagated error of $1\sigma$ in concentration and solubility.**
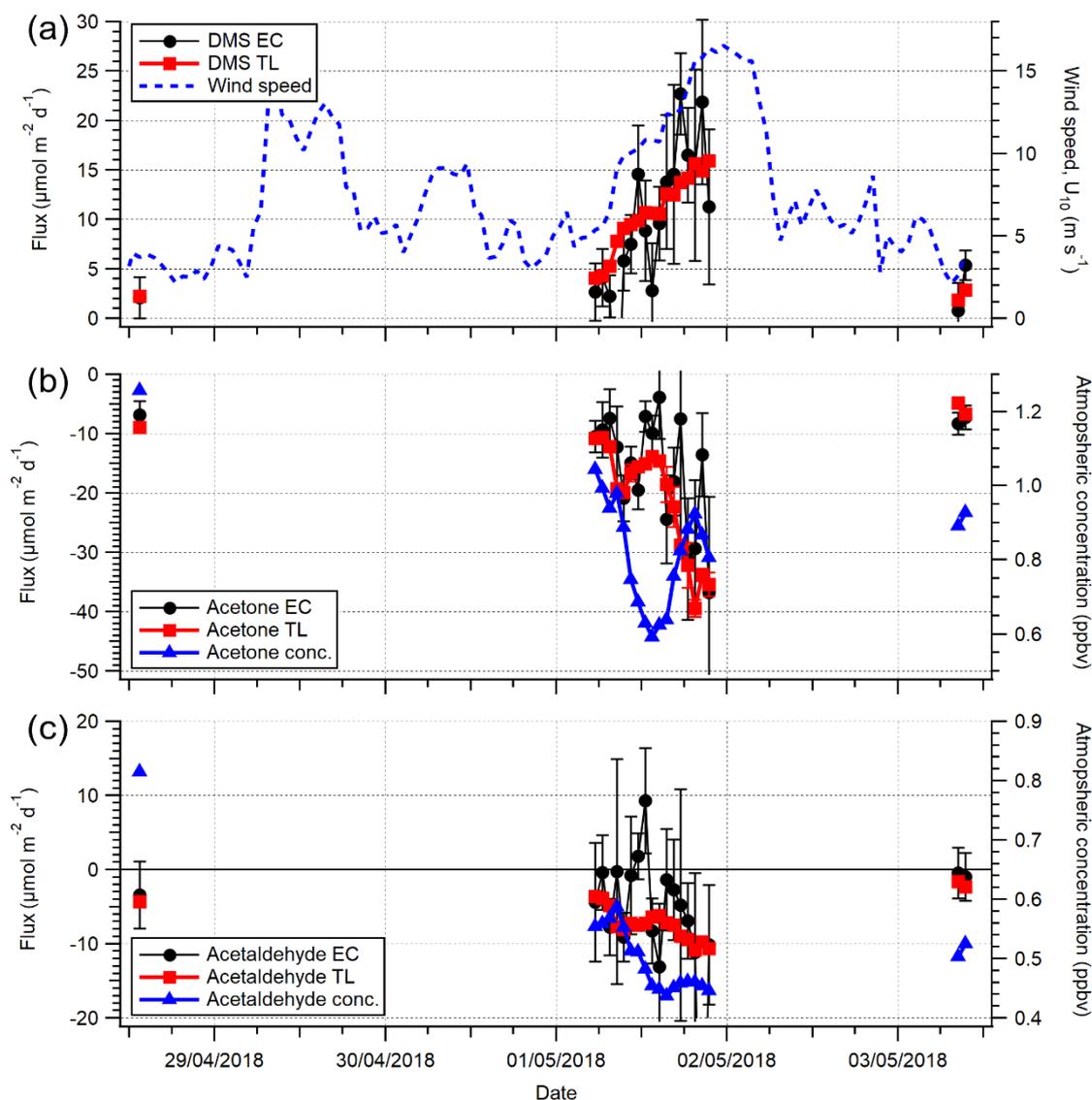
**Figure 14: A comparison between (a) DMS, (b) acetone and (c) acetaldehyde EC and TL fluxes (hourly) for the open-water sector during the dates 27/04/18–03/05/18. Wind speed ($U_{10}$) is provided in (a). The error on EC measurements is $1\sigma_{\bar{x}}$, whilst the error on TL is the propagated error of $1\sigma$ in concentration and solubility.**

To assess the wind speed dependence on gas transfer velocities at the PPAO, $K_a$ is calculated by equating the EC flux (Equation 4) with TL flux (Equation 5b). Figure 15 shows the calculated $K_a$ and $K_w$ ($K_w = HK_a$) values for acetone, acetaldehyde and DMS using 1 h flux data, compared to calculated $K$ from parameterisations of $k_a$ and $k_w$. In the mean, the expected solubility dependence in these VOCs is observed – the measurements show mean $K_a$ of 2121, 1894 and 183 cm h$^{-1}$ for acetone, acetaldehyde and DMS (in order of decreasing solubility), respectively. These translate to $K_w$ values of 2.0, 2.6 and 9.9 cm h$^{-1}$.
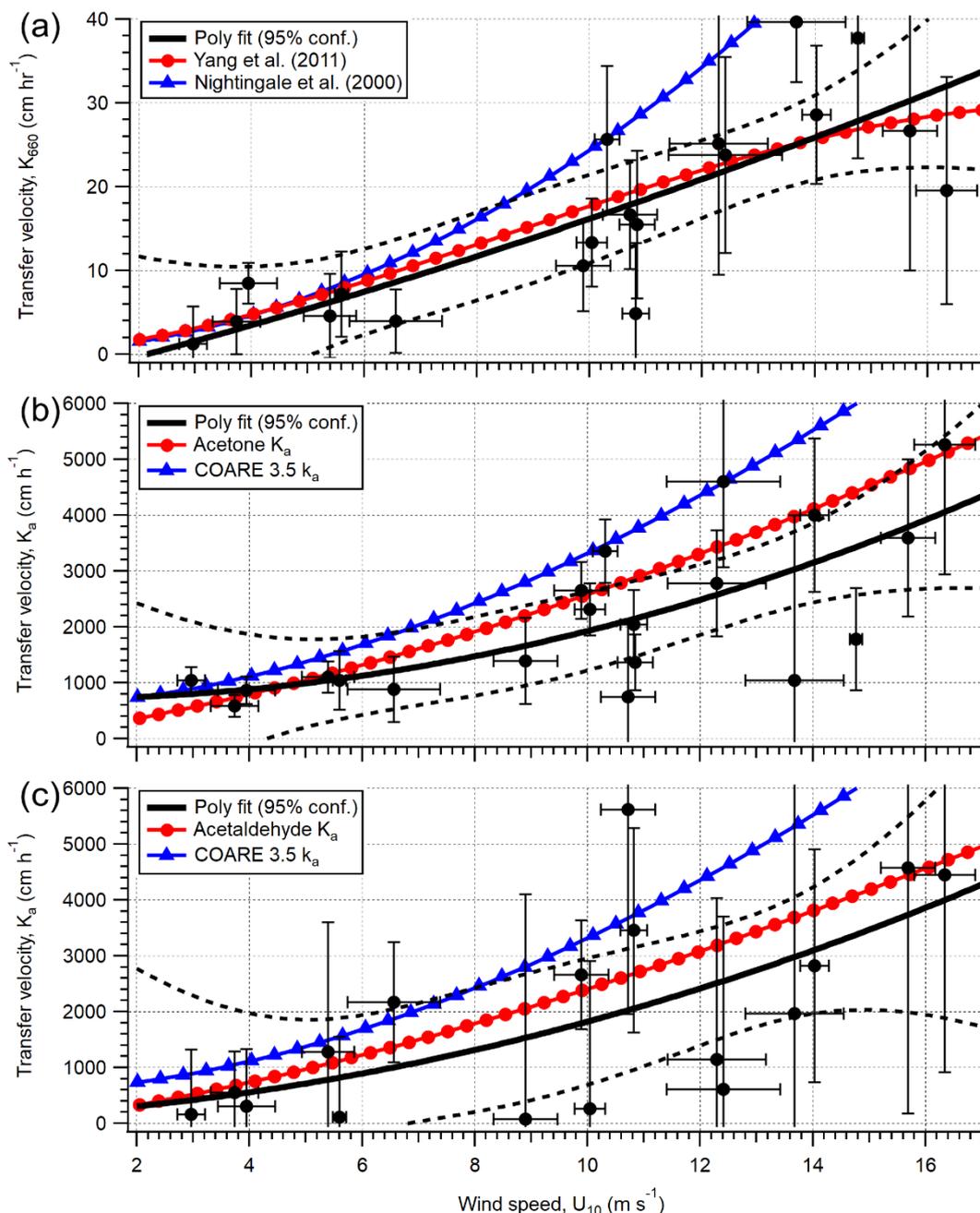
**Figure 15: Calculated transfer velocities (hourly) for (a) DMS ($K_{w,600}$), (b) acetone ($K_a$), and (c) acetaldehyde ($K_a$) in the open-water footprint of the Penlee Point Atmospheric Observatory during the dates 27/04/18–03/05/18. Error bars on the experimental data (black circles) are propagated uncertainty from the eddy covariance measurement. The black poly fit lines are fit to the experimental data, with the dashed black lines representing 95 % confidence in the poly fit. The red circle and blue triangle lines in panel (a) are theoretical transfer velocities using the $k_w$ parameterisations of Yang et al. (2011a) and Nightingale et al. (2000) respectively. The red circle lines in panels (b)–(c) are theoretical transfer velocities calculated from the $k_w$ parameterisation of Yang et al. (2011a) and $k_a$ from the COAREG 3.5 model (shown as blue triangles).**

For DMS, to facilitate comparison with previous measurements, the derived $K_w$ is adjusted to a standard $S_{C_w}$ of 660;

$$K_{660} = K_w \left(\frac{660}{S_{Cw}}\right)^{-0.5} \qquad\qquad 19$$

The mean $K_{660}$ for DMS (16.7±2.7 cm h⁻¹) is in good agreement when compared to published measurements (~17 cm h⁻¹; Blomquist et al., 2006; Yang et al., 2011a; Bell et al., 2013) at similar

wind speed in the North Atlantic Ocean. Data from this short campaign suggest that the mean wind speed dependence in DMS transfer velocity at the PPAO (open-water sector, depth of ~20 m) is largely comparable to deeper water, in agreement with previous $CO_2$ gas exchange measurements at this site (Yang et al., 2019a). The measured acetone and acetaldehyde $K_a$ are also of the expected magnitudes. Processes important for shallow estuaries, such as bottom-driven turbulence and tidal current, do not appear to be the main controlling factors in gas exchange in this environment.

There is a large amount of scatter in Figure 15, especially for acetone and acetaldehyde. This is likely in part due to the poor temporal resolution (weekly) in seawater concentration measurements that do not capture any rapid changes in this dynamic region (e.g. changes in riverine outflow, biological bloom). The DMS transfer velocity measurements imply that the outflow of the estuary Tamar does not substantially dilute the seawater DMS concentration within the open-water flux footprint compared to L4, while spatial gradients in the carbonyl concentrations could be more significant relative to their air–sea concentration differences. Higher resolution measurements within the flux footprints in the future are needed to better constrain the influence of riverine outflow.

If the concentrations between the flux footprint and L4 are assumed to be identical and the interpolation does not induce any error (likely a good match considering the close similarity between L4-concentration derived TL fluxes and PPAO EC fluxes of DMS), the lower deposition EC fluxes of acetone and acetaldehyde compared to those predicted by the TL model may be driven by wind-speed-dependent contributions to the flux at the air–sea interface (2.5±1.3 and 2.6±1.6 µmol m$^{-2}$ d$^{-1}$ respectively (±SE, n=14), estimated as the difference). An example source would be the heterogeneous production of carbonyl compounds (Zhou et al., 2014) that increased with wind speed because of subsequent changes in the $O_3$ deposition flux (e.g. Loades et al., 2020). This source is discussed in more detail in Chapter 3 (see Section 3.3.3.4 for resolving data here).

As mentioned in Section 2.2.4, I used a revised acetone solubility from Wohl et al. (2020). Focusing on the last week of the campaign (Table 7), a mean TL acetone flux of -19.0±2.2 and -21.5±2.5 µmol m$^{-2}$ d$^{-1}$ (±$\sigma$, propagated error in concentration only) is calculated with and without the solubility revision. The flux with revised solubility is in better agreement with the EC measurement (-14.9±2.1 µmol m$^{-2}$ d$^{-1}$).

### 2.3.4.  Comparison to other flux estimates

The acetone fluxes presented here are in good agreement with previous EC measurements (-7.0±2.2 µmol m$^{-2}$ d$^{-1}$) from 50° N on the 22$^{nd}$ Atlantic Meridional Transect (AMT-22) research cruise in Autumn 2012 (Yang et al., 2014b). However, the acetaldehyde flux here shows an opposite mean direction to their 50° N average (1.8±1.3 µmol m$^{-2}$ d$^{-1}$). Acetone and acetaldehyde bulk fluxes from 50° N during AMT-19 in 2009, estimated using CAM–Chem modelled atmospheric concentrations, were -5.7±1.1 and -2.4±0.7 µmol m$^{-2}$ d$^{-1}$ respectively (Beale et al.,

2013). The PPAO fluxes are in reasonable agreement with these earlier indirect estimates. Further acetone and acetaldehyde bulk fluxes estimated from a time series of L4 water measurements and static atmospheric mixing ratios (0.66 and 0.40 ppbv respectively) were -7.4±1.4 and 1.4±1.0 µmol m$^{-2}$ d$^{-1}$, respectively, for spring 2011 and -6.4±0.1 and -1.5±0.1 µmol m$^{-2}$ d$^{-1}$, respectively, as annual averages. The spring acetone fluxes of Beale et al. (2015) are in good agreement with the PPAO direct measurements, however, their acetaldehyde flux was in the opposite direction. Importantly, Beale et al. (2015) identified that the L4 water saturation of acetaldehyde was highly sensitive to the atmospheric mixing ratio (changing it between 0.1–0.4 ppbv was enough to switch the direction of flux). Thus variability and uncertainty in the atmospheric acetaldehyde mixing ratio are probably among the main causes of the discrepancies in these air–sea flux estimates (Yang et al. (2014b), Beale et al. (2013, 2015), and PPAO measurements presented here).

The PPAO DMS flux is in agreement with previous EC DMS flux observations from the eastern North Atlantic Ocean during the summer of 2007 (2.6±0.2 and 4.4±0.4 µmol m$^{-2}$ d$^{-1}$ with and without a short, intense phytoplankton bloom; Huebert et al., 2010). The campaign ended before the spring phytoplankton bloom started at L4 (Archer et al., 2009), which typically starts in May or June. Yang et al. (2016c) estimated bulk DMS fluxes of ~3 and ~10 µmol m$^{-2}$ d$^{-1}$ in the winter and summer, respectively, using the L4 annual seawater DMS concentration time series (Archer et al., 2009). The DMS flux measurement at the PPAO is also in reasonable agreement with previous observations in the North Atlantic Ocean without the phytoplankton bloom (5.58±0.15 µmol m$^{-2}$ d$^{-1}$; Bell et al., 2013).

Although isoprene EC fluxes were unresolvable, the estimated open-water TL flux was similar to NECS April estimates of ~0.8 µmol m$^{-2}$ d$^{-1}$ (Palmer and Shaw, 2005) and ~1.0 µmol m$^{-2}$ d$^{-1}$ (Booge et al., 2016, supplement) using MODIS satellite observations of chlorophyll *a* for production models. A mean direct flux (0.7 µmol m$^{-2}$ d$^{-1}$) was observed in the northern Atlantic Ocean (Kim et al., 2017); they estimated seawater concentrations (~0.02 nM) that were ~78 % lower than measured here but also experienced much higher wind speed. Importantly, discrepancies between top-down and bottom-up isoprene budget analyses show the ocean fluxes necessary to explain remote MBL concentrations of isoprene are an order of a magnitude higher than predicted from seawater concentrations alone (Arnold et al., 2009; Booge et al., 2016). Future simultaneous comparisons between EC and TL isoprene fluxes might observe this difference.

The direct VOC fluxes are also compared to global model predictions at this location. Typical global models and climatologies operate with a 1° latitudinal and longitudinal resolution (e.g. Wang et al., 2019, 2020a, 2020b). At the PPAO this equates to a grid size of ~110 km N–S and ~85 km E–W, which is much coarser compared to the flux footprint areas (on the order of a few square kilometres). Nevertheless, this comparison allows us to qualitatively assess the spatial representativeness of the PPAO fluxes and identify potential shortcomings in the models.

The GEOS-Chem and CAM-Chem models predict a mean annual acetone flux in the eastern North Atlantic Ocean coastal shelves (NECS; biogeochemical province that includes the PPAO

coastal site) of ~-2.5 µmol m$^{-2}$ d$^{-1}$ (Fischer et al., 2012) and Mar–May flux of ~-2.9 µmol m$^{-2}$ d$^{-1}$ (Wang et al., 2020a), respectively. These two predictions are much lower than those measured in the PPAO open-water sector (-8.01±0.77 µmol m$^{-2}$ d$^{-1}$, Table 6) because the models predict a smaller air–sea concentration difference. Fischer et al. (2012) and Wang et al. (2020a) used water concentrations of 15 (static) and ~8 nM respectively (182 % and ~50 % higher than L4 concentrations) and a modelled atmospheric mixing ratio of ~0.45 ppbv (~45 % lower than the PPAO concentration). Seawater acetone has a highly variable lifetime (Beale et al., 2013; de Bruyn et al., 2013; Dixon et al., 2013) so the higher estimated seawater concentration in the Wang et al. (2020a) model may be because of a slower removal rate. Here an atmospheric acetone mixing ratio that is higher than in the model was measured likely because the measurement, even from the open-water sector, has some terrestrial influence (e.g. via the diurnal sea-breeze effect or advection of air masses previously in contact with land).

The small negative acetaldehyde fluxes measured at the PPAO imply a weak ocean sink (mean of -1.55±1.14 µmol m$^{-2}$ d$^{-1}$, Table 6), which does not agree with the global model results. The NECS acetaldehyde flux is ~0.22 µmol m$^{-2}$ d$^{-1}$ in GEOS–Chem (Millet et al., 2010) and ~1.4 µmol m$^{-2}$ d$^{-1}$ in CAM–Chem (Wang et al., 2019) in the Mar–May period. The seawater concentrations used by Wang et al. (2019) (~11 nM) are higher than L4 measurements for the same period (54 % higher than L4 conc.). In the models, the short marine lifetime of acetaldehyde (de Bruyn et al., 2013, 2017; Dixon et al., 2013) is coupled with an estimate of its production rate to predict the seawater concentration. Wang et al. (2019) use a constant lifetime of 0.3 d for the global ocean, whereas previous measurements at L4 suggest a much shorter acetaldehyde lifetime (0.01–0.13 d; Beale et al., 2015). de Bruyn et al. (2017) showed shorter seawater acetaldehyde lifetimes at another coastal location directly after rainfall or during the wet season. It is possible that the shorter lifetime at L4/PPAO, and hence lower seawater acetaldehyde concentration, may be related to riverine input. The atmospheric acetaldehyde mixing ratios from the models are also lower than the coastal observations presented here, similar to acetone as discussed above.

From the perspective of climatology and global modelling, the NECS was predicted to have an April DMS flux of ~14 µmol m$^{-2}$ d$^{-1}$ (Lana et al., 2011) and ~6 µmol m$^{-2}$ d$^{-1}$ (Wang et al., 2020b). The estimate of Lana et al. (2011) is ~3 times higher than the PPAO measurements; however, that of Wang et al. (2020b) is in good agreement. Waterside concentrations of ~7 and ~3 nM were predicted (52 % higher and 43 % lower than the L4 concentration) by Lana et al. (2011) and Wang et al. (2020b) respectively. The high concentrations in the Lana et al. (2011) climatology likely correspond to phytoplankton blooms in the Apr–May period, which did not occur at the time of measurements here or appear as intensely in the estimations of Wang et al. (2020b). This could be partly related to the interannual variability in plankton dynamics and hence seawater DMS cycling.

All the models and climatologies discussed here (except for Wang et al. (2020b)) used the Nightingale et al. (2000) $k_w$ parameterisation, which leads to ~26, ~14 and ~26 % higher $k_w$

values for acetone, acetaldehyde and DMS, respectively, than those of Yang et al. (2011a) over this campaign because of the solubility dependence in bubble-mediated gas exchange (Yang et al., 2011a; Bell et al., 2017). Substituting the Nightingale et al. (2000) $k_w$ parameterisation with the Yang et al. (2011a) $k_w$ would generally reduce the flux magnitude in these models, estimated as ~5, ~6 and ~19 % for acetone, acetaldehyde and DMS, respectively ($k_a$ unchanged and from COAREG 3.5).

### 2.3.5.  Significance of fluxes

The measured open-water acetone and acetaldehyde air–sea fluxes exhibit stronger deposition flux than estimated by global modelling. Here the lifetimes of these gases within the atmospheric MBL are evaluated. The MBL lifetimes ($\tau_x$) are calculated similarly to a 0D model;

$$\tau = \frac{C_a}{C_a + \frac{D_F}{h}}$$

20

where $C_a$ represents concentration (here, the mean of the PPAO observations; Table 7), $L_x$ represents chemical loss, $D_F$ represents the net deposition flux (here, the mean of the PPAO EC observations; Table 6) and $h$ represents MBL height. The assumptions are the VOCs are homogeneously mixed within the MBL upwind of the PPAO, $h$ is 500 m and $L_x$ is $2.7\times10^{-7}$ s$^{-1}$ for acetone and $2.1\times10^{-5}$ s$^{-1}$ for acetaldehyde. $L_x$ is calculated from literature OH reaction rates ($1.7\times10^{-13}$ and $1.5\times10^{-11}$ cm$^3$ molec.$^{-1}$ s$^{-1}$, respectively; Atkinson and Arey, 2003), April surface 50° N zonal average OH concentration (~$10^6$ molec. cm$^{-3}$; Horowitz et al., 2003) and summer surface photolysis rates for acetone (~$10^{-7}$ s$^{-1}$; Blitz et al., 2004) and acetaldehyde (~$5.5\times10^{-6}$ s$^{-1}$; Warneck and Moortgat, 2012).

From this simple model and the values described above, the MBL lifetimes of acetone and acetaldehyde are calculated to be 2.0 and 0.5 d respectively. The deposition to the ocean above accounts for 95 and 8 % of all losses for MBL acetone and acetaldehyde respectively, which highlights the importance of acetone air–sea exchange. The calculated PPAO open-water acetone lifetime is much shorter than the 11–18 d estimates for the mean troposphere (Marandino et al., 2005; Fischer et al., 2012; Khan et al., 2015; Wang et al., 2020a), where surface deposition is less substantial (16–56 %; Jacob et al., 2002; Fischer et al., 2012). The acetaldehyde lifetime is in good agreement with literature values (0.1–0.8 d; Millet et al., 2010; Wang et al., 2019) because photochemistry is the main loss mechanism for MBL acetaldehyde rather than deposition, and the April surface 50° N zonal average OH concentration is similar to the tropospheric mean ($1.1\times10^6$ molec. cm$^{-3}$; Li et al., 2018).

The noticeable increase in acetone and acetaldehyde deposition fluxes within the Plymouth Sound compared to the open-water sector suggests that deposition can represent a large loss term for atmospheric VOCs in the coastal atmosphere. Importantly, enhanced coastal deposition fluxes of acetone and acetaldehyde are not well captured in global models. The boundary layer lifetimes during periods of offshore winds are calculated using the same approach as before, resulting in 1.7 d for acetone and 0.5 d for acetaldehyde. Here deposition to the ocean accounts for 96 and 17

% of losses, respectively. The estimated lifetimes in the Plymouth Sound sector are similar to the open ocean even though the deposition fluxes were stronger because the increased deposition fluxes correspond to a greater atmospheric burden. As air masses from the Plymouth Sound (or further inland to the NE) are advected offshore over the coastal seas, the mixing ratios of carbonyls tend to decrease due to a combination of deposition to the sea, chemical losses and mixing with marine air. If additional x–y dimensional constraints are added to the Plymouth Sound 0D box (e.g. 4 km N–S, 1 km E–W), dilution becomes an important loss term.

## 2.4. Conclusion

This chapter presents measurements of air–sea fluxes of acetone, acetaldehyde and DMS at the coastal PPAO in the SW UK. A PTR-quadrupole-MS (2.2 Hz) was used to simultaneously resolve the fluxes of these gases with the eddy covariance method. Comparisons between the open-water sector and a terrestrially influenced sector show stronger deposition fluxes of acetone and acetaldehyde from the latter because of higher atmospheric carbonyl concentrations from that wind direction. Emission fluxes of DMS from the terrestrially influenced sector are weaker than from the open-water sector, likely because of lower wind speed and lower seawater concentrations due to estuarine influence/dilution.

Bulk fluxes computed from seawater and atmospheric concentrations using the TL approach agree reasonably well with the EC measurements of open-water acetone, acetaldehyde and DMS fluxes. The derived air–sea transfer velocities of acetone, acetaldehyde and DMS are largely consistent with previous estimates over the open ocean in the mean. Along with previous measurements of air–sea $CO_2$ exchange, these data suggest that wind speed, rather than processes such as bottom-driven turbulence, is the dominant control for gas exchange at this site for the open-water sector (depth of ~20 m).

While the DMS flux at PPAO was in reasonable agreement with recent climatological estimates, the measured open-water acetone fluxes show stronger deposition compared to climatological and model estimates for the NE Atlantic Ocean coastal shelf. This is likely because the models/climatologies do not fully capture the spatial and temporal variability in the distribution of atmospheric and seawater acetone concentrations. The PPAO acetaldehyde flux (net sink in the mean) is in the opposite direction to global models that suggest the Northern Hemisphere oceans to be a net acetaldehyde source. This is mostly because models predict higher seawater acetaldehyde concentrations and lower atmospheric acetaldehyde mixing ratios at this coastal location.

Future experiments at PPAO should strive to increase the temporal and spatial resolutions of the $C_w$ observations in order to better match up with the EC fluxes. The accuracies in the air/water concentration measurements can be further improved by using blanks that have the same $CO_2$ and humidity levels as the samples, especially for acetaldehyde. The use of a higher resolution PTR-time-of-flight-MS at ≥10 Hz would improve the precision of the flux measurement and reduce the magnitude of the high-frequency flux loss. Simultaneous methanol fluxes would enable the

derivation of $k_a$ and benefit the lag correlation calculation (methanol flux is typically large; see Yang et al. (2014a)). Important future work would involve measuring EC fluxes, $C_w$ and $C_a$ at high resolution from the anthropogenically/terrestrially dominated coast through to the continental shelf edge and open ocean on a ship in order to develop our understanding of the impact of coastal seas biogeochemistry on local atmospheric chemistry and air quality. Such transect measurements would help to further constrain global models for improved estimations at the coast and ideally determine whether the reversed direction acetaldehyde fluxes (compared to open ocean fluxes) are a typical finding.

# Chapter 3 – The heterogeneous production of VOC from the ozonolysis of surface ocean DOM

## 3.1. Introduction

Large uncertainty exists in the role the ocean plays as a net source or sink for atmospheric VOCs partly because of poorly quantified processes near the air–sea interface. This includes a very limited understanding of some VOC production mechanisms in and around the ocean interface, as introduced/identified in Chapters 1 and 2, and also because only a relatively small number of environmental measurements exist over remote marine areas.

An introduction to acetone, acetaldehyde and isoprene chemistry, including their atmospheric importance, can be found in Chapter 1 or briefly in Section 2.1. Importantly for this chapter, the discrepancy in the top-down and bottom-up budgets of some VOCs (Section 1.2.3) may be lowered/eliminated with the incorporation of heterogeneous processes at the air–sea interface. Zhou et al. (2014) showed the production of PTR-MS masses $m/z$ 45 and 59, which were allocated to acetaldehyde and acetone/propanal respectively, from the ozonolysis of coastal and oceanic SML samples. Additional masses were observed in the coastal SML only: for example $m/z$ 69 which is likely isoprene. Their experiment involved gently passing 300 ppbv $O_3$ over a small open sample boat (10 mL volume, 40 cm$^2$ area) filled with stored natural SML water or a linoleic acid monolayer on seawater, which showed that VOCs can be produced from a stagnant surface uptake of $O_3$ and subsequently diffuse into the gas phase. Schneider et al. (2019) further showed the reactions are interfacial and not gas phase reactions.

In this chapter, ozonolysis experiments using fresh seawater are undertaken to quantify production yields of acetone, acetaldehyde and isoprene. An efficient and turbulent bubble column is used to achieve a high production signal. Various types of water are investigated: (1) natural seawater from the L4 marine station in the south-west UK, (2) aged seawater spiked with *Emiliania huxleyi* (*E. huxleyi*) algal culture, (3) aged seawater spiked with fatty acids, (4) aged seawater spiked with natural organic matter (NOM), and (5) natural water spiked with I$^-$. A seasonal comparison is made between natural seawater sampled in Feb-May (pre/during spring algal bloom), Jun–Oct (summer bloom) and Sep–Nov. I attempt to scale the production yield of the VOC to the global ocean and then discuss the importance of these $O_3$ driven fluxes for the atmospheric budgets of VOCs. The seasonality in the VOC productions from natural seawater and the precursor addition experiments are used to show the likely origin of the precursor organics for VOC production.

**Disclaimer**

This chapter includes some results from a University of Plymouth MRes Applied Marine Science dissertation; Chen, Y.: Quantifying the Productions of Volatile Organic Compounds from Surface Reactions between Ozone and Seawater, University of Plymouth, Plymouth., 2017. The results I used are the 2017 production time series and the fatty acid, algal culture, NOM and $O_3$ concentration experiments; these results are clearly referenced in the text. In all cases, I reanalysed these experiments using the method described below to enable additional conclusions, including the global scaling first discussed in this thesis. I furthermore account for the fragmentation of isoprene in the PTR-MS, which was not considered by Chen (2017).

### 3.2. Method

### 3.2.1. Experimental set-up

Experiments were carried out using a custom-built 1.45 L cylindrical borosilicate glass column fitted with a gas sparger made from a fine glass frit (Figure 16). A ~200 mL volume below the sparger was fitted with a gas inlet and stopcock. With the stopcock closed, 1.2 L of the sample was siphoned into the column above the sparger, using silicone tubing to limit bubble formation. 250 mL of headspace remained in the column above the sample, which also contained the gas outlet. The column was rinsed three times with ~5 % hydrochloric acid (HCl; Acros Organics 37 % fuming HCl) and then three times with Milli-Q water (18.2 MΩ; MilliPor Milli-Q Direct (Type 1)) before each filling.
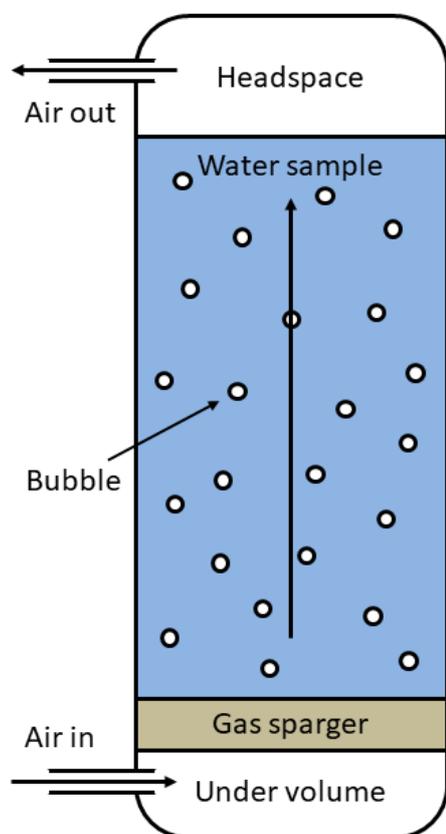


**Figure 16: Design of the bubble column. Dimensions: external height = ~30 cm, internal sample height = ~23 cm, internal diameter = ~9 cm, under volume height = ~3 cm.**

Compressed artificial air (BOC BTCA 178) was used as the main carrier gas and was scrubbed of organics using a custom-built Pt catalyst heated to ~450 °C. The efficiency of the catalyst was shown to be complete oxidation for VOC with orders of magnitude higher concentration than in the artificial air (Yang and Fleming, 2019). A flowrate of 150 nmL min$^{-1}$ (at 1 atm, 0° C) was established using mass flow controllers (MFC; Bronkhurst EL-FLOW Select series); this corresponds to a volumetric flow of ~165 mL min$^{-1}$ at room temperature. Opening the stopcock allowed gas in the stream to pass through the sparger and form a dense turbulent plume of bubbles (~0.5 mm diameter each, ~3 mL total volume) that rose through the sample. Bubble residence time in the water phase was ~1.2 s. The bubble exchange interface area ($A$) was estimated to be 360 cm$^2$, using; $A = 3V/r$, where $V$ represents the total bubble displacement volume and $r$ represents the radius of a single bubble. $V$ was measured by observing the volume displacement with and without the gas flow, while $r$ was roughly estimated using photographs of the column bubbles with a ruler as a reference. Importantly, in my calculation of the VOC production ratio, the bubble interface area is cancelled out and thus does not affect the VOC production estimate (see Section 3.2.4.2). The estimated bubble diameter of 0.5 mm is of the same order of magnitude as the dominant diameter of bubbles generated in wave breaking and is much smaller than the maximum size (Loewen et al., 1995).

O$_3$ was generated from the artificial air using a corona discharge (Enaly 1000BT-12 O$_3$ generator) and variably mixed into the gas stream to achieve concentrations between 1–15 ppmv (rarely above 3 ppmv). While the O$_3$ concentrations used were high compared to ambient MBL concentrations (×25–150 higher), the response was experimentally shown to be linear by regression below ~4 ppmv (see Section 3.3.1.1). Gas-phase O$_3$ concentration in the column headspace was measured with a dual-channel (simultaneous blank correction) instrument (2B-Technologies model 205 O$_3$ monitor) which provided a good temporal resolution. The inlet flow rate of the model 205 O$_3$ monitor was ~2 L min$^{-1}$. To make up the remaining flow required, an O$_3$ scrubber vented to laboratory air was connected to the bubble column outflow via a tee. The dilution factor for the O$_3$ monitor is approximately 93–98 %, which is in part why the input O$_3$ concentration needed to be high. The total O$_3$ monitor and scrubbed dilution air flows were measured using a digital bubble meter (Gilian Gilibrator-2). The O$_3$ generator and monitor were powered up for 1–2 h before experiments with artificial air flowing through to allow the equipment to stabilise. All tubing and unions between the O$_3$ generator and O$_3$ monitor were made from 3.2 mm ID PFA pieces, apart from the three-way valves and MFC which were made from stainless steel.

Gas-phase VOC concentrations in the column headspace were quantified using the same PTR-MS technique as Chapter 2. All tubing and unions between the column headspace and PTR-MS were made from 3.2 mm ID PFA. During measurements, the PTR-MS was set mainly to monitor methanol (*m/z* 33), acetaldehyde (*m/z* 45), acetone (*m/z* 59), DMS (*m/z* 63) and isoprene (*m/z* 69). Masses were added/removed each campaign to aid specific analyses and these details can be

found in Table 8. Mass data, literature ion ratios and dwell times can be found in Table 9. Two additional masses for isoprene were added (*m/z* 39 and 41) due to expected fragmentation (Schwarz et al., 2009). Overall, the temporal resolution of the measurement was 3.1–7.7 s (0.13–0.27 Hz). Internally corrected PTR-MS mixing ratio (ppbv) data were used for calculation. The PTR-MS method parameters used to achieve optimal signal-to-noise ratios can be found in Table 10.

**Table 8: Measurement frequencies and temporal resolutions in each experimental campaign.**

| Campaign | Frequency (Hz) | Time (s) | Notes |
|---|---|---|---|
| 2017 | 0.13 | 7.7 | Added *m/z* 21, 32, 33, 39, 42, 42, 43, 45, 47, 59, 60, 61, 63, 69, 71, 79, 93, 107, 137 |
| 2018 beginning | 0.32 | 3.1 | Removed *m/z* 39, 42, 43, 47, 60, 61, 71, 79, 93, 107, 137<br>Added *m/z* 37 |
| 2018 end | 0.27 | 3.7 | Added *m/z* 39 with increased dwell time<br>Increased *m/z* 32 and 37 dwell times |
| 2020 beginning | 0.16 | 6.2 | Added *m/z* 43, 47, 57, 61, 73 |
| 2020 end | 0.14 | 7.2 | Added *m/z* 55, 87 |

**Table 9: Chosen compounds with their dwell times for the PTR-MS quadrupole method. Literature sources are (a) Warneke et al. (2003), and (b) Schwarz et al. (2009).**

| Mass-charge ratio | Expected compound/s | Literature ion ratio (%) | Structural formula | Dwell time (ms) |
|---|---|---|---|---|
| 21 | Hydronium | - | $H_3^{18}O^+$ | 50 |
| 32 | Oxygen | - | $O_2^+$ | 20–50 |
| 33 | Methanol | 100[b] | $CH_3OH_2^+$ | 500 |
| 37 | Water dimer | - | $H_2O.H_3O^+$ | 20–50 |
| 39 | Isoprene (fragment) | 10[b] | $CH_2CCH^+$ | 50–500 |
|  | Isotopic water dimer | - | $H_2^{18}O.H_3O^+ / H_2O.H_3^{18}O^+$ |  |
|  | Pentanal (fragment) | 2[b] |  |  |
| 41 | Isoprene (fragment) | 39[b] | $CH_2CCH_3^+$ | 500 |
|  | Propanal (fragment) | 4[b] |  |  |
|  | Pentanal (fragment) | 23[b] |  |  |
| 43 | Propene | - | $CH_2CH_2CH_3$ | 500 |
|  | Acetone (fragment) | 10[a] |  |  |
| 45 | Acetaldehyde | 100[b] | $CH_3COOH_2^+$ | 500 |
|  | Pentanal | 2[b] |  |  |
| 47 | Formic acid | - | $HCOHOH$ | 500 |
| 55 | Butanal (fragment) | 57[a], 90[b] | $CH_2CH_2CHCH_2$ | |
|  | Butadiene | - |  |  |
| 57 | Butene | 100[a] | $CH_2CH_2CH_2CH_3$ | 500 |
| 59 | Acetone | 90[a], 98[b] | $CH_3COHCH_3^+$ | 500 |
|  | Propanal | 100[a], 89[b] | $CH_3CH_2CH_2O^+$ |  |
| 61 | Acetic acid | - | $CH_3COHOH$ | 500 |
| 63 | DMS | 100[a] | $CH_3SHCH_3^+$ | 500 |
| 69 | Isoprene | 100[a], 46[b] | $CH_2C(CH_3)CHCH_3^+$ | 500 |
|  | Pentanal (fragment) | 78[a], 68[b] |  |  |
| 73 | Butanal | 43[a], 7[b] | $CH_3CH_2CH_2COH_2$ | 500 |
|  | Butanone | - | $CH_3CH_2COHCH_3$ |  |
| 87 | Pentanal | 87[a], 5[b], | $CH_3CH_2CH_2CH_2COH_2$ | 500 |
|  | Pentanone | 100[a] | $CH_3CH_2CH_2COHCH_3$ |  |

**Table 10: PTR-MS method used for measurements.**

| Parameter | Value |
|---|---|
| Drift chamber pressure (mBar) | 2.21 |
| Drift chamber voltage (true) (V) | 690 |
| Drift chamber temperature (°C) | 80 |
| $H_2O$ mass flow controller (mL min$^{-1}$) | 5 |
| Inlet flow rate (mL min$^{-1}$) | 80–120 |
| Inlet temperature (°C) | 80 |

The experiments progressed by cycling/repeating four stages. Stage one and stage two involved bypassing the column to get an $O_3$ input measurement and dry VOC blanks, respectively.

Bypassing was controlled with manual three-way valves. Stage three involved passing artificial air through the water sample. This resulted in the transfer of some dissolved VOCs from the water phase into the gas phase and also flushed out the column headspace, and eventually resulted in sample gas that was in approximate steady-state with the seawater sample. Out of all the VOCs monitored, only isoprene shows a noticeable decrease in concentration during this stage due to its low solubility and thus ease of purging out of the water phase. Stage four involved adding $O_3$ to the carrier gas stream to achieve sample oxidation. Typically, two Milli-Q water samples were run to check for column cleanliness and also provide a humid VOC blank, followed by triplicate seawater samples. $O_3$ and VOC were measured continuously throughout all four stages. An experimental schematic is provided (Figure 17).
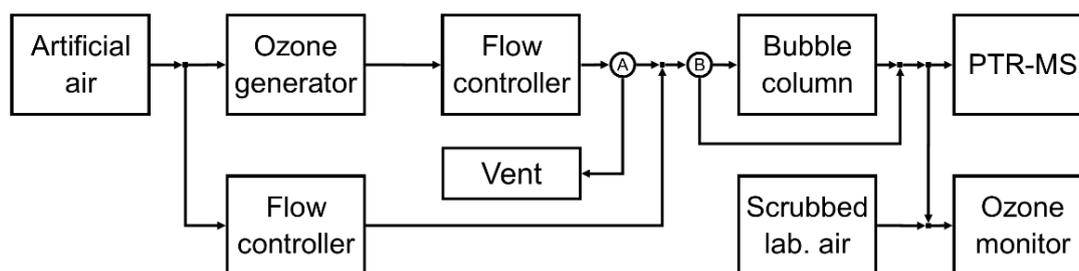


**Figure 17: Schematic for the laboratory setup used in the VOC production experiments. Arrows represent flow and A and B represent three-way valves.**

### 3.2.2. Sampling of natural water

Surface seawater was routinely sampled from the L4 marine station of the WCO, using the rosette sampler of the RV *Plymouth Quest* at a mean depth of 1.8±0.3 m (min=0.9 m, max=2.3 m). This usually occurred between 8–10 am local time. Sample seawater was transferred following a gas-sensitive method to gas-tight glass bottles, which were acid-washed with ~5 % HCl; each bottle was rinsed three times with sample and then filled from bottom to top using Tygon tubing before being overflowed to minimise bubbles or gas loss. The samples were stored in a dark cool box during transit and whilst at the laboratory. Samples were analysed as soon as possible to minimize the consumption/change of DOM (59 % were run within 3 h, 94% within 24 h).

Three seasonal measurement campaigns were undertaken for comparison of VOC production. The first campaign was conducted in the spring (14/02/17–03/05/17) and included a portion of the spring algal bloom. The second campaign was conducted in the autumn (04/09/18–05/11/18) after the summer biological activity. The third campaign (15/06/20–12/10/20) attempted to bridge the gap between the first two (however started late because of the COVID-19 pandemic) and occurred during intense summer biological activity through to autumn. Officially the autumnal equinox occurs between the 22nd–24th September, thus the first two 2018 measurements and the last 2020 measurement occur across two defined (i.e. 'summer' and 'autumn') campaign seasons. Four periods are therefore considered, the spring pre-bloom period, the spring bloom period, the summer period and the autumn period. Later in the analysis of the summer data, it became evident

that the data could be split to reduce seasonal variability, thus later (Section 3.3.1.3+) the summer will be discussed as early summer and late summer.

### 3.2.3.  Reactant addition experiments

Besides using natural seawater, some reactant addition experiments were also performed. Using the bubble column, select reagents were added to aged seawater (left in the dark in a gas-tight glass bottle for ~1 month at 20 °C) to determine oxidation products and identify potential structural characteristics for VOC production. Added reagents included a phytoplankton culture, NOM, fatty acids and I⁻. Aged seawater was used over Milli-Q water, as the lack of salinity in the latter would affect the bubble size distribution and potentially the rate of reaction if the surface area was significantly different (Scott, 1975); the effect of salt on bubble distributions is thought to be probably due to the stabilisation of the thin liquid films formed between approaching bubbles.

For the phytoplankton addition, a culture of *E. huxleyi* Rutgers 607 was grown on-site to senescence (mature, with possible cell lysis) and added directly to the column by removing the column cap and pipetting the culture (5–20 mL) into the water sample surface. Dilutions were made such that the final cell concentrations were within the range of ambient seawater (assuming no algal cells in the aged seawater used for dilution). NOM was sourced from the International Humic Substances Society (Suwannee River), dissolved in 10 mL of aged seawater and poured into the column (0–10 mg L⁻¹ column concentration). Two fatty acids (oleic acid and nonanoic acid) were injected directly into the water surface (0–400 µL) via the sidearm on the glass column.

Potassium iodide (KI, Acros Organics >99 %) was dissolved in Milli-Q water to prepare a 0.6 mM I⁻ standard, through serial dilution, which was injected into the seawater (0–500 µL). Aged seawater was not used as the matrix to limit I⁻ in the zero samples. The I⁻ concentration in natural surface seawater is ~100 nM (Chance et al., 2014) and each 100 µL standard addition here increased the concentration by ~50 nM.

### 3.2.4.  Data processing

### 3.2.4.1.  Calibration

VOC concentrations were averaged at 1 min intervals and then corrected with a calibration factor derived from gas-phase calibrations using dilutions of a certified gas standard (Apel-Riemer Environmental Inc.; 500 ppbv for all VOC here) (Table 11). $O_3$ data were also averaged at 1 min intervals to reduce noise and then corrected for zero drift and the scrubbed air dilution. The $O_3$ monitor was calibrated during routine servicing, through comparison with other instruments or using a portable calibration source (2B-Technologies model 306 $O_3$ source). Under standard operation, negligible drift in calibration was observed.

**Table 11: Calibration factors for the instruments.**

| Instrument | Compound | Calibration factor |
|---|---|---|
| PTR-MS | Acetaldehyde | 0.820±0.042 |
| | Acetone | 0.949±0.103 |
| | DMS | 0.549±0.146 |
| | Isoprene | 0.138±0.012 |
| $O_3$ monitor | $O_3$ | n/a, frequently updated with an internal correction |

### 3.2.4.2. Peak data

Figure 18 shows a typical time series of acetaldehyde, acetone, isoprene and $O_3$ concentration in the headspace of the bubble column at ~1 min intervals during an oxidation experiment of one seawater sample. Figure 18 is an example of the plots that were used to derive all the production data.
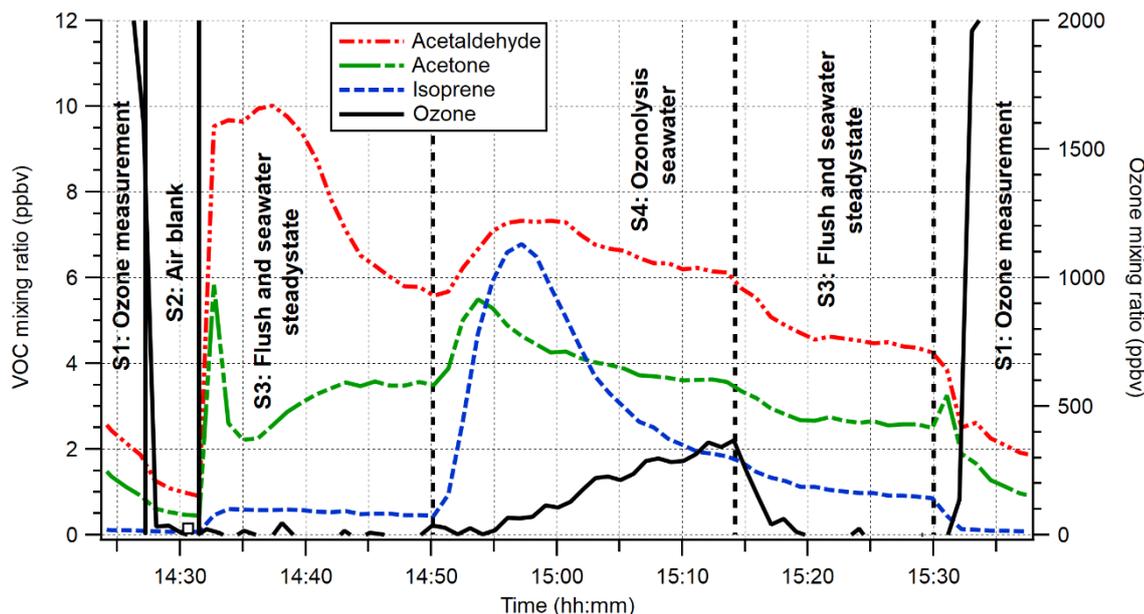


**Figure 18: Time series of acetaldehyde, acetone, isoprene and $O_3$ concentration in the headspace of the bubble column during an oxidation experiment. The four stages are identified. In this experiment, a second purge stage (stage three) was undertaken between about 15:14 to 15:30.**

The main experimental data from stage four are VOC peak height (ppbv) and initial gradient (ppbv $s^{-1}$). The concentration of VOC in the column headspace, after steady-state was achieved in stage three, is modelled by the integrated form of the differential equation;

$$\frac{dC_{VOC}}{dt} = \frac{P_{VOC}A_{bub}}{V_{air}} - \frac{F_{air}C_{VOC}}{V_{air}}$$
21

where $C_{VOC}$ represents headspace VOC concentration, $P_{VOC}$ represents the production of VOC at the air–sample interface, $A_{bub}$ represents the interfacial area (bubble area), $V_{air}$ represents headspace volume and $F_{air}$ represents gas flow rate. The headspace concentration was controlled by VOC produced from the reaction (Equation 21 first term right-hand side (RHS)) and the loss from the purge gas continuously moving through the headspace (Equation 21, second term RHS). VOC concentrations raise quicker and peak sooner than $O_3$ in Figure 18 because $O_3$ is lost rapidly to DOM and other aqueous compounds (i.e. $I^-$). Reactions with other compounds likely outcompete the small percentage of DOM that becomes measured VOC, hence a large initial loss of injected $O_3$.

The VOC peak height is the maximum concentration of VOC in the headspace of the column upon $O_3$ addition, which was measured by taking the difference between the steady-state point of the artificial air purge and the peak maximum (Figure 19). The VOC initial gradient is the maximum rate of increase before the peak maximum (Equation 21, maximum of left-hand side term) and was measured by linear regression through the initial linear portion of the peak. The

area under the peak corresponds to the total amount of VOC produced for the available DOM in the sample. This was rarely measured because full DOM consumption would take >1.5 h and shorter reaction times gave greater confidence in the stability of the injected $O_3$ concentration. The small peak height increase between 14:50–14:51 in Figure 19, compared to the maximum gradient represented by the green line, was an artefact of the 1 min averaging intervals and not representative of the reaction.
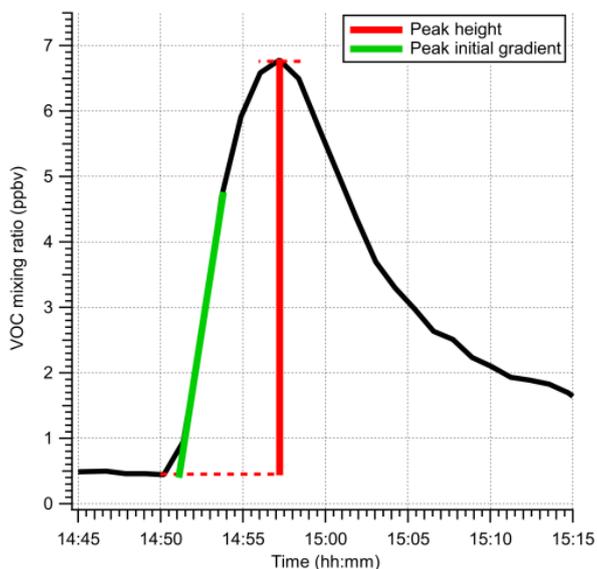


**Figure 19: Measurement system for VOC peak height and initial gradient**

To calculate the production of VOC scaled to the $O_3$ added, Equation 21 was rearranged for $P_{VOC}$ (mol m$^{-2}$ s$^{-1}$). As the peak height gradient ($dC_{VOC}/dt$) is maximum in the first few seconds, where headspace concentration is lowest, the $F_{air}C_{VOC}$ term (Equation 21, second term RHS) is small and should not be significant; an example initial $V_{air}\frac{dC_{VOC}}{dt}$ value from Figure 19 was $2.4\times10^{-5}$ ppbv s$^{-1}$, compared to the $F_{air}C_{VOC}$ value of $1.3\times10^{-6}$ ppbv s$^{-1}$ (5 %), when $C_{VOC}$ was 0.5 ppbv. Removing $F_{air}C_{VOC}$ leads to the estimation of $P_{VOC}$;

$$P_{VOC} \approx \frac{V_{air}\dfrac{dC_{VOC}}{dt}}{A_{bub}} \qquad\qquad 22$$

$O_3$ is added to the sample from a constant source at a constant rate and the flux into the sample (deposition, $D_{F,O_3}$) can be calculated (mol m$^{-2}$ s$^{-1}$);

$$D_{F,O_3} = \frac{F_{air}\left(C_{O_3,G} - C_{O_3,H}\right)}{A_{bub}} \approx \frac{C_{O_3,G}F_{air}}{A_{bub}} \qquad\qquad 23$$

where $C_{O_3,G}$ and $C_{O_3,H}$ represent $O_3$ concentration injected (from the generator) and in the headspace respectively. In the first few minutes of oxidation, all $O_3$ added to the sample is removed – if the concentration is low enough and $O_3$ remains the limiting reactant – which gives the good approximation in Equation 23. Deposition/loss of $O_3$ on the stainless-steel fittings, glass walls of the column and internal PFA tubing walls is small and considered negligible (all $O_3$ loss is assumed a result of the sample). The ratio of VOC produced for a given injected $O_3$ is calculated by dividing Equation 22 by the approximation of Equation 23;

$$P_{VOC:O_3} = \frac{P_{VOC}}{D_{F,O_3}} \approx \frac{V_{air} \frac{dC_{VOC}}{dt}}{C_{O_3,G} F_{air}} \qquad\qquad 24$$

Values calculated from Equation 24 – 'production ratios' – are dimensionless and represent a ratio of VOC produced for a known $O_3$ uptake. Other experimental results included the purge and oxidation loss of DMS. When a high DMS concentration was observed, $O_3$ was not observed in the headspace until a significant proportion of DMS had been lost. In this case, the loss rate of DMS from the artificial air purge (stage three) and the loss rate from oxidation (stage four) were measured with linear regression. The loss rate solely from $O_3$ addition was calculated by subtracting the stage three loss rate from the stage four loss rate.

### 3.2.4.3.   Reproducibility of peak data

The VOC peak data was reasonably reproducible using triplicate samples with a typical $R\sigma$ of 20–30 % (Table 12). Possible causes of variability in replicate samples may be insufficient cleanliness in the glass column, fluctuations in $O_3$ input concentration, or natural variability in the replicate seawater samples (e.g. if not well mixed from the sampling Niskin). The sample bottles and column were acid washed with HCl and then rinsed with Milli-Q water before the first usage, therefore any residual organics should be removed/destroyed. The ozonolysis of Milli-Q water (used to check for residual organics and usually has negligible VOC production) would also destroy any residual reactive DOM in the column. The column was rinsed with Milli-Q water between each sample and then conditioned with seawater sample from autumn 2018 onwards. Fluctuations in $O_3$ input concentration are identified by regular monitoring; once stabilised (running for ~1 h), the $O_3$ concentration very rarely varies by more than 10 % between the first and last measurement (max=8 h). The same amount of water ($\pm 2$ %) is used in all experiments to maintain the same bubble interface area and headspace volume.

**Table 12: Averages of the relative standard deviations of VOC peak data in triplicate samples across all measurements in a seasonal campaign. Number of runs (n) in each campaign: spring = 11, autumn = 7, summer = 14, total = 32.**

| Measurement | Acetaldehyde $R\sigma$ (%) | | Acetone $R\sigma$ (%) | | Isoprene $R\sigma$ (%) | |
|---|---|---|---|---|---|---|
| | Peak height | Peak grad. | Peak height | Peak grad. | Peak height | Peak grad. |
| Spring 2017 | 16.4±7.7 | 19.4±13.8 | 22.8±15.2 | 19.8±13.6 | 28.8±21.7 | 27.6±13.2 |
| Autumn 2018 | 11.9±7.4 | 20.6±10.7 | 21.6±10.5 | 27.6±12.2 | 15.4±8.4 | 11.4±6.0 |
| Summer 2020 | 13.1±7.2 | 17.7±8.9 | 15.0±8.4 | 21.5±8.3 | 30.4±20.5 | 29.6±13.7 |
| All meas. | 14.0±7.4 | 19.0±10.9 | 19.1±11.8 | 22.3±11.2 | 26.6±19.5 | 24.9±14.0 |

The temperature of the water sample was not explicitly controlled in the experiments. The triplicate seawater samples were generally measured over a continuous ~3 h period in the autumn 2018+ measurements shortly (~3 hrs) after water collection. As the initial seawater temperature was always below laboratory temperature, it is likely that the temperature increased slightly from sample one to sample three. This might have introduced some variability in the VOC production. On occasions where measurements were conducted a day after sampling, the triplicate samples were uniform at room temperature. Preliminary measurements of production vs. temperature showed a potential minimum at 15 °C (Chen, 2017); therefore, if the temperature of sample three was higher (due to heating in a relatively warmer laboratory compared to the L4 water), greater

production would be expected. Temperature is important not only for reaction kinetics but also for the bubble plume size distribution and the $O_3$ solubility. Increasing temperatures are expected to increase kinetic rates (more production) and reduce bubble size (more production) but also reduce the $O_3$ solubility (possibly less production). For acetaldehyde, the rise from 10 °C to 20 °C leads to a reduction in $P_{VOC:O_3}$ of ~8 %, while for acetone and isoprene the rise in temperature caused a ~58 % increase in $P_{VOC:O_3}$.

The spring 2017 measurements were run in much quicker (three in ~1 h) time compared to the autumn 2018+, therefore the earlier measurements are more likely to be reproducible with regards to temperature changes. However, as the experiments were much quicker, there was less column cleaning between samples. Residual organics, especially those created in the reaction process, were more likely to remain between samples and are, therefore, a potential source of deviation in the spring 2017 measurements. Sample 3 was on average 12±13 % higher ($\pm\sigma_{\bar{x}}$) compared with sample 1 in all measurements that occurred on the day of sampling (no difference between 2017 and 2018+; t-test, $p$=0.92), therefore temperature increase between samples was likely not a problem. The higher production in sample 3 must have been due to insoluble organic residues that could not be removed with column cleaning.

### 3.2.4.4. Compound identification

High mass resolution literature results of Zhou et al. (2014), using a PTR-time of flight instrument, were used to confirm the production of acetaldehyde and acetone at $m/z$ 45 and 59 (recorded as $m/z$ 45.03 and 59.04 at higher resolution) respectively. In principle, acetone, propanal and glyoxal can all be produced from heterogeneous oxidation and be detected at $m/z$ 59.04 (Zhou et al., 2014). Acetaldehyde and acetone/propanal production has also been identified in other experiments (Schneider et al., 2019). Glyoxal is not directly measured with our PTR-MS because the proton affinity of glyoxal (161.41 kcal mol$^{-1}$; Wróblewski et al., 2007) is lower than that of the hydronium reagent ion for efficient proton transfer (165.2 kcal mol$^{-1}$; Lindinger et al., 1998). Furthermore, the very high solubility of glyoxal ($4.2\times10^5$ M atm$^{-1}$; Burkholder et al., 2015; Sander, 2015) should cause the vast majority of produced glyoxal to dissolve into the seawater sample before measurement in the column headspace, leading to a very low signal. Propanal (an aldehyde with one more methyl group than acetaldehyde) is a possible interference for acetone measurement and the experiments here are not able to differentiate the two compounds. However, previous seawater measurements using our PTR-MS with $NO^+$ as the reagent ion showed that the contribution of propanal towards $m/z$ 59 is usually only ~10% (Rogerson, 2016). Moreover, in the VOC production measurements $m/z$ 45 and $m/z$ 59 also show markedly different temporal evolution; thus $m/z$ 59 seems more likely to be primarily acetone and not propanal because propanal would potentially have a similar mechanism to acetaldehyde (both being low mass monoaldehydes)

Zhou et al. (2014) speculated the observed $m/z$ 69 peak (recorded as $m/z$ 69.06) was dehydrated pentanal ($M-18+1$). However, they did not find a correlation between $m/z$ 69 and

the *m/z* 87 parent ion (*m/z* 87 was observed when *m/z* 69 was not, however *m/z* 87 might also be pentanone). Schneider et al. (2019) also observed the production of *m/z* 69 during the ozonolysis of SML samples taken from a phytoplankton culture. The *m/z* 69:41 fragmentation ratio during my $O_3$ oxidation experiments was 0.46±0.04. In comparison, I measured fragmentation ratios of 0.542±0.037 and 0.550±0.033 of standards of isoprene and pentanal, respectively. A GC-MS was not available during the research to separate interferences of isoprene and pentanal, thus the resolved peak at *m/z* 69 is assumed to be isoprene.

## 3.3. Results and Discussion

### 3.3.1. Seawater production

#### 3.3.1.1. Dependence in VOC production on ozone input

The experiments used a mean $O_3$ concentration of 7.7±0.7, 1.7±0.7, and 2.1±1.1 ppmv (±$\sigma$) in the spring, summer and autumn experiments respectively. Experiments conducted by Chen (2017) with variable $O_3$ concentration in spring 2017 showed increasing rates of production that plateaued at higher $O_3$ input concentration (Figure 20a), which could be fit to the curve $y = A(1 - \exp(-Bx - Cx^2))$. A plateau at higher $O_3$ concentration was indicative of a limiting process in the reaction; possibly $O_3$ or DOM cannot adsorp/replenish fast enough at the bubble surface or $O_3$ adsorps too readily and occupies all the available active sites (Section 1.5.2.4). The initial linear portion of each VOC curve suggests that below the limiting threshold (4–6 ppmv), the reaction rate is linearly proportional to $O_3$ concentration. The uptake of $O_3$ by the ocean is generally thought not to significantly deplete the amount of reactants available near the sea surface (Fairall et al., 2007) and the fact the experiments are also $O_3$ limited at low $O_3$ input (linear response) suggests that the experimental reaction regime behaves similarly to the ocean. An approximately linear relationship was also observed in summer 2020 (Figure 20b). These results suggest that the spring 2017 measurements were likely DOM reagent limited in part but also limited by the concentrations of reactants, probably due to a combination of high $O_3$ input and fairly low reactant concentration, whilst the autumn 2018 and summer 2020 measurements were only $O_3$ input limited. Thus, when Equation 24 is applied to the 2017 data, the $P_{VOC:O_3}$ may be slightly underestimated because the reactions were not purely limited by $O_3$ input.
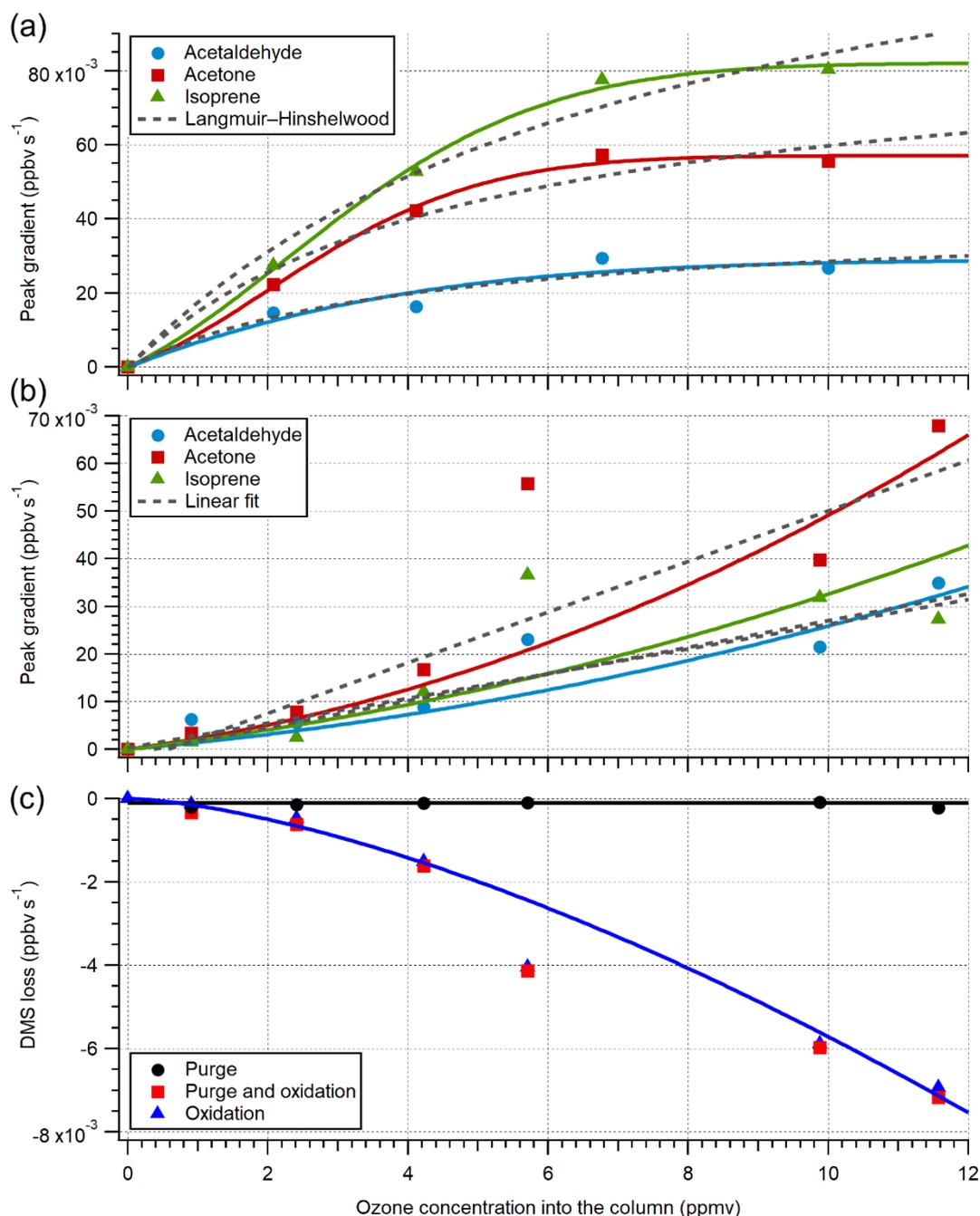
**Figure 20: The effect of increasing ozone concentration with WCO L4 surface seawater using ozone heterogeneous oxidation on (a) the rate of VOC production from April 2017, (b) the rate of VOC production (Oct 2020) and (c) loss rate of DMS from Oct 2020. In (b) & (c) 5.7 ppmv measurement was ignored in regression analysis for all VOC. April 2017 data from Chen (2017).**

Also shown in Figure 20a are fits to the Langmuir–Hinshelwood mechanism (Section 1.5.2.4), $y = Ax/(B + x)$, which has been shown to model surface reaction of $O_3$ and some aqueous species (Mmereki et al., 2004; Raja and Valsaraj, 2005; Clifford et al., 2008; Sakamoto et al., 2009; Reeser and Donaldson, 2011). Here, the $A$ term represents the product of the $O_3$ chemical activity ($O_3$ destroying species surface bimolecular rate constants and interfacial concentrations) and total surface binding sites, while the $B$ term represents the reciprocal of the adsorption:desorption ratio of surface equilibrium constants for $O_3$ (Reeser and Donaldson, 2011). It is clear that the acetaldehyde production rate matches the Langmuir–Hinshelwood mechanism reasonably well, while acetone and isoprene show a poorer fitting. If error bars from triplicate

measurements were included on the acetone and isoprene data points (only one measurement per sample was undertaken), the uncertainty would likely incorporate the Langmuir–Hinshelwood fitted curves; thus the Langmuir–Hinshelwood mechanism is assumed to model all three VOC. Interfacial heterogeneous reactions that produce acetaldehyde and acetone are also shown by Schneider et al. (2019). Table 13 shows the measured values of $A$ and $B$ for the three VOC.

**Table 13: Measured Langmuir–Hinshelwood mechanism coefficients (fit to $y = Ax/(B + x)$) for reactions of $O_3$ (2–10 ppmv) and seawater (constant).**

| VOC | $A$ | $B$ | $B^{-1}$ |
|---|---|---|---|
| Acetaldehyde | 0.0404±0.0116 | 4.19±2.90 | 0.239±0.165 |
| Acetone | 0.0895±0.0184 | 4.97±2.29 | 0.201±0.095 |
| Isoprene | 0.1489±0.0336 | 7.57±3.21 | 0.132±0.056 |

Similar experiments in summer 2020 showed increasing rates of production with higher $O_3$ concentrations (Figure 20b). This differs from the 2017 experiment and suggested the reactions were not in agreement with the Langmuir–Hinshelwood mechanism, which is either due to (1) shifting of the DOM plateau to higher $O_3$ input, or (2) the reactions were better modelled by a different surface mechanism. For point (1), this would be the case if the summer seawater contained higher DOM concentrations, which is commonly observed at L4 (Smyth et al., 2010), thus the linear trend shown in Figure 20b is the extended range of the linear portion (0–4 ppmv) of Figure 20a. Under this scenario, the increased abundance of DOM in the seawater enabled a greater interfacial DOM renewal. For point (2), the data reasonably fit an Eley–Rideal mechanism (Section 1.5.2.4), where $O_3$ is the non-absorbing gas-phase species and the surface-absorbing DOM is in relatively high concentration; here the reaction would be linear with respect to $O_3$ concentration. The linear fits in Figure 20a show a coefficient of determination, $r^2 \geq 0.93$; therefore, this is potentially an acceptable explanation.

Figure 21 generally shows that for most VOCs in spring 2017 and summer 2020, the sensitivity in the $P_{VOC:O_3}$ towards $O_3$ input was small. Acetaldehyde, acetone and isoprene observed a mean ~31 % reduction and ~6 and ~33 % increase, respectively, in $P_{VOC:O_3}$ at the higher $O_3$ input using common regressions. Importantly, however, for all three VOC, the spring 2017 and summer 2020 regressions were found to be statistically similar and similar to zero; thus further correction is not necessary.
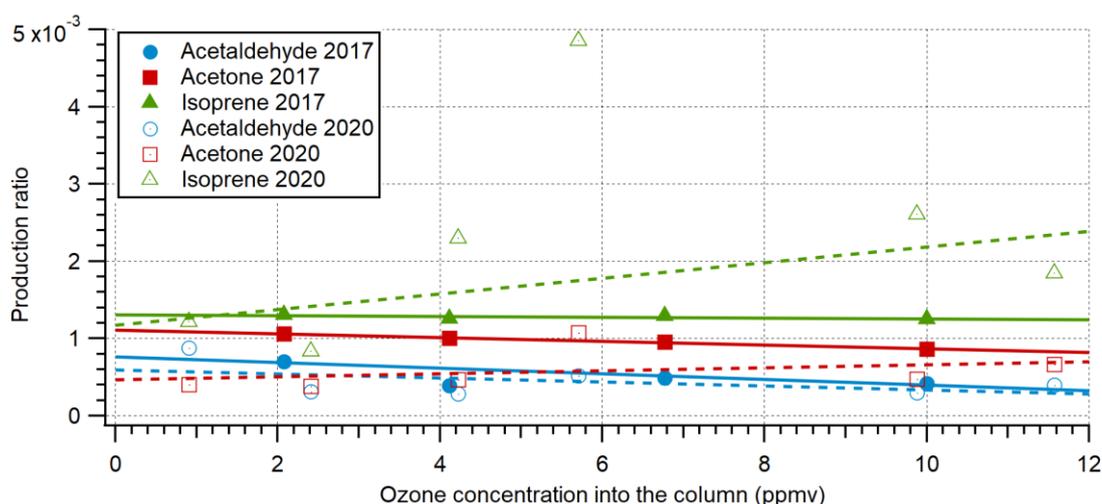
**Figure 21: The effect of increasing ozone concentration on the production ratio using WCO L4 surface seawater in spring 2017 (full shapes and solid lines) and summer 2020 (empty shapes and dashed lines). April 2017 data from Chen (2017).**

During the 2020 experiment, a large increase in the DMS loss rate was observed with higher concentrations of injected $O_3$ (Figure 20c). The loss rate of DMS during the headspace purge was near-constant between samples (expected as the only loss process was bubble stripping). While DMS can be oxidised by $O_3$ in both the gas phase (Du et al., 2007) and aqueous phase (Lee and Zhou, 1994; Gershenzon et al., 2001), the gas phase reaction is considered negligible, therefore loss processes in the experiment were assumed to be solely aqueous $O_3$–DMS reactions. The $O_3$–DMS aqueous rate constant ($1.1 \times 10^9$ $M^{-1}$ $s^{-1}$ at 20 °C; Gershenzon et al., 2001) was used to calculate the amount of $O_3$ reacting with the DMS; rate $= -kC_{O_3}C_{DMS}$, where rate represents the measured DMS loss, $k$ represents the second order rate constant and $C_{O_3}$ and $C_{DMS}$ represent the concentration of $O_3$ and DMS respectively. The concentration of available $O_3$ to react with aqueous DMS (~2.5 nM) was calculated to be $2.0 \times 10^{-6}$ and $9.9 \times 10^{-5}$ nM for the 0.9 and 10.8 ppmv $O_3$ concentrations respectively. These very low $O_3$ concentrations show extreme loss, compared to the 8 and 103 nM $O_3$ concentrations injected ($C_{O_3}/H$), and suggest high competition of other $O_3$ depleting species (i.e. DOM for VOC production, I⁻) in the seawater sample, consistant with values in Table 1.

### 3.3.1.2.  Raw peak data

The maximum peak height and initial peak gradient for each VOC during ozonolysis, not adjusted for the variable $O_3$ input for the different periods, are shown in Figure 22. Here changes are discussed for measurements with similar $O_3$ inputs. The spring bloom observed on average a 65, 348 and 136 % increase in acetaldehyde, acetone and isoprene mean peak height, compared to the pre-bloom weeks before. Acetone observed the largest increase in mean peak height over the spring bloom with a range of 2.5–15.5 ppbv. In contrast, no change was observed for acetone between the summer and autumn. For acetaldehyde and isoprene, 35 and 438 % increases were observed, respectively, in the autumn compared to the summer. Generally, higher production of acetone and isoprene was observed in the summer compared to the pre-bloom period (even though the spring measurements used higher $O_3$ input, Section 3.3.1.1).
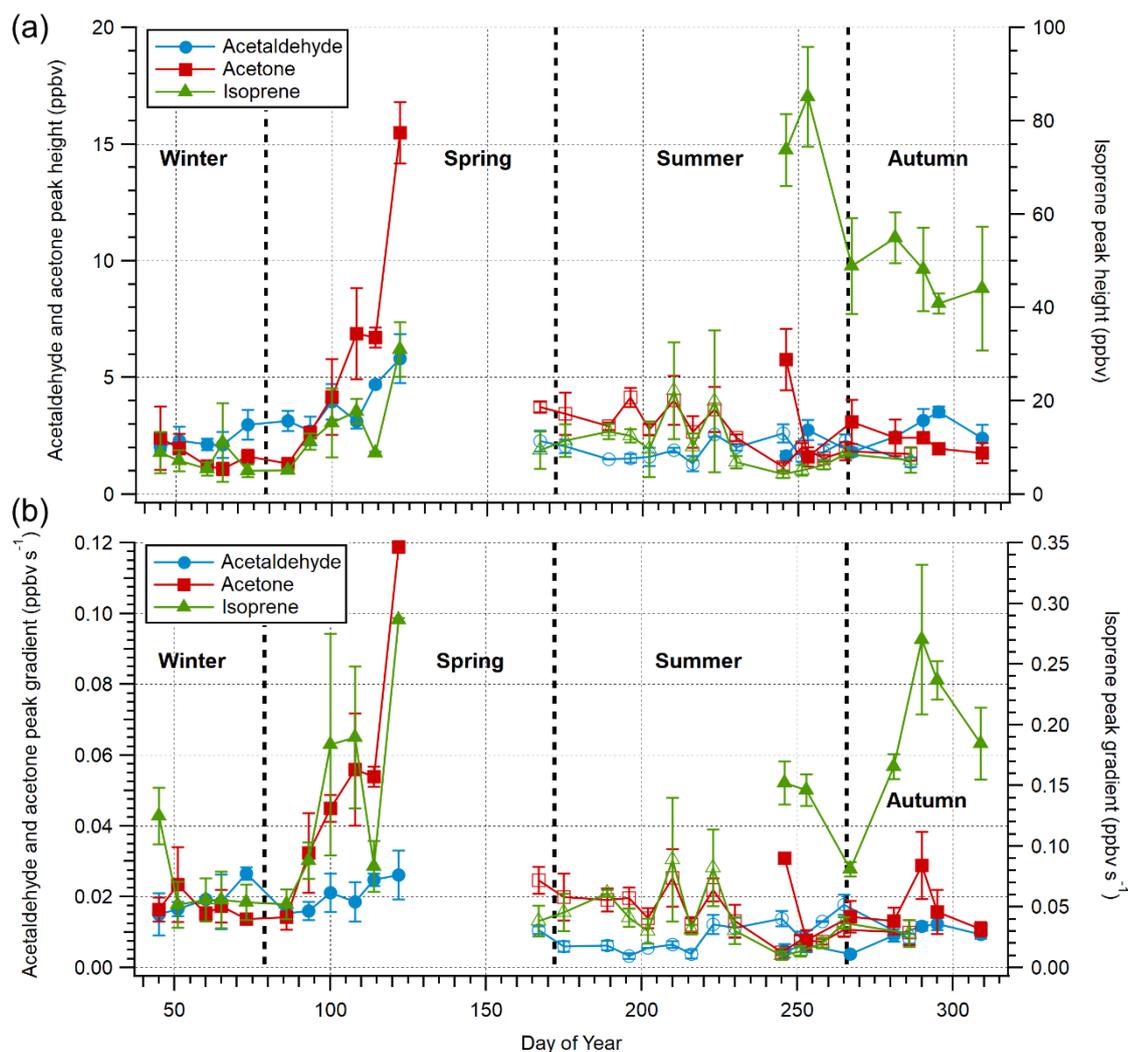
**Figure 22: Combination of three measurement campaigns of VOC peak (a) height and (b) gradient from WCO L4 surface seawater using ozone heterogeneous oxidation. Data are not corrected for variable ozone input concentration. Error bars are 1 standard deviation of triplicate measurements. Spring (DOY 45–122) data from Chen (2017). The full markers represent the spring 2017 and the autumn 2018 measurements. The hollow markers represent the summer 2020 measurements.**

Similar mean initial peak gradients were observed for acetaldehyde between the two spring periods (15 % average increase in the bloom), however, for acetone and isoprene, seasonal average increases of 266 and 153 % were observed during the bloom, respectively. For acetone the change between the summer and autumn was small (a small 16 % increase in autumn). For acetaldehyde and isoprene, a 10 % decrease and 344 % increase were observed from summer to autumn, respectively. Isoprene observed a large increase in both peak height and initial peak gradient in the autumn of 2018 compared to the late summer of 2020. In contrast, the acetaldehyde gradient decreased while the peak height increased.

Clear peak height:gradient correlations, by linear regression, were observed for the VOCs in at least two campaigns (Table 14). A Tukey multiple comparison regression test (multi-comparisons between >2 regressions, $\alpha$=0.05) showed acetone and acetaldehyde had statistically similar positive height:gradient slopes across all the campaigns (129.2±56.4 and 151.1±75.0 s, respectively, ±propagated $\sigma$). The 2017 and 2020 isoprene slopes were both very tight ($r^2 \geq 89$ %, likewise for acetone) but very different in magnitude. Positive slopes between peak height and

gradient are expected considering the strong coupling between production rate and maximum concentration. However, the 2018 isoprene data showed a negative slope between peak height and initial gradient with a very low $r^2$. If one outlier is removed, the correlation strength increases ($r^2$=0.52) and the gradient becomes more negative at -255 s. If two outliers are removed, the strength remains similar ($r^2$=0.14) and the gradient becomes statistically similar to zero. Due to the few data points in the 2018 time series, further detailed correlation analysis is unavailable nor is the cause of the dissimilar trend known.

**Table 14: Linear regressions for peak height:gradient of heterogeneous production of the three VOCs from L4 seawater for the three experimental campaigns. Here $y$ is the peak height and $x$ is the peak gradient.**

| Year | Acetaldehyde | Acetone | Isoprene |
|------|-------------|---------|----------|
| 2017, $n$=11 | $y = 196.6x - 0.711$ $r^2$=0.50 | $y = 134.9x - 0.313$ $r^2$=0.98 | $y = 93.1x + 1.177$ $r^2$=0.89 |
| 2018, $n$=7 | $y = 181.8x + 1.050$ $r^2$=0.77 | $y = 116.6x + 0.691$ $r^2$=0.53 | $y = -101.8x + 74.499$ $r^2$=0.15 |
| 2020, $n$=14 | $y = 74.9x + 1.211$ $r^2$=0.53 | $y = 136.1x + 0.682$ $r^2$=0.89 | $y = 217.6x + 1.848$ $r^2$=0.95 |

### 3.3.1.3.  Production ratio data

Interpretations of the raw peak data (Section 3.3.1.2) are complicated by the fact that different $O_3$ inputs were used. Here I account for the $O_3$ input and discuss the variability in the VOC $P_{VOC:O_3}$. The $P_{VOC:O_3}$ values calculated from Equation 24 are shown in Figure 23 with mean values in Figure 24 and Table 15. It was evident that the summer campaign period data contained a large amount of variability, which I interpret by splitting the period into two sections for the remainder of the results and discussion: early summer and late summer, with the break appearing at DOY ~230. As discussed earlier (Section 3.3.1.1), the spring $P_{VOC:O_3}$ may be a slight underestimation for acetaldehyde and acetone due to the non-linearity in VOC production at high $O_3$ input (26 and 13 % underestimation respectively) but not for isoprene (2 % underestimation); this does not affect the comparison between the two spring periods.
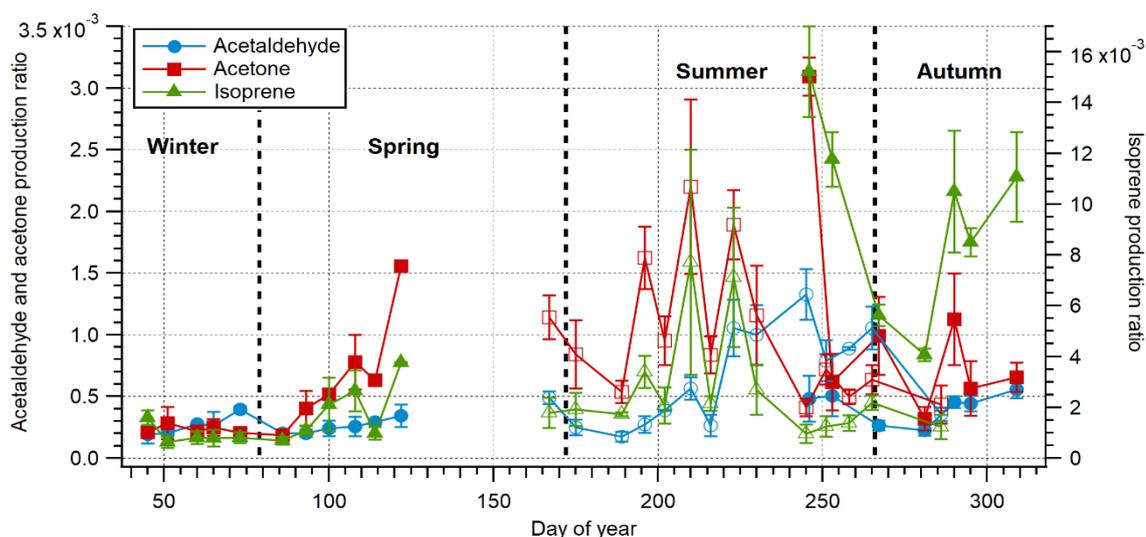


**Figure 23: Combination of three measurement campaigns of VOC production ratio (VOC produced per ozone added) from WCO L4 surface seawater using ozone heterogeneous oxidation. Error bars are 1 standard deviation of triplicate measurements. Spring (DOY 45–122) data from Chen (2017). The full markers represent the spring 2017 and the autumn 2018 measurements. The hollow markers represent the summer 2020 measurements.**
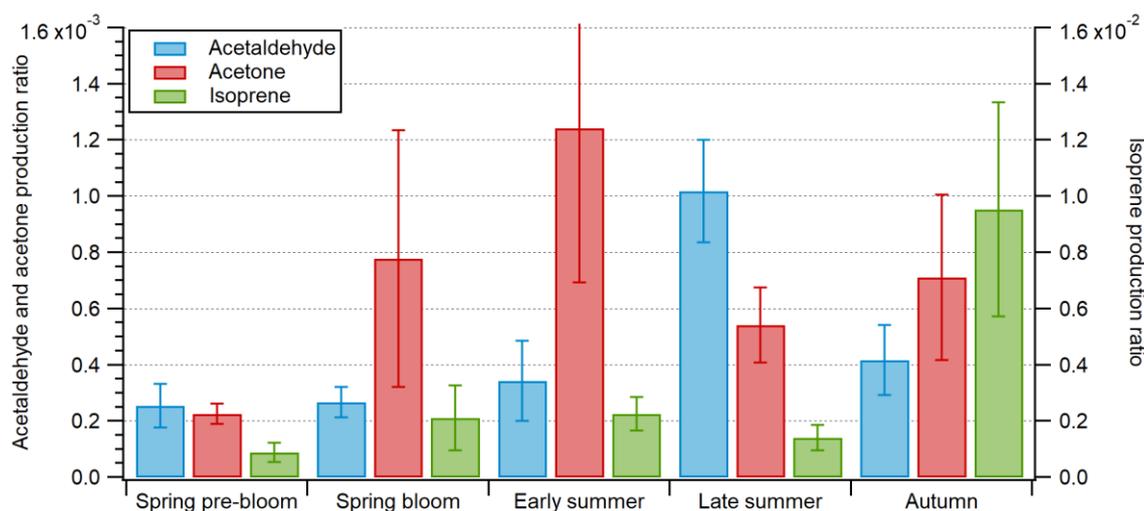
**Figure 24: Combination of three measurement campaigns of VOC production (spring, summer and autumn) from WCO L4 surface seawater using ozone heterogeneous oxidation. Data provided as a ratio of VOC produced to ozone input. Error bars are 1 standard deviation. VOC appear in the order acetaldehyde, acetone and isoprene per category.**

**Table 15: Mean VOC production ratio ($\times 10^4$) from the ozone heterogeneous oxidation of WCO L4 seawater. Uncertainty is 1 standard deviation. 'All data' is the average of all recorded production data.**

| VOC | Statistic | Spring pre-bloom | Spring bloom | Early summer | Late summer | Autumn | All data |
|---|---|---|---|---|---|---|---|
| Acetald. | Mean | 2.6±0.8 | 2.7±0.5 | 3.4±1.4 | 10.2±1.8 | 4.2±1.3 | 4.6±3.0 |
|  | Median | 2.3 | 2.6 | 2.7 | 10.0 | 4.2 | 3.5 |
| Acetone | Mean | 2.3±0.4 | 7.8±4.6 | 12.4±5.5 | 5.4±1.3 | 7.1±3.0 | 8.3±6.5 |
|  | Median | 2.1 | 6.3 | 11.4 | 5.0 | 6.5 | 6.4 |
| Isoprene | Mean | 8.8±3.5 | 21.2±11.5 | 22.5±6.0 | 14.0±4.6 | 95.3±38.0 | 37.5±38.6 |
|  | Median | 8.0 | 21.1 | 21.5 | 12.5 | 105.0 | 20.9 |

Acetaldehyde showed no substantial change in mean $P_{VOC:O_3}$ in the spring but was increased on average by 34, 299 and 64 % in the early summer, late summer and autumn respectively (Table 15). The acetone mean $P_{VOC:O_3}$ was 246, 452, 140 and 216 % higher in the bloom, early summer, late summer and autumn periods, respectively, compared to the pre-bloom period. Similar mean isoprene $P_{VOC:O_3}$ values were observed in the bloom and early summer period (early summer was 7 % lower), which were 140 and 154 % higher, respectively, than the pre-bloom period. The late summer period was between the pre-bloom and bloom / early summer (59 % higher than pre-bloom). Significantly higher isoprene $P_{VOC:O_3}$ was observed in the autumn (980 %) compared with the pre-bloom.

A one-way ANOVA test ($\alpha$=0.05) followed by a Tukey test determined that the late summer acetaldehyde data were statistically different from all other periods, whilst the remaining pairings were confidently statistically similar (i.e. far from Tukey test significance thresholds). The test for acetone found that the early summer data were statistically different from the pre-bloom and late summer data, and the remaining pairing combinations were not different. Here the early summer and autumn data were close to the threshold for swapping significance (becoming different). Unsurprisingly, the test identified the isoprene autumn data were statistically different from the remaining seasons, which themselves were all similar. For isoprene, all pairings were

comfortably separated from significance thresholds for becoming statistically different. Acetaldehyde and isoprene were not statistically similar during the overlap in the summer 2020 and autumn 2018 periods (DOY 246–286). Isoprene was higher in the autumn, acetaldehyde was higher in the late summer and acetone was statistically similar between the periods. The unique annual pattern of these VOCs suggests the precursor DOM is different per compound. The annual cycling of specific DOM compounds and compound groups is strongly dependent on the dominant biological producer, which is likely to vary on a weekly/month scale as dynamic environmental conditions change.

For acetone and isoprene, the spring bloom produced a clear increase in $P_{VOC:O_3}$ (~DOY 90) likely because of an increase in biological production of DOM (Schneider et al., 2019). Banoub and Williams (1973) observed a ~35 µM increase in DOC concentration for the spring bloom, compared to the pre-bloom background, at the WCO E1 station (location reference; Figure 4) that started around DOY ~70 and peaked around DOY ~160. The 2017 bloom measurements reported here show increased production later around DOY ~90 (Figure 23), which is either (1) because of interannual variability or because the E1 station is further from the coast (~20 km) or (2) because total DOC concentration and the specific DOM required to produce the VOC here do no correlate. Chen (2017) measured surface DOC in the L4 water during the end of the spring phytoplankton bloom; a mean concentration of 257±33 µM was measured. Moderate-strong and moderate strength linear regressions between DOC concentration and $P_{VOC:O_3}$ were shown for isoprene and acetone (r²=0.63 and 0.43 respectively), which helps to invalidate point (2) above. Furthermore, high annual variability has been seen in the annual dominant diatom species, total carbon mass and rate of increase of carbon mass at the L4 station (Irigoien et al., 2000) and the spatial structure has been observed to vary on the order of ~1 km (Smyth et al., 2002), thus spatial/temporal variability between the L4 and E1 stations is expected. When DOC concentration was checked against VOC peak height, the isoprene regression improved (r²=0.72) however the acetone regression fell slightly (r²=0.31). No regression was shown for acetaldehyde for $P_{VOC:O_3}$ or peak height (r²=0.06 and 0.03 respectively) because acetaldehyde did not increase at the end of the 2017 spring bloom, while acetone, isoprene and DOC concentration did increase.

Autumn 2018 saw a significant order of magnitude increase in isoprene production. Carr et al. (2019) observed a higher mean concentration of DOC in the autumn (~84 µM), compared to ~65 µM in the spring and summer, to the north of the south-west UK peninsula at the coastal 'Site A' (51.2° N, -6.1° E; similar to L4 at 50.3° N, -4.2° E). The Central Celtic Sea in comparison did not show a large change in DOC concentration during any season (63.4–68.5 µM range). The high autumn DOC concentrations at Site A were a result of the summer bloom because high chlorophyll *a* concentrations were observed (Carr et al., 2019). Banoub and Williams (1973) observed a ~44 µM DOC increase in the summer bloom at the E1 station which started DOY ~220 and peaked DOY ~250. The peak of this summer bloom coincided with the start of the

autumn campaign (DOY 246); assuming some temporal and spatial differences between L4 and E1, the high autumn production may be a remnant of an intense summer phytoplankton bloom.

### 3.3.1.4.   Western Channel Observatory data and events

The variability in $P_{VOC:O_3}$ across different seasons are due to a combination of measurement uncertainty and natural variability. More than half of the seasonal means have variability >33 %, so a comparison to WCO data was made to determine if environmental changes could explain the observed variability. Here the $P_{VOC:O_3}$ time series from each campaign is compared to simultaneous data through linear regression. Note that the campaigns occur over different seasons, so the analysis below is essentially comparing seasonality in VOC production to other variables that also vary seasonally. As an example, the summer is expected to show the highest surface temperature and temperature may not have a direct cause-effect relationship on VOC production but may regulate biological activity which subsequently could affect VOC production. Thus correlations do not imply direct causation.

Figure 25 shows the measured temperature, salinity, chlorophyll *a* concentration and CDOM absorbance, alongside the decadal average measured from the L4 surface buoy (Smyth, 2021). It is clear that there are no large variations in temperature in spring 2017 or autumn 2018 (Figure 25a), while summer 2020 observed multiple ~2° C jumps between weekly measurements. Generally, the surface temperatures matched the decadal average, however, the slightly higher spring 2017 temperature suggests that spring 2017 was anomalously warm. High 2017 temperatures were also observed in measurements at Looe Bay (2014–2017).

Table 17 shows that acetone and isoprene had medium strength correlations with surface temperature for the spring 2017 and autumn 2018 campaigns. See Table 16 for an explanation of the correlation phrasing used in the text. No correlation with temperature was observed for acetaldehyde in these periods; however, acetaldehyde did show a medium strength correlation in the summer 2020 campaign while acetone and isoprene did not. Where a relationship was shown, the correlation was positive suggesting increased surface temperature increased VOC production. Because the water temperature at the time of laboratory measurement did not relate simply to the ambient seawater temperature (Section 3.2.4.3) these correlations are more likely reflections of relationships with biological VOC precursors.

**Table 16: Phrasing of correlation strengths used in the text.**

| Phrase | $r^2$ correlation values |
|---|---|
| Weak | $0.0 < r^2 \leq 0.2$ |
| Moderate–weak | $0.2 < r^2 \leq 0.4$ |
| Moderate | $0.4 < r^2 \leq 0.6$ |
| Moderate–strong | $0.6 < r^2 \leq 0.8$ |
| Strong | $0.8 < r^2 \leq 1.0$ |
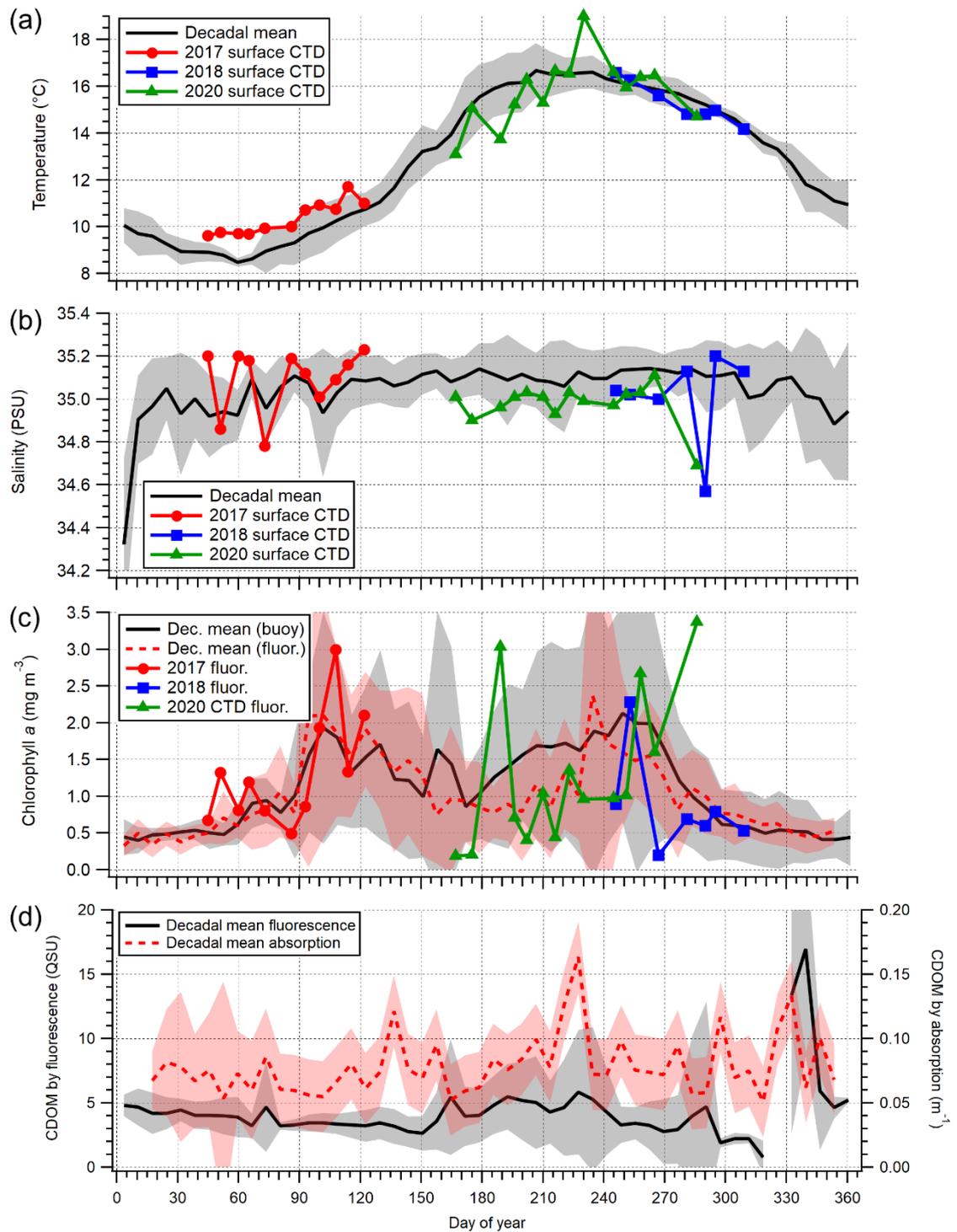
**Figure 25: Decadal averages (2009–2019) shown as weekly binned surface (a) temperature and (b) salinity from the RV *Plymouth Quest* CTD at L4, weekly binned surface (c) chlorophyll *a* concentration from the L4 buoy, laboratory fluorescence measurements (2017 and 2018) and CTD fluorescence measurements (2020), and (d) CDOM from the L4 buoy (2009–2019) and laboratory absorption measurement (2002–2009). Shaded regions are 1σ. Values from sampled seawater are also shown.**

**Table 17: Coefficient of determination ($r^2$) for linear regressions between the independent variable and VOC $P_{VOC:O_3}$ (dependant) for the three campaigns. The direction of correlation is provided when $r^2 \geq 0.05$. Temperature, salinity, transmission, fluorescence, oxygen and CTD depth were all measured during the rosette cast. Turbidity and wind speed were measured from the L4 buoy. Chlorophyll was either measured in situ (L4 buoy) or in the laboratory (HPLC) and the strongest regression was used. Inorganic nutrient data was measured in the laboratory. * data only available DOY 73–122. ** data is high and possibly biofouled. n/a means no data available. *** mixed layer depth that could not be determined (i.e. homogeneous vertical profile) were recorded as NaN.**

| Group | Variable | Year | Acetaldehyde | Acetone | Isoprene |
|---|---|---|---|---|---|
| Water parameters | Temperature (° C) | 2017 | 0.05 (+) | 0.43 (+) | 0.23 (+) |
| | | 2018 | 0.00 | 0.40 (+) | 0.21 (+) |
| | | 2020 | 0.36 (+) | 0.00 | 0.01 |
| | Salinity (PSU) | 2017 | 0.08 (–) | 0.09 (+) | 0.08 (+) |
| | | 2018 | 0.01 | 0.03 | 0.03 |
| | | 2020 | 0.18 (+) | 0.09 (+) | 0.06 (+) |
| | Transmission (%) | 2017 | 0.07 (+) | 0.18 (+) | 0.01 |
| | | 2018 | 0.04 | 0.01 | 0.04 |
| | | 2020 | 0.00 | 0.09 (+) | 0.02 |
| | Turbidity (NTU) | 2017* | 0.02 | 0.47 (–) | 0.42 (–) |
| | | 2018** | 0.06 (–) | 0.91 (–) | 0.45 (–) |
| | | 2020 | n/a | n/a | n/a |
| | Mixed layer depth (m)*** | 2017 | 0.00 | 0.85 (+) | 0.32 (+) |
| | | 2018 | 0.88 (–) | 0.26 (–) | 0.89 (–) |
| | | 2020 | 0.05 (+) | 0.02 | 0.01 |
| Physical forcing | Windspeed (m s$^{-1}$) | 2017* | 0.16 (–) | 0.07 (+) | 0.00 |
| | | 2018 | 0.37 (+) | 0.29 (–) | 0.02 |
| | | 2020 | n/a | n/a | n/a |
| | Windspeed (-6 hr) (m s$^{-1}$) | 2017* | 0.08 (–) | 0.41 (–) | 0.33 (+) |
| | | 2018 | 0.47 (+) | 0.01 | 0.30 (+) |
| | | 2020 | n/a | n/a | n/a |
| Biological proxies | CTD in situ fluorescence (QSU) | 2017 | 0.06 (+) | 0.03 | 0.13 (+) |
| | | 2018 | 0.43 (–) | 0.44 (–) | 0.58 (–) |
| | | 2020 | 0.00 | 0.16 (–) | 0.02 |
| | Chlorophyll $a$ laboratory fluorescence (µg L$^{-1}$) | 2017 | 0.04 | 0.48 (+) | 0.56 (+) |
| | | 2018 | 0.17 (+) | 0.59 (+) | 0.55 (+) |
| | | 2020 | n/a | n/a | n/a |
| | Oxygen (µM) | 2017 | 0.02 | 0.16 (+) | 0.07 (+) |
| | | 2018 | 0.24 (+) | 0.01 | 0.27 (+) |
| | | 2020 | 0.04 | 0.14 (+) | 0.04 |
| Inorganic nutrients | Nitrite (µM) | 2017 | 0.16 (–) | 0.30 (–) | 0.18 (–) |
| | | 2018 | 0.11 (–) | 0.27 (–) | 0.24 (–) |
| | | 2020 | 0.07 (–) | 0.22 (–) | 0.05 (–) |
| | Nitrate (µM) | 2017 | 0.05 (–) | 0.63 (–) | 0.46 (–) |
| | | 2018 | 0.05 (+) | 0.34 (–) | 0.02 |
| | | 2020 | 0.10 (+) | 0.31 (–) | 0.00 |
| | Ammonia (µM) | 2017 | 0.84 (+) | 0.89 (+) | 0.62 (+) |
| | | 2018 | 0.18 (–) | 0.37 (+) | 0.24 (+) |
| | | 2020 | 0.01 | 0.06 (+) | 0.00 |
| | Silicate (µM) | 2017 | 0.09 (–) | 0.77 (–) | 0.23 (–) |
| | | 2018 | 0.07 (–) | 0.09 (–) | 0.18 (–) |
| | | 2020 | 0.09 (+) | 0.16 (–) | 0.03 |
| | Phosphate (µM) | 2017 | 0.01 | 0.86 (–) | 0.59 (–) |
| | | 2018 | 0.06 (+) | 0.12 (–) | 0.01 |
| | | 2020 | 0.10 (–) | 0.03 | 0.05 (–) |
| ODS | Iodide (nM) | 2017 | 0.13 (–) | 0.01 | 0.05 (–) |
| | | 2018 | n/a | n/a | n/a |
| | | 2020 | n/a | n/a | n/a |
| Sampling & measurement | Measurement delay (d) | 2017 | 0.33 (–) | 0.21 (–) | 0.17 (–) |
| | | 2018 | 0.08 (–) | 0.00 | 0.05 (–) |
| | | 2020 | 0.04 | 0.07 (–) | 0.03 |
| | Rosette sampling depth (m) | 2017 | 0.62 (–) | 0.20 (–) | 0.08 (–) |
| | | 2018 | 0.22 (–) | 0.13 (–) | 0.31 (–) |
| | | 2020 | 0.01 | 0.01 | 0.03 |

The spring 2017 and autumn 2018 surface salinities were close to the decadal average (Figure 25b); both time series showed multiple rapid decreases that closely coincided with increased outflow from the River Tamar. Figure 26 shows the Tamar flow was below the decadal average (without large spike increases) for both spring 2017 and autumn 2018, likely because the spikes are a frequent non-routinely occurring event in the data set, and that the majority of increased Tamar flow is because of increased rain activity. River Tamar flow data was accessed from the Gunnislake station (50.531° N, -4.222° E) (Environment Agency; environment.data.gov.uk/hydrology/station/575d64ff-3205-4213-abe9-ed455d9bc49f) and rain data was accessed from the PPAO met station (filtered to reduce the effect of sea spray: wind speed <22 m s$^{-1}$, relative humidity >80 % if wind speed between 15–22 m s$^{-1}$) (Yang, 2021). The increased river flow rate during higher rainfall means the periods of increased flow will have higher terrestrial DOM concentrations because of increased terrestrial runoff. No change in VOC production was observed during low salinity events when increased terrestrial DOM is transported into coastal waters (low correlation, see Table 17). Therefore, terrestrial humic-like DOM is unlikely to be a significant part of the precursor DOM pool for heterogeneous VOC production discussed here. This is expected because the currently available literature data shows clear mechanisms for fatty acid-like compounds (Zhou et al., 2014) (more straight chain carbon compounds) produced in situ by marine organisms. In the 2017 data, a medium strength relationship was shown for surface turbidity – a measure of suspended particles – which, considering no relation with terrestrial runoff has been observed, typically suggests resuspension events from the benthic environment in shallow water. However, as the L4 water column is strongly stratified in the spring, the turbidity is likely a proxy for biological activity and the consumption of VOC precursors (the relationship is negative).
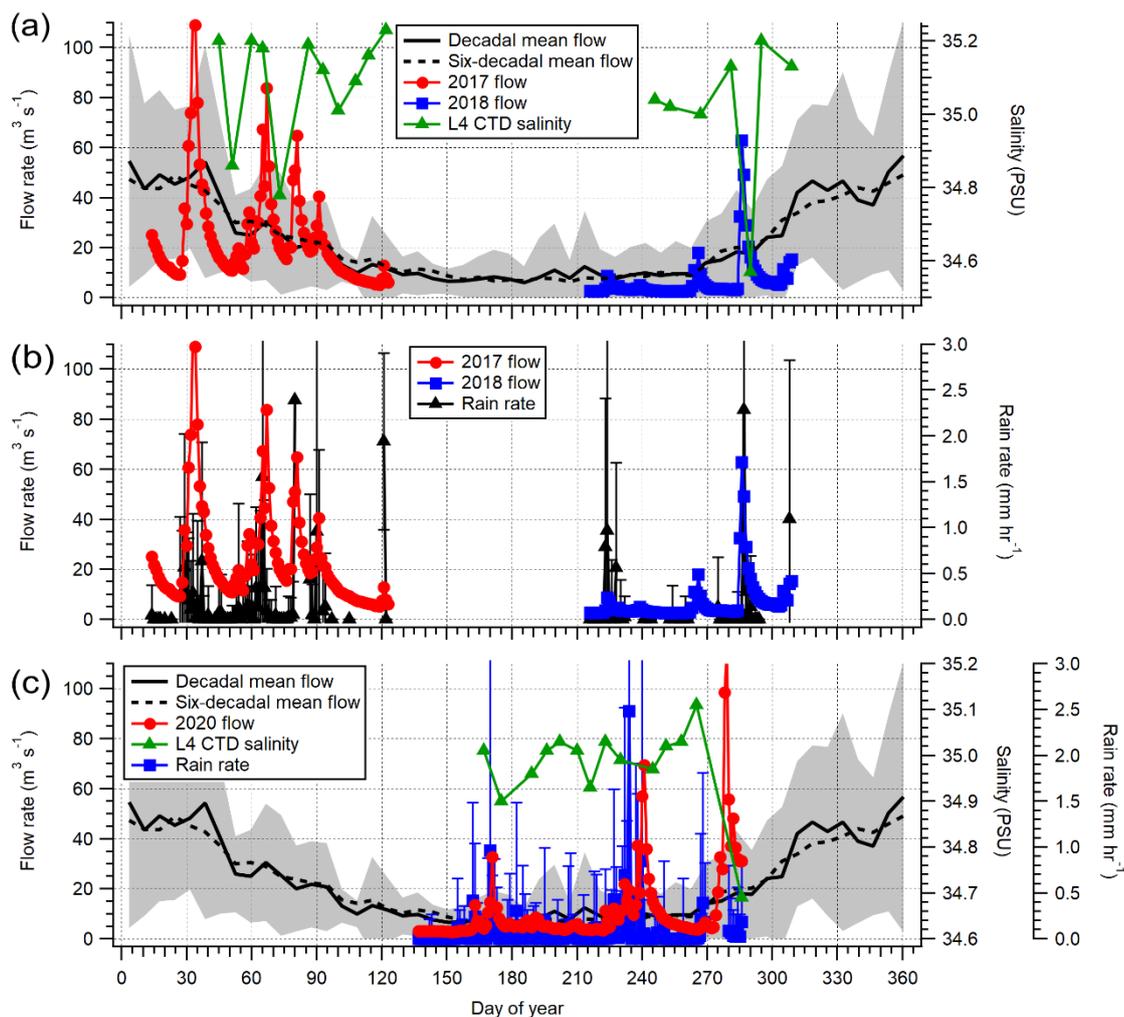
**Figure 26: Daily average flow data over the measurement campaigns compared with (a) weekly (2017 & 2018) binned Tamar River flow rate (Gunnislake Station, SX47F051) from decadal (2009–2019) and six-decadal (1969–2019) averages (the shaded region is 1σ of decadal average) with salinity values from sampled seawater (2017 & 2018), (b) daily average rain rates at Penlee Point Atmospheric Observatory and (c) weekly binned Tamar River flow rate, sample salinity and rain rate for 2020.**

The annual cycle of chlorophyll *a* concentration (Figure 25c) is highly variable because of the multiple annually occurring biological processes (hence the large $\sigma$), which includes two algal blooms (Smyth et al., 2010), that vary in terms of initiation time, dominant species and also duration. It is however clear to see the spring 2017 and autumn 2018 concentrations by pigment fluorescence (laboratory measurement) followed the decadal average. The summer 2020 concentrations by in situ CTD fluorescence were noisier than the previous campaigns, likely because of a change in methodology compared with the more precise laboratory fluorescence, and also were slightly lower than the decadal average. The lower chlorophyll *a* uncertainty between Nov–Mar on the decadal average is because of (1) limited buoy data and (2) less biofouling, which both lead to less overall annual (winter) variability. Chlorophyll *a* concentration showed medium strength positive correlation with $P_{VOC:O_3}$ (Table 17) especially for acetone and isoprene in spring 2017 and autumn 2018 (L4 surface in situ sensor). Here chlorophyll *a* is a proxy for a biological component in the DOM pool. In all campaigns, acetaldehyde showed a weak correlation with chlorophyll *a*. The difference in correlation of acetone and isoprene, compared

to acetaldehyde, suggests acetone and isoprene might be produced from similar precursor DOM while the acetaldehyde precursor is unique.

The annual cycle of CDOM (Figure 25d) is less variable than chlorophyll *a*. Two methods are used, fluorescence from in situ L4 buoy measurements and laboratory absorption measurements (Tilstone, 2009). The annual mean values were 4.0±3.1 QSU for fluorescence (2009–2019) and 0.077±0.046 m$^{-1}$ for absorption (2002–2009). No CDOM fluorescence measurements were available during production experiments because the buoy optical sensor was biofouled. In Figure 25d, a clear summer bloom peak is apparent (DOY 215–235) in the absorbance data that started and ended quickly. This appeared to happen on ~five occasions in the 8 year data set, in the few weeks before autumn 2018 measurements and in the middle of the summer 2020 measurements, which indicates strong interannual variability that probably depends on the dominant phytoplankton. High CDOM in autumn and low CDOM in the summer might suggest why isoprene production was significantly higher in the autumn measurements.

Strong to medium strength correlations were observed for inorganic nutrients (Table 17), with a clear relationship for acetone and isoprene, and weak/negligible for acetaldehyde. Nitrite, nitrate, silicate and phosphate generally exhibit negative correlations with $P_{VOC:O_3}$, which makes sense considering these nutrients are consumed for biomass growth by silicious diatoms in the spring and coccolithophores in summer in the Western English Channel (Smyth et al., 2010). The summer bloom is dominated by coccolithophores (e.g. *E. huxleyi*), because they survive the spring silicon depletion (Egge and Aksnes, 1992), however strong annual variation in cell concentration is shown (Widdicombe et al., 2010). On the other hand, ammonia shows a strong positive correlation with $P_{VOC:O_3}$ in the spring 2017, medium positive correlation in autumn 2018 and no correlation in summer 2020. Similar to ammonia was the positive weak–medium strength relationship with dissolved O$_2$ concentration.

High wind speed has been shown to enhance surface enrichment of surfactants (Wurl et al., 2011; Mustaffa et al., 2018), with stronger correlations from wind speed history (6 h before sampling), which is thought to occur by increased bubble scavenging of bulk surfactants by breaking waves. Considering sampling here occurred at ~2 m, a relationship of $P_{VOC:O_3}$ with wind speed could potentially hint at VOC DOM precursors. Surface in situ wind speed showed a positive medium relationship for acetaldehyde in autumn 2018, which increased slightly when the wind speed 6 h before was tested (Table 17). Whereas the acetaldehyde relationship was positive in autumn 2018, the relationship was negative in spring 2017. A positive medium relationship was only shown for isoprene when the wind speed 6 h before was used; no relationship was seen with in situ wind speed. Acetone showed medium negative strength relationships with varying wind times (spring 2017 6 h before and autumn 2018 in situ) but also weak/no relationships as well (spring 2017 in situ and autumn 2018 6 h before). Negative relationships observed for acetone can be due to increased stripping of DOM leading to a separation of organics by their surfactant activities. This is evidenced by strong to moderate

negative relationships with rosette sampling depth (Table 17) which implies surface organic gradients. Deeper sampling was on average associated with reduced $P_{VOC:O_3}$, implying near-surface (<2 m) gradient in DOM. This may be because the precursor DOM was surface active. On the other hand, high wind speed has also been shown to deepen the mixed layer depth (MLD) in a shallow stratified sea (Lincoln et al., 2016) which would dilute the near-surface DOM or entrain DOM from depth. Positive strong and moderate–weak correlations were observed for acetone and isoprene $P_{VOC:O_3}$, respectively, with MLD in spring 2017. Furthermore, negative strong correlations were observed for acetaldehyde and isoprene and a moderate–weak correlation was observed for acetone in autumn 2018. No correlation was observed for acetaldehyde in spring 2018 or any VOC in summer 2020. The L4 water column is strongly stratified in the spring and weakly/not stratified in the autumn, therefore increased production in the autumn could be due to increased mixing which brought deep DOM to the surface, while reduced production in the spring could be due to increased mixing which brought diluting DOM-depleted water to the surface. Importantly, as each VOC experienced unique relationships with in situ wind speed and wind speed 6 h before, this is further evidence that each VOC has a unique DOM precursor.

Finally, weak negative correlations were observed for the duration between seawater sampling and VOC production measurement. As already mentioned, 59 % of experiments were run within ~3 h of sampling and 94% were within 24 h, thus DOM loss due to biology in the sample was minimal.

**Table 18: Summary of Western Channel Observatory data. n/a means no data available.**

| Value | Pre-bloom | Bloom | Early summer | Late summer | Autumn |
|---|---|---|---|---|---|
| L4 temperature (° C) | 9.8±0.2 | 11.0±0.4 | 15.7±1.7 | 16.0±0.8 | 15.3±0.9 |
| L4 salinity (PSU) | 35.1±0.2 | 35.1±0.1 | 35.0±0.1 | 35.0±0.1 | 35.01±0.2 |
| L4 transmission (%) | 87.9±6.0 | 91.5±1.9 | 88.9±6.1 | 86.9±4.5 | 86.3±7.8 |
| L4 turbidity | 1.1±0.2 | 0.6±0.4 | n/a | n/a | 24.9±0.1 |
| Tamar flow rate ($m^3$ $s^{-1}$) | 28±17 | 12±8 | 16±4 | 18±25 | 7±9 |
| PPAO rain rate (mm $hr^{-1}$) | 0.09±0.25 | 0.26±0.35 | 0.06±0.14 | 0.07±0.17 | 0.11±0.45 |
| L4 fluorescence | 0.17±0.02 | 0.17±0.02 | 0.92±1.13 | 1.34±0.64 | 1.0±0.2 |
| L4 chlorophyll $a$ (µg $L^{-1}$) | 0.9±0.3 | 1.8±0.8 | n/a | n/a | 0.4±0.4 |
| L4 oxygen (µM) | 258±3 | 276±11 | 254±13 | 221±26 | 241±8 |
| L4 nitrite (µM) | 0.23±0.08 | 0.16±0.09 | 0.12±0.08 | 0.40±0.46 | 0.48±0.34 |
| L4 nitrate (µM) | 6.2±1.1 | 2.4±1.8 | 0.6±0.2 | 1.3±1.3 | 2.0±1.6 |
| L4 ammonia (µM) | 0.14±0.06 | 0.34±0.34 | 0.50±0.46 | 0.29±0.17 | 0.49±0.42 |
| L4 silicate (µM) | 3.3±0.4 | 1.7±0.9 | 0.8±0.4 | 2.5±1.0 | 2.3±0.7 |
| L4 phosphate (µM) | 0.45±0.02 | 0.26±0.09 | 0.11±0.06 | 0.14±0.08 | 0.27±0.14 |
| L4 iodide (nM) | 101.3±10.0 | 99.5±3.2 | n/a | n/a | n/a |

### 3.3.2.  Added compound production

In the following experiments, I describe results where different reactants were added to aged seawater or samples of seawater in the bubble column. Organic compound addition (algal culture and fatty acids) was used to probe potential DOM precursors, while I⁻ addition was used to study the effect of competition with DOM towards reactions with $O_3$. Additional experiments not important for discussion can be found in Appendix A.

### 3.3.2.1. Algal (*Emiliania huxleyi*) culture

Experiments conducted by Chen (2017) with the addition of cultured (senescent) *E. huxleyi*, a coccolithophore, showed increasing VOC peak height and $P_{VOC:O_3}$ with increasing addition of algal culture (Figure 27). The peak height production of acetone and acetaldehyde here is similar in magnitude to the time series experiments. The 20 mL culture addition showed similar peak heights to those observed in the spring bloom period, while the 5–10 mL additions were similar to the rest of the seasonal periods. This result shows that some of the DOM released from *E. huxleyi* (and probably other marine algae) are among the main precursors for acetone and acetaldehyde productions from the O₃ reaction, consistent with the cultured diatom SML samples from Schneider et al. (2019). High molecular weight DOC typically makes up ~2.5 % of the total organic carbon in a mature *E. huxleyi* culture (Aluwihare and Repeta, 1999). The results presented here are also consistent with the time series measurements (Section 3.3.1) that suggest heterogeneous production of acetone and acetaldehyde are of autochthonous biological DOM origin and are not formed from terrestrial originating DOM. In contrast to acetone and acetaldehyde, additions of *E. huxleyi* culture showed only a minor response in isoprene production compared to the natural L4 seawater samples.
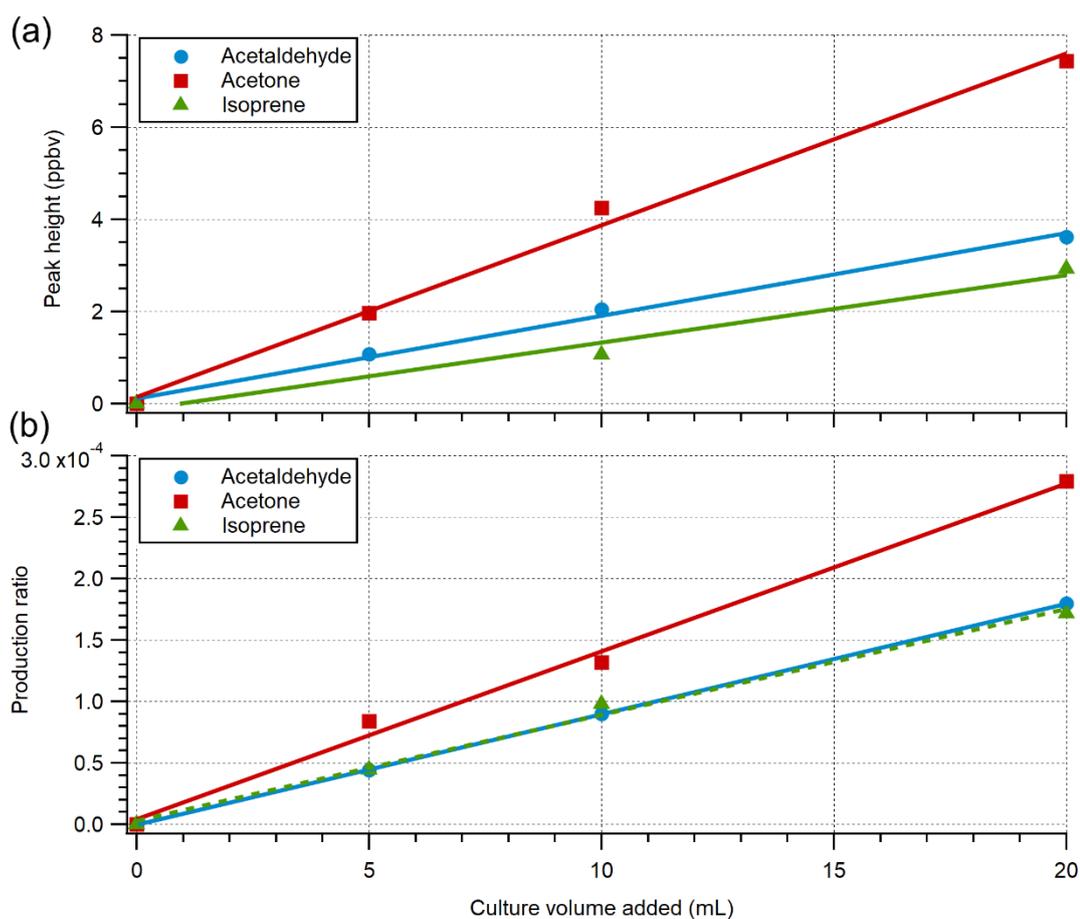


**Figure 27: VOC a) peak height and b) production ratio due to ozone heterogeneous oxidation from the addition of an *Emiliania huxleyi* culture diluted in aged seawater. Aged seawater from the Western Channel Observatory L4 station. Data from Chen (2017).**

The $P_{VOC:O_3}$ of all three VOC were lower using the *E. huxleyi* culture, especially for isoprene, compared to natural samples. The added DOC concentrations in the sample water were ~170 and ~690 µmol L$^{-1}$ for the 5 mL and 20 mL algal culture additions respectively (extrapolated from 2–6 mg L$^{-1}$ *E. huxleyi* additions; Chen, 2017). In comparison, DOC concentrations in surface L4 waters were ~260 µM for the spring bloom, as measured by Chen (2017), which shows the DOM concentration should have been high enough, especially for the 20 mL addition.

The *E. huxleyi* algal culture experiments resulted in fairly low isoprene $P_{VOC:O_3}$. *E. huxleyi* was clearly capable of producing isoprene precursor DOM (i.e correct class of compounds), however not in the abundance seen in the natural seawater. This could be either because (1) *E. huxleyi* releases limited isoprene precursor DOM in the senescence stage (i.e. greater DOM release during grazing or cell lysis), (2) another algal species dominated in autumn 2018, or (3) natural ageing processes to labile DOM might be necessary to achieve an abundance of isoprene precursor DOM. For point (2), the summer WCO bloom is dominated by dinoflagellates (*Karenia mikimotoi*, *Prorocentrum minimum / balticum*) or cocolithophores (*E. huxleyi*) (Pingree et al., 1975; Smyth et al., 2002; Widdicombe et al., 2010), thus the dinoflagellates might be the cause, especially in the period of these measurements. Schneider et al. (2019) observed the production of *m/z* 69 in their work with cultured diatom SML samples therefore isoprene precursor DOM may be very specific to phytoplankton functional type. Point (3) arises because the DOM produced from the cultured senescent algae is essentially fresh and had minimal time to age/degrade.

### 3.3.2.2. Fatty acids

Fatty acids are a known (but minor; Section 1.3.2) component of the SML (Momzikoff et al., 2004; Triesch et al., 2021) and nonanoic acid (an oxidation product of oleic acid) can be used as a proxy (Ciuraru et al., 2015a). Experiments conducted by Chen (2017) with the addition of nonanoic acid and oleic acid showed variable productions of the three VOCs. The saturated nonanoic acid was shown to produce an approximately equal proportion of acetaldehyde and isoprene (Figure 28), however minimal acetone was produced. Acetaldehyde and acetone showed good linearity to increasing surface concentrations of nonanoic acid (r$^2$>0.94 for acetaldehyde, 0.92 and 0.76 for acetone peak height and $P_{VOC:O_3}$ respectively), whereas isoprene showed more variance around the linear trend (r$^2$=0.47 and 0.28 for isoprene peak height and $P_{VOC:O_3}$ respectively).
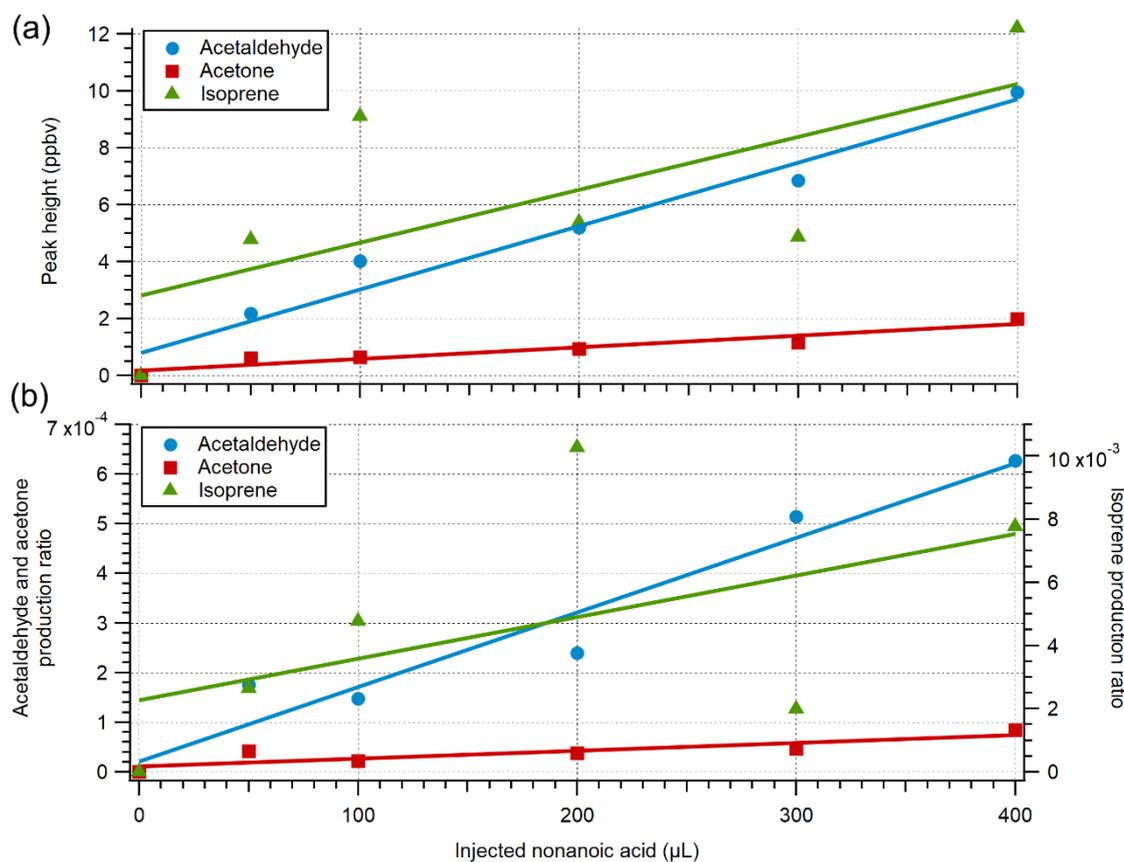
**Figure 28: VOC a) peak height and b) production ratio from the addition of nonanoic acid to aged seawater (1.2 L) using ozone heterogeneous oxidation. Aged seawater from the Western Channel Observatory L4 station. Data from Chen (2017).**

The unsaturated oleic acid was shown to produce extremely high quantities of isoprene and minimal amounts of acetaldehyde and acetone (not shown). The isoprene $P_{VOC:O_3}$ for 0.3 and 1 µL addition of oleic acid were 0.83 and 0.78, respectively, to produce peak heights >2.5 ppmv. Peak isoprene concentrations during the air purge phase were >700 ppbv, suggesting oleic acid contained isoprene as a contaminant, thus the true production of isoprene during ozonolysis is uncertain. The minimal production of acetaldehyde and acetone could be due to the formation of nonanoic acid as a minor product of the Criegee biradical reaction from the primary ozonide of oleic acid (Katrib et al., 2004).

### 3.3.2.3. Iodide

I$^-$ and DOC have approximately equal reactivities with $O_3$ (Martino et al., 2012), therefore I$^-$ is expected to compete with DOM to quench $O_3$-driven VOC production. I$^-$ should also compete with all oxidisable species, however, the reactivities of individual small organic species like DMS, ethene and propene are much lower (Chang et al., 2004). Experiments with changing I$^-$ concentration caused a lower rate of DMS oxidation with higher concentrations of I$^-$ (Figure 29a). No effect was observed for the rate DMS was stripped from the seawater, as expected. The oxidation of I$^-$ occurs as a surface reaction at the air–sample interface (Reeser and Donaldson, 2011) or a reaction within the aqueous phase (Carpenter et al., 2013), while the $O_3$–DMS reaction is predominantly in the aqueous phase. The addition of I$^-$ depleted $O_3$, which meant less $O_3$ was available to oxidise DMS. Apart from the 50 nM spike measurement, good

linearity/reproducibility was shown between sequential measurements of 1.2 L seawater. This increases confidence in the reproducibility of the methodology used in the production experiments.
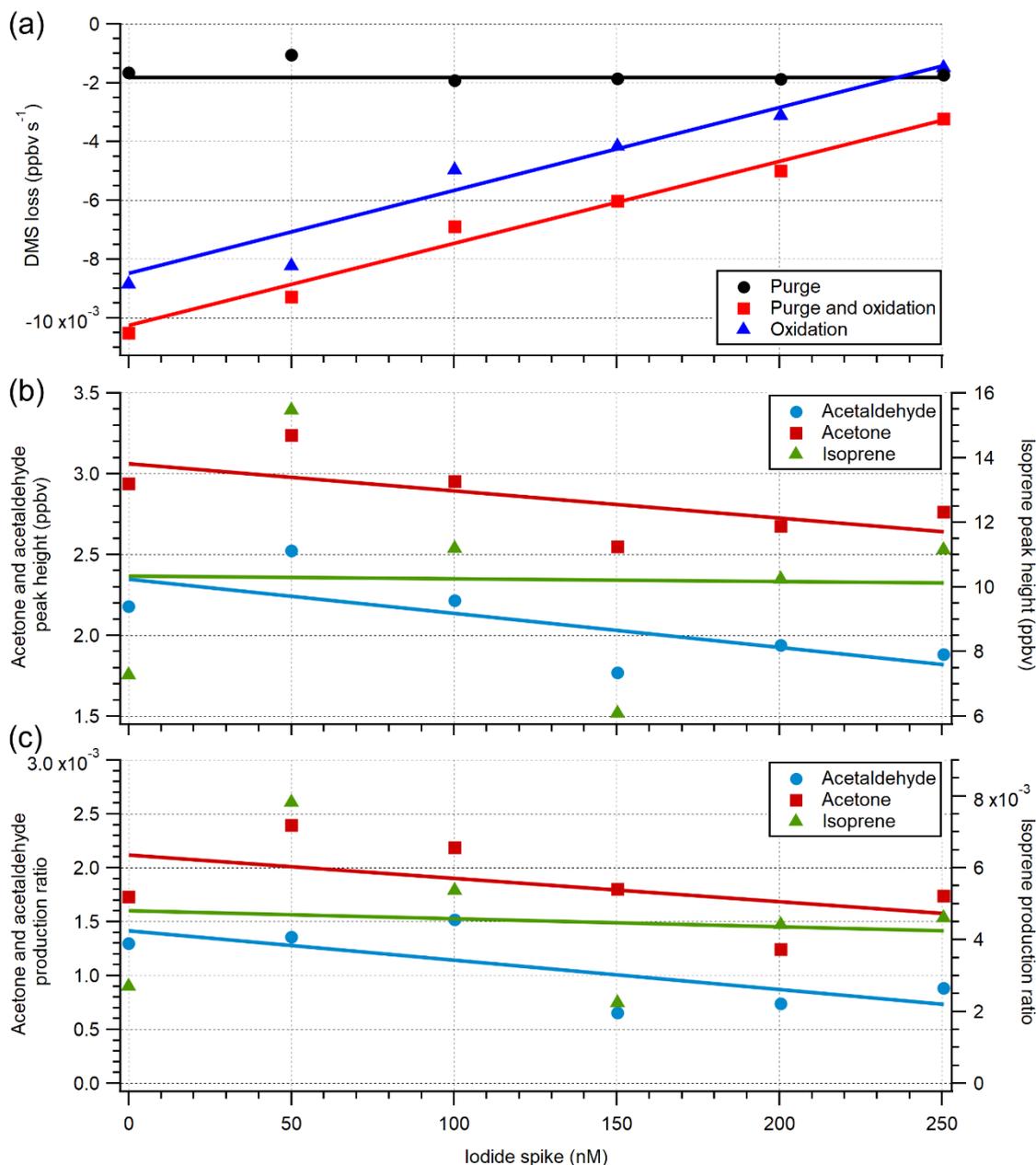


**Figure 29: The effect of injected iodide in natural seawater on (a) DMS loss rates, (b) VOC peak height and (c) VOC production ratio. The oxidation loss rate is calculated as the difference between the observed purge rate and the total (purge + oxidation) rate.**

Similar to the changing $O_3$ concentration experiment (Section 3.3.1.1), the $O_3$–DMS aqueous rate constant was used to calculate the amount of $O_3$ reacting with DMS. Assuming full uptake of $O_3$ to the sample, a 1176±44 ppbv gaseous concentration equated to 11.2±0.4 nM $O_3$ aqueous concentration ($C_a/H$). The initial concentration of available $O_3$ to react with aqueous DMS was calculated to be $1.1 \times 10^{-4}$ and $1.8 \times 10^{-5}$ nM for the 0 and 250 nM I$^-$ spike respectively (the remaining spikes fit linearly between these values). Again, these very low $O_3$ concentrations show either extreme loss at the bubble interface (i.e. DOM for VOC production) or the importance of other $O_3$ destroying species in the seawater sample.

The produced VOC data appears noisier compared to the DMS measurement, but because of the good reproducibility shown with the DMS measurements (from the same samples) the variability in VOC production is most likely a result of variability in the replicate seawater samples or complex mechanism not captured by the simple peak data. Generally, peak height and $P_{VOC:O_3}$ decreased slightly with increasing $I^-$ for acetaldehyde and acetone (Figure 29c; $r^2$=0.50 and 0.25 respectively), which suggested the reactions that produce them have competition with $I^-$ and are therefore either interfacial or aqueous layer reactions. Interfacial reactions seem more likely considering the overall large rate of reaction along with the mechanism fit (curve matching) in Section 3.3.1.1. The overall trends for isoprene suggested isoprene production was not influenced by $I^-$ addition, though the large variability may be masking the true trend. Strong correlations between peak gradient and peak height were observed in this experiment, especially for isoprene, which was why peak height and production trends were so similar. This was expected considering the organic precursors, injected $O_3$ concentration and column mechanics were unchanged between repeat measurements. Importantly, across the full range of $I^-$ concentrations studied here (which exceeds the natural $I^-$ concentration range at L4 by ~100 nM), the sensitivity in VOC production is fairly weak (gradient statistically similar to zero). Thus no correction to VOC production data by $I^-$ concentration is necessary.

### 3.3.2.4.  Nominal organic matter

Marine DOM is a complex mixture of high molecular mass organic species that are typically sourced through in situ biological processes, thus the composition of DOM is highly temporally and spatially variable (Aluwihare and Repeta, 1999; Bodineau et al., 1999; Shimotori et al., 2016; Carr et al., 2019; Hansell et al., 2021). No commercially available certified DOM is available, however, NOM sourced from the Suwannee River is expected to be very similar between repeated standardised batches (IHSS, 2020), therefore repeatable experimentation is possible. Experiments conducted by Chen (2017) with the addition of NOM using an $O_3$ input concentration of ~9 ppmv showed negligible production of acetaldehyde, acetone and isoprene. This is further evidence that the VOC precursor DOM is of in situ biological origins because Suwannee River NOM is more unsaturated (contains more humic-like substances) and dominated by terrestrial/riverine DOM (Benner, 2002; Martino et al., 2012). The experiments did show, however, that increasing NOM concentration substantially increased the $O_3$ uptake (e.g. reduced the concentration of $O_3$ in the headspace 5 min after addition; Figure 30a), which shows that the higher degree of unsaturation in the NOM does increase $O_3$ reactivity. The ratio of $O_3$ in the headspace ($O_3$ out / $O_3$ in) initially decreased linearly at low NOM concentration, where the reactions are largely reactant limited. The ratio of 0.124 observed at 0 mg $L^{-1}$ NOM was likely due to other $O_3$ destroying species (i.e. $I^-$) present in the aged seawater and also the dissolution of $O_3$ in water. At high NOM concentration, the ratio decreases and approaches zero (plateau observed at 0.008), where the reactions are largely limited by $O_3$ input. The reaction shifted between the two regimes and was dependent on multiple reagents around ~6 mg $L^{-1}$. Due to the presence of other $O_3$ destroying

species, the reaction was never fully NOM limited. Further experiments with a static NOM concentration (6 mg L$^{-1}$) (Figure 30b) showed low sensitivity in O$_3$ uptake towards O$_3$ concentration below 18 ppmv. Here the plateau at low concentration had the same 0.008 ratio as the NOM curve (>6 mg L$^{-1}$). Due to a lack of data points between 17–21 ppmv, the true trend in this region is uncertain.
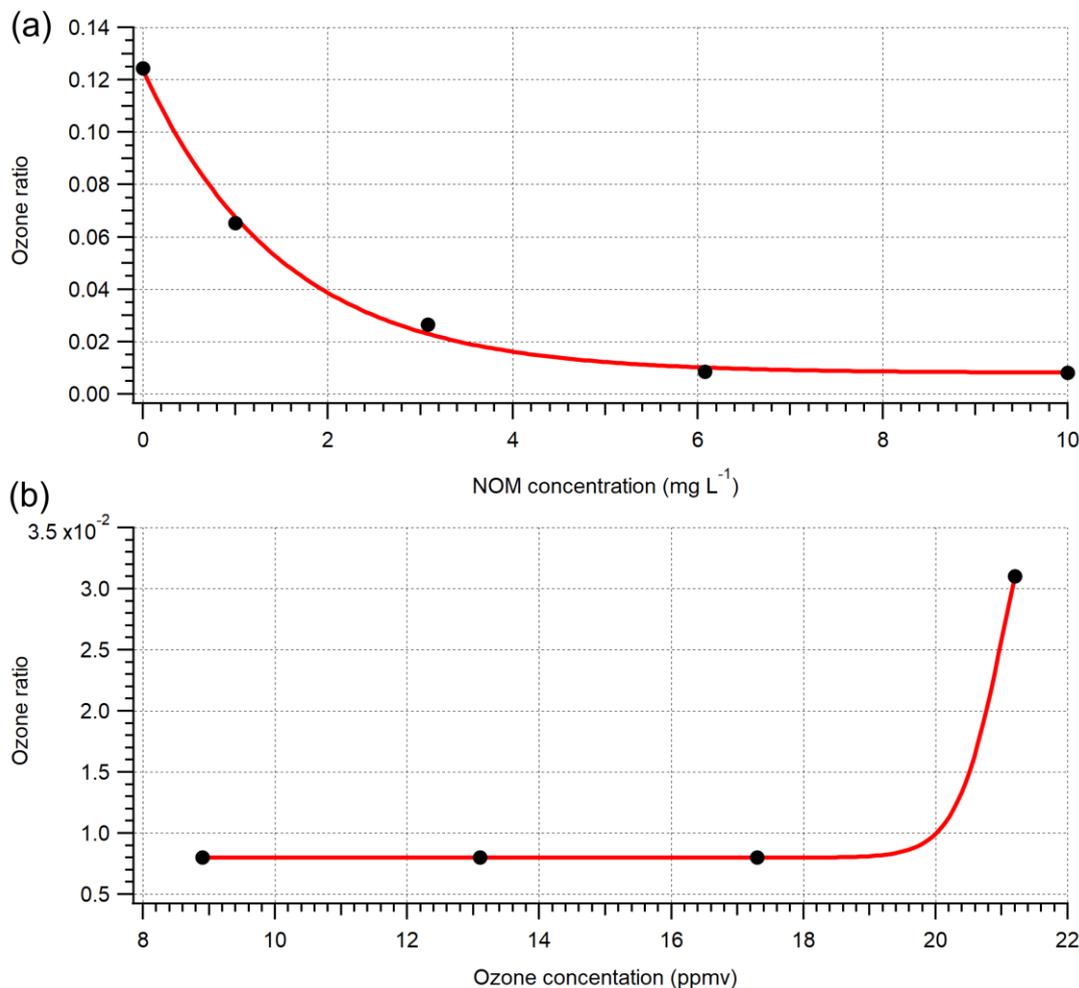


**Figure 30: The effect of increasing (a) NOM concentration and (b) ozone input concentration on the ratio of ozone leaving the column headspace (ozone out / ozone in) after 5 minutes. NOM dissolved in aged seawater from the Western Channel Observatory L4 station. O$_3$ input was 9 ppmv in panel (a) and NOM concentration was 6 mg L$^{-1}$ in panel (b). Data from Chen (2017).**

### 3.3.3.  Production significance

### 3.3.3.1.  Surface turbulence

To understand the significance of the laboratory measurements, it is necessary to consider the similarities and differences between the bubble column air–sample interface and the realistic ocean air–sea interface. I use this information to scale the laboratory measurements to the global ocean.

Literature over the last two decades has shown surface reactions of O$_3$ and aqueous species ($A_g + B_{aq} \rightarrow C$), especially organics, follow a Langmuir–Hinshelwood mechanism (Mmereki et al., 2004; Raja and Valsaraj, 2005; Clifford et al., 2008; Sakamoto et al., 2009; Reeser and

Donaldson, 2011), which for two species can be modelled following Equation 9a–c. The ratio of surface equilibrium constants can be expressed in the form;

$$R_X = \frac{1}{C_{X,\text{bulk}}} \exp\left(-\frac{E - TS}{RT}\right) \qquad\qquad 25$$

where $E$ and $S$ represent the free energy and entropy, respectively, of adsorption, $R$ represents the ideal gas constant and $T$ represents temperature (Bakaev, 2004; Liu, 2009).

With organic films, $k_{\text{surf}}N_{\text{surf}}^{\text{max}}$ is on the order of $\sim 10^{-3}$–$10^{-2}$ s$^{-1}$ and $R_{O_3}$ is on the order of 300–8600 L mmol$^{-1}$ (Mmereki et al., 2004; Kahan et al., 2006; Clifford et al., 2008). For Tween 20 and Triton X-100 surfactants at an air–water interface, $R_X$ was measured as 500–3150 L mmol$^{-1}$ (Giribabu and Ghosh, 2007). Tween 20 and Triton X-100 are efficient chemical surfactants that show similar surface-tension reduction as biologically-originating surfactants (more so for Tween 20 than Triton X-100) (Ćosović and Vojvodić, 1998; Rodríguez-López et al., 2018). High $R_X$, as seen above, causes efficient organic cumulation at the interface, such that $C_{X,\text{surf}}$ is dominated by $C_{X,\text{bulk}}$ and $N_{\text{surf}}^{\text{max}}$ and not the rate of movement between the surface and the bulk. In reality there are multiple competing surfactant species in an oceanic sample, which reduces the available surface sites each species can occupy (thus all present species ratios, $\sum R_{X_i} C_{X_i,\text{bulk}}$, are to be included in the isotherm) and the resulting $C_{X,\text{surf}}$. The turbulant rising bubbles in the seawater sample act to keep the sample well mixed.

The $k_{\text{surf}}N_{\text{surf}}^{\text{max}}$ should be similar at the bubble and ocean air–water interfaces because sampled natural seawater was used in the laboratory measurements. It is important to note for clarity that in this analysis, I do not argue that bubbles in the bubble column are directly comparable to bubbles in the surface ocean (i.e. equal bubble size spectra and the volume of bubbles per unit time, although the two are similar). Rather, the area of bubbles in the bubble column can transform – like a 3D shape net – to equal an approximately flat surface like the ocean air–sea interface. In comparisons of turbulence, Raja and Valsaraj (2005) show that the Langmuir–Hinshelwood mechanism, designed for stagnant surfaces, can be applied to falling micrometre water droplets. Thus, the application of this surface mechanism to rising bubbles should also be reasonable. Furthermore, the same turbulence that drives O$_3$ uptake in the bubble column also drives VOC emission, thus the scaling of $P_{VOC:O_3}$ to VOC flux ($P_{VOC:O_3}F_{O_3}$, see Section 3.3.3.4) is valid. $k_{\text{surf}}$ and $R_X$ (Equation 25) will likely have some temperature dependence but these effects should be minor, as the maximum possible difference between the laboratory and L4 water was relatively small (3.5 % in units of K).

The key mechanism that may drive differences between the two systems is how DOM accumulates at the air(bubble)–sample interface and at the real air–sea interface (i.e. the oceanic SML). SML thickness is approximately 1–1000 μm (Engel et al., 2018) (depending on the solubility of organics) which is very large relative to interfacial monolayers of organics (~0.7 nm; King et al., 2020). As such, the $C_{X,\text{bulk}}$ term in Equation 9c maybe more comparable to the SML itself and not the true bulk ocean (underlying water). A static laboratory seawater sample does

not efficiently form a SML because of a lack of mixing or scavenging by rising air bubbles. In this case, the only mode of organic regulation at the interface is by a Langmiur isotherm (Langmuir–Hinshelwood mechanism) from the bulk sample. Conversely, at the ocean surface, multiple mechanisms drive the enhancement of organic concentration at the surface to form a SML from which a Langmiur isotherm would pool organic (bulk) material from to produce a monolayer at the interface. This is a potential issue to be considered in these experiments since seawater samples were collected at a mean depth of 1.8±0.3 m and not using a surface technique; thus, a scaling factor should potentially be applied.

### 3.3.3.2. Surfactant enrichment and L4 organic concentration

To further understand the significance of the laboratory measurements, the bubble column samples and the realistic SML must be shown to observe the same concentration of seawater organics/DOM.

DOM (e.g. carbohydrates, proteins, and lipids) in the global oceans is typically increased in the SML by an enrichment factor (EF = $C_{X,SML}/C_{X,bulk}$) of 0.5–6, with mean nearshore and oceanic EFs of 1.9±1.1 and 2.7±1.3 respectively (Wurl et al., 2011); medium to high wind speed (average of 6 h before) appears to increase these EFs. A statistical difference between enrichment was only observed when average wind speed, 6 h before sampling, was tested, which suggested wind history played a role in enrichment. In the North and South Atlantic Ocean, the mean EFs were 2.0±0.8 and 1.5±0.7 (AMT-24, 2014) and 1.8±0.7 and 1.5±0.5 (AMT-25, 2015) respectively (Sabbaghzadeh et al., 2017). EFs in oligotrophic, mesotrophic and eutrophic waters do not correlate with SML surfactants concentration, which is thought to be due to the nature/source of the material; oligotrophic, mesotrophic and eutrophic waters have mean EFs of 2.7±1.3, 2.0±1.0 and 1.7±0.8, respectively, and mean SML surfactant concentration of ~320, ~500 and ~660 μg L$^{-1}$, respectively (Wurl et al., 2011). Wurl et al. (2011) map global EFs, predicted from satellite primary production data and shows the majority of the ocean has EFs >1.5, with the highest EFs in the region encompassing the tropics and subtropics. The contribution of the ocean at each latitude to the overall ocean area is calculated using data from Kossinna (1921); tropical zone = 0–23.5°, subtropical zone = 23.5–40°, temperate zone = 40–60° and cold zone 60–90° where zones are symmetrical around the equator. The region encompassing the tropics and subtropics (-40–40° N) accounts for ~67 % of the ocean surface, thus the majority of the ocean surface has a high (>1.5) EF. Generally, the EFs in this region are constant all year around, apart from higher coastal EFs in the spring. The region north of the northern subtropics generally has an EF of 1–2 for the majority of the year (EF of 1 in the spring) while the subantarctic water ring (SANT) and Antarctic biogeochemical provinces have no enrichment all year round. The same EF map predicts the WCO (or specifically the NECS) has EFs between 1.5–2, thus the important conclusion here is that L4 waters have similar EFs to those seen in the global oceans.

While it is clear DOM is enhanced in the SML, the underlying bulk waters at L4 and in the ocean must be shown to be similar. Furthermore, there is no certainty that the DOM available for

VOC production is hydrophobic or scavenged by rising bubbles, therefore comparisons between other ocean carbon pools are made.

Moderate strength relationships were shown for DOC concentration and $P_{VOC:O_3}$ (Section 3.3.1.4). Global estimations for surface DOC concentration in the Atlantic Oceans show increased concentrations near the equator (-20–20° N; 75–90 µmol kg$^{-1}$) because of coastal upwelling on the west coast of Africa (Romera-Castillo et al., 2016). The region from north of the tropics to the artic (20–90° N) is reasonably homogeneous in DOC (60–70 µmol kg$^{-1}$), likewise for the region between the tropics and SANT (-20–-40° N). The SANT and further south to the Southern Ocean have the lowest DOC concentrations (-40–-90° N; 40–55 µmol kg$^{-1}$). Following on with a similar ocean area analysis as above, the majority of the surface ocean (northern cold to southern subtropics; ~79 % ocean area) has DOC concentrations in the range 65–85 µmol kg$^{-1}$. Here the Pacific Ocean and the Indian Ocean are assumed to follow similar latitudinal trends as the Atlantic Oceans because similar in situ concentrations are observed (Ogawa and Tanoue, 2003). Multi-year measurements at L4 (2011–2014) had an average surface DOC concentration of 120±43 µM (Tapin, 2014), while measurements at the end of the 2017 spring phytoplankton bloom had an average of 257±33 µM (Chen, 2017). A large range of DOC concentrations was measured in the central English Channel (40–200 µM; Bodineau et al., 1999), over a transect from England to France, with the highest concentrations from a mixture of terrestrial origin, resuspension events and a spring phytoplankton bloom. These high concentrations were not seen in other measurements around the western English Channel (Banoub and Williams, 1973; Carr et al., 2019), which were approximately 50–90 µM, possibly because they were further offshore or diluted with strong water movements. The L4 DOC measurements suggest L4 is on average ~70 % (range of 20–300 %) higher than ~79 % of the ocean surface.

Similarly, moderate strength relationships were shown for chlorophyll $a$ concentration and $P_{VOC:O_3}$ (Section 3.3.1.4). Global estimates for chlorophyll $a$ show oceanic concentrations are generally 0.01–0.20 µg L$^{-1}$ (-35–45° N; ~65 % of ocean surface) (McClain, 2009) because of the strongly chlorophyll $a$ depleted gyres. The northern temperate zone typically has chlorophyll $a$ between 0.25–2.50 µg L$^{-1}$ with the highest measurements (~5 µg L$^{-1}$) at the coast. The southern temperate zone is similar to the gyres with 0.10–0.25 µg L$^{-1}$. No information is given for the cold regions, which are assumed to match their respective temperate zones. A long multi-year time series (1992–2019) showed the mean L4 surface chlorophyll $a$ concentration was 1.34±1.29 µg L$^{-1}$ (Airs, 2010); uncertainty decreases to 0.04 µg L$^{-1}$ when using $\sigma_{\bar{x}}$ ($n$=1084). The latter 10 yr of the data series showed a slightly reduced concentration of 1.04±0.92 µg L$^{-1}$ which was shown statistically different (t-test, p=2×10$^{-7}$, $n$=473). These chlorophyll $a$ results suggest L4 is on average ~300 % (range of 70–9900 %) greater than the open ocean at -35–45° N.

Global estimates for CDOM, known to be a small component of the DOM pool, show the lowest absorption coefficients in the region encompassing the tropics and subtropics (-40–40° N; ~67 % of ocean surface) with values of 0.005–0.025 m$^{-1}$ (Nelson and Siegel, 2013). The open-

ocean region north of the northern subtopics had an absorption of ~0.04 m$^{-1}$, while the region south of the southern subtropics had an absorption of ~0.03 m$^{-1}$. The highest CDOM absorption was estimated for the coastal regions; this is potentially due to substantial terrigenous inputs of detrital particulates that contribute a significant fraction of absorption (Nelson and Siegel, 2013). In the estimates by Nelson and Siegel (2013), the L4 water (NECS) had an absorption of 0.05–0.10 m$^{-1}$, which was similar to direct measurements of 0.077±0.046 m$^{-1}$ over a multi-year campaign (Tilstone et al., WCO data); these CDOM values are on average ~670 % (range of 100–1900 %) higher than the ocean at -40–40° N.

It is unclear whether DOC or CDOM is an appropriate estimate for DOM reactants that lead to the production of the VOCs measured here if the concentrations at L4 are easily biased towards terrestrial inflow considering no correlation between terrestrial output and VOC production was seen (see Section 3.3.1.4).

### 3.3.3.3.   Ozone deposition to the global ocean

Multiple literature sources provide estimates for the global oceanic dry deposition flux of tropospheric $O_3$. Ganzeveld et al. (2009) estimated a dry deposition of 280–300 Tg yr$^{-1}$, using variable $v_d$ when solely investigating the influence of the ocean, while Hardacre et al. (2015) estimated 250–591 Tg yr$^{-1}$ and 209–538 Tg yr$^{-1}$, using two different data sets for land coverage. The large range in ocean deposition from Hardacre et al. (2015) is due to large temporal and spatial uncertainty across an ensemble of models. Luhar et al. (2018) and Pound et al. (2020) estimate lower deposition of 98±30 Tg yr$^{-1}$ and ~122 Tg yr$^{-1}$, respectively. These estimates are lower, in part, because (1) differentiation is made between model boxes with 100 % water and mixed water/land, and (2) the parameterisations differ in approach to chemical species (point (2) discussed later, see Section 4.3.4.4). Luhar et al. (2018) add the mixed water/land deposition to the land value (624.4±82.0 Tg yr$^{-1}$), while Pound et al. (2020) separate deposition into mixed (248 Tg yr$^{-1}$) and land (386 Tg yr$^{-1}$) averages; assuming a fifth of the mixed deposition is due to water, the Pound et al. (2020) deposition lies between Luhar et al. (2018) and Ganzeveld et al. (2009). The value of a fifth was estimated from the mean $v_d$ to the oceans (0.05 cm s$^{-1}$) compared the mean to the land (0.25 cm s$^{-1}$) from Hardacre et al. (2015).

Direct measurements in the open-ocean have shown $O_3$ air–sea fluxes of ~-27.5, ~-9.3 and ~-6.6 µmol m$^{-2}$ d$^{-1}$ in the Western Atlantic Ocean, Eastern Pacific Ocean and the Southern Ocean, respectively (Helmig et al., 2012), which are 60–90 % lower than the coastal WCO measurements (-67.5 µmol m$^{-2}$ d$^{-1}$; Loades et al., 2020). Interestingly, if the Loades et al. (2020) direct measurements are scaled to the total ocean (427±11 Tg yr$^{-1}$), good agreement is shown to the average of the Hardacre et al. (2015) model ensemble (~420 Tg yr$^{-1}$; OW11 data set); this will be important later.

#### 3.3.3.4. L4 VOC measurements with heterogeneous production

As discussed in Chapter 2 (Section 2.3.3), there is a potential missing $2.5\pm1.3$ and $2.6\pm1.6$ $\mu mol\ m^{-2}\ d^{-1}$ net source of acetone and acetaldehyde respectively, as inferred by the difference between EC and TL VOC fluxes measured at PPAO in spring 2018. Over the same period of satisfactory blanking, the mean $O_3$ EC deposition flux at the PPAO in spring 2018 was determined to be $-65.4\pm4.9\ \mu mol\ m^{-2}\ d^{-1}$ ($\sigma_{\bar{x}}$ over 49 intervals; Loades et al., 2020). Scaling the average $P_{VOC:O_3}$ of the spring campaign periods using the measurements of Loades et al. (2020) results in an acetone production of 0.015 and 0.051 $\mu mol\ m^{-2}\ d^{-1}$ for the pre-bloom and bloom periods respectively. Acetaldehyde production of 0.017 $\mu mol\ m^{-2}\ d^{-1}$ was calculated for both spring periods. These $O_3$-driven production values are negligible compared to the inferred missing source; to achieve the difference here (avg: ~2.55 $\mu mol\ m^{-2}\ d^{-1}$), a much larger $O_3$ deposition flux of 6917 $\mu mol\ m^{-2}\ d^{-1}$ (using the average $P_{VOC:O_3}$ of all spring acetone and acetaldehyde measurements) or a much higher $P_{VOC:O_3}$ of 0.039 (using the Loades et al. (2020) $O_3$ flux for the end period) would be required.

As discussed in Chapter 2 (Section 2.3.2), the bulk sea-to-air emission flux of isoprene at L4 in Apr–May 2018 was 0.30 $\mu mol\ m^{-2}\ d^{-1}$. Similar scaling to the previous carbonyl calculations, however now using the full measurements of Loades et al. (2020) ($67.5\pm1.7\ \mu mol\ m^{-2}\ d^{-1}$, 342 intervals), gives an isoprene heterogeneous production of 0.060 and 0.14 $\mu mol\ m^{-2}\ d^{-1}$ for the spring pre-bloom and spring bloom periods respectively (20 and 48 % respectively of the bulk emission). Bulk emission flux during summer/autumn from L4 is not available to compare to the early summer, later summer or autumn production, which is calculated to be 0.15, 0.095 and 0.64 $\mu mol\ m^{-2}\ d^{-1}$ respectively (51, 32 and 214 % respectively of the spring bulk emission). All of these results, especially the high autumn result, are below the 3 h LOD of the EC flux system (Section 2.2.3) and thus cannot be ruled out as being too high.

#### 3.3.3.5. Extrapolations of $O_3$-driven VOC fluxes to the real world

In this section, the discussions above are used to first derive a scaling factor for a conservative approach to estimate a lower-bound $O_3$-driven VOC emission from the laboratory data (Section 3.3.1.3) and secondly to derive a scaling factor for a liberal approach to estimate an upper-bound $O_3$-driven VOC emission from the data. Both approaches are compared with the current global VOC budgets.

Listed below are the considerations and subsequent laid out assumptions for the lower-bound scaling.

- The average ocean is less productive than L4 (reduced bulk seawater organic concentration; ×0.3 [specifically $0.3\pm0.2$, $n=3$]). Here the scaling is the average of the DOC (~0.58), chlorophyll a (~0.24) and CDOM (~0.13) measurements between L4 and the majority of the ocean surface with respect to the ocean concentration.
- Organic concentration between the SML and underlying bulk water is the same (no enrichment; ×1.0). This is a conservative assumption.

- The $O_3$ deposition to the ocean is conservative (low atmospheric sink; 100 Tg yr$^{-1}$ from Luhar et al. (2018) for the open-ocean).

Now using the global $O_3$ ocean deposition instead of a directly measured deposition, Table 19 shows the extrapolated lower-bound global production of VOCs due to the $O_3$ reaction with seawater. The yields of acetone and acetaldehyde are negligible compared to the estimated net contribution of the ocean to atmospheric carbonyl burden (Wang et al., 2019, 2020a). In the case of acetone, the lack of a surface source is unsurprising since measurements in the open Atlantic Ocean during the autumn found good agreement between direct and estimated fluxes (Yang et al., 2014b).

**Table 19: Scaled production yield of the three VOCs using an oceanic dry deposition of 100 Tg yr$^{-1}$ and a coastal organic scaling factor of 0.3 compared to the mean ocean. See the main text for the derivation of these values. Units are Tg yr$^{-1}$ for mean values and % for relative standard deviations. All data is the unweighted average of all recorded production data.**

| VOC | Spr. p.-bloom | | Spring bloom | | Ea. summer | | Late summer | | Autumn | | All data | |
|---|---|---|---|---|---|---|---|---|---|---|---|---|
| | Mean | R$\sigma$ | Mean | R$\sigma$ | Mean | R$\sigma$ | Mean | R$\sigma$ | Mean | R$\sigma$ | Mean | R$\sigma$ |
| Acetald. | 0.01 | 30 | 0.01 | 20 | 0.01 | 41 | 0.03 | 18 | 0.01 | 30 | 0.01 | 0.01 |
| Acetone | 0.01 | 16 | 0.03 | 59 | 0.05 | 44 | 0.02 | 25 | 0.03 | 41 | 0.03 | 0.02 |
| Isoprene | 0.04 | 40 | 0.09 | 54 | 0.10 | 29 | 0.06 | 33 | 0.41 | 40 | 0.16 | 0.16 |

The majority of the seasonal isoprene yields here (Table 19) are below the estimated 0.31 Tg yr$^{-1}$ production from phytoplankton communities or the estimated missing source of ~1.6 Tg yr$^{-1}$ (Arnold et al., 2009). The annually averaged VOC production from $O_3$ (mean of all recorded production data across spring, summer and autumn) is similar to the phytoplankton community production, with a significant uncertainty because of the large annual variability, which is still ~90 % lower than the estimated missing source. The annual average is strongly weighted upwards due to the autumn isoprene yield which accounted for ~25 % of the estimated missing source. Importantly, using the conservative approach, the global scaled isoprene yields are not of the same magnitude as the missing remote ocean source (one magnitude below or lower).

Next, I look at the upper-bound scaling of global significance using the same discussion above (Section 3.3.3.1–3.3.3.3) to derive a scaling factor for a liberal approach. Listed below are the considerations and subsequent laid out assumptions for the upper-bound scaling.

- The average ocean is equally productive as L4 (same bulk seawater organic concentration; ×1.0). This is a liberal assumption.

- Organic concentration is higher in the SML compared to the underlying bulk water (enrichment; ×2.0). Here the scaling parameter is the average of the Wurl et al. (2011) and Sabbaghzadeh et al. (2017) oceanic EFs.

- The $O_3$ deposition to the ocean is relatively large (high atmospheric sink; 420 Tg yr$^{-1}$ from Hardacre et al. (2015) model range using the OW11 data set).

Now using the global $O_3$ ocean deposition, Table 20 shows the extrapolated upper-bound global production of VOCs due to the $O_3$ reaction with seawater. The yields of acetone and acetaldehyde are still small compared to the estimated net contribution of the ocean to the atmospheric carbonyl burden. The maximum acetone yield is 16 % of the modelled ocean sink

(-8.1 Tg yr$^{-1}$; Wang et al., 2020a) while the maximum acetaldehyde yield is 7 % of the modelled net ocean missing source (~11 Tg yr$^{-1}$; Wang et al., 2019).

**Table 20: Scaled production yield of the three VOCs using an oceanic dry deposition of 420 Tg yr$^{-1}$ and a coastal organic scaling factor of 2.0 compared to the mean ocean. See the main text for the derivation of these values. Units are Tg yr$^{-1}$ for mean values and % for relative standard deviations. All data is the unweighted average of all recorded production data.**

| VOC | Spr. p.-bloom | | Spring bloom | | Ea. summer | | Late summer | | Autumn | | All seasons | |
|---|---|---|---|---|---|---|---|---|---|---|---|---|
| | Mean | R$\sigma$ | Mean | R$\sigma$ | Mean | R$\sigma$ | Mean | R$\sigma$ | Mean | R$\sigma$ | Mean | R$\sigma$ |
| Acetald. | 0.20 | 30 | 0.21 | 20 | 0.26 | 41 | 0.79 | 18 | 0.32 | 30 | 0.35 | 66 |
| Acetone | 0.23 | 16 | 0.79 | 59 | 1.26 | 44 | 0.55 | 25 | 0.72 | 41 | 0.84 | 79 |
| Isoprene | 1.05 | 40 | 2.52 | 54 | 2.68 | 29 | 1.67 | 33 | 11.36 | 40 | 4.48 | 103 |

With the upper-bound estimations, nearly all seasons exceeded the estimated missing isoprene source of 1.6 Tg yr$^{-1}$ (Arnold et al., 2009); the spring pre-bloom, spring bloom, early summer, late summer and autumn account for 66, 158, 167, 104 and 710 % of the missing source. The spring bloom, early summer and autumn are high enough to exceed the top-down estimate of total production necessary to explain remote MBL isoprene concentrations (Arnold et al., 2009) without the inclusion of seawater marine organism production. This shows that all seasons, other than the very high autumn, can be considered significant for isoprene production.

In summary, these calculations suggest that O$_3$-driven production is potentially very important for the marine atmospheric budget of isoprene, but is less important (relative to diffusive air–sea fluxes) for acetone and acetaldehyde.

### 3.3.4. Likelihood of heterogeneous isoprene source

Booge et al. (2016) concluded isoprene air–sea fluxes would need to be more than an order of magnitude higher than predicted from seawater concentration alone to explain the atmospheric mixing ratios in the Indian and Eastern Pacific Oceans; additional flux needed was 2.08±1.33 and 2.04±1.00 μmol m$^{-2}$ d$^{-1}$ respectively. When the estimates were binned into day or night, a statistical difference was shown (Section 1.2.3.2), though the difference could be explained by reduced atmospheric sinks at night.

An atmospheric concentration arising from an air–sea flux, at sites distant from terrestrial sources, can be estimated with Equation 2. The isoprene air–sea flux is typically estimated as $F_{\text{bulk}} \approx K_w C_w$ (valid approximation for bulk fluxes of sparingly soluble compounds that are supersaturated in water, see Chapter 2). Equation 2 is rearranged and the flux sum is subtracted to estimate the additional required flux ($F_?$) necessary to explain remote marine atmospheric concentrations:

$$F_? \approx \frac{C_a h}{\tau} - K_w C_w \qquad\qquad 26$$

Figure 31 shows the additional flux necessary to explain a 2.5 ppt isoprene concentration, a concentration typical of remote MBL measurements (3.33±4.88 pptv mean, 2.44 median; Booge et al., 2016), with and without heterogeneous production. Here the assumptions are $h$ is 500 m, $F_{O_3}$ is 67.5±1.7 μmol m$^{-2}$ d$^{-1}$ (Loades et al., 2020) and $P_{VOC:O_3}$ is the overall seasonal means of 0.0011 and 0.0075, lower- and upper-bounds, respectively. Lateral transport of isoprene is not considered here because the main scientific concern is isoprene production in the remote ocean

(far from terrestrial sources). Isoprene $\tau$ is estimated from literature reaction rates with OH ($1\times10^{-10}$ cm$^3$ molec.$^{-1}$ s$^{-1}$; Atkinson and Arey, 2003) and annual surface 50° N zonal average OH concentration (~$8\times10^5$ molec. cm$^{-3}$; Horowitz et al., 2003) which estimate $\tau = 3.5$ h (Figure 31b). The $\tau = 1$ h approximation (Figure 31a) that comes from Booge et al. (2016) may be more appropriate for a tropical summer midday. $K_w$ is calculated with a $U_{10}$ of 6.0 m s$^{-1}$, temperature of 14 °C and a salinity of 35.1 PSU (averages of WCO L4 measurements) using isoprene parameterisations from Chapter 2 (Section 2.2.4). Typical seawater isoprene concentrations are 1–100 pM (Milne et al., 1995; Broadgate et al., 1997; Hackenberg et al., 2017; Booge et al., 2018; Wohl et al., 2020).
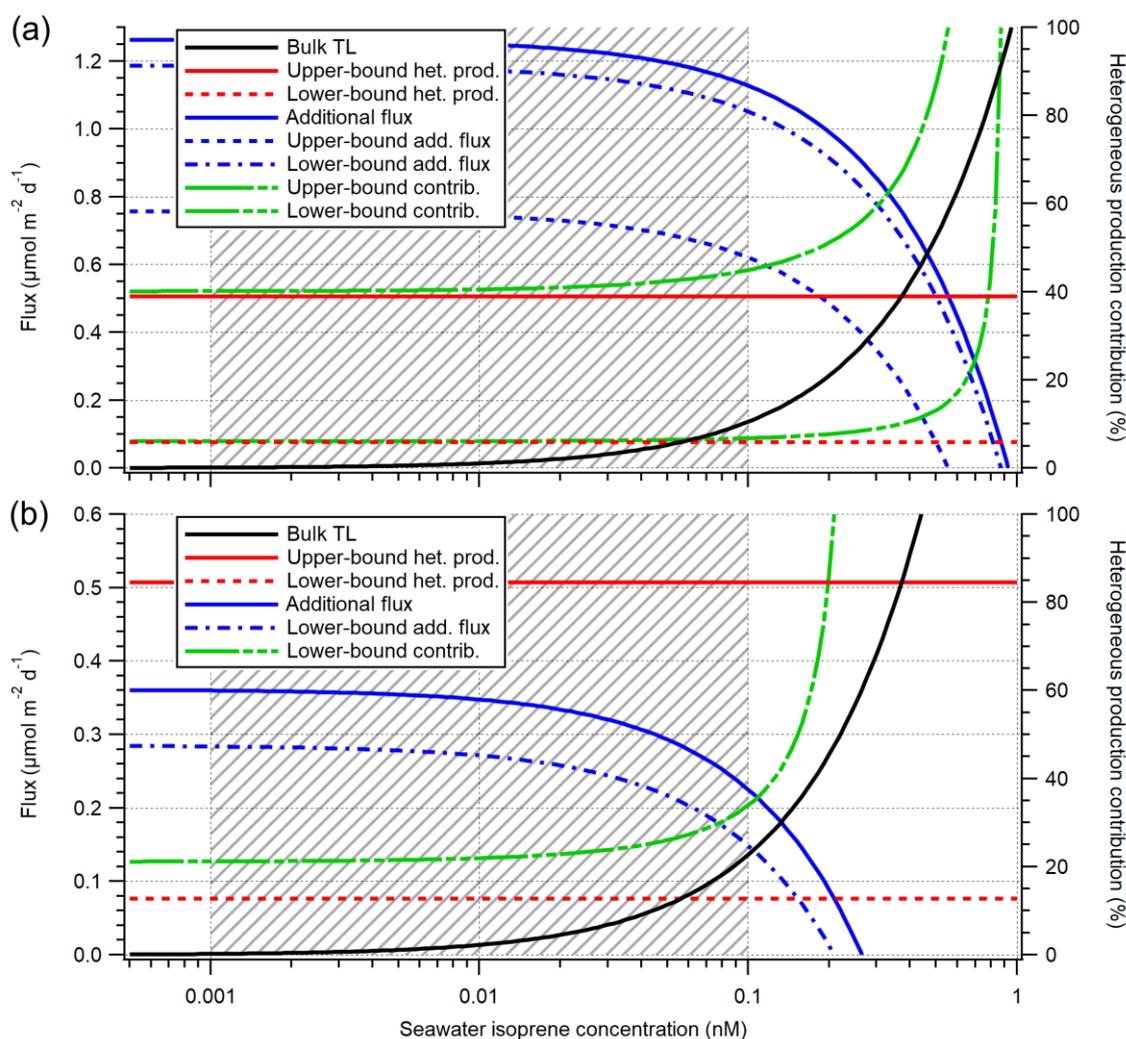


**Figure 31: Contribution of isoprene fluxes required to match atmospheric concentration using an atmospheric isoprene lifetime of (a) 1 h and (b) 3.5 h. The solid black line is the estimated bulk flux from seawater concentration. The red solid and dashed lines are the upper- and lower-bound heterogeneous production estimates, respectively. The blue solid, dashed and dash-dot lines are the additional flux needed (top-down minus bottom-up; $F_?$) for no heterogeneous production, upper-bound production and lower-bound production, respectively. The green long-dash and long-double-dash lines are the percentage contribution of heterogeneous production to the additional flux needed. The forward slash shaded area represents typically observed isoprene seawater concentrations. The blue dashed line (upper-bound production) is not provided for panel (b) as the value was below zero.**

Figure 31a shows the seasonal mean upper-bound heterogeneous production of isoprene at L4, when substituted into environmental measurements and using $\tau = 1$ h, can account for ~41 %

of the additional flux required in the open-ocean when seawater concentrations are <10 pM. Here the direct flux is near identical to the upper-bound global ocean deposition. As the seawater concentration increases above 10 pM, the bulk flux becomes more significant and the required additional flux becomes less. In this scenario, heterogeneous production can contribute an even higher percentage towards the additional flux required (50 % contribution at ~190 pM and 100 % at ~550 pM). On the other hand, the mean lower-bound isoprene heterogeneous production can only account for 8 % of the additional flux required in the open-ocean when seawater concentrations are <100 pM. Here the direct flux is double the lower-bound global ocean deposition, thus if the $O_3$ deposition was any lower, the contribution would approach zero. As the seawater concentration increases above 100 pM, a small increase in the contribution of bulk TL flux towards the isoprene production is observed however the contribution does not increase past 10 % of the required flux until at a seawater concentration of 190 pM (50 % at ~400 pM and 100 % at ~870 pM, as an example).

Figure 31b shows the seasonal mean upper-bound heterogeneous production of isoprene at L4, using $\tau = 3.5$ h, overestimates the additional flux required in the open-ocean (40 % higher when seawater concentration <10 pM). At a seawater concentration of 100 pM, the upper-bound heterogeneous production of isoprene accounts for 225 % of the necessary ocean production. On the other hand, the mean lower-bound isoprene heterogeneous production accounts for 22 % of the additional flux required in the open-ocean when seawater concentrations are <10 pM; this rises to 34 % as the seawater concentration increases above 100 pM. Increasing $h$ to 800 m (Booge et al., 2016) (60 % increase) causes the upper- and lower-bound contribution from heterogeneous production to decrease to 88 and 13 % of required ocean flux in the remote MBL.

It is clear that, with a reasonable isoprene $\tau$, heterogeneous production can represent an important source of MBL isoprene. With shorter $\tau$ and larger $h$, the heterogeneous production accounts for less of the required ocean flux in the remote MBL. The largest disadvantage of this scaling analysis is the use of static parameters that induce sensitivity in $F_?$. Large improvements could be made to this analysis if global modelling is used in the future; here MBL OH concentrations, and subsequently $\tau$, can be resolved at higher resolutions along with $h$, $K_w$ and $C_w$ and possibly even $F_{O_3}$. Higher resolution $P_{VOC:O_3}$ would not yet be available, however, reducing sensitivity and uncertainty in the remaining parameters would be advantageous. Conducting this modelling, using a model that can derive the bottom-up and top-down MBL estimates, would further aid our understanding of the contribution of heterogeneous production toward the marine atmospheric isoprene budget. Importantly, for this thesis, it is clear that the heterogeneous oxidation source of isoprene is comparable to diffusive emission flux at L4 using both the high autumn and lower spring/summer values and that the scaled production is the correct order of magnitude for top-down budget estimates.

### 3.4.  Conclusions

This chapter presents measurements of the $O_3$-driven heterogeneous production of acetone, acetaldehyde and isoprene using near-surface water from the L4 marine station in the western English Channel. Comparisons between measurement campaigns in spring, summer and autumn (virtual year, 2017, 2020, 2018 respectively) show the greatest production of acetone, acetaldehyde and isoprene in the early summer, late summer and autumn respectively, which suggests the DOM precursors for the productions of these three VOCs are different. The isoprene production in the autumn was ~5.7 times larger than the spring and summer measurements and shows the large effect of variability of the DOM pool. Correlations between production and temperature (+), fluorescence (–), chlorophyll *a* (+) and inorganic nutrients (–), along with no relationship between production and salinity, river flow and rain rate (the latter two are qualitative) suggest the DOM pool is of autochthonous biological origin. Experiments with the injection of a phytoplankton culture (*E. huxleyi*, commonly found at L4) and fatty acids (organic surface-active compounds) provide further evidence for the biological origin. However, algal culture and fatty acids do not fully represent the marine DOM pool, which is known to contain 1000s of compounds. It is thus unsurprising that these reactant addition experiments yield VOC productions that are at least several times lower than the observed total productions using natural seawater.

Scaling of the VOC production data from natural seawater to the global ocean, attempted with conservative and liberal approaches, shows the global yield of isoprene is on the same order of magnitude as the bottom-up oceanic emission for the conservative approach ($0.32\pm0.33/0.06$ Tg $yr^{-1}$ [$\pm\sigma/\sigma_{\bar{X}}$]) and on the same order of magnitude as the top-down oceanic emission ($2.24\pm2.30/0.41$ Tg $yr^{-1}$, one magnitude higher) for the liberal approach. This is strong evidence that the heterogeneous production of isoprene at the ocean surface is, at least, comparable to the ocean bulk flux and is a significant process that must be further understood. On the other hand, scaling of the production data shows the global yield of acetaldehyde and acetone is small – even with the liberal approach – compared to the estimated ocean fluxes. The maximum acetone yield is 16 % (~0.63 Tg $yr^{-1}$) of the net ocean sink while the maximum acetaldehyde is 6 % of the estimated missing ocean source. Of course, the estimate from the model could equally be wrong, however, this is not possible to gauge without more direct observations.

Future laboratory measurements should strive to (1) control/study the effect of temperature on the reactions and (2) develop a continuous methodology to enable higher temporal resolution measurements. Controlling temperature will be an important step for reducing variability between replicate measurements and also more accurately estimating the global $O_3$-driven VOC fluxes; employing a temperature-controlled jacket on the column and a temperature-controlled siphoning method will benefit future experiments. Furthermore, experiments studying the effect of temperature on the reactions will be important for deciding whether future experiments should be at the in situ sampling temperature (in situ production) or at a constant standardised temperature

(20 °C; standardised production). Developing a continuous semi-autonomous methodology will be crucial to enable higher temporal/spatial resolution measurements from the terrestrially influenced coast through to the continental shelf edge / open ocean (e.g. on a research cruise). Such transect measurements would importantly identify the significance of these reactions over the open ocean as well as near the coast.

Future sampling campaigns should strive to (3) make simultaneous DOM composition measurements and $O_3$ destroying species measurements (e.g. $I^-$), (4) undertake multi-year annual measurement cycles and (5) conduct simultaneous isoprene EC flux measurements to constrain the atmospheric–ocean loss. Measurements of DOM composition alongside VOC production would significantly enhance our understanding of the precursor DOM or, at the very least, remove specific DOM composition from contention to allow greater focus on unknown compounds. Similarly, measurements of seawater $O_3$ destroying species alongside VOC production would enable further understanding of whether the variability in weekly VOC production is due to changing DOM, changing $O_3$ destroying species competition or a mixture of both. Multi-year annual measurement cycles would importantly develop our understanding of interannual variability in VOC production and increase the amount of data to support these conclusions with a more rigorous statistical backing. Simultaneous isoprene EC fluxes and bulk seawater fluxes – like those attempted in Chapter 2 – would be beneficial to constrain the true ocean–atmosphere loss and determine the missing source with direct measurement. These measurements would be valuable alongside isoprene heterogeneous production experiments to more accurately and precisely discuss the contribution of heterogeneous production to the missing ocean source.

# Chapter 4 – The variability in ozone uptake by the Atlantic Ocean

## 4.1. Introduction

Deposition to the ocean surface is a large but poorly quantified sink for tropospheric $O_3$ (Hardacre et al., 2015). $O_3$ $v_d$ is typically given a constant 0.05 cm s$^{-1}$ value in most chemistry and climate models due to use of a constant resistance scheme (Ganzeveld and Lelieveld, 1995; Ganzeveld et al., 2009; Luhar et al., 2018; Pound et al., 2020), however direct measurements of $O_3$ $v_d$ to the ocean vary by more than an order of magnitude and show marked regional variability (Bariteau et al., 2010; Helmig et al., 2012; Loades et al., 2020). A large part of this variability is thought to be governed by the distributions of reactants in seawater (e.g. I$^-$ and organics).

An introduction to $O_3$ chemistry, including seawater reactions and deposition parameterisations, can be found in Chapter 1. Importantly for this chapter, reactions with I$^-$ and DOC are believed to together dominate $O_3$ seawater loss processes (Martino et al., 2012; Sarwar et al., 2016) with reactivities ($\lambda = C_i k_i$) of 12–400 and 102–800 s$^{-1}$, respectively, depending upon concentration and reaction kinetics (Table 1).

In this chapter, an investigation into the uptake of $O_3$ by near-surface seawater during a transect of the Atlantic Ocean in autumn 2019 from Southampton, UK to Punta Arenas, Chile (50° N to 45° S) is presented. A continuous and novel measurement method is developed that uses the defined $O_3$ uptake efficiency (OUE); the fraction of $O_3$ lost to seawater compared to the $O_3$ input. Direct observations of seawater I$^-$ concentration, coupled with laboratory rate experiments using I$^-$ standards diluted in artificial seawater, are used to determine the contribution of I$^-$ and DOM Atlantic Ocean towards $O_3$ uptake. Measurements of seawater from the deep chlorophyll maximum (DCM) and 1000 m depth are further used to explore vertical and latitudinal variability. In addition to the Atlantic Ocean measurements, a time series of OUE measurements at the L4 station in the summer algal bloom are also presented.

## 4.2. Method

### 4.2.1. Location

Experiments were undertaken onboard the research vessel RRS *Discovery* during a transect from Southampton, UK to Punta Arenas, Chile in autumn 2019 (13/10/19–23/11/19). This transect benefitted from measurements in multiple pelagic biogeochemical environments including the NECS, and the Atlantic tropical and subtropical gyres (Northeast Atlantic subtropical gyral (NASE), South Atlantic gyral (SATL) and western tropical Atlantic (WTRA)) (four-letter codes refer to Longhurst provinces; Longhurst et al., 1995; Longhurst, 2007). A full cruise transect with biogeochemical provinces is provided (Figure 32) using boundary data from Flanders Marine Institute (2009).
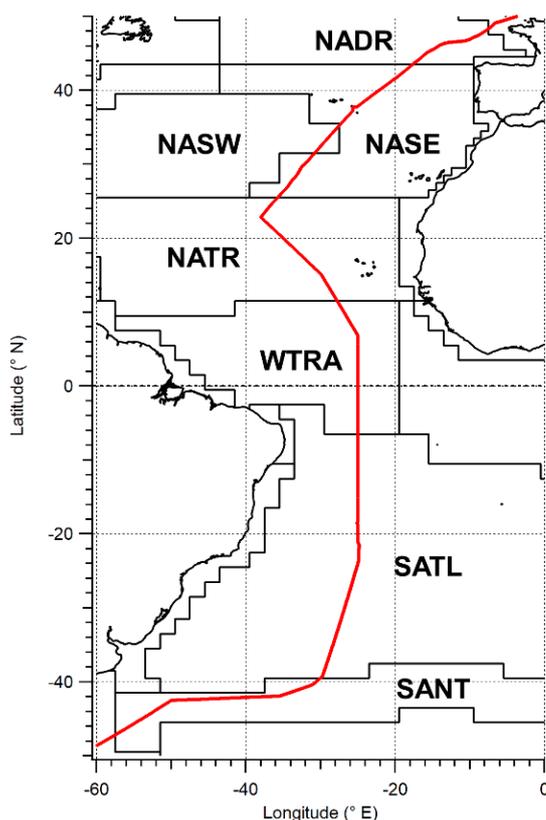
**Figure 32: Cruise transect with Longhurst provinces.**

All data were measured with respect to UTC, thus as the transect progressed from east to west, desynchronisation between solar noon (referred to as 'local time') and UTC noon occurred. A correction was applied to the UTC time, before hourly averaging occurred to aid the determination of any diurnal cycles, using the decimal longitude coordinate (240 seconds (° longitude)$^{-1}$).

### 4.2.2. AMT laboratory set-up

Atmospheric measurements were conducted on the meteorological mast (bow of the ship), which enabled clean air sampling with limited or no interaction from the ship, and in the meteorological laboratory. Atmospheric $O_3$ was measured by drawing atmospheric air to a monitor (2B-technologies model 202) in the laboratory. A downwards facing PTFE bottle (ID=~7 cm, length=~20 cm) was installed on the forward edge of the meteorological mast to minimalise the ingress of rain and sea spray. Atmospheric air was drawn into the bottle and through ~30 m of 4.8 mm ID tube at a flow rate of a few L min$^{-1}$, achieved using a 5 L min$^{-1}$ pump (KNF N86KT.18 diaphragm) and the internal pump of the monitor; no dilution was necessary upstream of the monitor. All tubing and unions between the PTFE bottle and the $O_3$ monitor were made from PFA.

For the OUE experiments, $O_3$ was generated similarly to Chapter 3 (Section 3.2.1). A total gas flow rate of 200 nmL min$^{-1}$ through the OUE measurement system (SFCE) was controlled using two MFC (Bronkhurst EL-FLOW Select series); typically 1 nmL min$^{-1}$ of air was passed through the $O_3$ generator and mixed into the remaining flow. A schematic is provided (Figure 33).
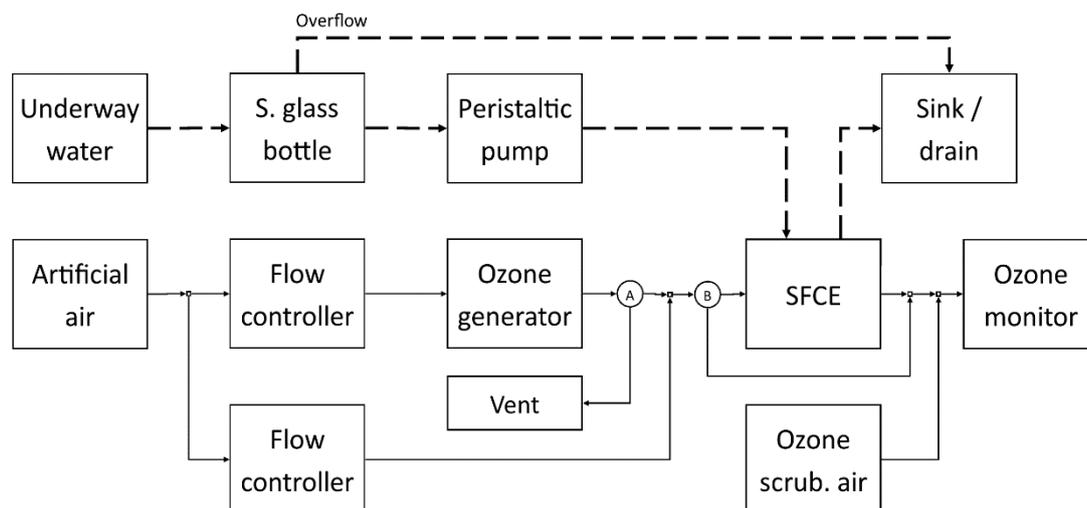
**Figure 33: Schematic for the laboratory setup used in the continuous measurement of ozone uptake efficiency using a segmented flow coil equilibrator (SFCE). Arrows represent flow direction, solid lines represent air transport, dashed lines represent water transport and A and B represent three-way valves. 'S. glass bottle' refers to the subsampling glass bottle.**

Underway water from the *Discovery*'s clean supply, sampled at ~5.5 m below the surface at the bow of the ship, was continuously flushed into a small overflowing narrow-necked glass bottle from which a peristaltic pump (Watson Marlow 120S/DV variable speed pump) drew the water into a 2 m 3.2 mm ID coiled PTFE tube (the SFCE). A water flow of ~100 mL min$^{-1}$ was controlled by routinely measuring flow with a graduated cylinder (every ~8 h) and manually varying the peristaltic speed as the tubing degraded. The peristaltic tubing used was 8 cm (Pumpsil platinum-cured silicone 4.8 mm bore, 1.6 mm wall).

The underway water and O$_3$-containing air were combined inside the SFCE, forming discrete water and air segments that allow for rapid gas exchange across the large and well mixed interface; the coil-specific residence time was ~6 s. A simple cross-sectional diagram is provided of the coil segments (Figure 34). The SFCE was based on the design of Wohl et. al (2019), with a few adaptions for the reactive O$_3$. After the coil, the water was discarded via a u-bend and the headspace air was measured for O$_3$ concentration (2B-technologies model 205 monitor). O$_3$ concentration, having gone through or bypassed the SFCE, was measured in alternation by using a three-way solenoid valve (Takasago Electric, Inc. MLV-3T-1/8NG) every 5 minutes. An activated charcoal scrubber (Thermo Scientific charcoal 4158) was installed upstream of the O$_3$ monitor at a tee with the experimental air and provided a source of O$_3$-free air. This fulfilled the ~2 L min$^{-1}$ flow requirement of the O$_3$ monitor and the dilution ratio was approximately 1:10. All tubing, unions and valves between the O$_3$ generator and monitor were made from PFA, while the valve was made from PTFE. OUE is determined as follows;

$$OUE_{\mathrm{meas}} = 1 - \frac{C_{\mathrm{SFCE}}}{C_{\mathrm{gen}}} \qquad\qquad 27$$

$$OUE_{\mathrm{corr}} = OUE_{\mathrm{meas}} - G\big(C_{\mathrm{gen}} - \overline{C_{\mathrm{gen}}}\big) \qquad\qquad 28$$

where $C_{\text{SFCE}}$ and $C_{\text{gen}}$ represent $O_3$ concentrations in the outflow of the SFCE or the bypass of the SFCE, respectively, $G$ represents an empirical correction and $\overline{C_{\text{gen}}}$ represents a reference mean/median concentration for normalisation. As shown later in Section 4.3.1.1, the OUE measurement from Equation 27 has a sensitivity towards $C_{\text{gen}}$; $OUE_{\text{meas}}$ is 10 % higher at an input concentration of 500 ppbv and 12 % lower at an input concentration of 2000 ppbv compared to a chosen reference of 1200 ppbv. An empirical correction is applied to the OUE data to normalise for variable $C_{\text{gen}}$ (Equation 28). For the remainder of this Chapter, unless specified, OUE refers to $OUE_{\text{corr}}$.
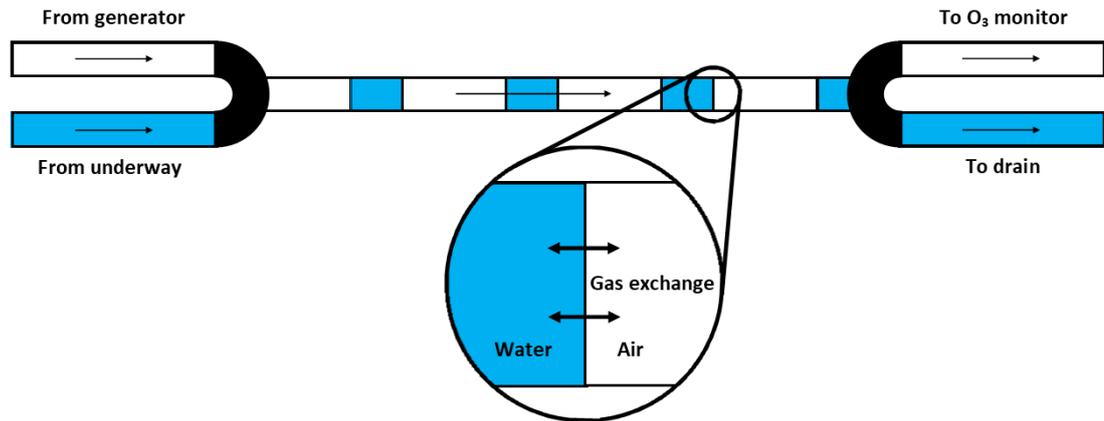


**Figure 34: Simplistic diagram of the air–water segmentation inside the segmented flow coil equilibrator. The black U pieces represent three-way tee connections.**

A higher OUE indicates more $O_3$ uptake by the seawater (i.e. higher chemical reactivity). OUE in the SFCE is measured at a fixed level of turbulence (determined by the water and air flows), thus represents the combined contribution from chemical reactivity and physical uptake of which the latter will be subtracted via the Milli-Q water blank. A Milli-Q water blank with added salt (salinity of ~35 PSU) is most appropriate for an uptake experiment using seawater because sampled seawater irradiated to remove OM or artificial seawater is hard to reproduce. Furthermore, seawater naturally low in I⁻ concentration is not available in the NECS studied here. If saline Milli-Q water is not available, traditional Milli-Q water can be used with a salting-out factor adjustment.

The three-way valve sequencing was automated by a USB-controlled relay (SAINSMART 4-channel 5V USB relay) via Python 3.7 code I wrote using the `ftd2xx` module, whereas in the previous SFCE measurements (Wohl et al., 2019; Yang et al., 2021) the valve sequencing was controlled by I/O ports of the PTR-MS. The relay approach worked for the vast majority of the cruise, however, occasionally the USB connection failed for reasons unknown. When failure was discovered, the relay was reset and sequencing reinitiated. If external valve automation is required in the future, I would recommend using a relay that connects to the I/O ports of a Raspberry Pi (or similar equipment) to reduce USB interferences. A custom-built digital thermometer (Omega ultra-precise 1/10 DIN immersion RTD), constructed from stackable microcontrollers (Tinkerforge master brick 2.1 and PTC bricklet, as per Sims et al. (2017)), was installed in an

overflowing bucket (in which the glass bottle, that was sub-sampled by the SFCE, was partially submerged) to measure the underway water temperature entering the laboratory. A second custom-built thermometer was installed between the looped SFCE, on the outer surface of the coil wall, to measure the tubing surface temperature. This was an indication of the effect the temperature-controlled laboratory (17–25 °C depending on latitude) might have had. The average temperature difference between the coil surface and underway seawater was 0.9±3.2 °C (i.e. coil was slightly warmer). Thus the temperature of the laboratory had minimal effect on the temperature of the experiment.

The SFCE was cleaned each week with 2 L of 5–10 % HCl and then Milli-Q water to remove any biofouling or contamination build-up inside the system. The gas sampling instruments were disconnected during acid washing. Measurements of OUE before and after the cleaning showed little difference, suggesting biofouling was negligible (expected considering $O_3$ is industrially used for biofouling prevention in water supplies, see Von Gunten (2003a, 2003b)).

Advantages of the SFCE technique for the measurement of $O_3$ uptake include (1) continuous measurements of underway seawater, which is an improvement over previous methods (e.g. stirred-flask (Martino et al., 2012; Moore, 2014), wetted-wall flow tube (Barcellos da Rosa et al., 2003; Clifford et al., 2008)), (2) making discrete measurements with ease, and (3) the apparatus is easy to clean. The disadvantages of the SFCE, especially in the set-up used here, include (1) the measurement of bulk seawater instead of the SML (discussed later in Section 4.3.4.2) and (2) the use of high $O_3$ input concentration compared to atmospheric concentrations (discussed later in Section 4.3.1.1).

### 4.2.3.   AMT discrete sampling

Underway water was sampled, filtered and frozen for $I^-$ concentration analysis during the noon rosette station on 36 of the 41 days at sea. $I^-$ is a known $O_3$ destroying species within seawater, so this measurement might help to explain the variability in OUE. Samples were filtered through GF/F filter paper using a glass syringe and stainless-steel filter holder and stored in 50 mL plastic tubes. The syringe, filter holder and plastic tubes were rinsed three times with Milli-Q water and then underway water before sampling. Samples remained frozen (~-20 °C) on the *Discovery* for ~8 months before measurement. Concentration was determined by the Wolfson Atmospheric Chemistry Laboratories (University of York) using square wave voltammetry (refer to method 3 from Chance et al. (2019)).

The OUE measurements were typically made on the continuous supply of surface seawater for the majority of the cruise measurements (an OUE value every 10 min), however occasionally discrete water samples from 1000m, 2000 m and/or the DCM were taken from *Discovery*'s rosette sampler and measured for OUE to compare with near-surface values (Table 21). Discrete water samples were collected into 2 L glass bottles using a gas-sensitive method; each bottle was rinsed three times with sample and then filled from bottom to top using the silicone peristaltic tubing

before being overflowed to minimise any bubbles or gas loss. The glass bottles were rinsed three times with Milli-Q water before and after each use.

**Table 21: Coordinates and depths for sampled CTD water for the OUE experiment. The deep chlorophyll maximum (DCM) was unique to each station.**

| Latitude (° N) | Longitude (° E) | Depths (m) |
|---|---|---|
| 48.522 | -7.204 | DCM (70) |
| 46.165 | -13.882 | 1000 |
| 43.914 | -17.148 | DCM (70) |
| 41.465 | -20.189 | 1000 |
| 35.091 | -27.625 | 1000 |
| 32.402 | -30.024 | 1000 |
| 30.268 | -31.861 | DCM (115) |
| 25.301 | -35.301 | DCM (120), 1000 |
| 19.799 | -34.778 | DCM (100), 1000 |
| 17.279 | -32.151 | DCM (80), 1000 |
| 14.845 | -27.961 | DCM (50), 1000 |
| 5.522 | -25.000 | DCM (69), 1000 |
| -5.044 | -25.001 | 1000, 2000 |
| -11.882 | -25.008 | 2000 |
| -21.437 | -24.837 | DCM (162), 2000 |
| -27.709 | -26.085 | 1000 |
| -34.777 | -28.252 | 1000 |

### 4.2.4. PML laboratory measurements

In spring/summer 2021 (25/05/21–19/07/21), a comparison between the VOC heterogeneous production measurements (Chapter 3) and the OUE measurements was undertaken. Seawater was again sampled from the L4 marine station using the rosette sampler of the RV *Plymouth Quest*, however, samples were now taken at depths of ~2 m and 40 m. Over this period, the L4 water column was strongly stratified with a MLD of 10–15 m. The samples were each transferred into a clean 10 L bottle. Bottle cleaning, filling and transport followed the method of Chapter 3. Here, however, the samples were always measured the day after sampling (~24 hr). This allowed the production and uptake experiments to be done in near succession on the same day, though the sample temperature was ~20 °C instead of at ambient.

Additional laboratory experiments were undertaken to assess the impact of experimental parameters on the AMT OUE data. The effect of changing $O_3$ input concentration on OUE was assessed on two different seawater samples in the laboratory over an input range of 150–2300 ppbv (the AMT $O_3$ input concentration range was 400–2200 ppbv). The water samples were prepared by (1) mixing two L4 samples ('L4 mix', surface and deep in an approximate 50:50 ratio to increase water volume) and (2) by preparing a large volume of 100 nM KI standard in Milli-Q water (similar to Chapter 3), however now with the addition of ~35 g L$^{-1}$ of 24 h oven-baked (400 °C) sodium chloride (NaCl; Sigma Aldrich S9625 >99 %) and ~0.3 g L$^{-1}$ of sodium bicarbonate (NaHCO$_3$; VWR 27778 >99.7 %) to increase the salinity and buffer the pH to ~8, respectively. The KI standard was prepared through serial dilution. Experimental parameters between these two experiments (and others that follow) can be found in Table 22 below.

**Table 22: Control parameters for laboratory experiments on the controlling variables for ozone uptake efficiency.**

| Experiment | Sample / standard | Sample flow rate (mL min$^{-1}$) | Gas flow rate (mL min$^{-1}$) | Sample temperature (°C) | Ozone conc. (ppbv) |
|---|---|---|---|---|---|
| Changing ozone | L4 mix | 104±8 | 200 (MFC) | 19.6 | *150–2100* |
| concentration | Iodide std. | 98±1 | 200 (MFC) | 20.5 | *200–2300* |
| Changing iodide | Milli-Q | 99±2 | 217.1±1.1 | 18.8±0.4 | 1274±17 |
| concentration | Milli-Q (sea std.) | 100±0 | 200 (MFC) | 20.1±0.5 | 1260±18 |
| Changing sample | Eddystone | 98±1 | 213.7±1.1 | *5–35* | 1256±46 |
| temperature | Iodide std. | 101±3 | 232.4±24.5 | *5–35* | 1596±108 |
| Changing sample | Exp 1. | *80–105* | 200 (MFC) | 19.8±0.3 | 1051±27 |
| flow rate | Exp 2. | *80–115* | 200 (MFC) | n/a | 1381±10 |

The effect of changing I$^-$ concentration on OUE was undertaken, at a fixed O$_3$ input concentration of ~1200 ppbv, by preparing standards of KI in Milli-Q water (similar to Chapter 3) using serial dilution. A 0.24 mM stock solution was prepared by dissolving 24 h oven-baked KI in Milli-Q water and repeatedly diluting to achieve stock concentration. Aliquots of the stock solution (80–830 μL) were added to 1 L of Milli-Q water to achieve desired standard concentration. In a repeat experiment, ~35 g L$^{-1}$ of NaCl and ~0.3 NaHCO$_3$ were added to the KI standards to simulate seawater effects.

The effect of changing sample temperature on the OUE was undertaken with an Eddystone water sample and a 100 nM standard of KI in Milli-Q water. The Eddystone samples mentioned here and below are aged seawater supplied to the PML laboratories from an external tank that is filled routinely from the Eddystone Reef (approximately 8.5 km SW of L4 and 17 km NE of E1, see Figure 4). The Eddystone water tank is continuously aerated with atmospheric air (i.e. not gas-tight), kept in the dark and is circulated continuously through the piping to limit stagnant water. The temperature of the samples in both experiments was varied by pumping the sample through a ~20 m coil in a temperature-regulated water bath before entering the SFCE. Sample temperature was measured with a clean glass thermometer and also two of the custom-built digital thermometers; one thermometer in the bath and the other in SFCE u-bend.

The effect of changing sample flow rate on the OUE was assessed with an L4 water sample and also Milli-Q water. Here, the flow rate was controlled by changing the rotational speed of the pump. Two experiments were undertaken, the first using flows in a randomised order and the second using flows in a linear order. The first experiment also used alternating Milli-Q water and L4 water, while the second experiment used just L4 water.

### 4.2.5. Data processing

The O$_3$ data from the AMT and PML experiments was continuously measured at 0.1 Hz. The timing where the solenoid switched from generator output (i.e. bypass) to the SFCE was determined for each 10 min window by searching for a large negative gradient between consecutive data points. A record of valve timings was additionally made with the valve Python code, which aided the development of the differential approach. During the AMT deployment, $C_{gen}$ was determined as the average of the 15 data points (~150 s) before the determined valve change, whilst $C_{SFCE}$ was the final 15 data points of the 300 s period after the valve change. Example data is shown in Figure 35a. Initial OUE was calculated using Equation 27 (including

discrete measurements of Milli-Q water blanks and CTD samples), corrected for variable $O_3$ concentration using an empirically derived correction factor ($G$=-7.87×10$^{-5}$ OUE ppbv$^{-1}$ and $\overline{C_{gen}}$=1200 ppbv, Equation 28), and filtered for periods of maintenance (i.e acid washing, blanking etc.) and the CTD sampling by removing ±15 min of data. Filtered 10 min OUE measurements were averaged into 1 h bins to reduce experimental noise. The average hourly $\sigma$ was 0.01 or ~2 % of the mean OUE. The in-situ blank measurements were fitted to an exponential curve and subtracted from the hourly OUE to estimate the residual chemical component (see Section 4.3.3.4). The approximately daily I$^-$ concentration measurements were linearly interpolated to the 1 h bin timestamp, converted to OUE values using an empirically derived fit (see Section 4.3.1.2) and subtracted from the OUE chemical component to estimate the influence of remnant reactions on OUE.
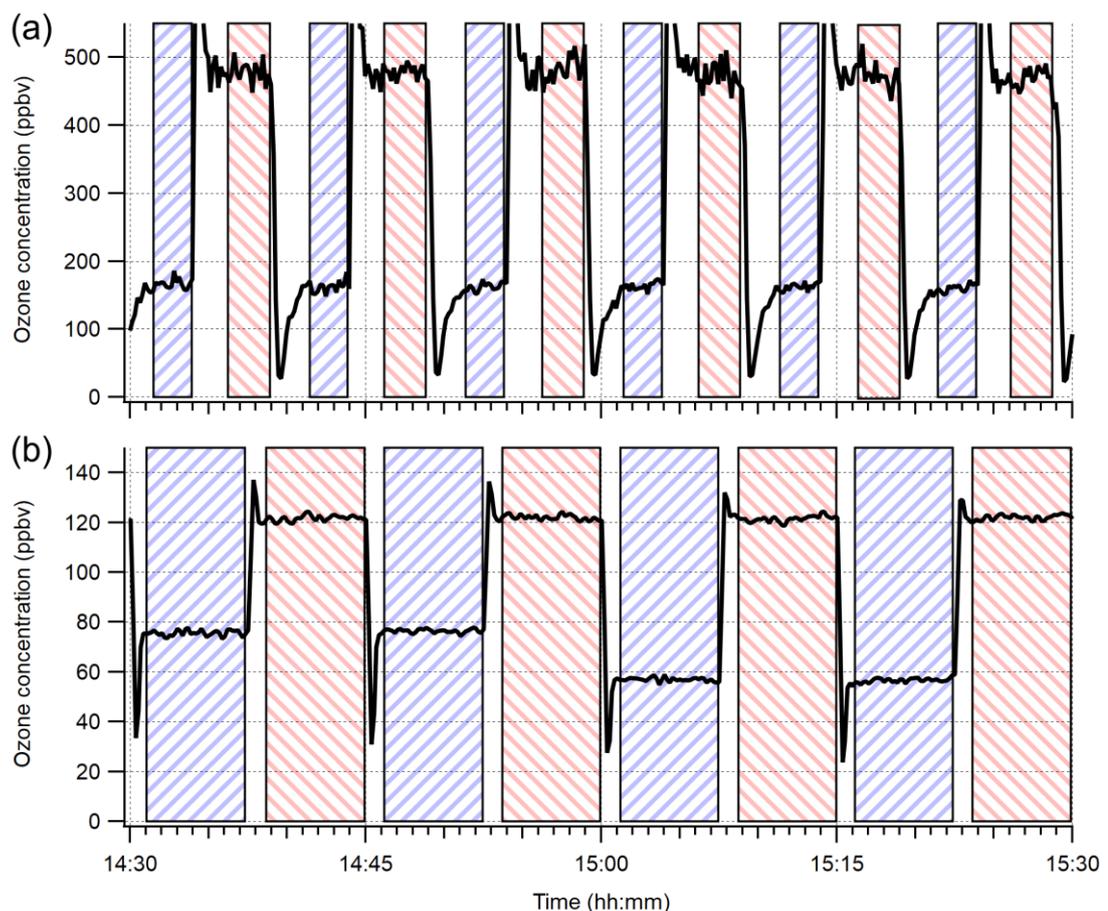


**Figure 35: Representation of the periods in the raw O₃ data where generator O₃ concentration (red backslash shaded) and SFCE O₃ concentration (blue forward-slash shaded) were measured in the (a) AMT continuous data and (b) laboratory experiment data. The time axis is shared vertically, although the absolute time in panel (b) is not important.**

In Figure 35, the initially raised peak before a $C_{gen}$ measurement and the initially lowered peak before a $C_{SFCE}$ measurement is thought to be because of a changing pressure balance of the MFC which quickly stabilised. During the PML experiments, the valve sequencing was extended to 7.5:7.5 min to gain a larger window of concentration averaging. Example data are shown in Figure 35b. Here, $C_{gen}$ was calculated as the average of the generator output before and after a

coil measurement, which helped limit any generator output fluctuation during a coil measurement (0–50 ppbv per repeat).

## 4.3.  Results and Discussion

### 4.3.1.  Laboratory control experiments

In this section, laboratory experiments undertaken to determine the impact of varying control parameters, including $O_3$ concentration, $I^-$ concentration and temperature, are discussed. The results of these experiments are used in the discussion in the sections that follow. Further control parameters, including flow rates, not important for discussion are included in Appendix B.

#### 4.3.1.1.  Variable ozone input concentration

The $O_3$ input concentration during AMT-29 was not very constant due to inconsistent output from the $O_3$ generator (400–2200 ppbv range, 1195±412 ppbv mean) likely because of the low flow used to conserve compressed gas. Laboratory measurements show that the measured OUE depends linearly on the $O_3$ input concentration, with higher $O_3$ uptake at lower input concentration. Figure 36 shows the $O_3$-concentration-dependent gradient for OUE was statistically similar for the L4 mixture and $I^-$ standard, with a combined gradient of $-7.87\times10^{-5}$ OUE ppbv$^{-1}$. Each gradient was shown to be very tightly correlated ($r^2 > 0.98$) and extremely statistically different from a gradient of zero (F-statistic $>274$ for an F-critical $<5.6$).
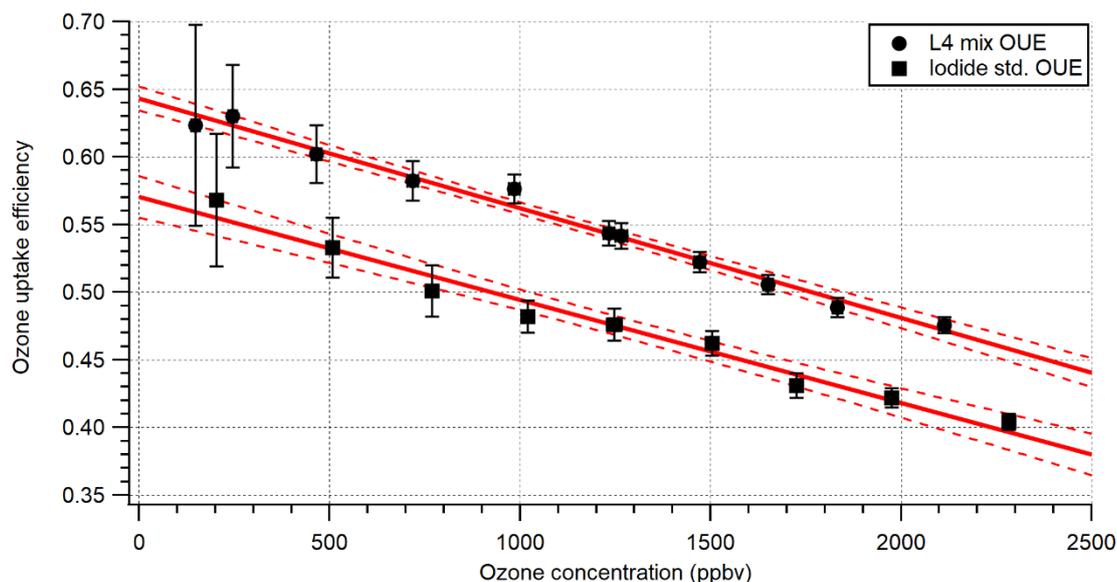


**Figure 36: The effect of changing ozone concentration on OUE for an L4 mixture (approx. 50/50 surface and deep water) and a 100 nM iodide standard.**

Over the range of $O_3$ concentrations observed in the AMT data set (500–2000 ppbv), a range in OUE of 0.48–0.60 (L4 sample) was observed. Relative to the mean $O_3$ concentration (~1200 ppbv), OUE is 10 % higher at an input concentration of 500 ppbv and 12 % lower at an input concentration of 2000 ppbv. To make data from the entire AMT transect comparable, I normalise the initial OUE data ($OUE_{meas}$) to a fixed value of $O_3$ input ($OUE_{corr}$) (the cruise mean 1200 ppbv) using Equation 28. Figure 37 shows the OUE with and without this correction and also shows the $O_3$ input concentration. Linear regression between $OUE_{corr}$ and $O_3$ concentration showed a gradient of $1.76\times10^{-5}$ OUE ppbv$^{-1}$ (~78 % absolute lower than the laboratory-measured

gradient) and an $r^2$=0.02. This gradient was shown to be statistically different from a gradient of zero (F statistic of 15.1, compared to critical 3.9), using regression analysis for equality of slope=zero. However, the lack of correlation suggested that $O_3$ input concentration no longer induced any variability in OUE. For completeness, the regression between $OUE_{meas}$ (pre-correction) and $O_3$ concentration showed a gradient of $-6.11\times10^{-5}$ OUE ppbv$^{-1}$ (~22 % less steep than the laboratory gradient as shown in Figure 36) and an $r^2$=0.17.
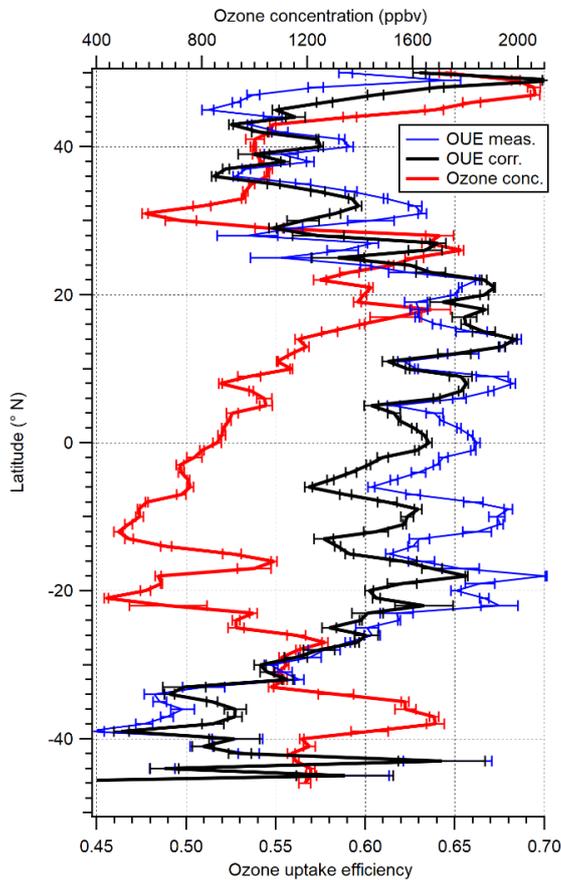


**Figure 37: 1° latitude bins of measured OUE (blue thin), O₃-corrected OUE (black thick) and input ozone concentration (red thick).**

Figure 36 also showed that at $O_3$ input concentration >500 ppbv, $OUE_{meas}$ had a relative uncertainty <4 %. At lower $O_3$ input, the uncertainty in OUE increases due to increased relative error in the $O_3$ concentration measurement. Relative propagated OUE uncertainty can be predicted by $\sigma_{OUE} \approx 7.37 C_{O_3}^{-0.84}$, using the combined data of the L4 sample and the I⁻ standard. Here the ~1:10 dilution by the $O_3$-free makeup flow is included in the calculation of concentration, but it is primarily the measured concentration (i.e. without dilution correction) that affects the uncertainty. Duplicate $O_3$ input concentrations for the 149 ppbv samples in the L4 experiment were 16.1±0.8 and 15.0±0.9 ppbv without dilution correction, while the SFCE output was 5.9±1.1 ppbv. The SFCE output, while detectable, was lower than the limit of quantification (LOQ; measured as ~8.7 ppbv) of the 2B model 205 $O_3$ monitor and approached the LOD (measured as ~2.6 ppbv). For reliable measurements, the undiluted concentration would need to be above the LOQ, thus with a typical dilution of 1:10 and a potential OUE of 0.8, input $O_3$ concentration needs to be >350 ppbv.

### 4.3.1.2. Changing iodide concentration

Figure 38 shows that I⁻ concentration and OUE are tightly correlated with a square root dependency. A square root fit is incorporated in the calculation of $v_d$ for O₃ where the dominant loss processes are aqueous reactions (Carpenter et al., 2013). The O₃ deposition velocity can be calculated from resistances following Equation 8a–d. For the sample used here, $\lambda$ can be simplified to $k_{O_3+I^-}C_{I^-}$. Experiments have shown the aqueous phase reactions dominate over surface reactions between O₃ and I⁻, and that the O₃ concentration is insignificant, when the I⁻ concentrations are <0.1 mM (Moreno et al., 2018).
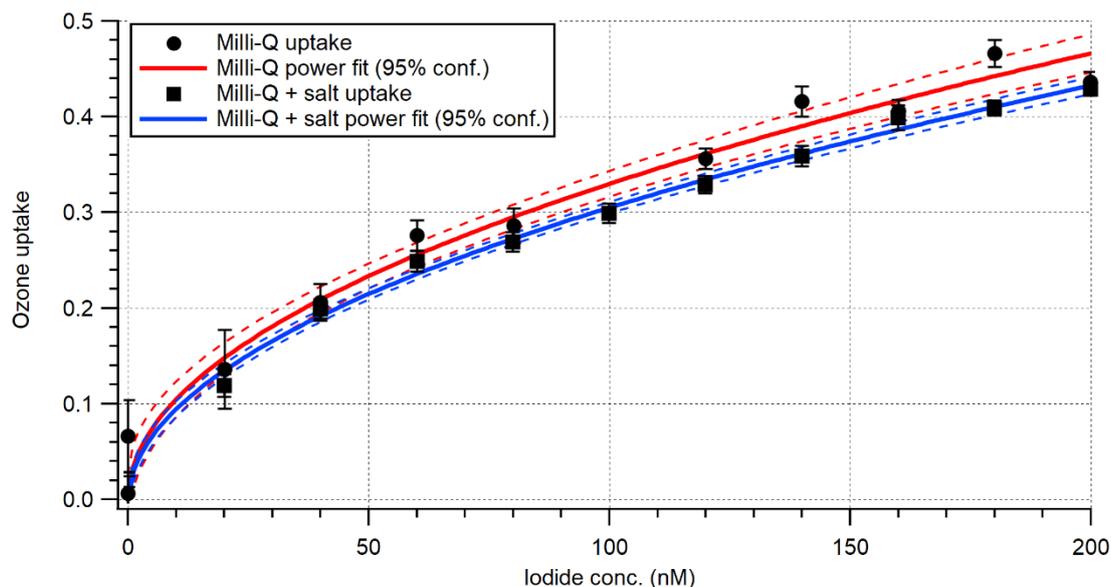


**Figure 38: OUE as a function of I⁻ concentration in Milli-Q water (red) and Milli-Q water at 35 PSU and pH 8 (blue). The solid lines are fits to a power-law fixed at 0.5, $y = Ax^{0.5}$, and the dashed lines are 95 % confidence bands.**

For the pure Milli-Q water I⁻ standard and the buffered and saline Milli-Q water I⁻ standard, the power fit coefficients (A) were determined to be 0.033±0.001 and 0.031±0.001, respectively, with an r²=0.99 and 1.00. The I⁻ standard in buffered and saline water yielded a lower OUE than the I⁻ standard in Milli-Q water, which is due to the salting-out effect on $H$ in $R_3$ (Equation 8d). The salting-out factor was calculated to be 1.21, following Johnson (2010) with solubility data from Sander (2015), whereas the difference between the two fits was determined to be 1.08 (~11 % lower than the salting-out factor). This reduction is expected considering the influence of the salting-out factor upon the final derived OUE; an identical reduction is shown with theoretical calculations of $R_3$. Any remaining discrepancy, however small, maybe due to the temperature dependence of $k_{O_3+I^-}$, $D$ and $H$ in $R_3$ because the pure and saline standards were at 18.8±0.4 and 20.1±0.5 °C, respectively. Temperature influence is discussed below. Importantly, it is very clear to see, with the very strong r², that the measurements of OUE in these experiments demonstrate high reproducibility and consistency.

### 4.3.1.3.   Changing sample temperature

There is considerable debate within the literature on whether the $O_3$–$I^-$ reaction kinetics are temperature-dependent and even less understanding is provided for $O_3$–organic reactions. In this section, the influence of temperature on the OUE measurement is presented.

Figure 39a shows the Eddystone OUE was not dependent upon changing sample temperature. Here the gradient was -0.00014 OUE $K^{-1}$ ($r^2$=0.02) which was shown to be statistically equal to zero. The $\lambda$ for the Eddystone water is uncertain because the $k_{O_3+X}$ or concentration of $O_3$ destroying species are not known. However, if the Eddystone OUE is dominated by aqueous loss, then OUE is expected to decrease with temperature because of the stronger dependence of $H$ over the dependence in $k_{O_3+I^-}$ and $D$ in the calculation of $R_3$ (Equation 8d) (Ganzeveld et al., 2009; Carpenter et al., 2013).
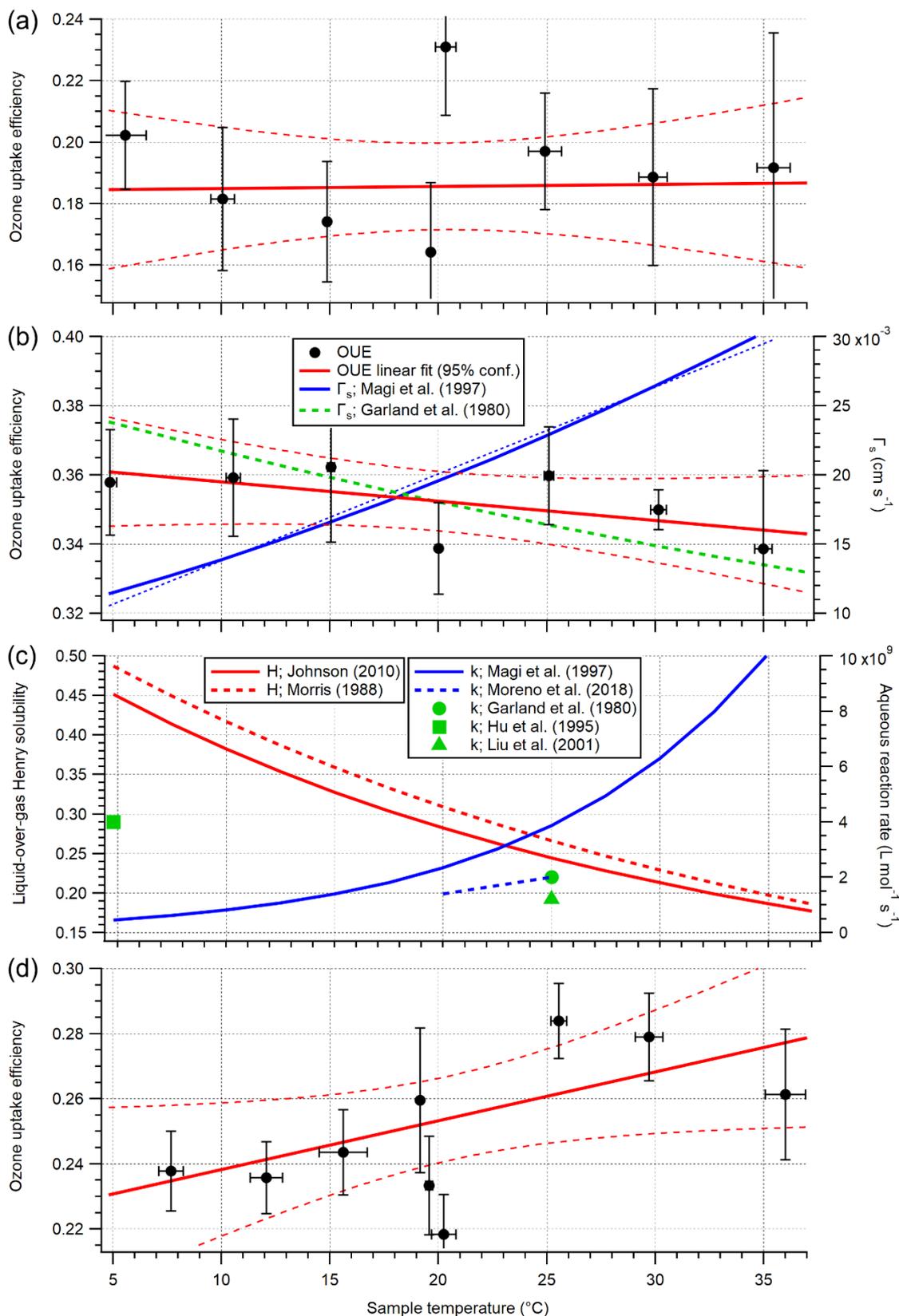
**Figure 39: (a) OUE for a sample of Eddystone Reef water, (b) OUE for a 100 nM I⁻ in Milli-Q water standard and predicted surface aqueous phase resistance ($R_3$ also given as $\Gamma_s$), (c) O₃ solubility (Morris, 1988; Johnson, 2010) and O₃–I⁻ rate constants (Garland et al., 1980; Hu et al., 1995; Magi et al., 1997; Liu et al., 2001; Moreno et al., 2018) and (d) OUE for a Milli-Q water sample, as a function of sample temperature.**

Figure 39b shows the I⁻ OUE was slightly dependent upon changing sample temperature, however, decreasing OUE was observed for increasing temperature. Here the gradient was -0.0006 OUE K⁻¹ (r²=0.36) and was shown to be statistically similar to zero. A lack of temperature dependency for the global ocean was observed by Ganzeveld et al. (2009). For the observed AMT water temperature range (12–29 °C), this gradient would equate to a change of 0.01 OUE between the maximum and minimum temperature, which is small compared to the mean signal. Because $\lambda$ for an I⁻ standard is more certain, the theoretical $R_3$ can be calculated for comparison firstly following Pound et al. (2020); $k_{O_3+I^-} = \exp(-8772.2/T + 51.5)$ (Magi et al., 1997), $D = 1.1 \times 10^{-6} \exp(-1896/T)$ (Johnson and Davis, 1996) and $H^{-1} = 10^{-0.25 - 0.013(T - 273.15)}$ (Morris, 1988). Figure 39b shows an ~11 % increase in sample temperature (K) is matched with a ~167 % increase in $R_3$, which was not seen in the OUE measurement. The kinetic experiments of Magi et al. (1997) report an Arrhenius expression pre-exponential that is ~10 orders of magnitude higher than the diffusion-limited reaction rate, which makes the results "unphysical" (Macdonald et al., 2014). Far better agreement of OUE temperature-dependence was observed using the non-temperature-dependant $2 \times 10^9$ M⁻¹ s⁻¹ $k_{O_3+I^-}$ from Garland et al. (1980), which had a good fit to the experimental OUE (r²=0.91). This is evidence that the $k_{O_3+I^-}$ measurements of Garland et al. (1980), Liu et al. (2001) and Moreno et al. (2018) are the most accurate.

Figure 39d shows a positive influence of temperature on a Milli-Q water blank, which accounted for approximately half of the variance of the blank signal (r²=0.51). Here the gradient was 0.0015 OUE K⁻¹, which was shown to be statistically different from zero by a very small margin (F statistic of 6.1 compared to critical 6.0). Over the AMT-29 temperature range, a ~7 % increase in temperature (in K) leads to a ~13 % increase in OUE. Using the mean and quartile temperature data (Table 25), a ±2% change in temperature leads to a ±3 % change in OUE. These two analyses show that the effect of temperature on the blank is very minor. Coupled with the knowledge that the laboratory-blank accounts for only ~25 % of the non-temperature-corrected OUE, correction for any temperature dependence in the blank seems unnecessary. Furthermore, the inclusion of a third 20 °C measurement (>95 % confidence band) lowered the F-statistic (4.1) and caused the gradient to be statistically similar to zero. While the I⁻ OUE temperature dependence appears to be dominated by the influence of solubility, the Milli-Q water OUE temperature dependence is likely dominated by diffusion because of the positive trend and also because the Milli-Q water uptake (in the absence of chemical reaction) can be shown to be far from equilibration. It is, however, unknown why the blank OUE in this set of experiments were higher than the ~20 °C measurements in the L4 time series (0.16±0.01, see Section 4.3.2); the only method change was the incorporation of a thermalising tube.

### 4.3.2. Laboratory OUE

In this section, laboratory experiments undertaken for a time series of coastal OUE measurements are discussed to support the Atlantic Ocean measurement conclusions and also link more discussion between Chapters 3 and 4.

Over nine weeks, the OUE of surface and deep L4 water were compared using triplicate repeats. Note that during the first week, the water at L4 was weakly/not stratified, thus for some analyses the first data point was removed to check for correlations during strong stratification. Figure 40a shows that the surface water OUE was higher than the deep water; with mean OUE of $0.57\pm0.02$ and $0.53\pm0.02$, respectively, which are statistically different (t-test, $p$=0.003). When the Milli-Q water blank ($0.15\pm0.01$) was subtracted, the deep sample was on average ~9 % lower than that of the surface.
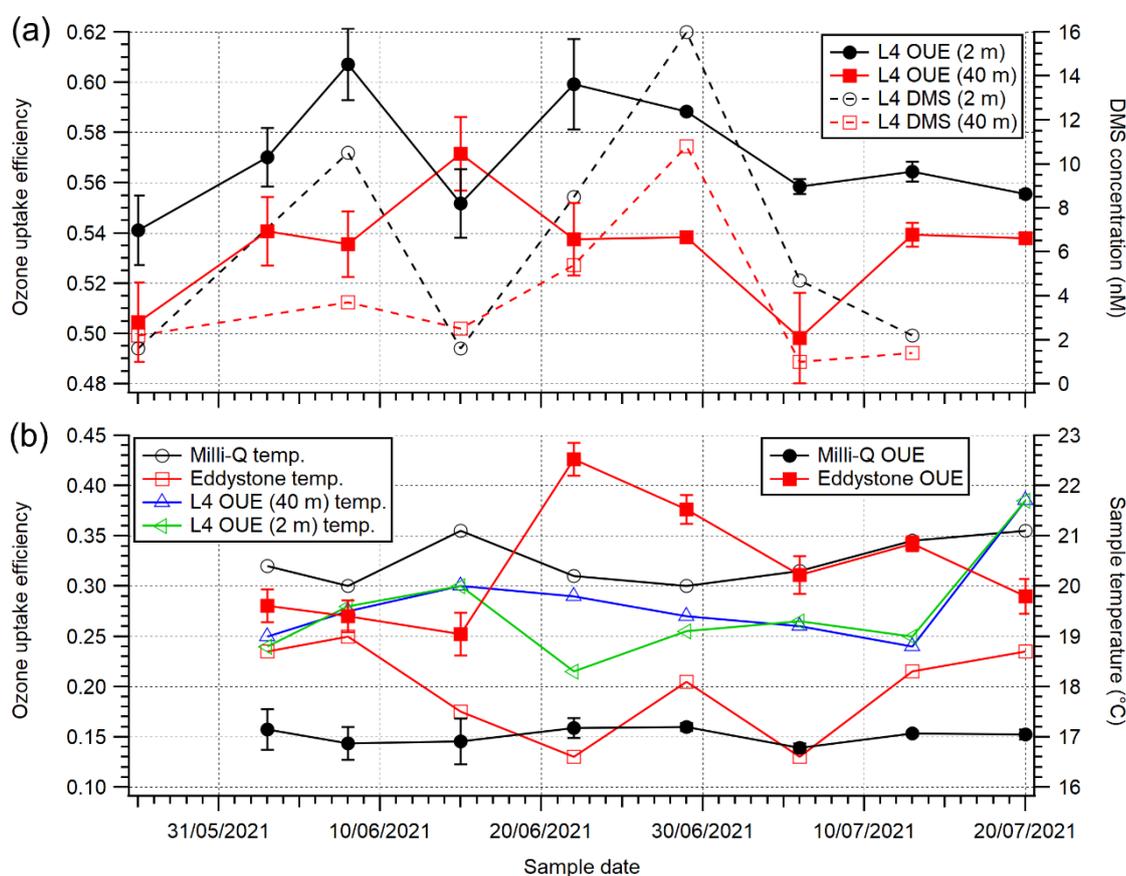


**Figure 40: Timeseries of (a) L4 surface and deep OUE and matching DMS concentrations and (b) Milli-Q water and Eddystone Reef seawater OUE and matching sample temperatures along with L4 surface and deep.**

Figure 40a also shows L4 DMS concentrations that were measured at the same time as the OUE experiments (Hopkins pers. comm.), following Hopkins and Archer (2014). OUE and DMS showed a moderate–strong positive correlation ($r^2$=0.70) for the surface water, but, showed no correlation ($r^2$=0.00) for the deep water (the 40 m DMS concentration was linearly interpolated between 25 m and 50 m). The lack of correlation in the deep water suggests that the correlation observed in the surface water was not directly due to the low DMS reactivity towards $O_3$ (compared to $I^-$ and DOC, see Table 1), but likely a sign that DMS was a proxy of biological

activity. Leck et al. (1990) demonstrate clear correlations between DMS concentration and zooplankton biomass ($r^2$=0.64, +), nutrients ($r^2$=0.46, –), temperature ($r^2$=0.37, +) and primary production ($r^2$=0.18, +) all at $\alpha$<0.05. Biological activity can influence the concentration of DOC/DOM but also shift the seawater $I^-$:$IO_3^-$ equilibrium in favour of $I^-$ (Farrenkopf et al., 1997; Chance et al., 2014). Further analysis between OUE and DMSP concentration (Hopkins pers. comm.) showed a weak positive correlation ($r^2$=0.15) for the surface water and no correlation for the deep water. Importantly, these results show that OUE is sensitive to biological activity.

With the first data point removed (26/05/21, weak stratification), strong to moderate correlations were observed for surface OUE and water fluorescence (+), water transmission (–) and $O_2$ concentration (+) (Table 23). Here fluorescence is typically associated with chlorophyll *a*. No significant trends have been observed between DMS and chlorophyll *a* concentrations (Leck et al., 1990; Archer et al., 2009; Bell et al., 2021), which suggests the strong OUE:DMS and OUE:fluorescence correlations are covariant to a third variable that is likely linked to biological activity because these measurements occurred during the summer algal bloom. The strong negative correlation of surface OUE with water transmission, coupled with the strong correlation with fluorescence, suggests OUE increases with marine biological particles that lower transmission. The moderate–weak negative correlation with salinity implies a small terrestrial output from nearby rivers and estuary (rivers Tamar and Plym) because $O_3$ loss from riverine NOM, which is generally comprised of terrestrial humic-like DOM, has been shown previously (Section 3.3.2.4). However, as discussed earlier, the laboratory-blank-corrected L4 measurements OUE (0.41±0.02) are generally similar to (if not slightly lower than) the laboratory-blank-corrected AMT-29 underway OUE (0.48±0.02, 50° N latitude bin). Therefore any immediate terrestrial influence at L4 is minor. The inclusion of the first data point was enough to substantially lower the correlations between variables which suggests a strong dependence on the thermal stratification during the algal bloom.

**Table 23: Coefficient of determination ($r^2$) for linear regressions between independent variable and OUE (dependant). The direction of correlation is provided when $r^2$≥0.05. All independent variable data ($n$=9), apart from mixed layer depth (MLD), were measured during the rosette cast. Filtered data is the data with a strong thermal stratification (temperature difference >1° C).**

| Variable group | Variable | Surface OUE | Surface OUE filt. | Deep OUE | Deep OUE filt. |
|---|---|---|---|---|---|
| Physical properties | Temperature (° C) | 0.00 | 0.24 (–) | 0.00 | 0.13 (–) |
|  | Salinity (PSU) | 0.02 | 0.23 (–) | 0.01 | 0.07 (+) |
|  | MLD (m) | 0.01 | 0.00 | 0.02 | 0.00 |
| Water clarity | Transmission (%) | 0.20 (–) | 0.72 (–) | 0.37 (–) | 0.36 (–) |
|  | PAR ($\mu$E m$^{-2}$ s$^{-1}$) | 0.11 (–) | 0.18 (–) | 0.00 (–) | 0.16 (–) |
| Biological proxy | Oxygen ($\mu$M) | 0.28 (+) | 0.53 (+) | 0.00 | 0.09 (+) |
|  | Fluorescence | 0.25 (+) | 0.86 (+) | 0.00 | 0.06 (+) |

Generally, the L4 deep OUE experienced weaker correlations than the surface values. The strongest correlation was observed for transmission, which showed a moderate–weak negative correlation with deep OUE. However, all the remaining correlations were weak. The lack of correlations for the deep OUE, especially fluorescence, suggests that the algal bloom was not a dominant driver for deep OUE and other $O_3$ destroying species played a role in $O_3$ loss. Depth profiles of fluorescence and transmission from the rosette's CTD show increased fluorescence

and decreased transmission at the surface, over Jun–Jul (see Figure 62 in Appendix C), which indicates the bloom was efficiently contained in the surface mixed layer and no/limited leakage into the deeper waters occurred.

The Eddystone sample had a measured OUE of 0.33±0.06 and exhibited the largest variability of the four samples. Figure 40b shows a slow decline in Eddystone OUE before a rapid increase and then a slow decline again, which was due to the repeated ageing and replenishing of the stored sample. The much lower Eddystone OUE compared to the L4 waters was due to the biological/chemical consumption of DOM, the chemical oxidation of $I^-$ to $IO_3^-$ or a mixture of both. While the Eddystone sample was variable, the Milli-Q water blank was low and very consistent across nine weeks of measurements (0.15±0.01, R$\sigma$=5 %). Linear regressions between all four OUE and their respective sample temperature (Figure 40b) showed moderate–weak to weak correlations ($r^2$=0.29 (–), 0.23 (–), 0.13 (+) and 0.05 (+)) for Eddystone, L4 surface, Milli-Q water blank and L4 deep respectively. Overall, the gradients were shown to all be statistically similar to each other, and independently similar to zero, with confidence that the similarity together was not a coincidence. The low dependency of OUE on sample temperature, an indication of kinetic rates and not biological production, is in agreement with previous results (Section 4.3.1.3).

### 4.3.3. Cruise data

### 4.3.3.1. Ozone and iodide

The mean Atlantic Ocean OUE, after $O_3$ input correction and before blank subtraction, was 0.593±0.057 ($\pm\sigma$) ($\pm 0.002$ $\sigma_{\bar{X}}$, $n$=918). Over the entire transect, OUE was generally highest in the central equatorial Atlantic Ocean and lowest in the northern and southern regions (although these regions did have hotspots of high OUE), qualitatively consistent with literature estimates of $O_3$ loss (Ganzeveld et al., 2009; Luhar et al., 2018; Pound et al., 2020). Figure 41a shows that the lowest OUE (~0.50) was observed in the eastern North Atlantic Drift (NADR), NASE, SATL and SANT regions. Thus, high OUE did not occur only at the coast (Section 4.3.2). An immediate comparison to the seawater $I^-$ concentration (Figure 41b) showed a similar trend to the OUE suggesting that the OUE was likely dominated by seawater $I^-$. A correlation between OUE and $I^-$ concentration was positive ($OUE = 0.00066 \times C_{I^-} + 0.527$, $r^2$=0.26). The non-zero intercept and moderate–weak strength correlation suggest other $O_3$ destroying species or thermodynamic properties related to physicochemical gas exchange played an important role in the variability of observed OUE. Over the transect, the seawater $I^-$ concentration range was 26–174 nM, which gives reactivities of 50–350 s$^{-1}$, whereas the open-ocean DOC range is estimated between 40–80 µM (Romera-Castillo et al., 2010) which gives similar but slightly lower reactivities of 130–255 s$^{-1}$. The DOM reactivity is based on the reactivity of bulk DOC towards $O_3$ (Coleman et al., 2010; Sarwar et al., 2016), which is highly uncertain. Some of the lowest estimated $I^-$ and DOC concentrations are in the SANT (<40° S) where some of the lowest OUE was observed. A

qualitative match, in terms of maximum and minimum between OUE and I⁻ concentration, was also seen when the data were binned into 1° latitude bins (Figure 42).
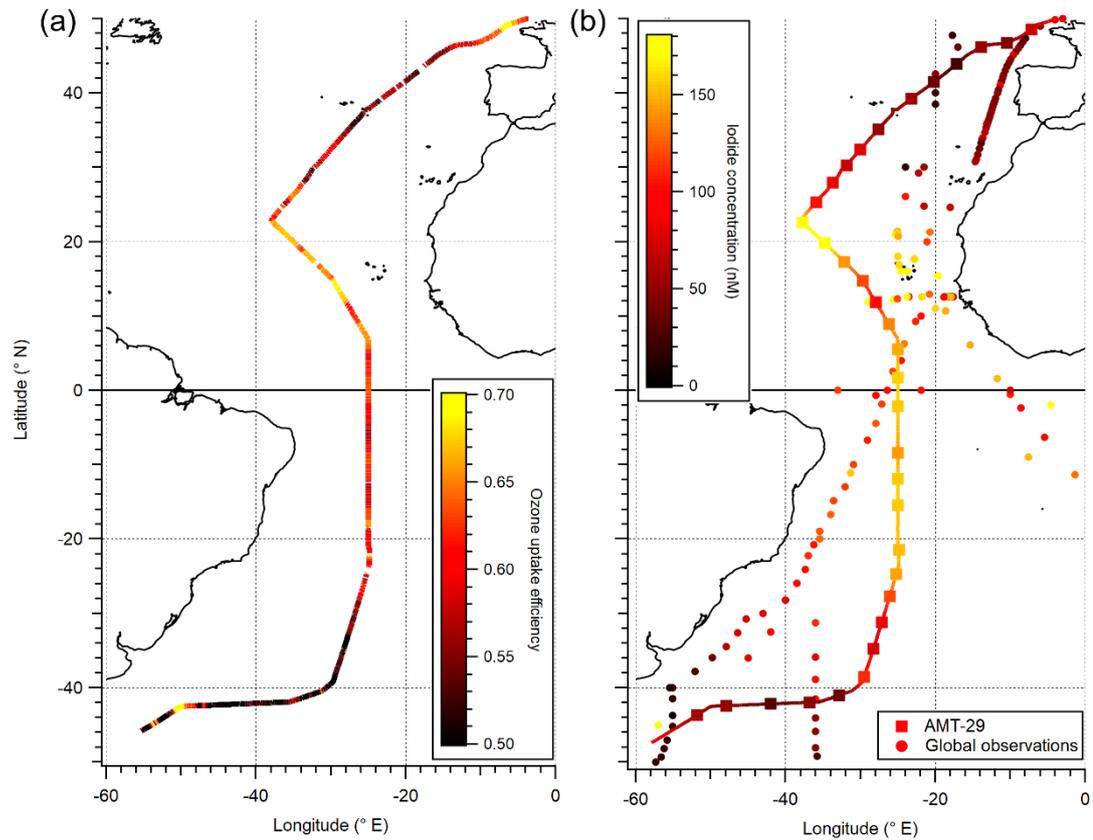


**Figure 41: Underway data (~5 m) over the period 13/10/19–23/11/19 for seawater a) OUE and b) iodide concentration. In panel b, the squares and circles represent the location of the discrete sampling from AMT-29 and Chance et al. (2019). The line through the AMT-29 iodide measurements was linearly interpolated.**
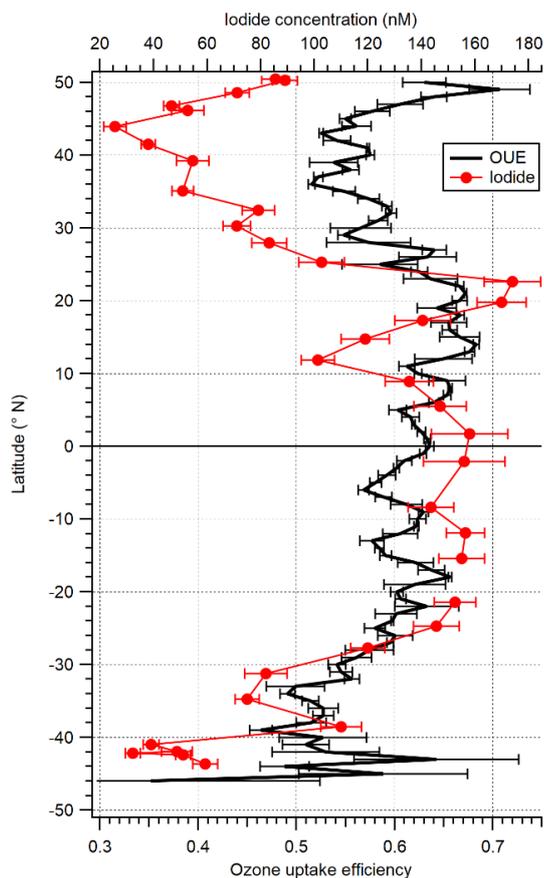
**Figure 42: 1° latitude bins of OUE and iodide concentration in the surface Atlantic Ocean for Autumn 2018. Discrete measurements of iodide concentrations were taken at solar noon. Error bars are 1$\sigma$.**

As mentioned before, the measured OUE contains a contribution from chemical reactions and physical uptake. Two approaches were used to remove the latter, the OUE blank from the in situ measurements (0.26±0.05, see Section 4.3.3.4) and laboratory measurements (0.16±0.01, Section 4.3.2) was subtracted from the hourly average OUE to leave the chemical component; the in-situ-blank-corrected and laboratory-blank-corrected OUE was ~44 and ~25 % lower than the total measured OUE. The 50° N latitude bin of the in-situ-blank-corrected and laboratory-blank-corrected OUE was 0.24±0.03 and 0.48±0.02 respectively, therefore the laboratory-blank-corrected OUE was in better agreement with the blank-corrected OUE from the L4 measurements from the same latitude (0.41±0.02; Section 4.3.2). This implies that the in-situ-blank is potentially erroneous (see Section 4.3.3.4 for potential causes), however as this cannot be directly proven, the in-situ-blank-corrected and laboratory-blank-corrected OUE are discussed simultaneously in the following sections.

Figure 43a shows reaction with I$^-$, as a fraction of the I$^-$-dependant OUE parameterisation, was the dominant contribution of blank-corrected OUE with total OUE contributions of 36–101 % (61±11 and 72±13 % mean in the North and South Atlantic Oceans respectively) when subtracting the laboratory-blank. The average OUE from I$^-$ alone was 0.29±0.07, which accounted for ~66 % of the laboratory-blank-corrected OUE measurement. Here the I$^-$ reaction contribution rarely exceeded the total OUE beyond the measurement uncertainties. On the other hand, I$^-$ contributions of 45–155 % (91±16 and 89±17 % mean in the North and South Atlantic Oceans

respectively) were determined when subtracting the in-situ-blank, which accounted for ~90 % of the blanked OUE measurement (Figure 43b). The use of the in-situ-blank caused the I⁻ contribution to exceed 100 % for significant durations of the transect, but this seems unlikely given (1) the laboratory measurements of $O_3$ driven VOC production (Chapter 3) and (2) the expected contribution, given measured concentrations and reactivities, of DOM (Coleman et al., 2010; Martino et al., 2012; Sarwar et al., 2016).
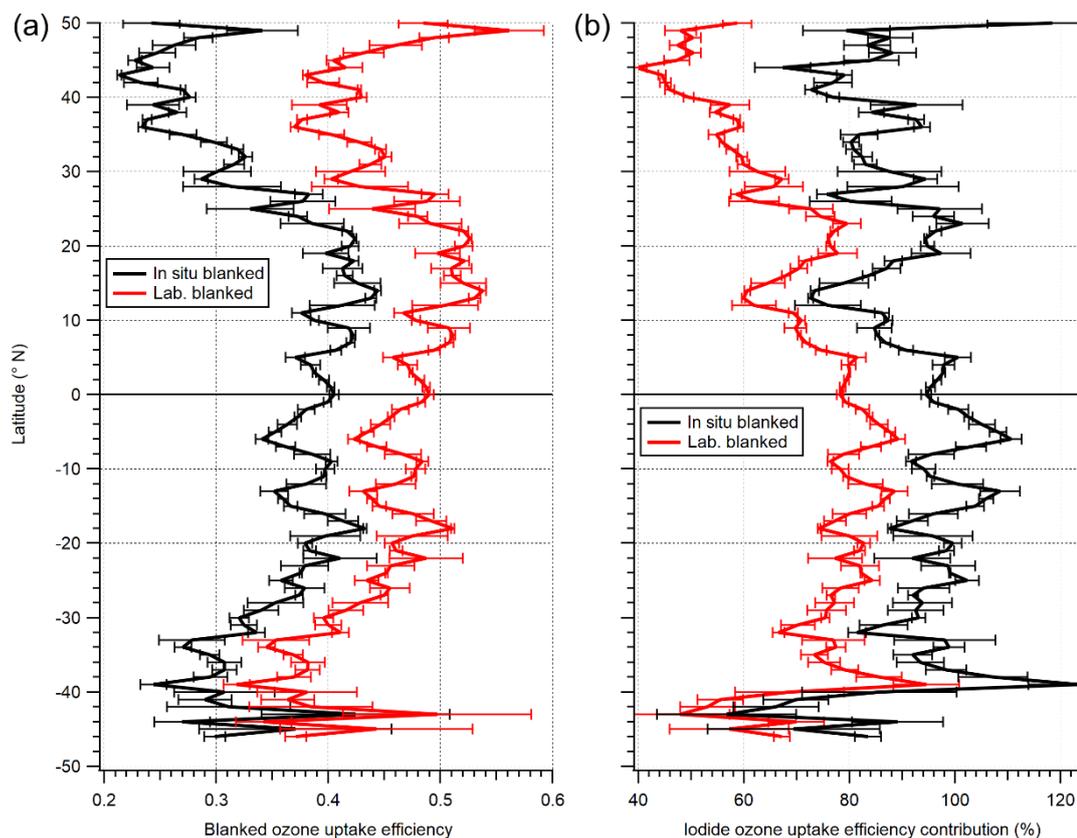


**Figure 43: 1° latitude bins of (a) in-situ-blank-corrected OUE with the respective iodide reaction contribution and (b) laboratory-blank-corrected OUE with the respective iodide contribution in the surface Atlantic Ocean for Autumn 2018. Error bars are 1$\sigma$.**

The binned OUE data had an apparent oscillation (Figure 42 and Figure 43). The average latitude difference between minima in the oscillation was 6.4±2.4°. At an average ship speed of 2.3±1.6° d⁻¹, the period of oscillation was 2.8±2.1 d. Firstly, the >1 d period suggested that a diurnal cycle was not causing an oscillation. Secondly, the 77 % R$\sigma$ suggested the cause of the oscillation was not regular (i.e. scheduled CTD sampling/station). One would expect rapid changes in I⁻ with equal frequency, considering the 61–91 % contribution of I⁻ concentration to OUE, if the source of the oscillation was from the seawater. However, the low frequency of the I⁻ sampling (about once a day) does not allow me to investigate such variability. Whilst there is no evidence of a diurnal cycle in seawater I⁻ concentration or a correlation with in situ MLD (Chance et al., 2014), the oscillation could be linked with MLD history. Chance et al. (2014) showed correlations of moderate–weak strength with summed MLD and also MLD maximum ($r^2$=0.37 and 0.34 respectively).

**4.3.3.2.   Remnant (unaccounted for) OUE in the Atlantic Ocean**

As already discussed, multiple processes control the loss of $O_3$ at the ocean surface. Theoretically, if one could accurately remove the influence of each individual known $O_3$ destroying species, what remains would be the influence of the unknown $O_3$-destroying species. If $I^-$-driven reactivity and physical uptake (related to solubility and diffusion) are subtracted, the remaining OUE here is hypothesised to be due to marine organics. The Milli-Q water blanks and $I^-$-dependant OUE (Section 4.3.2/4.3.3.4 and 4.3.1.2 respectively) were subtracted from the total measured OUE to estimate the unknown dependency on OUE – "remnant OUE".

As with Section 4.3.3.1, two sets of values are provided when subtracting the in-situ-blank and the laboratory-blank. Figure 44a shows the remnant OUE latitudinal distribution, which is homogeneous for in-situ-blank-corrected remnant OUE. The mean remnant OUE when subtracting the in-situ-blank was 0.037±0.053 (±0.002 $\sigma_{\bar{X}}$, $n$=918), which represents on average ~10 % of the total in-situ-blank-corrected OUE (range of -55–55 %). If the Atlantic Ocean is split, 9±16 and 11±17 % mean contribution is calculated in the North and South respectively (Figure 44b). Importantly here, the in-situ-blank-corrected remnant OUE contribution is not within the possible contributions set by bounds of the total OUE measurement, the independent $I^-$ contribution and the blank (i.e. has a negative contribution, at maximum -55 % of the blank-corrected OUE). On the other hand, the mean laboratory-blank-corrected remnant OUE was 0.151±0.063 (±0.002 $\sigma_{\bar{X}}$, $n$=918), representing on average ~34 % of the total laboratory-blank-corrected OUE (range of -1–63 %). In this case, if the Atlantic Ocean is split, 38±11 and 28±13 % mean contribution is calculated in the North and South respectively. Assuming the remnant OUE contribution is organic in nature, the ~34 and ~66 % contribution of organic material and $I^-$ is similar to the findings of Martino et al. (2012); a slightly lower percentage loss to organic material is shown here because the marine DOM from L4 is slightly more saturated than the riverine NOM used by Martino et al. (2012).
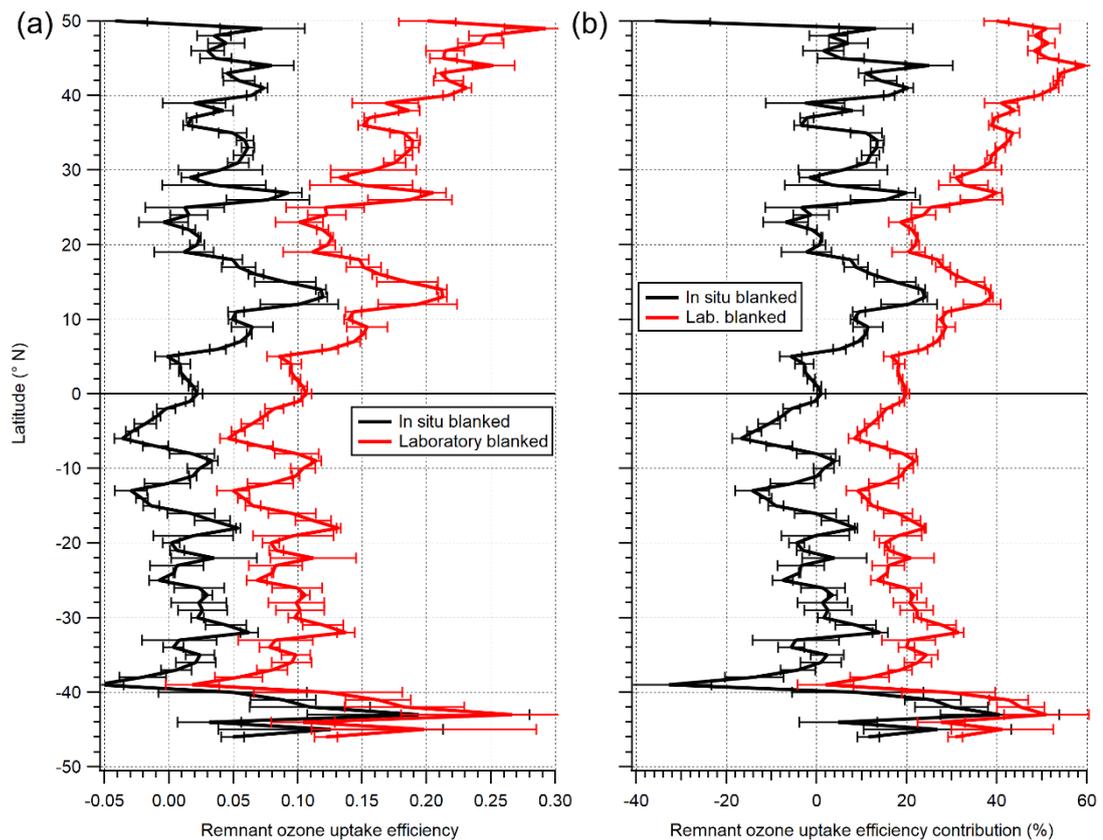
**Figure 44: 1° latitude averages of (a) remnant ozone uptake efficiency, using the in-situ blank and the laboratory blank, and (b) the non-iodide ozone uptake efficiency contribution to the blanked OUE measurement in the surface Atlantic Ocean for Autumn 2018. Error bars are $1\sigma$.**

### 4.3.3.3.    Relationships of OUE and remnant OUE to ocean variables

In this section, correlations between ocean variables and OUE, and I⁻ concentration and remnant OUE are discussed. While other groups have identified relevant correlations for seawater I⁻ concentration (Chance et al., 2014; Macdonald et al., 2014; Sherwen et al., 2019), their work on producing I⁻ concentration parameterisations was done with some estimated ocean variables. In the first half of this section, OUE and I⁻ concentration are discussed together with directly measured ocean variables. In the second half, laboratory- and in-situ-blank-corrected remnant OUE are discussed.

In terms of the direct measurements, surface temperature, salinity and fluorescence were measured in situ from *Discovery*'s clean underway supply, while chlorophyll *a* concentration was measured by adsorption by Dall'Olmo et al. (PML) and nutrient data were measured using an auto-analyser by Woodward et al. (PML) respectively. MLD was calculated from the pre-dawn and solar noon CTD downcast data using the +0.03 kg m⁻³ and ±0.2 °C methodology following de Boyer Montégut et al. (2004). $CO_2$ fugacity ($fCO_2$) was measured by Yang et al. (PML) using an SFCE approach. Refer to the BODC cruise inventory for detailed documentation and data ownership; bodc.ac.uk/resources/inventories/cruise_inventory/report/17230. CDOM values were taken from the daily MODIS-Aqua 443 nm absorption product (GIOP model) at 4 km resolution. Here underway OUE data was averaged onto the MODIS pixel grid.

**4.3.3.3.1.    OUE and iodide**

Figure 45 shows the surface temperature, salinity, fluorescence and chlorophyll *a* concentration data with latitude on AMT-29. Qualitatively, temperature exhibits the same latitudinal trend as surface OUE and I⁻ concentration (Figure 42). Linear regression between temperature and OUE showed a moderate–weak positive correlation (Table 24), while a regression between temperature and I⁻ concentration (interpolated to hourly timestamp) showed a stronger moderate correlation. The correlation of OUE with temperature is slightly higher than the laboratory measurements of OUE temperature dependence (see Section 4.3.1.3) and potentially suggests an indirect co-dependency. The correlation of temperature with I⁻ concentration is quantitatively consistent with the results of Chance et al. (2014), who discuss that the positive temperature correlation could be due to a co-dependency on vertical mixing (i.e. MLD; increased dilution with deep water in the colder waters) or an indirect link with an I⁻ source/sink through plankton community composition (varies with temperature) or surface photochemistry (solar radiation raised temperature). Thus the OUE:temperature correlation may be in large part indirectly mediated through the effect of temperature on seawater $O_3$ destroying species concentration, and not primarily due to the effect of temperature on reaction kinetics.
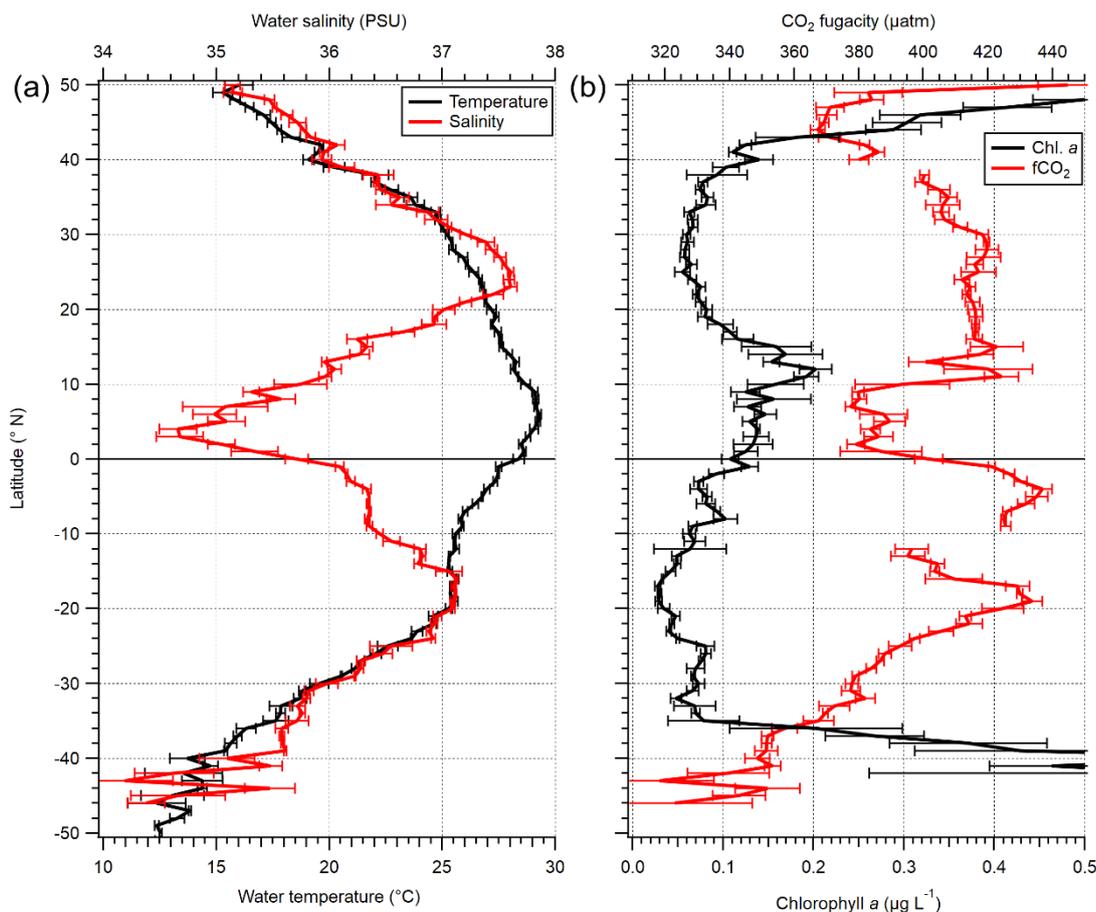


**Figure 45: Underway data (~5.5 m) over the period 13/10/19–23/11/19 for seawater (a) temperature and salinity and (b) chlorophyll *a* concentration and fCO₂, binned into 1° latitude intervals.**

**Table 24: Coefficient of determination ($r^2$) for linear regressions between the independent variable and ozone uptake efficiency, surface iodide concentration and non-iodide ozone uptake efficiency (iodide and blank influence subtracted). The direction of correlation is provided when $r^2 \geq 0.05$. Temperature and salinity ($n=984$ and $948$ respectively, 1 h average), chlorophyll $a$ ($n=911$, 1 h int.), mixed layer depth ($n=55$ stations). DOC and additional nitrate, nitrite, phosphate and silicic acid data from the CLIVAR A16S-2013 cruise (Hansell et al., 2021) ($n=102$, 1° latitude average, italic font). CDOM values were from the MODIS-Aqua 443 nm absorption product (filtered for open-ocean) ($n=102$, MODIS pixel average).**

| Variable | Variable | Iodide conc. (nM) | Total OUE | Remnant OUE (in situ) | Remnant OUE (lab.) |
|---|---|---|---|---|---|
| Water properties | Temperature (°C) | 0.57 (+) | 0.24 (+) | 0.03 | 0.16 (−) |
| | Salinity (PSU) | 0.21 (+) | 0.03 | 0.07 (−) | 0.13 (−) |
| | Salinity (\|latitude\|≥20°) (PSU) | 0.32 (+) | 0.03 | 0.08 (−) | 0.13 (−) |
| | Salinity (\|latitude\|<20°) (PSU) | 0.04 | 0.01 | 0.02 | 0.03 |
| | Mixed layer depth (m) | 0.11 (−) | 0.11 (−) | 0.00 | 0.01 |
| ODS | Iodide concentration (nM) | 1.00 (+) | 0.26 (+) | 0.15 (−) | 0.41 (−) |
| | DOC concentration (µM) | *0.37 (+)* | *0.42 (+)* | *0.01* | *0.03* |
| Biological proxy | Chlorophyll $a$ concentration (µg L$^{-1}$) | 0.20 (−) | 0.00 | 0.13 (+) | 0.28 (+) |
| | Chl. $a$ conc. (-35–40° N) (µg L$^{-1}$) | 0.00 | 0.10 (+) | 0.15 (+) | 0.11 (+) |
| | Chl. $a$ conc. (<-35 & >40° N) (µg L$^{-1}$) | 0.06 (+) | 0.23 (+) | 0.13 (+) | 0.11 (+) |
| | CO$_2$ fugacity (µatm) | 0.27 (+) | 0.18 (+) | 0.32 (−) | 0.04 |
| | CDOM absorption (m$^{-1}$) | 0.13 (−) | 0.02 | 0.00 | 0.20 (+) |
| | CDOM absorption filtered (m$^{-1}$) | 0.62 (−) | 0.52 (−) | 0.46 (+) | 0.31 (+) |
| Inorganic nutrients | Silicate concentration (µM) | 0.06 (+) | 0.04 | 0.00 | 0.01 |
| | | *0.13 (+)* | *0.00* | *0.09 (−)* | *0.28 (−)* |
| | Nitrite concentration (µM) | 0.08 (−) | 0.23 (−) | 0.47 (+) | 0.24 (−) |
| | | *0.13 (−)* | *0.23 (−)* | *0.16 (+)* | *0.06 (+)* |
| | Nitrate concentration (µM) | 0.11 (−) | 0.16 (−) | 0.23 (+) | 0.00 |
| | | *0.03* | *0.14 (−)* | *0.10 (+)* | *0.02* |
| | Phosphate concentration (µM) | 0.03 | 0.06 (−) | 0.11 (+) | 0.00 |
| | | *0.03* | *0.12 (−)* | *0.06 (+)* | *0.00* |

Surface salinity showed the same trend as temperature when |latitude|≥20° (i.e. in the subtropical, temperate and cold zones) (Figure 45a). Regressions between OUE and salinity were very weakly positive (Table 24), which did not improve when the salinity data was filtered for |latitude|≥20° or |latitude|<20°. On the other hand, I⁻ concentration showed a moderate–weak positive correlation with salinity, which was also quantitatively consistent with Chance et al. (2014). Chance et al. (2014) indicate precipitation, evaporation and mixing are not dominant controls on seawater I⁻. Here these three processes are also not dominant towards seawater OUE because of the very weak correlation. The reduction in variability between I⁻:temperature and OUE:temperature was approximately similar to the reduction between I⁻:salinity and OUE:salinity. Filtering the salinity data for |latitude|≥20° slightly improved the correlation with I⁻, with a significantly lower correlation at |latitude|<20°.

Latitudinal trends in surface chlorophyll $a$ concentration differed from the other underway parameters shown in Figure 45a. No correlation was shown between OUE and chlorophyll $a$ concentration over the full transect (Table 24). However, I⁻ concentration and chlorophyll $a$ concentration showed a moderate–weak negative correlation that was not seen by Chance et al. (2014) (who found no correlation between seawater I⁻ and chlorophyll $a$). OUE and chlorophyll $a$ concentration showed a weak positive correlation for the gyre/equator and non-gyre/equator transects. Here chlorophyll $a$ is likely a proxy for seawater organic content and not a direct O$_3$ loss reagent because chlorophyll $a$ has a very low O$_3$ reactivity (compared to I⁻ and DOC, see Table 1). Furthermore, a moderate negative correlation was observed between OUE and CDOM

only when the CDOM data were filtered for the open-ocean data (outliers that affected correlation were in the NECS and near the Cape Verde archipelago). Regressions between OUE and $fCO_2$ showed a positive weak correlation because a slightly stronger moderate–weak correlation was observed for I⁻ concentration. The positive correlation with I⁻ suggests a relationship with dissolved inorganic carbon (DIC) from remineralisation or the co-dependency of fCO2 on seawater temperature (Thomas et al., 2005).

MLD was calculated from CTD data measured on station and inorganic nutrients were sampled at station, which occurred twice a day (pre-dawn and solar noon) for the majority of the open-ocean days. Figure 46a shows the latitudinal distribution of MLD and the surface nutrient concentrations on the AMT cruise. MLD closely matched the expected depth from a monthly climatology to within a few degrees latitude (de Boyer Montégut et al., 2004), which helps validate the calculations. Linear regression between MLD and OUE and I⁻ concentration showed a near-identical (spread of variability) weak negative correlation (Table 24). The I⁻:MLD correlation was quantitatively similar to that with the monthly MLD (±0.5 °C thermocline) seen by Chance et al. (2014), who showed the duration of stratification over the course of a year was more important than the in situ MLD, hence the weak correlation observed in both works.
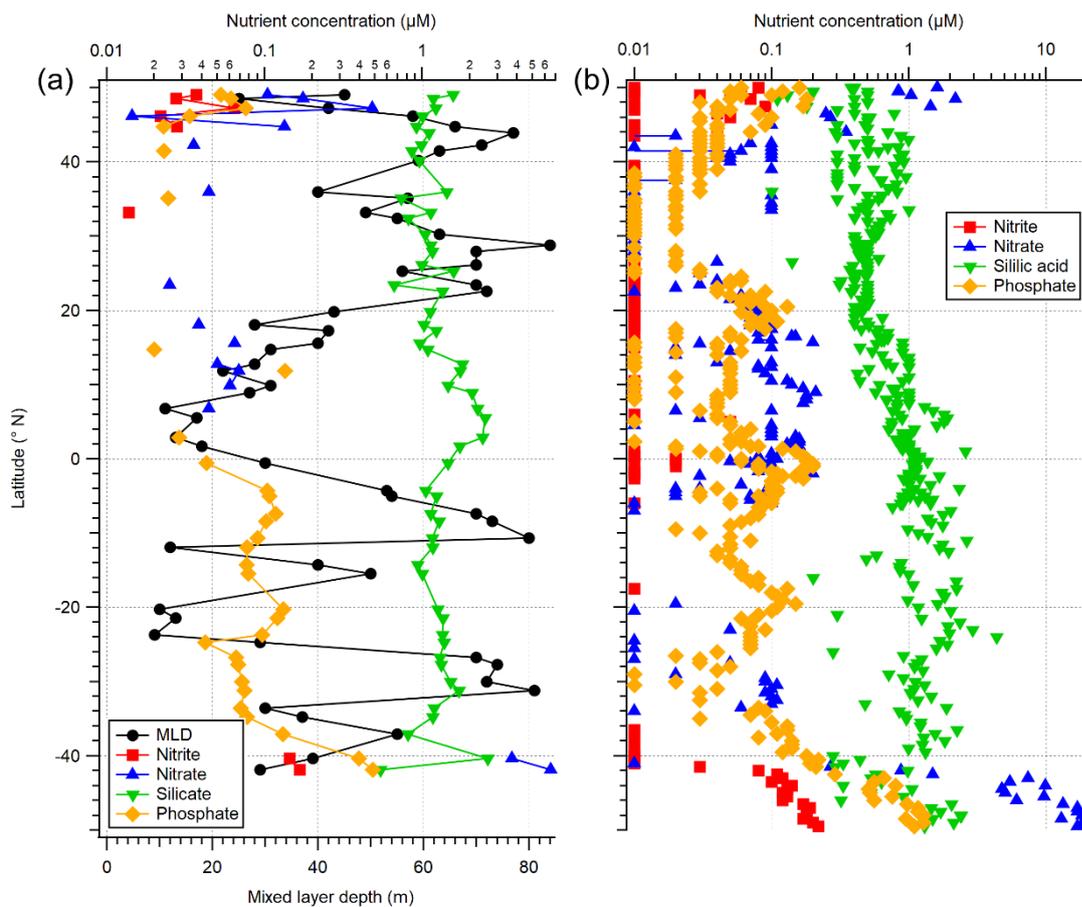


**Figure 46: Latitude distribution of (a) mixed layer depth and surface inorganic nutrients measured at station on AMT29 and (b) surface inorganic nutrients measured on the CLIVAR A16S-2013 cruise (Hansell et al., 2021).**

The station nutrient data has variable $n$ count (8, 16, 32 and 55 for nitrite, nitrate, phosphate and silicate respectively) because different nutrients were below their respective LOD at different

latitudes along the transect (Figure 46a). Regressions between inorganic nutrients and OUE show moderate–weak and weak negative correlations (Table 24). Nitrite and nitrate had the strongest correlation while phosphate and silicate were much weaker. Negative correlations are expected if the nutrients are a proxy for biological DOM/organic production, however, the regression strength suggests the link is poor. For regressions with $I^-$ concentration, nitrate and nitrite were strongest (both negative), while silicate and phosphate were much weaker (positive and negative respectively). The $I^-$:nitrate regression strength was under half of the strength observed by Chance et al. (2014), likely because their data compilation incorporated larger temporal and spatial variability especially in more productive nitrate-rich waters (>2 µM). Figure 46b shows high resolution literature measurements of surface nutrients (Hansell et al., 2021). Unfortunately, no measurements occur over the same period as AMT-29 (autumn), however, the CLIVAR A16S-2013 cruise – highlighted in Figure 47a – occurred in winter (Dec–Feb). Linear regressions between OUE and inorganic nutrients from the CLIVAR A16S-2013 cruise show moderate–weak to weak negative correlations (Table 24). Interestingly, all four nutrients showed identical correlations, in terms of predicted variability, gradient and intercept via multi-comparison regression analysis, to their respective AMT OUE:nutrient regressions.

Figure 47 shows literature measurements of surface DOC concentration (Hansell et al., 2021), which loosely follow the latitudinal trend of OUE and $I^-$ concentration. Linear regression between surface DOC from the CLIVAR A16S-2013 cruise and OUE and $I^-$ concentration show moderate and moderate–weak strength positive correlations (Table 24). OUE and DOC see a moderate strength positive correlation, which was surprisingly strong despite being many annual cycles apart. The approximate similarity in the variability of OUE and $I^-$ concentration predicted by DOC suggests a co-dependency on biological activity or biogeochemical processes (Chance et al., 2014). The slightly improved regression for OUE:DOC, compared to OUE: $I^-$, is likely the organic component in OUE.
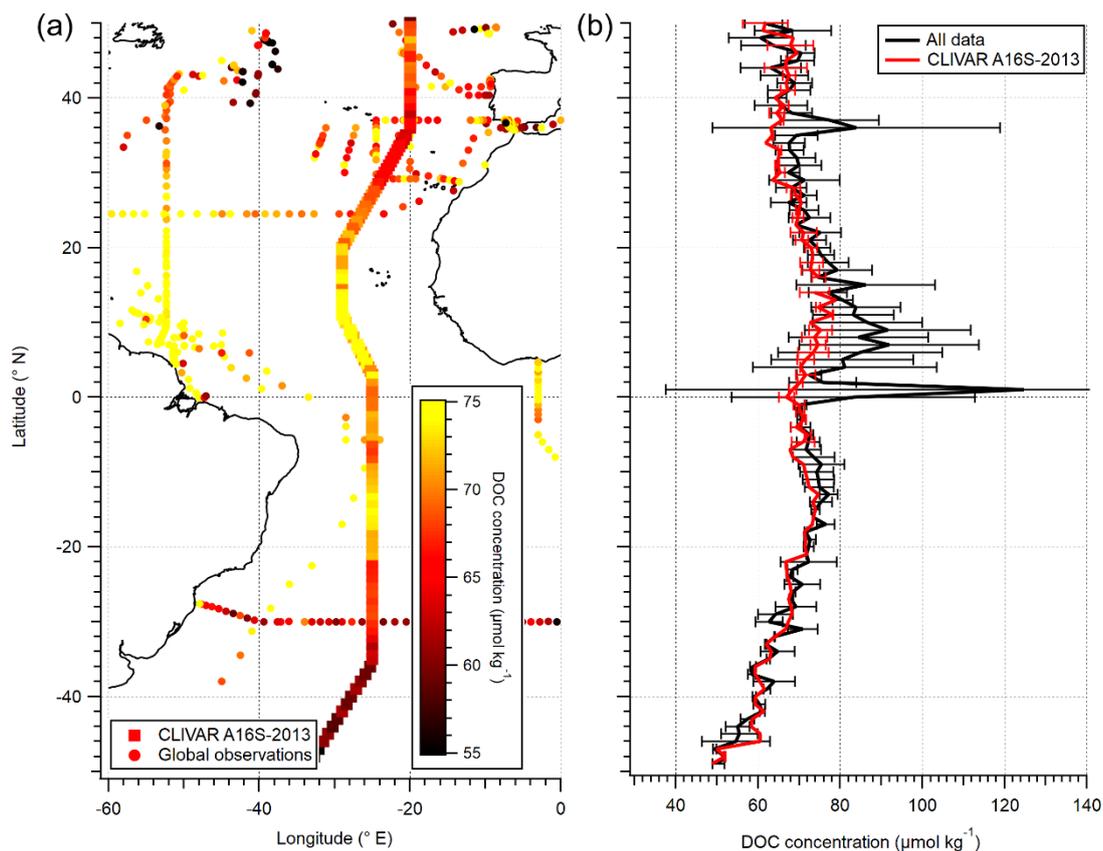
**Figure 47: Literature DOC concentration in the Atlantic Ocean by (a) coordinates and (b) latitude bins, filtered for <10 m depth. Data from Hansell et al. (2021). The north-south transect in panel (b) is the CLIVAR A16S-2013 cruise, which is highlighted with square shapes in panel (a).**

The important take-home message from these analyses of OUE measurements in the Atlantic Ocean are (1) OUE and nutrients are inversely correlated on large spatial scales, (2) OUE and $O_3$ destroying species (i.e. $I^-$, DOC, chlorophyll $a$) are correlated on large spatial scales, and (3) $I^-$ accounts for more than half of $O_3$ chemical loss in the bulk mixed surface layer seawater.

### 4.3.3.3.2.    Remnant laboratory-blank-corrected OUE

In this subsection, correlations with laboratory-blank-corrected remnant OUE are discussed. Figure 44b shows that if the lab-blank is used, the highest percentage contribution from reactants other than $I^-$ was found in the northern and southern temperate zones. Of the three available seawater organic concentration climatologies (DOC, chlorophyll a and CDOM; Section 3.3.3.2), the contribution of remnant OUE in Figure 44b is most consistent with the geospatial distribution of CDOM (Nelson and Siegel, 2013); highest CDOM above and below ~40° with a smaller increase just above the equator. The work of Nelson and Siegel (2013) is a decadal average, so some variability is to be expected. Satellite-derived CDOM absorption showed a moderate–weak positive relationship with remnant OUE, which slightly increased in strength when filtering for non-coastal water, which provides evidence for a biological organic sink. The filtering for non-coastal likely removed the influence of terrigenous detrital material from the coast (Bélanger et al., 2008).

Seawater $I^-$ concentration showed a moderate strength negative correlation with the remnant OUE (Table 24) which was opposite in direction to the total OUE. Considering the influence of

I$^-$ has been subtracted to calculate remnant OUE, a negative correlation may be an indication of biological activity. This is consistent with the positive correlations with chlorophyll *a* and negative correlation with in situ nitrite concentration, especially because the correlations here are significantly stronger than [total OUE]:[chlorophyll *a*] and similar to [total OUE]:nitrate. This suggests the remnant OUE should correlate with seawater organic content assuming chlorophyll *a* is a proxy for seawater organic content through co-relation with phytoplankton abundance (i.e. primary production biomass; Suratman et al., 2009). The remnant OUE showed a moderate–weak correlation with chlorophyll *a*, which was stronger than the total OUE. However, with the gyre and equator only transect and the non-gyre-equator transect, weaker positive correlations were observed. Whilst the variability predicted between the gyre-equator-only transect and the non-gyre-equator transect were identical, the gradients suggested the gyres and equator were more sensitive (~x6) to chlorophyll *a*. Ganzeveld et al. (2009) show a chlorophyll *a*–$O_3$ reaction scheme in the open-ocean only weakly increases $O_3$ loss, which is further evidence the correlations presented here are not a result of a direct chlorophyll *a*–$O_3$ reaction.

As already discussed, a moderate–weak negative correlation was observed between remnant OUE and nitrite. Interestingly, the same correlation is observed for [remnant OUE]:nitrite and [total OUE]:nitrite. The remaining in situ nutrients showed no correlation with remnant OUE. Silicate and nitrite nutrient data from the CLIVAR A16S-2013 cruise showed a moderate–weak negative correlation and a weak positive correlation, respectively, with remnant OUE while the other nutrients did not.

No correlation was observed between remnant OUE and DOC concentration, possibly because (1) DOC concentration represents too large an organic pool, and only a fraction of that reacts with $O_3$, and (2) interannual and annual variability in the Atlantic Ocean between winter 2013 and autumn 2019 causes a poor match between data. Point (2) is further evidenced with weak, but non-zero, correlations with in situ nutrients as already discussed. Moreover, no correlation was observed between remnant OUE and $fCO_2$.

Temperature showed a weak negative correlation with remnant OUE, which was in the opposite direction to the [total OUE]:temperature correlation. Moreover, salinity and non-tropical salinity (|latitude|≥20°) showed identical negative weak correlations with remnant OUE, via multiple regression analysis, which was not observed for [total OUE]:salinity.

### 4.3.3.3.3.    Remnant in-situ-blank-corrected OUE

Finally, in-situ-blank-corrected remnant OUE is discussed last in this subsection; last, because there is the least evidence that the in situ blanks are a true signal and not – as an example – a result of a contaminated Milli-Q water generating machine. Hence this discussion is minimal.

In situ nitrite showed the strongest correlation, via linear regression, with remnant OUE (Table 24). The correlation was positive and had a moderate strength fit, which was opposite and stronger than total OUE. Likewise, nitrate and phosphate both showed positive correlations, however with moderate–weak and weak fitting respectively. Comparisons with the CLIVAR

A16S-2013 cruise data showed similar moderate–weak and weak positive correlations. In situ silicate did not show any correlation while the CLIVAR A16S-2013 cruise data showed a weak negative correlation.

Seawater $I^-$ concentration showed a weak negative correlation with remnant OUE (Table 24), which was opposite to [total OUE]:$I^-$. Similar to the discussion above for laboratory-blank-corrected remnant OUE, a negative correlation here is likely an indication of biological activity, however, for this remnant OUE the correlation with nitrite was positive. Again, this is consistent with the positive correlations with chlorophyll *a* which were stronger than for [total OUE]:[chlorophyll *a*]. Remnant OUE showed very similar weak positive relationships with chlorophyll *a* for the total transect, gyre and equator only transect (-35–40° N) and the non-gyre-equator transect (<-35 & >40° N). Here the gradient of the -35–40° N data was ~4 times steeper than the <-35 & >40° N data; the gyres and equator were more sensitive to chlorophyll *a* even though concentrations were lower (i.e. less productive waters). Similarly again, no correlation was observed between either remnant OUE and DOC concentration. On the other hand, a large increase in correlation between CDOM and remnant OUE was observed when CDOM was filtered for non-coastal. A moderate strength relationship was observed that was stronger than for laboratory-blank-corrected remnant OUE.

A moderate–weak relationship was observed for remnant OUE and $fCO_2$. This suggests that DIC uptake and the conversion to organic material correlate better with in-situ-blanked-corrected remnant OUE than laboratory-blank-corrected remnant OUE.

No correlation between in-situ-blank-corrected remnant OUE and temperature was seen. Moreover, salinity and non-tropical salinity (|latitude|≥20°) showed identical negative weak correlations with in-situ-blank-corrected remnant OUE and laboratory-blank-corrected remnant OUE, via multiple regression analysis, which was not observed for [total OUE]:salinity.

### 4.3.3.4.  Additional data: Milli-Q blanking

Over the course of the transect, ultrapure Milli-Q water was used as a measure of the OUE blank as in theory Milli-Q water does not contain any reactant; thus physical $O_3$ loss processes are the most relevant (i.e. gas exchange/uptake, which is related to solubility, diffusivity, and turbulence within the SFCE). While $O_3$ does react with the auto-dissociation components of $H_2O$ (i.e. hydroxide ion (HO$^-$), $O_3 + HO^- \rightarrow HO_2^- + O_2$) and the subsequent products (i.e hydroperoxide anion (HO$_2^-$), $O_3 + HO_2^- \rightarrow HO + O_2^- + O_2$) (Staehelin and Holgné, 1982; Von Gunten, 2003a), the rate-determining reaction with HO$^-$ is very slow (70 M$^{-1}$ s$^{-1}$ (Staehelin and Holgné, 1982), compared to ~$2\times10^9$ M$^{-1}$ s$^{-1}$ for $I^-$ (Moreno et al., 2018)).

Figure 48 shows that for the first week of the cruise, the in situ Milli-Q OUE was elevated compared to the remaining cruise. Here the first week's mean OUE was $0.36\pm0.04$ ($\pm\sigma$, $n$=4) and the remaining mean OUE was $0.25\pm0.03$ ($n$=15). Overall, the mean in situ blank OUE was $0.28\pm0.06$. An exponential fit through the in situ measurements, $y = 0.233 + 0.154 \exp\left(\frac{-t}{720393}\right)$, was used to produce the in-situ-blank-corrected OUE discussed in Section

4.3.3. In the equation, $t$ represents time in s since 01/01/1904 (a property of time data in the Igor Pro software used).
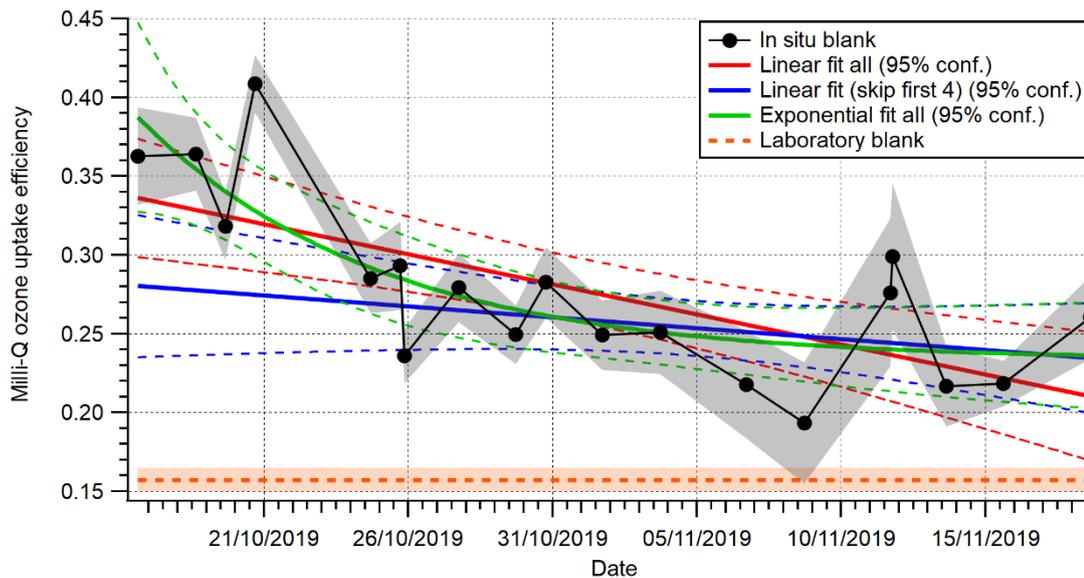


**Figure 48: Timeseries of blank OUE measurements during the transect. The shaded region is $1\sigma$. The average blank from the laboratory time series is provided for comparison.**

Potential causes for the initial raised in situ blank are, but are not limited to, (1) a contaminated Milli-Q system, (2) a contaminated SFCE and (3) changing turbulence within the SFCE. Considering $O_3$ is used for biofouling prevention in water supplies (Von Gunten, 2003a, 2003b) and $O_3$ was running through the SFCE (starting mean $1194\pm411$ ppbv, ending mean $498\pm211$ ppbv) for over ~200 h before the fourth Milli-Q blank (just before 21/10/19, Figure 48), a contaminated SFCE is unlikely. Furthermore, considering the SFCE was attached to a frame that wasn't altered, an orientation change that may have affected internal turbulence is unlikely. Thus, of the causes suggested, a contaminated Milli-Q system is thought to be most likely. In this scenario, a small amount of biological activity/fouling had likely built up during inactivity between ship deployments that was partially flushed with repeat usage; this also could explain why the latter blanks were still higher than the laboratory blank (see Section 4.3.2).

The Milli-Q water is essentially fresh water and does not take into account the influence of salinity on the solubility of $O_3$. The average $O_3$ salting-out factor along the transect was calculated to be $1.24\pm0.01$ following Johnson (2010) with solubility data from Sander (2015). Incorporating the salting-out factor into theoretical calculations of $R_3$ causes a reduction factor of 1.08, which is also seen with the direct measurements of OUE from saline and non-saline samples (see Section 4.3.1.2). The exponential blank fit was corrected by in situ temperature and salinity measurements.

### 4.3.3.5. Additional data: CTD data

During rosette casts, the DCM was sampled at 9 stations predominantly in the North Atlantic Ocean (Figure 49). The mean DCM OUE was $0.56\pm0.05$ ($\pm\sigma$), which was compared to a mean surface OUE of $0.62\pm0.04$ (h average of the station). These two means were found to be statistically different (t-test, $p=0.03$), although this difference is likely driven by three or four of

the data points. The DCM was sampled because it was expected to contain the highest concentration of fresh DOM, however, I⁻ concentration could have been lower at the DCM relative to the surface. Linear regression between the DCM OUE and the near-simultaneous surface showed no correlation ($r^2$=0.00), however without knowing the extent of the I⁻ concentration in the DCM, it is difficult to make sense of the correlation (or lack of) in OUE between the DCM and the surface. For all stations where the DCM was sampled, apart from the second station (CTD#6) which was 7 m above, respectively, the DCM was below the MLD (mean 60±37 m, not including CTD#6); thus the northern tropical and subtropical variability is not a result of the MLD. It is however interesting that the DCM OUE was lower than the surface OUE. If the DCM was lower in I⁻ (generally lower at depth, see Chance et al. (2014)), it implies that the reduced I⁻ at DCM outweighs any potential increase in fresh DOM at the DCM.
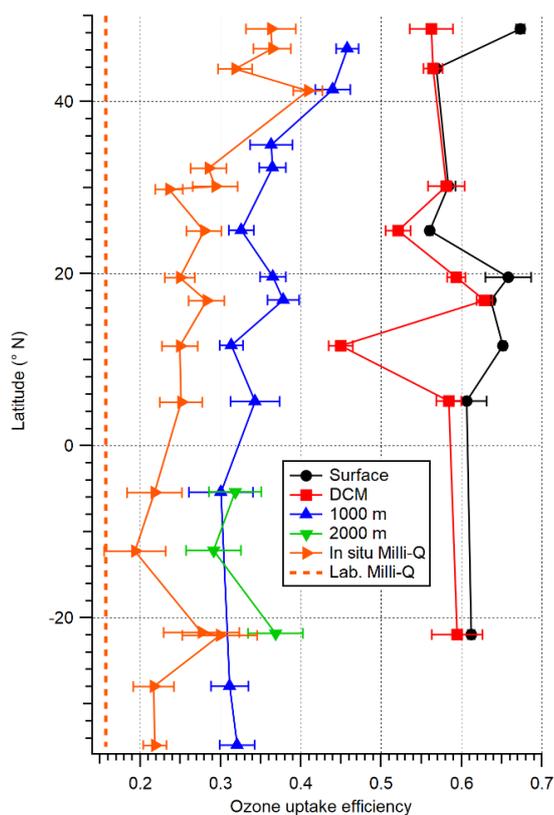


**Figure 49: Latitudinal distribution of OUE measurements from the deep chlorophyll maximum (DCM), 1000 m deep and 2000 m deep in the Atlantic Ocean in Autumn 2019. Surface is the hour average of the station. The shaded regions are 1$\sigma$. CTD#6 (see main text) is at ~44° N.**

Seawater from 1000 m was sampled at 12 stations, again predominantly in the North Atlantic Ocean, while seawater from 2000 m was sampled at 3 stations in the South Atlantic Ocean (Figure 49). Overall, the mean 1000 m and 2000 m OUE were 0.36±0.05 and 0.33±0.04 respectively. A linear regression of 1000 m CTD with latitude showed a gradient that was statistically different from zero (F-statistic of 12.6 compared to an F-critical of 5.0), which suggests that the Atlantic Ocean 1000 m seawater is heterogeneous on large latitudinal scales. The South Atlantic 1000 m OUE and the 2000 m OUE was shown statistically similar with a t-test ($p$=0.58) and F-test ($p$=0.58) that implies deep water is homogeneous on short latitudinal scales.

It is clear the 1000 m OUE in the northern temperate and subtropics had both the highest OUE and the highest variance of the deep water; because of the small sample size, the statistical similarity with the remaining 1000/2000 m samples may shift to a statistical difference if more stations were collected. Linear regressions between 1000 OUE and 1000 m salinity and temperature showed moderate strength positive correlations ($r^2$=0.57) which suggest that the raised 1000 m OUE in the Northern Hemisphere was due to a separate water mass. However, the lower 1000 m OUE in the Southern Hemisphere likely was because the CTD was sampling the AAIW which was bringing low temperature, low salinity waters from the Southern Ocean (see Figure 60 in Appendix C). The water in the AAIW is shown to be 41 % older than the North Atlantic deep water (Romera-Castillo et al., 2019). Therefore the lower OUE in the AAIW (difference of 0.057 or ~15 %) may be linked to degradation/consumption of some organic materials (i.e. labile/semi-labile DOM) in the older water. In total, the AAIW water is shown to have an equal DOC concentration to the North Atlantic deep water (Romera-Castillo et al., 2019), which further suggests this labile/semi-labile DOM fraction is small.

An interesting and easily overlooked result is that the deep Atlantic water had a measurable OUE. The in-situ blanked and laboratory-blank-corrected 1000 m OUE were 0.099±0.024 and 0.211±0.050 respectively, which equated to ~30 and ~47 % of blanked surface OUE respectively. Considering the surface water has a high $I^-$ concentration and also higher DOM concentration (Ogawa and Tanoue, 2003; Romera-Castillo et al., 2016, 2019) and that the deep water has low/negligible $I^-$ concentration (Chance et al., 2014), this suggests that the refractory DOC present in the deep water (Ogawa and Tanoue, 2003) had substantial $O_3$ reactivity.

### 4.3.3.6.  Additional data: Atmospheric ozone concentration

Atmospheric $O_3$ concentrations were measured alongside OUE. The mean $O_3$ concentration measured was 27.9±8.3 ppbv (±$\sigma$, 0.3 ppbv $\sigma_{\bar{X}}$), with a median of 25.9 ppbv and quartiles of 21.6 and 34.4 ppbv. Figure 50 shows the measured $O_3$ concentration was highest in the Northern Hemisphere (33.0±7.2 and 21.5±4.0 ppbv per hemisphere respectively) which is consistent with previous measurements (Winkler, 1988). Figure 50 also shows measured $O_3$ concentrations on AMT-22 (Hackenberg et al., 2012) and AMT-23 (Hackenberg and Read, 2013), which are qualitatively consistent with AMT-29 measurements for the Southern Hemisphere, and also $O_3$ concentrations from the Cape Verde Atmospheric Observatory (CVAO) (Read, 2019). The largest discrepancy is in the northern tropics (3–16° N) where AMT-29 measured ~40 ppbv whilst other literature and datasets showed ~20 ppbv (Winkler, 1988; Hackenberg et al., 2012). HYSPLIT (Stein et al., 2015; Rolph et al., 2017) backward trajectories for coordinates 8.094° N -25.731°E (29th Oct–1st Nov 2019) suggest the air mass trajectory was from the West African coast (see Figure 61 in Appendix C). Measurements from the CVAO for 29th Oct–1st Nov 2018 (2019 not available) show elevated concentrations compared to the AMT-22/-23 cruises, which were further west. The higher ozone concentrations during AMT29 and at CVAO closer to the African continent probably represent real spatial variability.
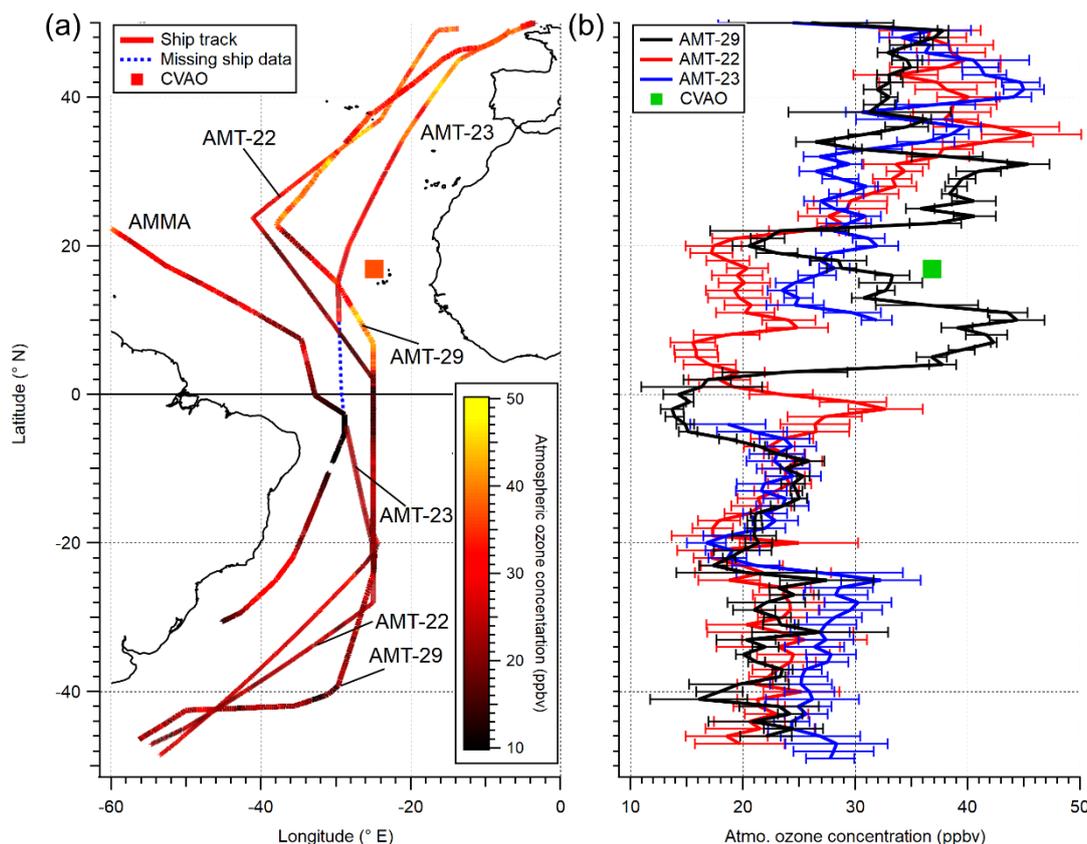
**Figure 50: O₃ concentration in the Atlantic Ocean marine boundary layer by (a) coordinate and (b) 1° latitude bins. AMT-22 data from Hackenberg et al. (2012), AMT-23 data from Hackenberg and Read (2013) and AMMA data from Helmig et al. (2012).**

### 4.3.4.  Cruise summary and implications

Table 25 and Table 26 summarise the continuous and discrete data in statistical and spatial (biogeochemical province) format respectively. Table 28 (Appendix C) describes the bounds used to aggregate data in Table 26.

**Table 25: Statistical summary of continuous underway data (~5 m) and station data on the AMT-29 research cruise during a transect from the North Atlantic to the South Atlantic. OUE and iodide are data presented here. Temperature and salinity are surface data from *Discovery*'s underway system and chlorophyll *a* concentration is based on absorption measurement from Dall'Olmo et al. (refer to BODC inventory for DY110). Mixed layer depth (MLD) is calculated as described in the main text. Error bars are 1σ.**

| Measurement | 25 % quartile | Median | Mean | 75 % quartile |
|---|---|---|---|---|
| OUE | 0.552 | 0.596 | 0.593±0.057 | 0.634 |
| Iodide conc. (nM) | 53.7 | 87.3 | 97.8±45.7 | 144.5 |
| Temperature (°C) | 16.4 | 22.7 | 21.6±5.4 | 26.4 |
| Salinity (PSU) | 35.44 | 36.02 | 36.03±0.88 | 36.79 |
| Chlorophyll a conc. (µg L$^{-1}$) | 0.07 | 0.11 | 0.25±0.31 | 0.33 |
| MLD (m) | 29 | 45 | 46.4±21.8 | 68 |

**Table 26: Same as Table 25 but separated by biogeochemical provinces (Longhurst provinces).**

| Biogeo. province | OUE | Iodide conc. (nM) | Temp. (°C) | Salinity (PSU) | Chlorophyll *a* conc. (µg L$^{-1}$) | MLD (m) |
|---|---|---|---|---|---|---|
| NECS | 0.60±0.04 | 82.0±9.4 | 16.2±0.9 | 35.1±0.1 | 0.75±0.20 | 45 |
| NADR | 0.54±0.02 | 41.7±14.3 | 16.9±0.7 | 35.6±0.1 | 0.37±0.09 | 53.5±20.5 |
| NASE | 0.58±0.04 | 62.8±17.8 | 22.9±2.5 | 36.7±0.6 | 0.09±0.03 | 61.9±12.0 |
| NATR | 0.64±0.03 | 134.6±32.3 | 27.0±0.4 | 37.1±0.4 | 0.08±0.02 | 43.2±17.6 |
| WTRA | 0.64±0.02 | 149.1±10.3 | 28.2±0.8 | 35.7±0.6 | 0.13±0.04 | 28.2±16.0 |
| SATL | 0.60±0.07 | 126.7±31.6 | 22.4±3.6 | 36.4±0.5 | 0.09±0.10 | 47.4±26.6 |
| SANT | 0.53±0.08 | 46.1±10.5 | 13.7±1.5 | 34.7±0.5 | 0.72±0.42 | 34.0±7.1 |

### 4.3.4.1.  Iodide interannual and annual variability

It is clear that seawater $I^-$ accounts for a significant proportion of the blanked OUE measurement in the Atlantic Ocean (66–90 % on average, depending on the choice of blanks; Section 4.3.3.1). How representative the AMT29 OUE measurement is of the Atlantic Ocean, in general, is likely therefore significantly related to the interannual and seasonal variability of seawater $I^-$ concentration. Limited measurements of $I^-$ concentration have been obtained in the open ocean. However, $I^-$ interannual variability has been shown to be large with 100 nM changes possible at a coastal station (Chance et al., 2010). An $I^-$ concentration increase of 100 nM equates to a 40–900 % increase in $I^-$-driven OUE depending on starting concentration (Section 4.3.1.2). On the other hand, annual variability in $I^-$ can be up to ±50 % in the temperate and cold climate zones (Sherwen et al., 2019), which equates to OUE which is 22 % greater and 29 % lower, in summer and winter respectively, irrespective of absolute concentration. In the tropics, the $I^-$ concentration variability is <10 %. Importantly, as already discussed, there is no evidence of a diurnal cycle in $I^-$ concentration (Chance et al., 2014) thus OUE is unlikely to vary significantly on short temporal scales.

The average of AMT-29 $I^-$ measurements was 98±46 nM (Table 25), which is remarkably similar to the average non-coastal $I^-$ concentration (100±135 nM; Chance et al., 2014). Figure 51 shows the measured $I^-$ samples were in good agreement with previous open-ocean measurements in the Atlantic Ocean (>20° N and <-30° N). However some disagreement is shown in the tropics (~-50–100 nM) due to a mix of spatial and interannual variability (majority of Atlantic $I^-$ measurements occur in Oct–Nov, thus no ability to assess variability).
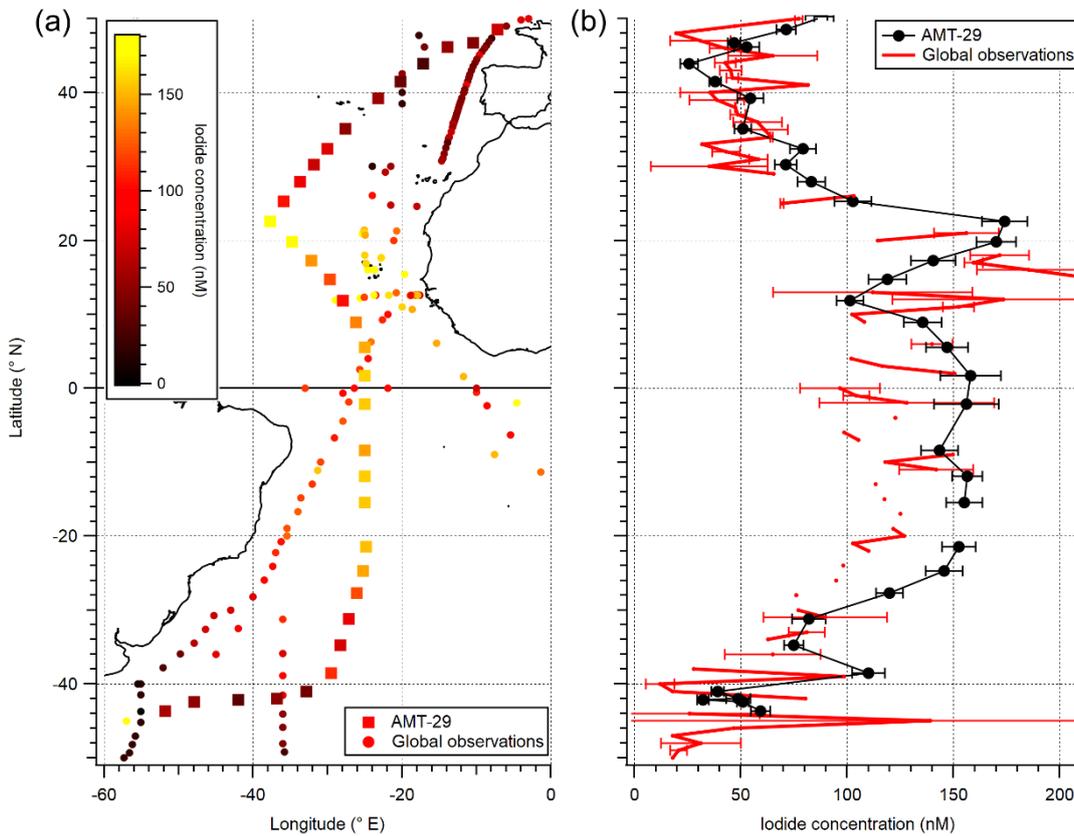
**Figure 51: Iodide concentration in the Atlantic Ocean from the AMT-29 cruise and literature observations in (a) coordinate format and (b) 1° latitude bins. Literature data from Chance et al. (2019).**

The I$^-$ concentration parameterisations of Chance et al. (2014) (Equation 29a) and MacDonald et al. (2014) (Equation 29b) were compared to my measured I$^-$ concentrations from -45–50° N in the Atlantic Ocean to examine the parameterisation accuracy. The parameterisations are as follows:

$$C_{I^-} = 0.28T^2 + 7S + 1.7|\text{latitude}| + 0.9C_{NO_3^-} - 0.020\text{sum}MLD - 309 \qquad 29a$$

$$C_{I^-} = 1.46{\times}10^6\exp\left(\frac{-3194}{T}\right) \qquad 29b$$

where sum$MLD$ is the annual sum of monthly average mean MLD. sum$MLD$ was calculated from the Ifremer 0.03 kg m$^{-3}$ MLD climatology (ifremer.fr/cerweb/deboyer/mld/Surface_Mixed_Layer_Depth.php). Figure 52 shows that neither parameterisation showed particularly good agreement with measured I$^-$ concentration. While both parameterisations had a similar gradient (multi-regression analysis, $\alpha$=0.05; common gradient: 0.5836), each parameterisation had a statistically different intercept which caused the Chance et al. (2014) parameterisation to overestimate at the lower concentration range (<120 nM) and the MacDonald et al. (2014) parameterisation to underestimate at the higher concentration range (>80 nM). Hence, each parameterisation was on average statistically different from the mean (one-way ANOVA followed by a Tukey-test). Underestimation by the MacDonald et al. (2014) parameterisation is up to ~40 % (Sherwen et al., 2019). Both parameterisations showed moderate correlation strength with measured concentrations (r$^2$=0.42 and 0.56 respectively) and large NRMSE (46 and 50 %, respectively, of mean).
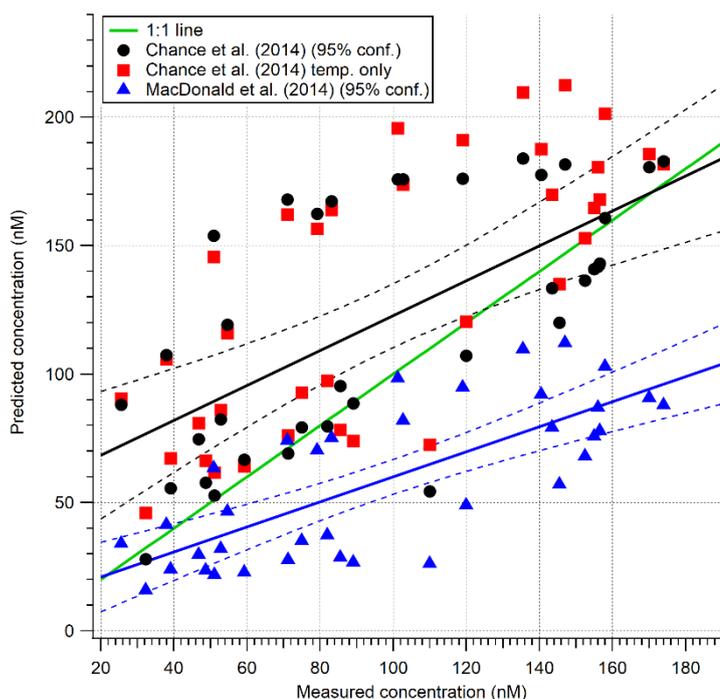
**Figure 52: Comparison of two iodide concentration parameterisations (Chance et al. (2014) and MacDonald et al. (2014)) to directly measured iodide in the Atlantic Ocean.**

### 4.3.4.2.   Subsurface measurements and the enhancement of organics

Most of the reactions between $O_3$ and reactants including $I^-$ and organics likely occur near/at the air-sea interface, likely within the SML. The seawater inlet was at ~5.5 m below the surface of the water. This has the potential to bias the OUE measurements if near-surface gradients in organic material or $I^-$ exist between the bulk measurements and the air–sea interface.

$I^-$ concentration is highest in the top ~40 m of the Mediterranean Sea (Tian and Nicolas, 1995) and the top ~100 m of the Pacific Ocean (Huang et al., 2005), although this is not specified to be due to the mixed surface layer, while in the tropical Atlantic Ocean $I^-$ concentration is near homogeneous in the mixed surface layer (Chance et al., 2014). Furthermore, no enrichment has been shown between the SML and underlying bulk water when measured (Chapman and Liss, 1981; Chance et al., 2014). On the other hand, clear evidence is shown for the enrichment of DOM between the SML and bulk water. A detailed discussion is given in Section 3.3.3.2. To briefly summarise, DOM is increased in the SML by an EF of 0.5–6, depending on material and environment, relative to the water below (Wurl et al., 2011). In the North and South Atlantic Ocean specifically, the mean organic enrichment factor was measured to be 1.9±1.1 and 1.5±0.9 respectively on similar AMT transects (Sabbaghzadeh et al., 2017).

Assuming the North and South Atlantic Ocean EF measured by Sabbaghzadeh et al. (2017) on a similar AMT transect apply here and assuming no SML enhancement in $I^-$ (EF=1), the percentage contribution of $I^-$ and remnant to chemical $O_3$ loss in the North and South Atlantic Ocean can be adjusted for the SML (Table 27). Here the contribution of the remnant OUE was increased by the organic EF (assuming remnant OUE is due to organics and organics have the same reactivity at the SML and in the bulk) and then the sum of contributions was normalised to 100 %. Table 27 shows a large increase in the contribution of remnant OUE for the laboratory-

blank; large enough that the remnant contribution was able to become the majority chemical loss mechanism in the North Atlantic Ocean. For the laboratory-blank-corrected OUE, the contribution of I⁻ and remnant compounds is consistent with the expected $O_3$ reactivities in Table 1. For the in-situ-blank-corrected OUE, even with the enrichment of DOM, I⁻ still dominates chemical $O_3$ loss by a factor of ~5.

**Table 27: Contributions of iodide and non-iodide toward blanked ozone uptake efficiency. In-situ-blank-corrected and laboratory-blank-corrected refer to the data blanking scheme. Adjustment for the enrichment factor of iodide (factor = 1.0) and remnant (non-iodide, assuming organics; enrichment factor = 1.9 and 1.5 in North and South Atlantic Ocean respectively).**

| Hemisphere | Species | In-situ-blank-corrected | | Laboratory-blank-corrected | |
|---|---|---|---|---|---|
| | | Measured (%) | Adjustment (%) | Measured (%) | Adjustment (%) |
| Northern | Iodide conc. | 90.6 | 83.9 | 61.6 | 46.4 |
| | Remnant | 9.4 | 16.1 | 38.4 | 53.6 |
| Southern | Iodide conc. | 88.7 | 83.8 | 72.3 | 63.2 |
| | Remnant | 11.3 | 16.2 | 27.7 | 36.8 |

### 4.3.4.3.  Atmospheric ozone loss

The ocean surface is not a significant sink for atmospheric $O_3$ on small spatial scales because of the small $v_d$, hence the atmospheric $O_3$ concentration and OUE do not correlate here ($r^2$=0.04). However, atmospheric $O_3$ concentration and surface deposition flux are affected by changes in $v_d$ over the large distances in the ocean (Ganzeveld et al., 2009; Hardacre et al., 2015). Large temporal and/or spatial variability exists in $v_d$ (Helmig et al., 2012; Loades et al., 2020), likely due to variability in seawater biogeochemistry which remains unknown (i.e. reaction kinetics for $O_3$ destroying species, especially DOM).

The range in the AMT OUE chemical component was a factor of 2.0–2.8 (depending on the blanking scheme) or 1.7 with no blank correction. During AMT-29 the average $U_{10}$, corrected for ship speed and motion (Yang et al., 2014b; Dong et al., 2021), was 7.7±3.2 m s⁻¹. At a $U_{10}$ of 8 m s⁻¹, Helmig et al. (2012) show a range of $v_d$ of at least a factor of ~5 over five distinct cruises. The highest $v_d$ were measured on the coastal TexAQS and GOMECC cruises (~0.055 and ~0.030 cm s⁻¹ respectively), whereas the lowest $v_d$ were measured on the open-ocean GasEx and STRATUS cruises (~0.011 cm s⁻¹). If the high TexAQS coastal cruise is excluded because of significant terrestrial influence (mean coastal $v_d$ of 0.24±0.02 cm s⁻¹ (Helmig et al., 2012), the mean is lowered to 0.07±0.02 cm s⁻¹ when filtered for sufficient over-water fetch, compared to an open-ocean 0.03±0.00 cm s⁻¹ (Bariteau et al., 2010)). Then the range of directly measured open-ocean $v_d$ is reduced to a factor of ~2.5 at moderate (5–10 m s⁻¹) wind speeds, which is quantitatively comparable with the AMT OUE. This suggests that the $v_d$ variability in the dataset of Helmig et al. (2012) at a given wind speed is most likely due to variability in seawater concentration of $O_3$ destroying species. An important unconsidered variability is the SML organic enrichment dependence on $U_{10}$ at medium and high $U_{10}$ (Wurl et al., 2011).

### 4.3.4.4.  Global deposition estimations

In Section 3.3.3.3, multiple literature estimates for the global oceanic dry deposition flux of tropospheric $O_3$ were discussed for the scaling of VOC production yields. A range of modelling

techniques, each focusing on different $v_d$ parameterisations, provides a large range of deposition estimates (98–591 Tg yr$^{-1}$).

The lowest two deposition estimates, those of Luhar et al. (2018) and Pound et al. (2020), are a result of recent attempts to produce multi-layer models of O$_3$ loss at the ocean surface. Pound et al. (2020) only consider I$^-$ (estimated from the machine-learning climatology of Sherwen et al. (2019)) as the sole O$_3$ destroying species in seawater. On the other hand, Luhar et al. (2018) considered multiple O$_3$-destroying species in seawater, however, they still found the best agreement between modelled $v_d$ and open-ocean direct measurements when only modelling I$^-$ loss. For Luhar et al. (2018), I$^-$ concentrations were estimated using the MacDonald et al. (2014) parameterisation (Equation 29b); the I$^-$ parameterisation of Chance et al. (2014) (simplified squared-temperature only) or incorporating estimates of O$_3$ loss from seawater DOC resulted in larger model–observation disagreement.

Considering I provide evidence that I$^-$ accounts for 48–84 % of chemical O$_3$ loss at the ocean surface (depending on the blanking scheme used, Section 4.3.3.1), this suggests that Luhar et al. (2018) and Pound et al. (2020) may be underestimating $v_d$ by up to 100 % in the Atlantic Ocean. This potential underestimation is quantitatively consistent with recent direct coastal $v_d$ measurements; median $v_d$ was 32 and 105 % higher than estimated by the Luhar et al. (2018) model with and without estimated DOM contributions respectively (Loades et al., 2020).

Luhar et al. (2018) and Pound et al. (2020) also use the rate constant parameterisation of Magi et al. (1997) because the parameterisation has a similar dependency on temperature as does directly measured $v_d$, however that parameterisation is thought to be erroneous (Macdonald et al., 2014). Figure 39b shows a slight negative dependency of OUE on sample temperature, which, when considering how temperature influences Equation 8d, implies the $v_d$ should either decrease or not be influenced by temperature. Figure 39c shows the large uncertainty in literature estimates for I$^-$ + O$_3$ reaction kinetics; within the uncertainty, it is possible that there is no significant temperature dependency.

The larger deposition estimate of Ganzeveld et al. (2009) was a result of the unification of the COARE gas transfer scheme with a chemistry–climate model, using monthly estimated concentrations of I$^-$, DMS, alkene and chlorophyll $a$ as a proxy for organics to simulate ocean surface destruction. While the incorporation of an organic proxy is in principle an improvement over the more recent work (Luhar et al., 2018; Pound et al., 2020), chlorophyll $a$ itself has low reactivity with O$_3$ (Table 1) and also does not show consistent relationships with DOC (Suratman et al., 2009). Therefore the estimated 15–52 % dependence of $v_d$ on organics shown on AMT-29 was not predicted by Ganzeveld et al. (2009) for the open ocean (~9 % increase) because of low chlorophyll $a$ concentrations. On the other hand, for coastal measurements with high chlorophyll $a$ concentration, a mean $v_d$ increase of ~153 % was modelled (Ganzeveld et al., 2009). This is evidence that organic material is important, however the spacial organic coverage will likely induce significant variability.

Overall, Ganzeveld et al. (2009) showed no dependency of $v_d$ on temperature because of competing effects of solubility and reactivity. With this is mind, the increased directly measured $v_d$ observed for increasing temperature over a large spatial range (Helmig et al., 2012) may in fact be a signal of increasing I$^-$ concentration with increasing temperature. Moreover, the $v_d$ trend with increasing temperature is unlikely to be a signal of increasing DOM, considering the variable relationships between temperature and chlorophyll $a$ (Nurdin et al., 2013; Siegel et al., 2013; Kumar et al., 2016) and generally negative relationships with CDOM (Siegel et al., 2013).

In summary, the majority of global estimates for the oceanic dry deposition flux of O$_3$ recognise/support the importance of seawater I$^-$ for O$_3$ loss, however, the role of organics on O$_3$ uptake has yet to be satisfactorily incorporated into global models.

## 4.4.  Conclusions

This chapter presents continuous measurements of the OUE to near-surface (~5 m) seawater in the Atlantic Ocean (-45–50° N) in Autumn 2019. OUE shows increased values in the tropics and temperate latitudes and lower values in the sub-tropical gyres; a latitudinal variability consistent with seawater I$^-$ concentration and organic proxies (e.g. DOC, CDOM, chlorophyll $a$). Correlations with I$^-$ (+) and DOC (+) concentration, temperature (+) and inorganic nutrients (–) suggests biological activity has an indirect control on OUE through mediating I$^-$ and DOC concentration. Discrete I$^-$ concentration measurements and empirical laboratory experiments, along with Milli-Q water blank measurements, were used to subtract the influence of I$^-$ and physical processes to leave the remnant OUE portion – hypothesised to be organic material related. Correlations with CDOM (+) absorption, chlorophyll $a$ (+) and silicate (–) concentrations suggest that the remnant OUE portion is organic in nature.

Atlantic Ocean SML enrichment of organic material (Wurl et al., 2011; Sabbaghzadeh et al., 2017) is used to adjust the organic (remnant) OUE portion at the air–sea interface; here the adjusted I$^-$:organic ratio is 46:54 and 63:37 for the North and South respectively, suggesting that I$^-$ and organics play a similar near-identical role in seawater O$_3$ loss. This result has important implications for the global modelling community that have generally parameterised O$_3$ $v_d$ using seawater I$^-$ concentration only. Further important results are the depth profiles that show a vertical gradient of reactivity; highest near the surface, then the DCM, and lowest at 1000 m. The deep water (1000–2000 m) is vertically homogeneous but shows latitudinal variability consistent with the AAIW incursion into the Atlantic Ocean. The non-zero OUE at depth indicates some of the refractory, long-life DOM in the deep ocean will react with O$_3$ once upwelled to the surface.

In addition to the Atlantic Ocean measurements, a time series of OUE measurements at the L4 station in the summer algal bloom is also presented. These measurements show that OUE in the coastal water is generally higher than OUE from the open ocean (with both blanking methods), probably due to terrestrial DOM sources.

Future improvements in OUE measurements include; (1) controlling/stabilising sample flow rate and O$_3$ concentration and (2) making use of in situ data processing. Controlling sample flow

rate and $O_3$ concentration will be key to reducing some of the measurement variability. The sample flow rate was maintained manually making the measurement less autonomous; incorporation of a liquid MFC would provide a digital record of flow (much like the gas MFC) and accurately maintain flow. A lack of a pulsating peristaltic pump could also provide a smoother flow. Stabilising $O_3$ concentration could be achieved by using a clean air generator (instead of using finite pressurised cylinders) which would allow a higher flow through the $O_3$ generator (like the set up in Section 3.2.1). Furthermore, installing a mass flow meter upstream of the $O_3$ sample dilution tee would provide useful information on the $O_3$ concentration and allow greater confidence in the true $O_3$ concentration. In situ data processing is the key to making any near-automated experimental process truly autonomous. Python code was already used to control valve timing for the OUE experiments; adding code that reads the instrument output and processes the data every 5 min would improve continuous/discrete measurements and aid diagnostics/maintenance.

Future sampling campaigns should strive to (3) make comparative measurements of the SML and bulk OUE and (4) undertake simultaneous $O_3$ EC fluxes. Here I simplistically used the previously measured surface enrichment of organic material to adjust the measured contribution of organic material towards $O_3$ loss at ~5 m depth to the surface. However, there is no guarantee that the reactivity of the surface-active and bulk organic material is identical. Thus, comparative OUE measurements of SML samples and the bulk can be used to predict the $O_3$ loss more accurately at the air–sea interface. Moreover, the measurement of simultaneous $O_3$ EC fluxes would also support the analysis of $O_3$ loss at the air–sea interface. EC provides a continuous measurement of total $O_3$ uptake (physical + chemical) and OUE provides a continuous measurement of chemical uptake and seawater $\lambda$. Thus combining these measurements would enable us to study the interplay between physical and chemical uptake (i.e. are these uptake processes additive?) and possibly validate the 1-layer vs. 2-layer deposition model schemes.

# Chapter 5 – Summary and Conclusions

### 5.1. Summary of research results

This section aims to summarise the main points of the thesis to facilitate further discussion and the unification of results. Detailed conclusions can be found at the end of Chapters 2–4.

In the first data chapter, EC measurements of the air–sea fluxes of acetone, acetaldehyde, DMS and isoprene are presented from the PPAO in the south-west UK. The main findings were:

- Air-to-sea deposition of acetaldehyde and acetone and the emission of DMS were observed in both open-water and Plymouth Sound influenced wind sectors. The open-water DMS flux agreed with recent climatological estimates. Isoprene flux could not be confidently resolved with the EC method using the PTR-quad-MS because of a lack of sensitivity.

- Acetone fluxes showed stronger deposition compared to climatological and model estimates probably because those estimates do not capture the spatial and temporal variability in the distribution of acetone air and sea concentrations.

- Observed acetaldehyde fluxes are in the opposite direction to global models that suggest the Northern Hemisphere oceans to be a net acetaldehyde source because the models predict higher seawater acetaldehyde concentrations and lower atmospheric acetaldehyde mixing ratios at this coastal location.

- Derived air–sea transfer velocities of acetone, acetaldehyde and DMS are approximately consistent with previous estimates over the open ocean and suggest that wind speed, rather than processes such as bottom driven turbulence, is the dominant control for gas exchange at this coastal location.

- The difference between EC measurements of net flux and computed bulk diffusive air–sea flux (from $C_a$ and $C_w$) provides a constraint for the magnitude of the net 'missing flux', which may be due to $O_3$ driven productions, which are explored in subsequent chapters.

In the second data chapter, laboratory production measurements of acetaldehyde, acetone and isoprene from the $O_3$ oxidation of seawater (and DOM) are presented from the L4 marine station over spring, summer and autumn. The main findings were:

- The greatest production of acetaldehyde was in the late summer, acetone in the early summer and isoprene in the autumn.

- The $O_3$ oxidation of seawater is an important source of isoprene. The scaled global production of isoprene is on the same order of magnitude as the bottom-up oceanic emission for a conservative scaling approach and on the same order of magnitude as the top-down oceanic emission for a liberal scaling approach.

- The scaled global productions of acetaldehyde and acetone are small – even with the liberal approach – compared to the estimated diffusive air–sea fluxes.

- Moderate relationships between $O_3$-driven productions and temperature (+), fluorescence (–), chlorophyll $a$ (+) and inorganic nutrients (–) suggest the precursor DOM pool is of biological origin. Experiments with the injection of phytoplankton culture and fatty acids provide further confirmation.

In the third data chapter, measurements of the $O_3$ uptake efficiency (OUE) by near-surface seawater in the Atlantic Ocean are presented. The main findings were:

- Higher OUE in the tropics and temperate latitudes and lower OUE in the sub-tropical gyres, which is broadly consistent with the spatial distribution in seawater $I^-$ concentration and organic proxies.

- Correlations of total OUE with $I^-$ (+) and DOC (+) concentration, temperature (+) and inorganic nutrients (–) suggest biological activity has an indirect control on OUE through controlling $I^-$ and DOC concentration.

- Correlations of remnant OUE (remaining OUE after the effects of $I^-$ and the blanks are subtracted) with CDOM absorption (+), chlorophyll $a$ (+) and silicate (–) concentrations suggest that the remnant OUE portion is organic in nature.

- $I^-$ and organics play a near equal role in seawater $O_3$ loss which has important implications for the global modelling community that have generally parameterised $O_3$ $v_d$ using seawater $I^-$ concentration only.

- The highest OUE was measured at the surface, then the DCM and the lowest at 1000–2000 m. The deepest water is vertically homogeneous but shows latitudinal variability consistent with the AAIW incursion into the Atlantic Ocean. The non-zero OUE at depth indicates that some of the refractory, long-life DOM in the deep ocean could react with $O_3$ once upwelled to the surface.

## 5.2. Unification of results

So far I have shown that $O_3$ reacts with marine organics, which leads to the outgassing of VOCs. But does greater $O_3$ uptake lead to more VOC production? Unifying the OUE and $P_{VOC:O_3}$ data helps to assess the relationship between oceanic $O_3$ uptake and subsequent $O_3$-driven VOC production.

Over four weeks, during the period of laboratory OUE experiments (Section 4.3.2), the $P_{VOC:O_3}$ of surface and deep L4 water were compared. These data have three main limitations, thus the data were not discussed in detail in Chapter 3, however the findings/conclusions are still of interest. Firstly, during this period only two replicate samples per depth were measured and the mean was calculated, therefore potentially these mean $P_{VOC:O_3}$ could be more variable compared to previous Chapter 3 measurements. Secondly, for some analyses, the first datum is removed to check for correlations during stratification ($n=3$), because, as with the L4 OUE time series (Section 4.3.2), the first week of data was weakly/not stratified. Finally, these correlations have the potential to be easily skewed by outliers and anomalies introduced by rapidly varying

parameters at the beginning of the summer bloom because $3 \leq n \leq 4$. With these three points in mind, only limited regression analysis is undertaken.

Figure 53a shows that for all three VOCs, peak height in the deep sample was generally on average higher than at the surface; acetaldehyde, acetone and isoprene peak height was 13, 16 and 31 % higher in the deep sample, respectively. Similar to the peak height, $P_{VOC:O_3}$ was generally higher in the deep sample than the surface. On average, the acetaldehyde, acetone and isoprene deep $P_{VOC:O_3}$ were 19, 41 and 46 % higher, respectively, than the surface samples. The higher acetaldehyde in the deep sample was driven by one datapoint (66 % of data were lower in the deep), whereas for acetone and acetaldehyde the majority (75 %) were higher in the deep. The mean surface acetaldehyde, acetone and isoprene $P_{VOC:O_3}$ were $(0.26 \pm 0.05) \times 10^{-3}$, $(0.50 \pm 0.05) \times 10^{-3}$ and $(0.83 \pm 0.15) \times 10^{-3}$, respectively, while the mean deep $P_{VOC:O_3}$ were $(0.31 \pm 0.26) \times 10^{-3}$, $(0.75 \pm 0.26) \times 10^{-3}$ and $(1.22 \pm 0.67) \times 10^{-3}$ respectively. It is clear that the deeper water has more potential to produce VOC, likely because the deeper water contained more DOM precursors for these VOCs. Recent experiments have shown a net benthic-to-pelagic transfer of dissolved material in the bloom months (Rühl et al., 2020), which could explain the higher $P_{VOC:O_3}$ in the deep water. Another potential cause of lower $P_{VOC:O_3}$ at the surface could be losses due to in situ ozonolysis and/or photochemistry. As with the OUE, the surface acetone and isoprene $P_{VOC:O_3}$ showed strong correlations with seawater DMS concentration ($r^2$=0.98 and 0.94 respectively). Here the correlation was negative, which suggested either DMS was directly competing with DOM for ozonolysis or DMS was a proxy for another competing compound.
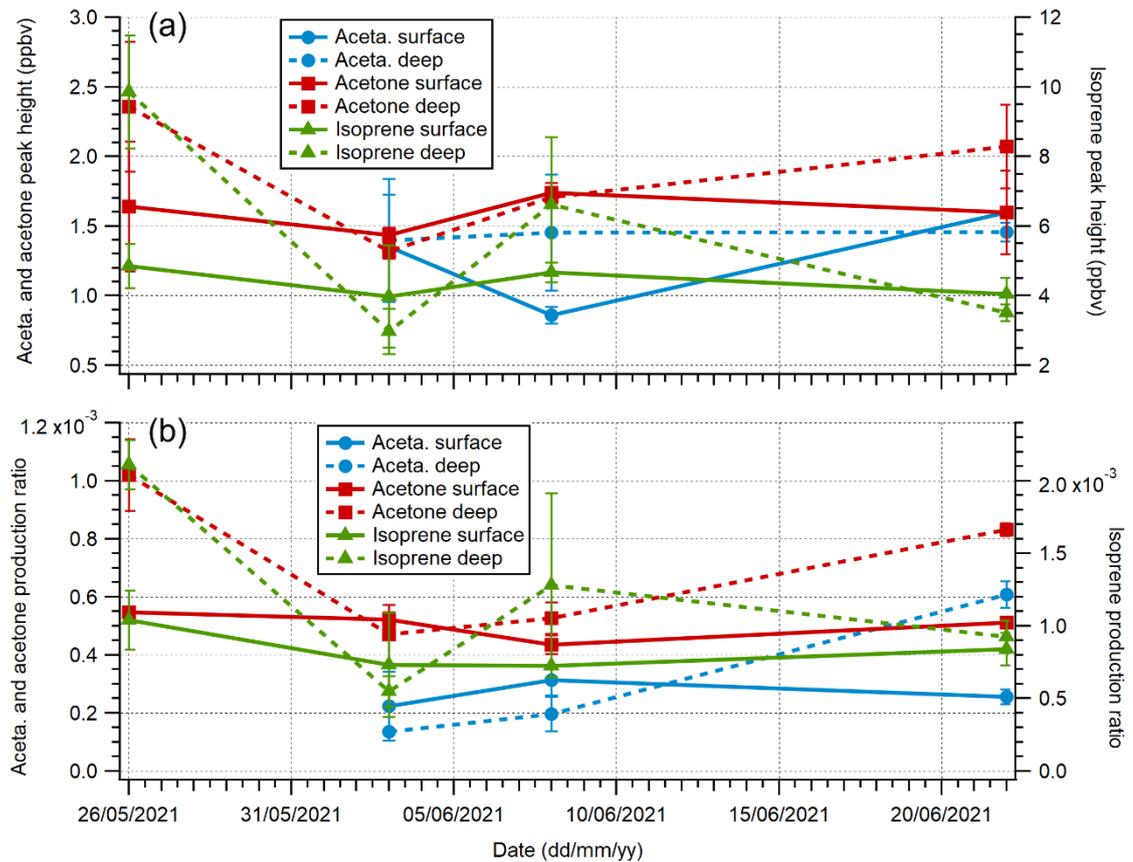
**Figure 53: Timeseries of (a) VOC peak height and (b) L4 surface and deep $P_{VOC:O_3}$.**

Strong to moderate $P_{VOC:O_3}$:OUE correlations were observed for the surface and deep samples (OUE have the Milli-Q water blank subtracted). The surface correlation was tightest for acetaldehyde ($r^2$=0.95), with acetone in the middle ($r^2$=0.84), and weakest for isoprene ($r^2$=0.51). The acetone and isoprene correlations were both negative (i.e. higher OUE, less VOC production) while the acetaldehyde correlation was positive. For the deep samples, the correlation was tightest for acetone ($r^2$=0.83), with acetaldehyde in the middle ($r^2$=0.72), and again weakest for isoprene ($r^2$=0.62). Counter to the surface correlations, all the deep $P_{VOC:O_3}$:OUE correlations were negative.

The common process between $P_{VOC:O_3}$ and OUE is the extent $O_3$ reacts with the seawater. A process that enhances $O_3$ $v_d$ will directly increase OUE and either increase $P_{VOC:O_3}$ (if increasing organic precursor concentration) or decrease $P_{VOC:O_3}$ (if increasing non-organic-precursor $O_3$ destroying species, i.e. I⁻). The negative $P_{VOC:O_3}$:OUE correlations imply an increase of $O_3$ destroying species; I⁻ is a good candidate which has directly been shown to increase OUE (Section 4.3.1.2) and decrease $P_{VOC:O_3}$ (Section 3.3.2.3). Unfortunately, I⁻ concentrations from these L4 waters were not measured to test the above hypothesis. Significantly stronger negative correlations were observed between the $P_{VOC:O_3}$:OUE ratio and DMS concentration ($r^2$=0.99 and 0.91 for acetone and isoprene respectively); the very strong relationship is possibly due to common sources of DOM, I⁻ and DMS. These results importantly show most of the variability in $P_{VOC:O_3}$ is dependent on OUE in the L4 water.

The half to near-full correlation strengths suggest I⁻, or a similar O$_3$ destroying species, has the strongest influence on the ratio between VOC production and O$_3$ uptake, consistent with the unadjusted measurements from the Atlantic Ocean because the L4 samples were also subsurface. The remaining variability in the $P_{VOC:O_3}$ is likely due to natural variability in DOM concentration and composition and also other O$_3$ destroying species competing with the organics. Interestingly, with the thought of scaling in mind, negative regressions (common gradient) were observed between the VOC production ratio and OUE for the deep and surface samples. A greater overall deposition of O$_3$ to seawater (i.e. higher OUE) did not result in relatively greater VOC production in general. This might be because (1) variability in I⁻ complicated the result, (2) the O$_3$ reaction with seawater does not necessarily lead to outgassing of VOCs (i.e. non-volatile products), and (3) the VOCs produced are not the compounds monitored by the PTR-MS.

## 5.3.   Implication of results

In this section, I draw together all the results to discuss '***The influence of oceanic ozone uptake on volatile organic compound production and air–sea exchange***'.

In the previous Chapters, it has been shown that approximately half of O$_3$ loss at the ocean surface is due to organic material (Section 4.3.4.2) and that the O$_3$ oxidation of organic material does produce VOCs including acetaldehyde, acetone and isoprene (Section 3.3.1). It has also been shown that other O$_3$ destroying species compete with organic material (Section 3.3.2.3), therefore it is not obvious whether a greater O$_3$ deposition flux would produce more VOCs. For example, a greater O$_3$ deposition flux driven by higher I⁻ concentration would probably lead to less VOC production at the same precursor DOM level and physical forcing.

The northern hemisphere temperate zone has the highest MBL O$_3$ concentration (Winkler, 1988), low I⁻ concentrations (Chance et al., 2014; Macdonald et al., 2014; Sherwen et al., 2019), highest seawater organics (McClain, 2009; Nelson and Siegel, 2013) and high wind speed in some seasons (Young, 1999; Laurila et al., 2021). Thus this zone seems most likely to have the highest O$_3$ deposition flux, and perhaps O$_3$-driven VOC emission. With the atmospheric mixing ratio of MBL O$_3$ in the northern hemisphere increasing by 2–3 ppbv decade$^{-1}$ (Parrish et al., 2009; Gaudel et al., 2018, 2020) as a result of increasing anthropogenic O$_3$ precursors, the influence of O$_3$-driven marine VOC production will likely only increase and become more significant.

The southern hemisphere temperate zone has low O$_3$ concentration (Winkler, 1988), low I⁻ concentrations (Chance et al., 2014; Macdonald et al., 2014; Sherwen et al., 2019), medium–high seawater organics in some areas (McClain, 2009; Nelson and Siegel, 2013) and high wind speed in all seasons (Young, 1999; Yu et al., 2020). Thus a medium level production of VOC is speculated. MBL O$_3$ in the southern hemisphere is increasing more rapidly by 4–5 ppbv decade$^{-1}$ (Gaudel et al., 2018, 2020), thus O$_3$-driven VOC production will also likely increase. The tropics and sub-tropics have high I⁻ concentration, low organic concentration and the lowest wind speed, therefore the lowest O$_3$-driven VOC production is expected in this region.

The influence of $O_3$-driven VOC production on air–sea VOC fluxes is two-fold; a formation of a new flux and a modification of the bulk flux. For sparingly soluble, supersaturated VOCs (e.g. isoprene with net emission), the heterogeneous production acts as an additional flux alongside the bulk seawater flux. Figure 54 shows a schematic of the two concurrent fluxes. The additional heterogeneous flux and the bulk flux, for supersaturated VOC, would be indistinguishable for a direct technique like EC, leading to a larger EC flux than predicted by the TL model based on bulk air/water concentrations.
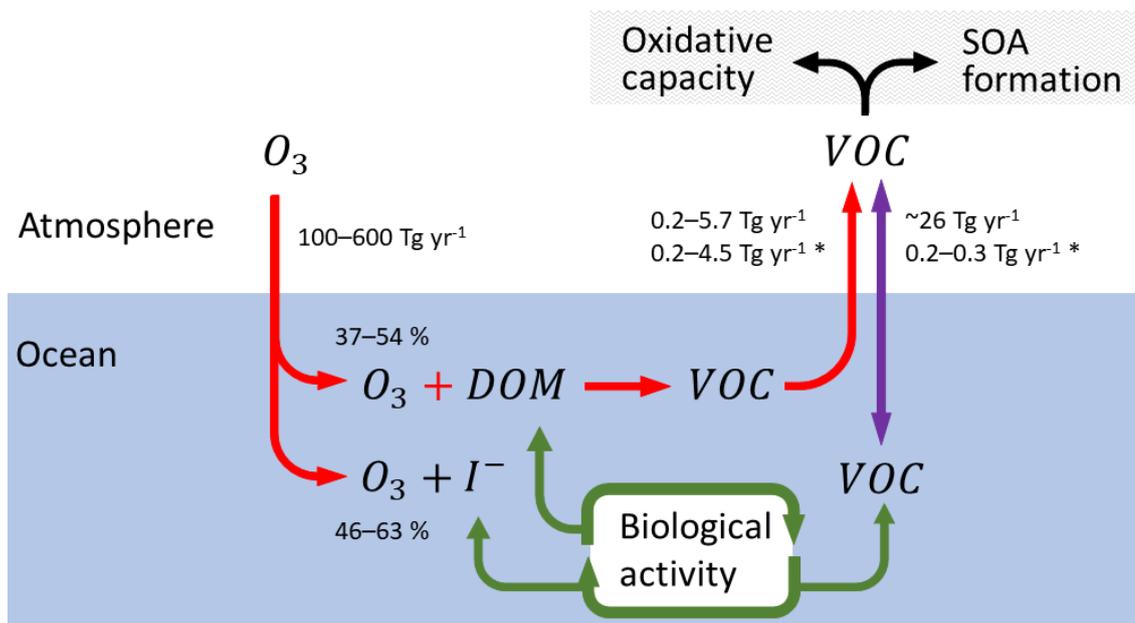


**Figure 54: A schematic of some of the main findings of the thesis, including the relative competition of dissolved organic matter (DOM) and iodide, the main source of VOC-producing DOM and the two concurrent air–sea fluxes. The \* refers specifically to isoprene. The red arrows are the main research themes of the thesis. The purple arrow is traditional bulk air–sea flux.**

For more soluble VOCs (e.g. acetaldehyde, acetone), the majority of the heterogeneous production leads to immediate outgassing and acts as an additional flux. This immediate outgassing is speculated because rapid production at the interface will likely supersaturate compounds at the immediate interface and subsequently suppress an atmosphere-to-interface concentration gradient. Note that some amount of $O_3$ does penetrate through the interface into the bulk water, as experiments of the $O_3$–I$^-$ reaction indicate. Thus any $O_3$–organic reactions that occur in the bulk may solely increase $C_w$ and contribute towards the bulk air-sea flux, either enhancing net emission (if supersaturated) or reducing net deposition (if undersaturated). This is important for flux estimations for VOC that are near seawater saturation (i.e. acetaldehyde at L4/NECS).

The VOC production results discussed here are important for MBL chemistry (Donaldson and George, 2012), especially in the remote ocean far from terrestrial and/or anthropogenic sources. In the lower troposphere, hydrocarbon/VOC oxidation is the main source of $O_3$ and subsequently OH (Section 1.4.2.1). Therefore these heterogeneous surface reactions may act to raise or lower the MBL oxidative capacity depending on VOC produced (either undergo hydrocarbon oxidation to produce $O_3$ or just consume $O_3$) and the available $NO_x$ and $HO_x$ precursors. This has important

applications for our understanding of the lifetimes of greenhouse gases (i.e. $CH_4$) and atmospheric pollutants in the remote MBL and lower troposphere. Furthermore, the oxidation products of some VOC can condensate to produce SOA, which could act as CCN and affect cloud albedo and the Earth's climate. Freshwater systems also contain large quantities of DOM, which tends to be more unsaturated, which could remove $O_3$ from the troposphere and produce VOC on shorter spatial scales.

It is interesting how the Atlantic OUE results indicated a similar contribution of $I^-$ and DOM (Section 4.3.4.2), yet the $P_{VOC:O_3}$ were only 0.0014–0.0038 (seasonal mean sum of individual acetaldehyde, acetone and isoprene $P_{VOC:O_3}$, min = pre-bloom, max = early summer). This indicates that every 487–1995 mol of atmospheric $O_3$ taken up by the ocean yields only 1 mol of acetaldehyde, acetone and/or isoprene combined. There are many possible reasons for this low yield: (1) the PTR-MS could not observe all the organic gases produced from the $O_3$ reactions with seawater, (2) non-volatile products from the reactions were lost (i.e. dissolved) to the water phase or interface, and/or (3) reaction stoichiometry is not 1:1. For point (1), glyoxal and MDA can be produced from the heterogeneous reaction of SML samples (Zhou et al., 2014) along with $C_5$–$C_{10}$ carbonyl compounds (Zhou et al., 2014; Schneider et al., 2019), which were not measured. Other important gases not able to be measured by PTR-MS include CO, $CO_2$, molecular hydrogen and low molecular weight hydrocarbons (e.g. $CH_4$) and some VOC. Thus, there is a high potential that other products could fill the yield discrepancy. Additionally, some analytes undergo further reactions and rearrangements in the PTR-MS drift chamber. For most important volatile gases, the characteristic fingerprint of fragmentation is known (Warneke et al., 2003; Schwarz et al., 2009). For point (2), evidence is provided that non-volatile reaction products stay at the interface or dissolve into the bulk depending on solubility (Voss et al., 2006, 2007; King et al., 2009, 2020; Zhou et al., 2014). At the interface or in the bulk sample, these non-volatile organic compounds may act as $O_3$ destroying species (i.e. DOC reactivity, Table 1), hence further compounded loss for $O_3$. Point (3) is mostly speculative for acetaldehyde, acetone and isoprene, however, multiple $O_3$ are necessary to convert seawater DOM to glyoxal and MDA (Zhou et al., 2014).

Considering the evidence that large molecular weight DOM is cleaved into smaller non-volatile compounds (Voss et al., 2006, 2007; King et al., 2009, 2020; Zhou et al., 2014) alongside the VOC production by $O_3$, $O_3$ oxidation clearly participates in the cycling of marine organics, alongside biology and photochemistry. The deep Atlantic Ocean OUE measurements (Section 4.3.3.5) further suggest refractory DOM can be rapidly oxidised.

## 5.4.  Thoughts on future work

In this section, some avenues of future research on seawater OUE and VOC production are provided. Future work discussion is also included in each conclusion of Chapter 2–4 which focuses on that specific experiment.

The experiments in this thesis focus on $O_3$–organic reactions at the ocean surface. In atmospheric chemistry, OH and $NO_3$ are more powerful oxidisers than $O_3$ (Atkinson and Arey,

2003). In seawater, the reactions of DOM and OH have been shown to produce acetaldehyde and acetone (De Bruyn et al., 2011) however OH and $NO_3$ may provide faster reaction kinetics than shown here for $O_3$ or additionally have unique products. In the current set-up of the bubble column, one could add a humidifying air supply and UV lamp between the $O_3$ generator and the column to produce OH or to inject $NO_2$ into the $O_3$ to produce $NO_3$. Further to studying the seawater reactions of OH and $NO_3$ and organic material, the POA emitted from the ocean acts as a source of VOC through reactions with OH, $NO_3$ and $O_3$. Recent literature measurements show the production of methanol, formaldehyde and acetaldehyde from the OH reaction with POA alkane and aromatic film substrates (Molina et al., 2004). In the current set-up of the bubble column, one could extend the tubing between column headspace and the PTR-MS and move the injection location of $O_3$ to observe the ozonolysis products of aerosols produced from the bubble-bursting nature of the column.

In this thesis, the VOC analytes were chosen due to their relatively high MBL concentrations, their importance within marine and atmospheric chemistry processes and their established atmospheric budget discrepancies. Isoprene, shown here to be produced in at least the same order of magnitude as marine biological production, is a known source of SOA (Carlton et al., 2009). Furthermore, Schneider et al. (2019) show the products of heterogeneous reactions of $O_3$ and DOM can very quickly condensate to form SOA. VOC not quantified by the PTR-MS or not chosen because of the criteria above might make a larger contribution to SOA than isoprene. Further work should be undertaken to address the impact of heterogeneous VOC production on MBL SOA abundance, especially considering the potential influence of heterogeneous VOC production modifying MBL oxidative capacity.

**Appendices**

**Appendix A – Additional characterisation of the bubble column**

To probe the VOC production mechanisms, the volume of the seawater sample was varied in one set of experiments (0.8–1.3 L) while the cross-sectional air-water interface area remained the same. This altered the maximum potential reaction time in and volume of the water phase, so also altering the residence time in the headspace. The 1.3 L experiment still had 150 mL of headspace which protected the instruments downstream of the column exit from exposure to water droplets/spray ejected from the water surface.

Experiments with changing water sample volume showed lower purge and lower oxidation of seawater DMS with increased water sample volume (Figure 55). The decreased loss (both purge and oxidation) at higher volumes suggests that the loss processes, relative to increased DMS amount, do not scale with the volume. Apart from the 1.1 L sample, the DMS measurements were linear indicating reproducibility in the experiment.
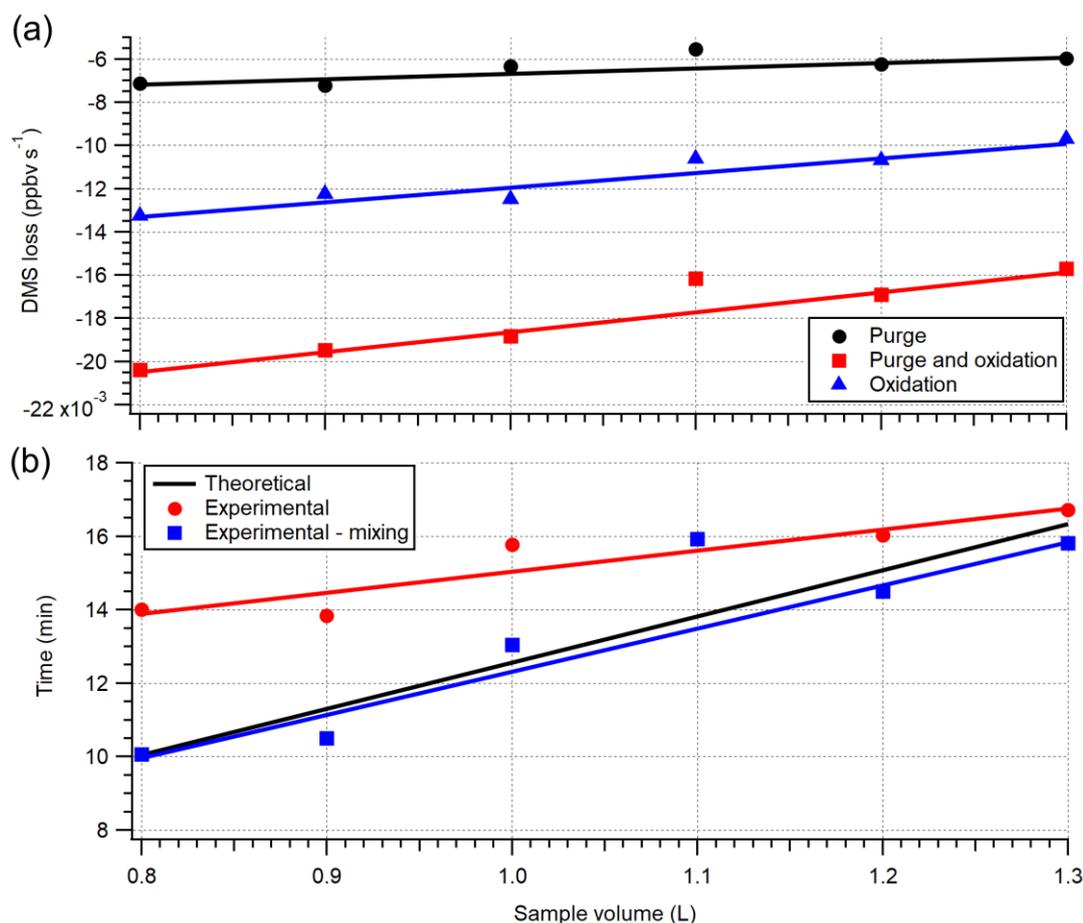


**Figure 55: The effect of changing sample volume on (a) DMS loss rates and (b) time to strip DMS from water. The oxidation loss rate is calculated as the differences between purge rate and purge + oxidation rate. The time taken to strip DMS from varying volumes of seawater (20 °C, 35 PSU). Theoretical time calculation from Mackay et al. (1979). 'Experimental – mixing' represents the experimental time corrected for the displacement time in the column (max volume 1.45 L). 1.1 L measurement ignored in regression analysis.**

The rate of stripping of gas from water, assuming gas equilibrium, can be calculated (Mackay et al., 1979);

$$\ln(C_t/C_0) = -(HF/VRT)\,t \qquad\qquad 30$$

where $C_0$ and $C_t$ represent concentrations of gas at 0 and $t$ seconds, respectively, and $V$ represents water volume. The theoretical time taken to strip DMS to 85 % of the starting concentration (~40 ppbv, during a summer bloom) is calculated and compared to the experimentally measured purge rates. 85 % was chosen to keep the loss rate pseudo-linear because the measured loss rate will slowly decrease as it is first-order with respect to DMS concentration. Noticeable offset was observed between the measured and theoretical stripping rates because Equation **30** does not account for changing headspace volume. Observed stripping times were in good agreement with the theoretical when the headspace displacement time was subtracted (RMSE of 3.4 %). Displacement time was calculated as $V_{\text{headspace}}/F$.

The produced VOC data was again noisier than the DMS data. The overall trend for peak height decreased with increasing sample volume for all VOC (Figure 56), which suggested the higher volume of seawater sample produced less VOC. This is unintuitive considering the larger sample had a larger reaction area, more total precursor organics and less headspace to dilute the initial produced VOC. On the other hand, the trends for the $P_{VOC:O_3}$ suggested that water sample volume had no significant effect on the initial production rate, which suggested $O_3$ was depleted before bubbles rose through 0.8 L of water (<240 cm$^2$ if bubble area scaling linearly with sample volume is assumed). A possible explanation for the apparent reduction of peak height with increased sample volume is gaseous VOC dissolving in the remainder of the sample (>0.8L) before the headspace is reached. With a smaller sample volume, less additional bubble area is given thus more VOC will purge into the headspace.
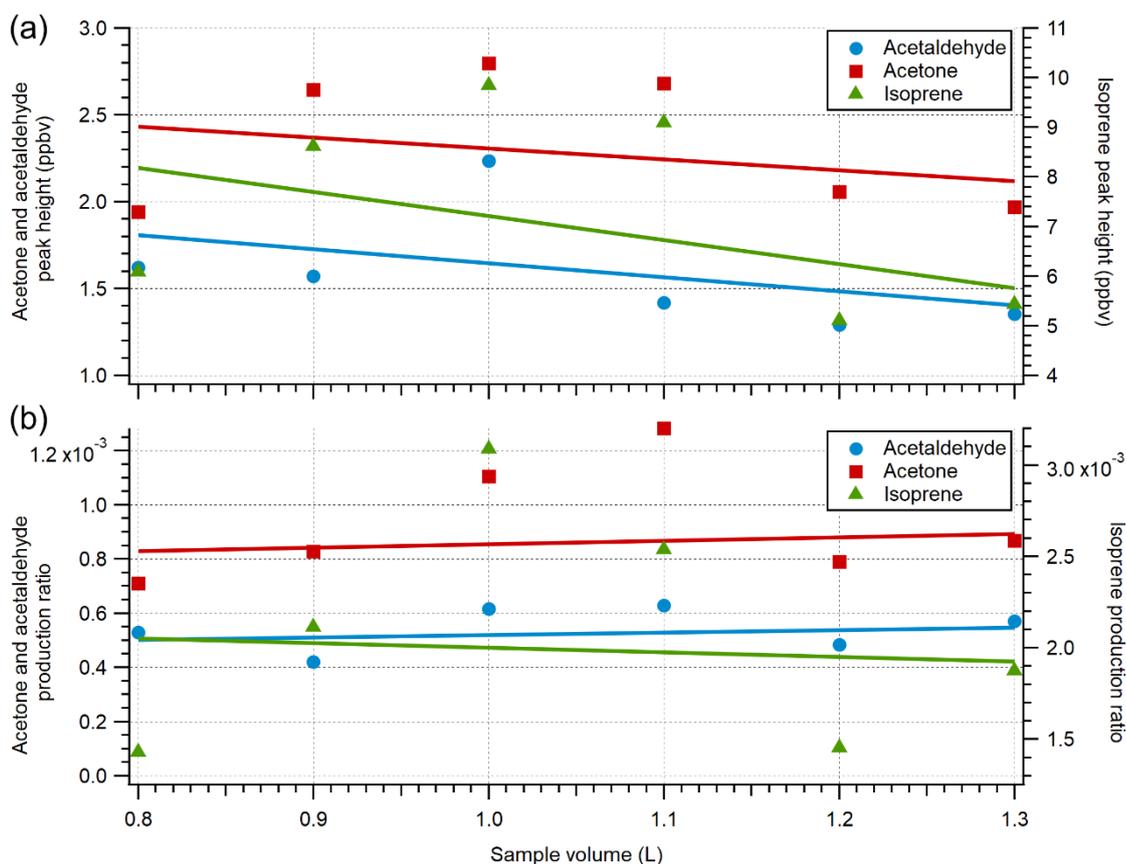
**Figure 56: The effect of changing sample volume on (a) VOC peak height and (b) VOC production ratio. 1.1 L measurement ignored in regression analysis.**

The response of DMS to the purge flow and acetone to the addition of $O_3$ was used to calculate the delay and response time. Delay time was the difference between a state change and the observation of that change. Response time was the difference between the state change observation and the state signal reaching $1 - e^{-1}$. The DMS delay time was found to not vary with changing sample volume because DMS was already degassed into the headspace before the artificial air purge (stage three) began. The acetone delay time did appear to slightly decrease with sample volume (the trend is not shown), however, it likely was constant if headspace mixing was fast enough because a constant trend would intercept the acetone response and column residence trendlines at 1.45 L. Both response times were shown to decrease with larger sample volumes (Figure 57), which implied that headspace mixing was involved with headspace measurements. The DMS response time was lower than the total headspace displacement time (~91 s) because the signal only needed to reach 63.2 % to be observed, whereas the residence time is a full renewal of the headspace volume. If the acetone signal had been laminar in the headspace, the delay, response and residence times would be in better agreement. The acetone response time was longer than the DMS time (linearly offset by ~69 s) because $O_3$ had to flush through the pre-sparger volume before reaction could take place.
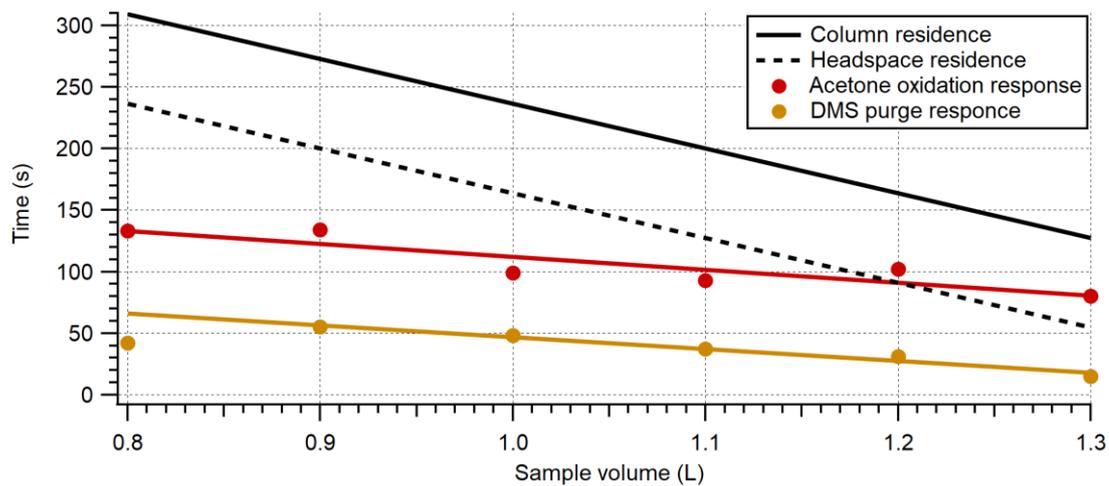
**Figure 57: The effect of changing sample volume on the measurement response of acetone and DMS. The theoretical residence time in the column and headspace provided for comparison (1.45 L empty column, 165 mL min$^{-1}$ gas flow).**

**Appendix B – Additional characterisation of the uptake coil**

Figure 58 shows that OUE is not sensitive to changing sample flow. The gradient of the L4 fit was -0.00030 OUE (mL min$^{-1}$)$^{-1}$ and was shown to be statistically different from a gradient of zero (the F statistic for the equally of slope zero was 6.7, compared to the critical value of 4.2). Over the entire cruise, the mean interpolated flow rate was 98.9±2.9 mL min$^{-1}$ (median: 99.5, 25 % quantile: 98.3, 75 % quantile: 100.2). A slight decrease in OUE with increasing flow rate is expected, considering coil residence time is a dominant factor for OUE, however, a flow rate change of ±5 mL min$^{-1}$ is small compared (<2 %) to the overall flow rate of 300 mL min$^{-1}$. On the other hand to the L4 sample, the slope of the Milli-Q fit was 0.0011 OUE (mL min$^{-1}$)$^{-1}$ and was shown to be statistically similar to a gradient of zero (F statistic of 1.6 compared to critical 4.4).
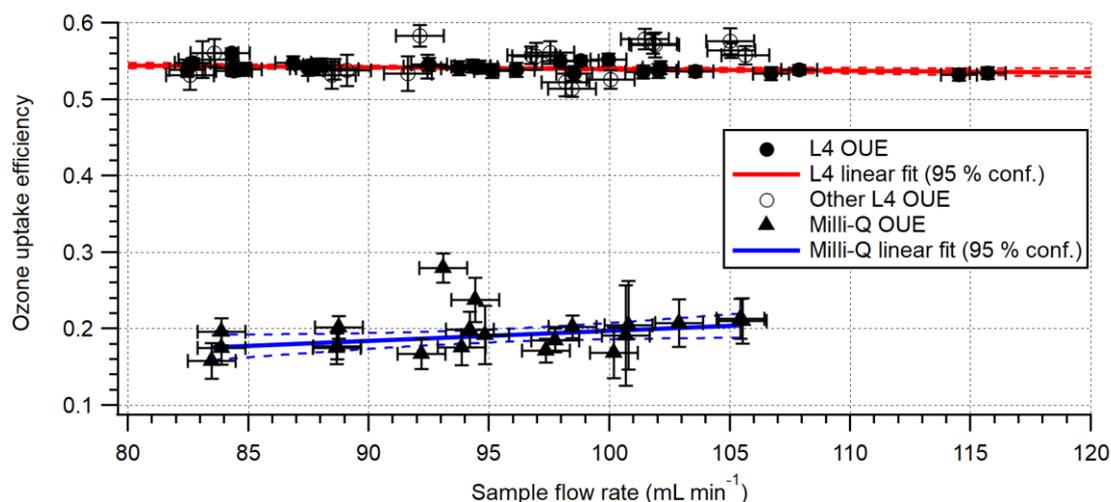


**Figure 58: The effect of changing sample flow rate on OUE for L4 seawater and a Milli-Q water sample.**

Figure 59 shows after 50 min the dry L4 OUE had stabilised to 0.068±0.012; over the remaining 70 min, the OUE dropped slightly to 0.051±0.013. With the high input O$_3$ concentration (1278±33 ppbv), the small amount of sample remaining in the tube should become quickly saturated, thus the OUE at infinite time predicted by the fit (0.048±0.020) should be the effect of the internal coil wall. Figure 59 also shows the dry Milli-Q water OUE stabilised to 0.043±0.011 in just 20 min. The reduced stabilisation time of the Milli-Q water experiment is due to negligible O$_3$ destroying species in the Milli-Q sample. Similarly, after a further period (150 min), the dry Milli-Q water OUE dropped slightly to 0.030±0.004. Here, the OUE at infinite time predicted by the fit was 0.027±0.012. The measured and predicted dry Milli-Q water OUE were lower than that of the L4 sample, which suggested a small amount of O$_3$ destroying species remained after 1 h of ozonolysis (half the measured time as the valve alternated between coil and generator). The predicted limited OUE for the Milli-Q was small (~18 %) compared to the mean Milli-Q blank (0.151±0.008) and suggests the wall accounts for just over a tenth of blank uptake (two-thirds of ~18 % because the water and air segments are 2:1 ratio respectively).
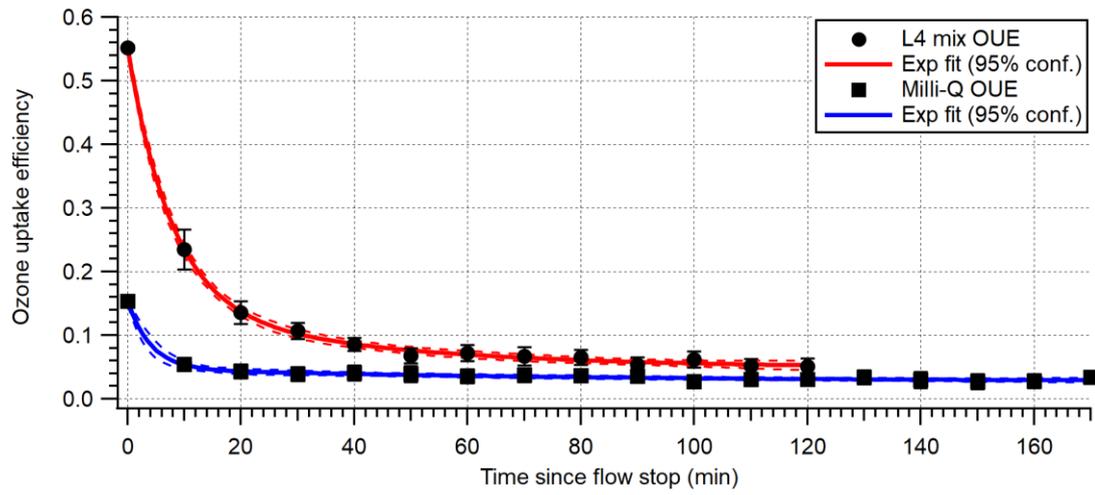
**Figure 59: The effect of time on OUE as the coil dries for L4 seawater and a Milli-Q water sample.**

**Appendix C – Additional figures, tables and equations**
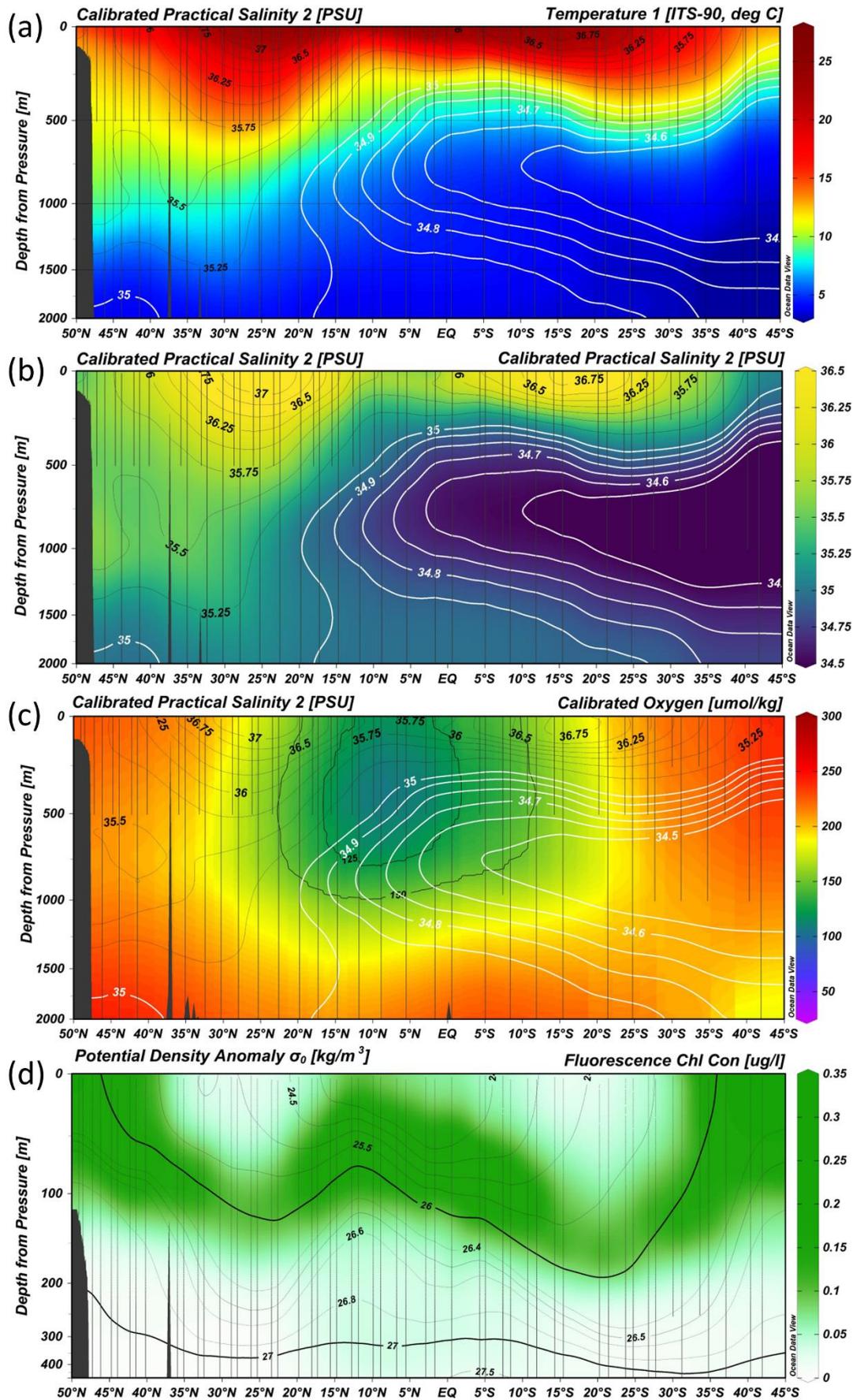


**Figure 60: Section plot along the AMT-29 transect of the (a) temperature, (b) salinity (c) oxygen concentration and (d) fluorescence depth profiles. Panels (a)–(c) show salinity contours and panel (d) shows potential density anomaly contours. Plots prepared by P. Strubinger (see cruise report).**
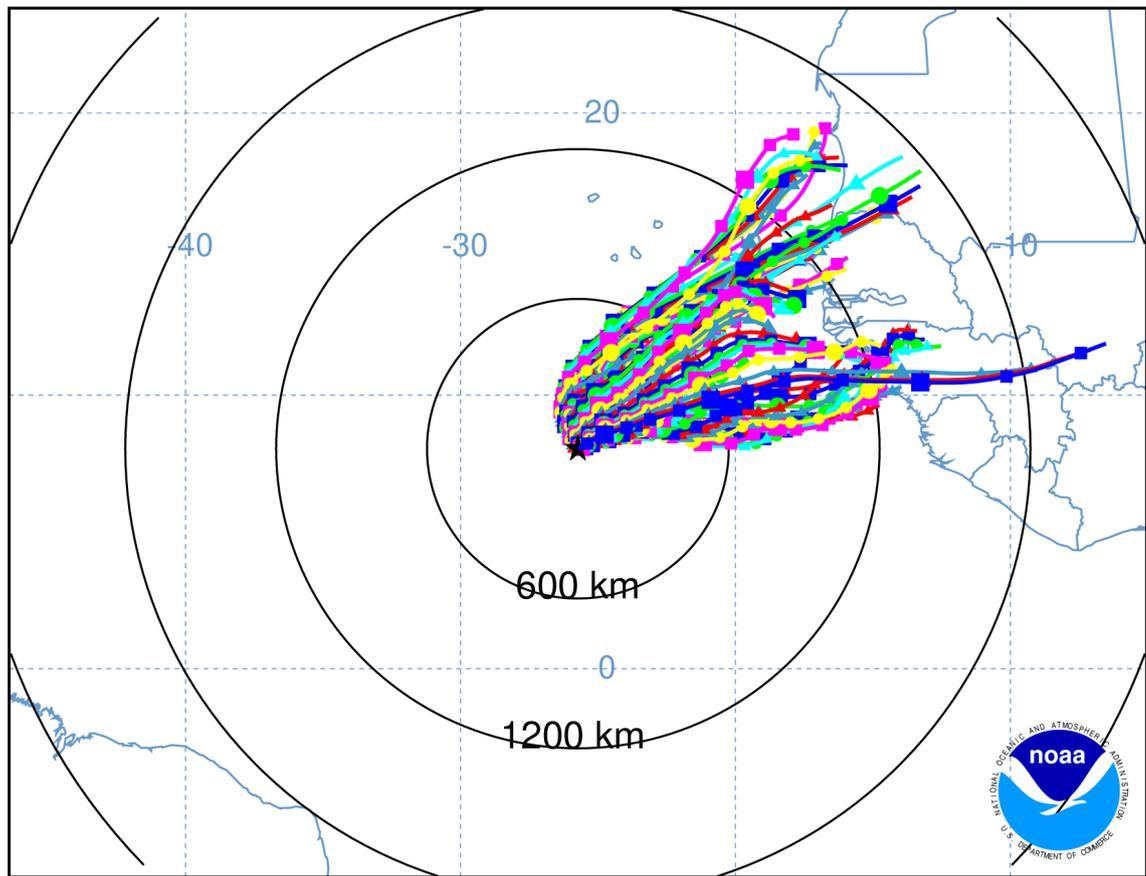
**Figure 61: 24 wind trajectories (72 h length) for a beginning 01/11/19 at 8.06° N, -25.73° E. Shapes represent 3 h travel distances. Plot produced from the NOAA HYSPLIT (Stein et al., 2015; Rolph et al., 2017) backward trajectory model.**

**Table 28: Latitude and longitude bounds used to divide the data in Table 26 into biogeochemical provinces. Time refers to the approximate duration in each province.**

| Province | Latitude and longitude bounds | Time |
|---|---|---|
| NECS | > -7.5° E | 4 d |
| NADR | > 43.5° N and > -7.5° E | 4 d |
| NASE | 25.5–43.5° N, includes linear transect (35.2° N, -27.5° E to 31.5 °N, -30.8° E.) of NASW. | 9 d |
| NATR | 11.5–25.5° N | 6 d |
| WTRA | -6.5–11.5° N | 6 d |
| SATL | -39.5– -6.5° N. | 12 d |
| SANT | <-39.5° N and <-57.5° E. | |

For the calculation of reduced electric field (Td) in a PTR-MS drift chamber (Chapter 2 and 3);

$$\text{Td} = \frac{V}{NL} \times 10^{17} \qquad\qquad 31$$

where $V$ represents the drift chamber voltage, $N$ represents the gas number density and $L$ represents the drift chamber length (7 cm for our PTR-MS).
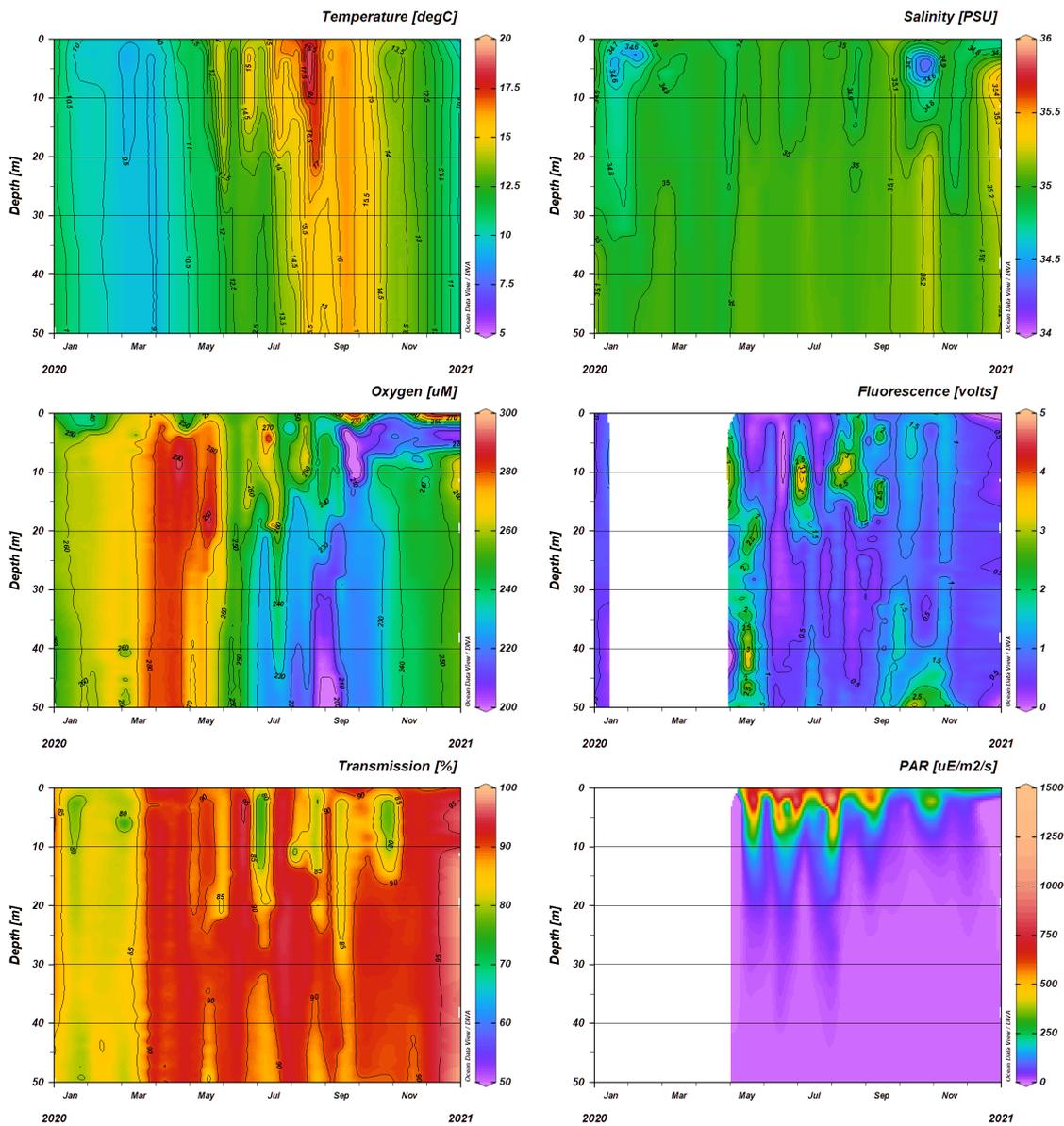
**Figure 62: Depth contour plots for the L4 marine station using the data from the RV Plymouth Quest's CTD instruments. Plot produced by Smyth et al. (WCO/PML).**

**Glossary**

**Acronyms and abbreviations**

| | | | |
|---|---|---|---|
| AAIW | Antarctic Intermediate Water | ODS | Ozone destroying species |
| AMT | Atlantic Meridional Transect (post-numerals refer to n$^{th}$ cruise) | OUE | Ozone uptake efficiency |
| CDOM | Chromophoric dissolved organic matter | PFA | Perfluoroalkoxy |
| CVAO | Cape Verde Atmospheric Observatory | PML | Plymouth Marine Laboratory |
| DCM | Deep chlorophyll maximum | POA | Primary organic aerosol |
| DIC | Dissolved inorganic carbon | PPAO | Penlee Point Atmospheric Observatory |
| DMS | Dimethylsulphide | ppbv | Parts per billion by volume |
| DOM | Dissolved organic matter | ppmv | Parts per million by volume |
| DOY | Day of year | pptv | Parts per trillion by volume |
| EC | Eddy covariance | PTFE | Polytetrafluoroethylene |
| EF | Enrichment factor | PTR | Proton transfer reaction |
| GC | Gas chromatography | PTR-MS | See PTR and MS |
| GC-MS | See GC and MS | SFCE | Segmented flow coil equilibrator |
| ID | Internal diameter | SML | Surface microlayer |
| IUPCA | International Union of Pure and Applied Chemistry | SST | Sea surface temperature |
| MBL | Marine boundary layer | SOA | Secondary organic aerosol |
| MFC | Mass flow controller | TL | Two layer |
| MLD | Mixed layer depth | UT | Union-tee |
| MS | Mass spectrometry | VOC | Volatile organic compound |
| NRSME | Normalised root mean squared error | WCO | Western Channel Observatory |
| OA | Organic aerosol | | |

**Chemicals**

| | | | |
|---|---|---|---|
| $CH_4$ | Methane | $O(^1D)$ | Oxygen (singlet) |
| CO | Carbon monoxide | $O_2$ | Oxygen (molecular) |
| $CO_2$ | Carbon dioxide | $O_3$ | Ozone |
| $HO_2$ | Hydroproxyl radical | OH | Hydroxyl radical |
| $H_2O$ | Water | NO | Nitric oxide |
| $H_3O^+$ | Hydronium ion | $NO_2$ | Nitrogen dioxide |
| $I^-$ | Iodide | $NO_3$ | Nitrate radical |
| $IO_3^-$ | Iodate | | |

**Symbols**

| | | | |
|---|---|---|---|
| $A_{bub}$ | Bubble surface area | D | Molecular diffusivity |
| $\lambda$ | Chemical reactivity | $P_{VOC}$ | Production (flux) of VOC |
| $C_a$ | Concentration in air | $P_{VOC:O_3}$ | Production ratio of VOC |
| $C_w$ | Concentration in water | $\Gamma_a$ | Resistance (aerodynamic) |
| $\rho_a$ | Density of air | $\Gamma_s$ | Resistance (surface) |
| $D_F$ | Deposition flux | $Sc_w$ | Schmidt number in water |
| $v_d$ | Deposition velocity | $\sigma$ | Standard deviation |
| $C_D$ | Drag coefficient | $R\sigma$ | Standard deviation (relative) |
| $k_a$ | Exchange velocities in air | $\sigma_{\bar{X}}$ | Standard deviation of the mean |
| $k_w$ | Exchange velocities water | $K_a$ | Total transfer velocity (airside) |
| $F_{air}$ | Flow rate of air | $K_w$ | Total transfer velocity (waterside) |
| $F$ | Flux | $K_{660}$ | Total transfer velocity normalised to a Schmidt number of 600 |
| $u_*$ | Friction velocity | $V_{air}$ | Volume of headspace |
| $H$ | Henry's air-over-water solubility | $U$ | Wind speed |
| $\tau$ | Lifetime | $U_{10}$ | Wind speed at height 10 m |
| $h$ | MBL height | $u, v$ and $w$ | Wind speed components in x, y and z directions |

**References**

Airs, R.: Chlorophyll a at L4, [online] Available from: https://www.westernchannelobservatory.org.uk/l4_pigments.php, 2010.

Aluwihare, L. I. and Repeta, D. J.: A comparison of the chemical characteristics of oceanic DOM and extracellular DOM produced by marine algae, Mar. Ecol. Prog. Ser., 186, 105–117 [online] Available from: http://www.jstor.org/stable/24853297, 1999.

Andreae, M. O., Ferek, R. J., Bermond, F., Byrd, K. P., Engstrom, R. T., Hardin, S., Houmere, P. D., LeMarrec, F., Raemdonck, H. and Chatfield, R. B.: Dimethyl sulfide in the marine atmosphere, J. Geophys. Res., 90(D7), 12891, doi:10.1029/JD090iD07p12891, 1985.

Archer, S. D., Cummings, D. G., Llewellyn, C. A. and Fishwick, J. R.: Phytoplankton taxa, irradiance and nutrient availability determine the seasonal cycle of DMSP in temperate shelf seas, Mar. Ecol. Prog. Ser., 394, 111–124, doi:10.3354/meps08284, 2009.

Archibald, A. T., Neu, J. L., Elshorbany, Y. F., Cooper, O. R., Young, P. J., Akiyoshi, H., Cox, R. A., Coyle, M., Derwent, R. G., Deushi, M., Finco, A., Frost, G. J., Galbally, I. E., Gerosa, G., Granier, C., Griffiths, P. T., Hossaini, R., Hu, L., Jöckel, P., Josse, B., Lin, M. Y., Mertens, M., Morgenstern, O., Naja, M., Naik, V., Oltmans, S., Plummer, D. A., Revell, L. E., Saiz-Lopez, A., Saxena, P., Shin, Y. M., Shahid, I., Shallcross, D., Tilmes, S., Trickl, T., Wallington, T. J., Wang, T., Worden, H. M. and Zeng, G.: Tropospheric ozone assessment report: A critical review of changes in the tropospheric ozone burden and budget from 1850 to 2100, Elementa, 8(1), 1–53, doi:10.1525/elementa.2020.034, 2020.

Ardura, D. and Donaldson, D. J.: Where does acid hydrolysis take place?, Phys. Chem. Chem. Phys., 11(5), 857–863, doi:10.1039/b812070f, 2009.

Arnold, S. R., Spracklen, D. V., Williams, J., Yassaa, N., Sciare, J., Bonsang, B., Gros, V., Peeken, I., Lewis, A. C., Alvain, S. and Moulin, C.: Evaluation of the global oceanic isoprene source and its impacts on marine organic carbon aerosol, Atmos. Chem. Phys., 9(4), 1253–1262, doi:10.5194/acp-9-1253-2009, 2009.

Atkinson, R.: Atmospheric chemistry of VOCs and NOx, Atmos. Environ., 34(12–14), 2063–2101, doi:10.1016/S1352-2310(99)00460-4, 2000.

Atkinson, R. and Arey, J.: Atmospheric Degradation of Volatile Organic Compounds, Chem. Rev., 103(12), 4605–4638, doi:10.1021/cr0206420, 2003.

Bakaev, V. A.: On the thermodynamics of adsorption on heterogeneous surfaces, Surf. Sci., 564(1–3), 108–120, doi:10.1016/j.susc.2004.06.187, 2004.

Baker, A. R., Turner, S. M., Broadgate, W. J., Thompson, A. M., McFiggans, G. B., Vesperini, O., Nightingal, P. D., Liss, P. S. and Jickells, T. D.: Distribution and sea-air fluxes of biogenic trace gases in the eastern Atlantic Ocean, Global Biogeochem. Cycles, 14(3), 871–886, doi:10.1029/1999GB001219, 2000.

Banoub, M. W. and Williams, P. J. L.: Seasonal changes in the organic forms of carbon, nitrogen and phosphorus in sea water at e1in the english channel during 1968, J. Mar. Biol. Assoc. United Kingdom, 53(3), 695–703, doi:10.1017/S0025315400058896, 1973.

Barcellos da Rosa, M., Behnke, W. and Zetzsch, C.: Study of the heterogeneous reaction of $O_3$ with $CH_3SCH_3$ using the wetted-wall flowtube technique, Atmos. Chem. Phys., 3(5), 1665–1673, doi:10.5194/acp-3-1665-2003, 2003.

Bariteau, L., Helmig, D., Fairall, C. W., Hare, J. E., Hueber, J. and Lang, E. K.: Determination of oceanic ozone deposition by ship-borne eddy covariance flux measurements, Atmos. Meas. Tech., 3(2), 441–455, doi:10.5194/amt-3-441-2010, 2010.

Bauer, J. E., Cai, W. J., Raymond, P. A., Bianchi, T. S., Hopkinson, C. S. and Regnier, P. A. G.: The changing carbon cycle of the coastal ocean, Nature, 504(7478), 61–70, doi:10.1038/nature12857, 2013.

Beale, R., Dixon, J. L., Arnold, S. R., Liss, P. S. and Nightingale, P. D.: Methanol, acetaldehyde, and acetone in the surface waters of the Atlantic Ocean, J. Geophys. Res. Ocean., 118(10), 5412–5425, doi:10.1002/jgrc.20322, 2013.

Beale, R., Dixon, J. L., Smyth, T. J. and Nightingale, P. D.: Annual study of oxygenated volatile organic compounds in UK shelf waters, Mar. Chem., 171, 96–106, doi:10.1016/j.marchem.2015.02.013, 2015.

Bélanger, S., Babin, M. and Larouche, P.: An empirical ocean color algorithm for estimating the contribution of chromophoric dissolved organic matter to total light absorption in optically complex waters, J. Geophys. Res. Ocean., 113(4), 1–14, doi:10.1029/2007JC004436, 2008.

Bell, T. G., de Bruyn, W. J., Miller, S. D., Ward, B., Christensen, K. and Saltzman, E. S.: Air-sea dimethylsulfide (DMS) gas transfer in the North Atlantic: Evidence for limited interfacial gas exchange at high wind speed, Atmos. Chem. Phys., 13(21), 11073–11087, doi:10.5194/acp-13-11073-2013, 2013.

Bell, T. G., Landwehr, S., Miller, S. D., De Bruyn, W. J., Callaghan, A. H., Scanlon, B., Ward, B., Yang, M. and Saltzman, E. S.: Estimation of bubble-mediated air-sea gas exchange from concurrent DMS and CO2 transfer velocities at intermediate-high wind speeds, Atmos. Chem. Phys., 17(14), 9019–9033, doi:10.5194/acp-17-9019-2017, 2017.

Bell, T. G., Porter, J. G., Wang, W. L., Lawler, M. J., Boss, E., Behrenfeld, M. J. and Saltzman, E. S.: Predictability of Seawater DMS During the North Atlantic Aerosol and Marine Ecosystem Study (NAAMES), Front. Mar. Sci., 7(January), doi:10.3389/fmars.2020.596763, 2021.

Benner, R.: Chemical composition and reactivity, in Biogeochemistry of Marine Dissolved Organic Matter, edited by D. A. Hansell and C. A. Carlson, pp. 59–90, Academic Press, London., 2002.

Blake, R. S., Monks, P. S. and Ellis, A. M.: Proton-Transfer Reaction Mass Spectrometry, Chem. Rev., 109(3), 861–896, doi:10.1021/cr800364q, 2009.

Blando, J. D. and Turpin, B. J.: Secondary organic aerosol formation in cloud and fog droplets: A literature evaluation of plausibility, Atmos. Environ., 34(10), 1623–1632, doi:10.1016/S1352-2310(99)00392-1, 2000.

Blitz, M. A., Heard, D. E., Pilling, M. J., Arnold, S. R. and Chipperfield, M. P.: Pressure and temperature-dependent quantum yields for the photodissociation of acetone between 279 and 327.5 nm, Geophys. Res. Lett., 31(6), doi:10.1029/2003gl018793, 2004.

Blomquist, B. W., Fairall, C. W., Huebert, B. J., Kieber, D. J. and Westby, G. R.: DMS sea-air transfer velocity: Direct measurements by eddy covariance amd parameterizarion based on the NOAA/COAREgas transfer model, Geophys. Res. Lett., 33(7), 2–5, doi:10.1029/2006GL025735, 2006.

Blomquist, B. W., Huebert, B. J., Fairall, C. W. and Faloona, I. C.: Determining the sea-air flux of dimethylsulfide by eddy correlation using mass spectrometry, Atmos. Meas. Tech., 3(1), 1–20, doi:10.5194/amt-3-1-2010, 2010.

Blomquist, B. W., Brumer, S. E., Fairall, C. W., Huebert, B. J., Zappa, C. J., Brooks, I. M., Yang, M., Bariteau, L., Prytherch, J., Hare, J. E., Czerski, H., Matei, A. and Pascal, R. W.: Wind Speed and Sea State Dependencies of Air-Sea Gas Transfer: Results From the High Wind Speed Gas Exchange Study (HiWinGS), J. Geophys. Res. Ocean., 122(10), 8034–8062, doi:10.1002/2017JC013181, 2017.

Bodineau, L., Thoumelin, G. and Wartel, M.: Fluxes and seasonal changes in composition of organic matter in the English Channel, Cont. Shelf Res., 19(15–16), 2101–2119, doi:10.1016/S0278-4343(99)00055-2, 1999.

Booge, D., Marandino, C. A., Schlundt, C., Palmer, P. I., Schlundt, M., Atlas, E. L., Bracher, A., Saltzman, E. S. and Wallace, D. W. R.: Can simple models predict large-scale surface ocean

isoprene concentrations?, Atmos. Chem. Phys., 16(18), 11807–11821, doi:10.5194/acp-16-11807-2016, 2016.

Booge, D., Schlundt, C., Bracher, A., Endres, S., Zäncker, B. and Marandino, C. A.: Marine isoprene production and consumption in the mixed layer of the surface ocean – a field study over two oceanic regions, Biogeosciences, 15(2), 649–667, doi:10.5194/bg-15-649-2018, 2018.

Borges, A. V., Vanderborght, J. P., Schiettecatte, L. S., Gazeau, F., Ferrón-Smith, S., Delille, B. and Frankignoulle, M.: Variability of the gas transfer velocity of CO2 in a macrotidal estuary (the Scheldt), Estuaries, 27(4), 593–603, doi:10.1007/BF02907647, 2004.

Borges, A. V., Delille, B. and Frankignoulle, M.: Budgeting sinks and sources of CO2 in the coastal ocean: Diversity of ecosystem counts, Geophys. Res. Lett., 32(14), 1–4, doi:10.1029/2005GL023053, 2005.

de Boyer Montégut, C., Madec, G., Fischer, A. S., Lazar, A. and Iudicone, D.: Mixed layer depth over the global ocean: An examination of profile data and a profile-based climatology, J. Geophys. Res. C Ocean., 109(12), 1–20, doi:10.1029/2004JC002378, 2004.

Broadgate, W. J., Liss, P. S. and Penkett, S. A.: Seasonal emissions of isoprene and other reactive hydrocarbon gases from the ocean, Geophys. Res. Lett., 24(21), 2675–2678, doi:10.1029/97GL02736, 1997.

Broadgate, W. J., Malin, G., Küpper, F. C., Thompson, A. and Liss, P. S.: Isoprene and other non-methane hydrocarbons from seaweeds: A source of reactive hydrocarbons to the atmosphere, Mar. Chem., 88(1–2), 61–73, doi:10.1016/j.marchem.2004.03.002, 2004.

de Bruyn, W. J., Clark, C. D., Pagel, L. and Singh, H.: Loss rates of acetone in filtered and unfiltered coastal seawater, Mar. Chem., 150, 39–44, doi:10.1016/j.marchem.2013.01.003, 2013.

de Bruyn, W. J., Clark, C. D., Senstad, M., Barashy, O. and Hok, S.: The biological degradation of acetaldehyde in coastal seawater, Mar. Chem., 192, 13–21, doi:10.1016/j.marchem.2017.02.008, 2017.

De Bruyn, W. J., Clark, C. D., Pagel, L. and Takehara, C.: Photochemical production of formaldehyde, acetaldehyde and acetone from chromophoric dissolved organic matter in coastal waters, J. Photochem. Photobiol. A Chem., 226(1), 16–22, doi:10.1016/j.jphotochem.2011.10.002, 2011.

Burba, G.: Eddy Covariance Method-for Scientific, Industrial, Agricultural, and Regulatory Applications, edited by R. Nelson, LI-COR Biosciences, Lincoln., 2013.

Burkholder, J. B., Sander, S. P., Abbatt, J. P. D., Barker, J. R., Huie, R. E., Kolb, C. E., Kurylo, M. J., Orkin, V. L., Wilmouth, D. M. and Wine, P. H.: Chemical Kinetics and Photochemical Data for Use in Atmospheric Studies, Evaluation No. 18, JPL Publ. [online] Available from: https://jpldataeval.jpl.nasa.gov/, 2015.

Calleja, M. L., Duarte, C. M., Prairie, Y. T., Agustí, S. and Herndl, G. J.: Evidence for surface organic matter modulation of air-sea CO 2 gas exchange , Biogeosciences Discuss., 5(6), 4209–4233, doi:10.5194/bgd-5-4209-2008, 2008.

Carlson, C. A.: Production and Removal Processes, in Biogeochemistry of Marine Dissolved Organic Matter, edited by D. A. Hansell and C. A. Carlson, pp. 91–154, Academic Press, London., 2002.

Carlton, A. G., Wiedinmyer, C. and Kroll, J. H.: A review of Secondary organic aerosol (SOA) formation from isoprene, Atmos. Chem. Phys., 9(14), 4987–5005, doi:10.5194/acp-9-4987-2009, 2009.

Carpenter, L. J. and Nightingale, P. D.: Chemistry and Release of Gases from the Surface Ocean, Chem. Rev., 115(10), 4015–4034, doi:10.1021/cr5007123, 2015.

Carpenter, L. J., MacDonald, S. M., Shaw, M. D., Kumar, R., Saunders, R. W., Parthipan, R., Wilson, J. and Plane, J. M. C.: Atmospheric iodine levels influenced by sea surface emissions of inorganic iodine, Nat. Geosci., 6(2), 108–111, doi:10.1038/ngeo1687, 2013.

Carr, N., Davis, C. E., Blackbird, S., Daniels, L. R., Preece, C., Woodward, M. and Mahaffey, C.: Seasonal and spatial variability in the optical characteristics of DOM in a temperate shelf sea, Prog. Oceanogr., 177(February 2018), 101929, doi:10.1016/j.pocean.2018.02.025, 2019.

Carslaw, N., Bell, N., Lewis, A. C., McQuaid, J. B. and Pilling, M. J.: A detailed case study of isoprene chemistry during the EASE96 Mace Head campaign, Atmos. Environ., 34(18), 2827–2836, doi:10.1016/S1352-2310(00)00088-1, 2000.

Chance, R., Weston, K., Baker, A. R., Hughes, C., Malin, G., Carpenter, L., Meredith, M. P., Clarke, A., Jickells, T. D., Mann, P. and Rossetti, H.: Seasonal and interannual variation of dissolved iodine speciation at a coastal Antarctic site, Mar. Chem., 118(3–4), 171–181, doi:10.1016/j.marchem.2009.11.009, 2010.

Chance, R., Baker, A. R., Carpenter, L. J. and Jickells, T. D.: The distribution of iodide at the sea surface, Environ. Sci. Process. Impacts, 16(8), 1841–1859, doi:10.1039/C4EM00139G, 2014.

Chance, R. J., Tinel, L., Sherwen, T., Baker, A. R., Bell, T. G., Brindle, J., Campos, M. L. A. M., Croot, P., Ducklow, H., Peng, H., Hopkins, F. E., Hoogakker, B., Hughes, C., Jickells, T. D., Loades, D., Macaya, D. A. R., Mahajan, A. S., Malin, G., Phillips, D. P., Roberts, I., Roy, R., Sarkar, A., Sinha, A. K., Song, X., Winkelbauer, H., Wuttig, K., Yang, M., Peng, Z. and Carpenter, L. J.: Global sea-surface iodide observations, 1967-2018, Sci. data, 6(1), 286, doi:10.1038/s41597-019-0288-y, 2019.

Chang, W., Heikes, B. G. and Lee, M.: Ozone deposition to the sea surface: Chemical enhancement and wind speed dependence, Atmos. Environ., 38(7), 1053–1059, doi:10.1016/j.atmosenv.2003.10.050, 2004.

Chapman, P. and Liss, P. S.: The sea surface microlayer: Measurements of dissolved iodine species and nutrients in coastal waters1, Limnol. Oceanogr., 26(2), 387–390, doi:10.4319/lo.1981.26.2.0387, 1981.

Charlson, R. J., Lovelock, J. E., Andreae, M. O. and Warren, S. G.: Oceanic phytoplankton, atmospheric sulphur, cloud albedo and climate, Nature, 326(6114), 655–661, doi:10.1038/326655a0, 1987.

Chen, Y.: Quantifying the Productions of Volatile Organic Compounds from Surface Reactions between Ozone and Seawater, University of Plymouth, Plymouth., 2017.

Cho, M., Kim, H., Cho, S. H. and Yoon, J.: Investigation of Ozone Reaction in River Waters Causing Instantaneous Ozone Demand, Ozone Sci. Eng., 25(4), 251–259, doi:10.1080/01919510390481577, 2003.

Ciuraru, R., Fine, L., van Pinxteren, M., D'Anna, B., Herrmann, H. and George, C.: Photosensitized production of functionalized and unsaturated organic compounds at the air-sea interface., Sci. Rep., 5(August), 12741, doi:10.1038/srep12741, 2015a.

Ciuraru, R., Fine, L., Pinxteren, M. Van, D'Anna, B., Herrmann, H. and George, C.: Unravelling New Processes at Interfaces: Photochemical Isoprene Production at the Sea Surface, Environ. Sci. Technol., 49(22), 13199–13205, doi:10.1021/acs.est.5b02388, 2015b.

Clifford, D., Bartels-Rausch, T. and Donaldson, D. J.: Suppression of aqueous surface hydrolysis by monolayers of short chain organic amphiphiles, Phys. Chem. Chem. Phys., 9(11), 1362–1369, doi:10.1039/b617079j, 2007.

Clifford, D., Donaldson, D. J., Brigante, M., D'Anna, B. and George, C.: Reactive uptake of ozone by chlorophyll at aqueous surfaces, Environ. Sci. Technol., 42(4), 1138–1143, doi:10.1021/es0718220, 2008.

Cloern, J. E., Foster, S. Q. and Kleckner, A. E.: Phytoplankton primary production in the world's estuarine-coastal ecosystems, Biogeosciences, 11(9), 2477–2501, doi:10.5194/bg-11-2477-2014, 2014.

Cohen, A. J., Brauer, M., Burnett, R., Anderson, H. R., Frostad, J., Estep, K., Balakrishnan, K., Brunekreef, B., Dandona, L., Dandona, R., Feigin, V., Freedman, G., Hubbell, B., Jobling, A., Kan, H., Knibbs, L., Liu, Y., Martin, R., Morawska, L., Pope, C. A., Shin, H., Straif, K., Shaddick, G., Thomas, M., van Dingenen, R., van Donkelaar, A., Vos, T., Murray, C. J. L. and Forouzanfar, M. H.: Estimates and 25-year trends of the global burden of disease attributable to ambient air pollution: an analysis of data from the Global Burden of Diseases Study 2015, Lancet, 389(10082), 1907–1918, doi:10.1016/S0140-6736(17)30505-6, 2017.

Coleman, L., Varghese, S., Tripathi, O. P., Jennings, S. G. and O'Dowd, C. D.: Regional-Scale Ozone Deposition to North-East Atlantic Waters, Adv. Meteorol., 2010, 1–16, doi:10.1155/2010/243701, 2010.

Ćosović, B. and Vojvodić, V.: Voltammetric Analysis of Surface Active Substances in Natural Seawater, Electroanalysis, 10(6), 429–434, doi:10.1002/(SICI)1521-4109(199805)10:6<429::AID-ELAN429>3.0.CO;2-7, 1998.

Crutzen, P. J. and Andreae, M. O.: Biomass Burning in the Tropics: Impact on Atmospheric Chemistry and Biogeochemical Cycles, Science (80-. )., 250(4988), 1669–1678, doi:10.1126/science.250.4988.1669, 1990.

Cunliffe, M., Engel, A., Frka, S., Gašparović, B. Ž., Guitart, C., Murrell, J. C., Salter, M., Stolle, C., Upstill-Goddard, R. C. and Wurl, O.: Sea surface microlayers: A unified physicochemical and biological perspective of the air-ocean interface, Prog. Oceanogr., 109, 104–116, doi:10.1016/j.pocean.2012.08.004, 2013.

Dani, K. G. S. and Loreto, F.: Trade-Off Between Dimethyl Sulfide and Isoprene Emissions from Marine Phytoplankton, Trends Plant Sci., 22(5), 361–372, doi:10.1016/j.tplants.2017.01.006, 2017.

Davis, C. E., Blackbird, S., Wolff, G., Woodward, M. and Mahaffey, C.: Seasonal organic matter dynamics in a temperate shelf sea, Prog. Oceanogr., 177(March 2018), 101925, doi:10.1016/j.pocean.2018.02.021, 2019.

Dixon, J. L., Beale, R. and Nightingale, P. D.: Production of methanol, acetaldehyde, and acetone in the Atlantic Ocean, Geophys. Res. Lett., 40(17), 4700–4705, doi:10.1002/grl.50922, 2013.

Dixon, J. L., Beale, R., Sargeant, S. L., Tarran, G. A. and Nightingale, P. D.: Microbial acetone oxidation in coastal seawater, Front. Microbiol., 5(MAY), 1–9, doi:10.3389/fmicb.2014.00243, 2014.

Dlugokencky, E. J., Houweling, S., Bruhwiler, L., Masarie, K. A., Lang, P. M., Miller, J. B. and Tans, P. P.: Atmospheric methane levels off: Temporary pause or a new steady-state?, Geophys. Res. Lett., 30(19), 1992, doi:10.1029/2003GL018126, 2003.

Donaldson, D. J. and George, C.: Sea-surface chemistry and its impact on the marine boundary layer, Environ. Sci. Technol., 46(19), 10385–10389, doi:10.1021/es301651m, 2012.

Donaldson, D. J. and Vaida, V.: The influence of organic films at the air-aqueous boundary on atmospheric processes, Chem. Rev., 106(4), 1445–1461, doi:10.1021/cr040367c, 2006.

Dong, Y., Yang, M., Bakker, D. C. E., Kitidis, V. and Bell, T. G.: Uncertainties in eddy covariance air–sea CO2 flux measurements and implications for gas transfer velocity parameterisations, Atmos. Chem. Phys., 21(10), 8089–8110, doi:10.5194/acp-21-8089-2021, 2021.

Du, L., Xu, Y., Ge, M., Jia, L., Yao, L. and Wang, W.: Rate constant of the gas phase reaction of dimethyl sulfide (CH3SCH3) with ozone, Chem. Phys. Lett., 436(1–3), 36–40, doi:10.1016/j.cplett.2007.01.025, 2007.

Duce, R. A., Liss, P. S., Merrill, J. T., Atlas, E. L., Buat-Menard, P., Hicks, B. B., Miller, J. M., Prospero, J. M., Arimoto, R., Church, T. M., Ellis, W., Galloway, J. N., Hansen, L., Jickells, T. D., Knap, A. H., Reinhardt, K. H., Schneider, B., Soudine, A., Tokos, J. J., Tsunogai, S., Wollast, R. and Zhou, M.: The atmospheric input of trace species to the world ocean, Global Biogeochem. Cycles, 5(3), 193–259, doi:10.1029/91GB01778, 1991.

Edson, J. B., Jampana, V., Weller, R. A., Bigorre, S. P., Plueddemann, A. J., Fairall, C. W., Miller, S. D., Mahrt, L., Vickers, D. and Hersbach, H.: On the exchange of momentum over the open ocean, J. Phys. Oceanogr., 43(8), 1589–1610, doi:10.1175/JPO-D-12-0173.1, 2013.

Egge, J. K. and Aksnes, D. L.: Silicate as regulating nutrient in phytoplankton competition, Mar. Ecol. Prog. Ser., 83(2–3), 281–289, doi:10.3354/meps083281, 1992.

Eliason, T. L., Aloisio, S., Donaldson, D. J., Cziczo, D. J. and Vaida, V.: Processing of unsaturated organic acid films and aerosols by ozone, Atmos. Environ., 37(16), 2207–2219, doi:10.1016/S1352-2310(03)00149-3, 2003.

Emberson, L.: Effects of ozone on agriculture, forests and grasslands: Improving risk assessment methods for O3, Philos. Trans. R. Soc. A Math. Phys. Eng. Sci., 378(2183), doi:10.1098/rsta.2019.0327, 2020.

Engel, A., Sperling, M., Sun, C., Grosse, J. and Friedrichs, G.: Organic matter in the surface microlayer: Insights from a wind wave channel experiment, Front. Mar. Sci., 5(JUN), doi:10.3389/fmars.2018.00182, 2018.

Exton, D. A., Suggett, D. J., McGenity, T. J. and Steinke, M.: Chlorophyll-normalized isoprene production in laboratory cultures of marine microalgae and implications for global models, Limnol. Oceanogr., 58(4), 1301–1311, doi:10.4319/lo.2013.58.4.1301, 2013.

Fairall, C. W., Helmig, D., Ganzeveld, L. and Hare, J.: Water-side turbulence enhancement of ozone deposition to the ocean, Atmos. Chem. Phys., 7(2), 443–451, doi:10.5194/acp-7-443-2007, 2007.

Fairall, C. W., Yang, M., Bariteau, L., Edson, J. B., Helmig, D., McGillis, W., Pezoa, S., Hare, J. E., Huebert, B. J. and Blomquist, B. W.: Implementation of the Coupled Ocean-Atmosphere Response Experiment flux algorithm with CO2, dimethyl sulfide, and O3, J. Geophys. Res. Ocean., 116(10), doi:10.1029/2010JC006884, 2011.

Farrenkopf, A. M., Dollhopf, M. E., Chadhain, S. N., Luther, G. W. and Nealson, K. H.: Reduction of iodate in seawater during Arabian Sea shipboard incubations and in laboratory cultures of the marine bacterium Shewanella putrefaciens strain MR-4, Mar. Chem., 57(3–4), 347–354, doi:10.1016/S0304-4203(97)00039-X, 1997.

Fischer, E. V., Jacob, D. J., Millet, D. B., Yantosca, R. M. and Mao, J.: The role of the ocean in the global atmospheric budget of acetone, Geophys. Res. Lett., 39(1), 3–7, doi:10.1029/2011GL050086, 2012.

Flanders Marine Institute: Longhurst Province Shapefile, [online] Available from: http://marineregions.org/mrgid/22538, 2009.

Flury, M. and Papritz, A.: Bromide in the Natural Environment: Occurrence and Toxicity, J. Environ. Qual., 22(4), 747–758, doi:10.2134/jeq1993.00472425002200040017x, 1993.

Fu, L., Wu, C., Zhou, Y., Zuo, J., Song, G. and Tan, Y.: Ozonation reactivity characteristics of dissolved organic matter in secondary petrochemical wastewater by single ozone, ozone/H2O2, and ozone/catalyst, Chemosphere, 233, 34–43, doi:10.1016/j.chemosphere.2019.05.207, 2019.

Fusco, A. C. and Logan, J. A.: Analysis of 1970-1995 trends in tropospheric ozone at Northern Hemisphere midlatitudes with the GEOS-CHEM model, J. Geophys. Res. Atmos., 108(15), doi:10.1029/2002jd002742, 2003.

Gantt, B., Meskhidze, N. and Kamykowski, D.: A new physically-based quantification of marine isoprene and primary organic aerosol emissions, Atmos. Chem. Phys., 9(14), 4915–4927, doi:10.5194/acp-9-4915-2009, 2009.

Ganzeveld, L. and Lelieveld, J.: Dry deposition parameterization in a chemistry general circulation model and its influence on the distribution of reactive trace gases, J. Geophys. Res., 100(D10), 20999, doi:10.1029/95JD02266, 1995.

Ganzeveld, L., Helmig, D., Fairall, C. W., Hare, J. and Pozzer, A.: Atmosphere-ocean ozone exchange: A global modeling study of biogeochemical, atmospheric, and waterside turbulence dependencies, Global Biogeochem. Cycles, 23(4), 1–16, doi:10.1029/2008GB003301, 2009.

Garland, J. A., Elzerman, A. W. and Penkett, S. A.: The mechanism for dry deposition of ozone to seawater surfaces, J. Geophys. Res. Ocean., 85(C12), 7488–7492, doi:10.1029/JC085iC12p07488, 1980.

Gaudel, A., Cooper, O. R., Ancellet, G., Barret, B., Boynard, A., Burrows, J. P., Clerbaux, C., Coheur, P. F., Cuesta, J., Cuevas, E., Doniki, S., Dufour, G., Ebojie, F., Foret, G., Garcia, O., Granados-Muñoz, M. J., Hannigan, J. W., Hase, F., Hassler, B., Huang, G., Hurtmans, D., Jaffe, D., Jones, N., Kalabokas, P., Kerridge, B., Kulawik, S., Latter, B., Leblanc, T., Le Flochmoën, E., Lin, W., Liu, J., Liu, X., Mahieu, E., McClure-Begley, A., Neu, J. L., Osman, M., Palm, M., Petetin, H., Petropavlovskikh, I., Querel, R., Rahpoe, N., Rozanov, A., Schultz, M. G., Schwab, J., Siddans, R., Smale, D., Steinbacher, M., Tanimoto, H., Tarasick, D. W., Thouret, V., Thompson, A. M., Trickl, T., Weatherhead, E., Wespes, C., Worden, H. M., Vigouroux, C., Xu, X., Zeng, G. and Ziemke, J.: Tropospheric Ozone Assessment Report: Present-day distribution and trends of tropospheric ozone relevant to climate and global atmospheric chemistry model evaluation, Elementa, 6, doi:10.1525/elementa.291, 2018.

Gaudel, A., Cooper, O. R., Chang, K. L., Bourgeois, I., Ziemke, J. R., Strode, S. A., Oman, L. D., Sellitto, P., Nédélec, P., Blot, R., Thouret, V. and Granier, C.: Aircraft observations since the 1990s reveal increases of tropospheric ozone at multiple locations across the Northern Hemisphere, Sci. Adv., 6(34), 1–12, doi:10.1126/sciadv.aba8272, 2020.

Gershenzon, M., Davidovits, P., Jayne, J. T., Kolb, C. E. and Worsnop, D. R.: Simultaneous uptake of DMS and ozone on water, J. Phys. Chem. A, 105(29), 7031–7036, doi:10.1021/jp010696y, 2001.

Giribabu, K. and Ghosh, P.: Adsorption of nonionic surfactants at fluid-fluid interfaces: Importance in the coalescence of bubbles and drops, Chem. Eng. Sci., 62(11), 3057–3067, doi:10.1016/j.ces.2007.03.002, 2007.

Goldstein, A. H. and Galbally, I. E.: Known and Unexplored Organic Constituents in the Earth's Atmosphere, Environ. Sci. Technol., 41(5), 1514–1521, doi:10.1021/es072476p, 2007.

De Gouw, J. A. and Warneke, C.: Measurements of volatile organic compounds in the earth's atmosphere using proton-transfer-reaction mass spectrometry, Mass Spectrom. Rev., 26(2), 223–257, doi:10.1002/mas.20119, 2007.

Griggs, D. J. and Noguer, M.: Climate change 2001: The scientific basis. Contribution of Working Group I to the Third Assessment Report of the Intergovernmental Panel on Climate Change, Weather, 57(8), 267–269, doi:10.1256/004316502320517344, 2002a.

Griggs, D. J. and Noguer, M.: Climate change 2001: The scientific basis. Contribution of Working Group I to the Third Assessment Report of the Intergovernmental Panel on Climate Change, Weather, 57(8), 267–269, doi:10.1256/004316502320517344, 2002b.

Guan, X. L., Wu, P. F., Wang, S., Zhang, J. J., Shen, Z. C., Luo, H., Chen, H., Long, L. H., Chen, J. G. and Wang, F.: Dimethyl sulfide protects against oxidative stress and extends lifespan via a methionine sulfoxide reductase A-dependent catalytic mechanism, Aging Cell, 16(2), 226–236, doi:10.1111/acel.12546, 2017.

Guenther, A. B. and Hills, A. J.: Eddy covariance measurement of isoprene fluxes, J. Geophys. Res. Atmos., 103(D11), 13145–13152, doi:10.1029/97JD03283, 1998.

Guenther, A. B., Karl, T. R., Harley, P., Wiedinmyer, C., Palmer, P. I. and Geron, C.: Estimates of global terrestrial isoprene emissions using MEGAN (Model of Emissions of Gases and Aerosols from Nature), Atmos. Chem. Phys., 6(11), 3181–3210, doi:10.5194/acp-6-3181-2006, 2006.

Guenther, A. B., Jiang, X., Heald, C. L., Sakulyanontvittaya, T., Duhl, T., Emmons, L. K. and Wang, X.: The model of emissions of gases and aerosols from nature version 2.1

(MEGAN2.1): An extended and updated framework for modeling biogenic emissions, Geosci. Model Dev., 5(6), 1471–1492, doi:10.5194/gmd-5-1471-2012, 2012.

Von Gunten, U.: Ozonation of drinking water: Part I. Oxidation kinetics and product formation, Water Res., 37(7), 1443–1467, doi:10.1016/S0043-1354(02)00457-8, 2003a.

Von Gunten, U.: Ozonation of drinking water: Part II. Disinfection and by-product formation in presence of bromide, iodide or chlorine, Water Res., 37(7), 1469–1487, doi:10.1016/S0043-1354(02)00458-X, 2003b.

Hackenberg, S. and Read, K. A.: Ozone (atmospheric), 2013.

Hackenberg, S., Lee, J. D. and Read, K. A.: Ozone (atmospheric), 2012.

Hackenberg, S. C., Andrews, S. J., Airs, R., Arnold, S. R., Bouman, H. A., Brewin, R. J. W., Chance, R. J., Cummings, D., Dall'Olmo, G., Lewis, A. C., Minaeian, J. K., Reifel, K. M., Small, A., Tarran, G. A., Tilstone, G. H. and Carpenter, L. J.: Potential controls of isoprene in the surface ocean, Global Biogeochem. Cycles, 31(4), 644–662, doi:10.1002/2016GB005531, 2017.

Halsey, K. H., Giovannoni, S. J., Graus, M., Zhao, Y., Landry, Z., Thrash, J. C., Vergin, K. L. and De Gouw, J. A.: Biological cycling of volatile organic carbon by phytoplankton and bacterioplankton, Limnol. Oceanogr., 62(6), 2650–2661, doi:10.1002/lno.10596, 2017.

Hansell, D. A.: Recalcitrant dissolved organic carbon fractions, Ann. Rev. Mar. Sci., 5, 421–445, doi:10.1146/annurev-marine-120710-100757, 2013.

Hansell, D. A., Carlson, C. A., Repeta, D. J. and Schlitzer, R.: Dissolved organic matter in the ocean a controversy stim ulates new insights, Oceanography, 22(SPL.ISS. 4), 202–211, doi:10.5670/oceanog.2009.109, 2009.

Hansell, D. A., Carlson, C. A., Amon, R. M. W., Álvarez-Salgado, X. A., Yamashita, Y., Romera-Castillo, C. and Bif, M. B.: Compilation of dissolved organic matter (DOM) data obtained from global ocean observations from 1994 to 2020, , doi:10.25921/s4f4-ye35, 2021.

Hardacre, C., Wild, O. and Emberson, L.: An evaluation of ozone dry deposition in global scale chemistry climate models, Atmos. Chem. Phys., 15(11), 6419–6436, doi:10.5194/acp-15-6419-2015, 2015.

Hartley, W. N.: XXI.—On the absorption of solar rays by atmospheric ozone, J. Chem. Soc., Trans., 39, 111–128, doi:10.1039/CT8813900111, 1881.

Heald, C. L., Goldstein, A. H., Allan, J. D., Aiken, A. C., Apel, E. C., Atlas, E. L., Baker, A. K., Bates, T. S., Beyersdorf, A. J., Blake, D. R., Campos, T., Coe, H., Crounse, J. D., DeCarlo, P. F., De Gouw, J. A., Dunlea, E. J., Flocke, F. M., Fried, A., Goldan, P. D., Griffin, R. J., Herndon, S. C., Holloway, J. S., Holzinger, R., Jimenez, J. L., Junkermann, W., Kuster, W. C., Lewis, A. C., Meinardi, S., Millet, D. B., Onasch, T., Polidori, A., Quinn, P. K., Riemer, D. D., Roberts, J. M., Salcedo, D., Sive, B., Swanson, A. L., Talbot, R., Warneke, C., Weber, R. J., Weibring, P., Wennberg, P. O., Worsnop, D. R., Wittig, A. E., Zhang, R., Zheng, J. and Zheng, W.: Total observed organic carbon (TOOC) in the atmosphere: A synthesis of North American observations, Atmos. Chem. Phys., 8(7), 2007–2025, doi:10.5194/acp-8-2007-2008, 2008.

Hedges, J. I.: Why Dissolved Organics Matter?, in Biogeochemistry of Dissolved Marine Organic Matter, edited by D. A. Hansell and C. A. Carlson, pp. 1–34, Academic Press, London., 2002.

Helmig, D., Lang, E. K., Bariteau, L., Boylan, P., Fairall, C. W., Ganzeveld, L., Hare, J., Huebert, B. J. and Pallandt, M.: Atmosphere-ocean ozone fluxes during the TexAQS 2006, STRATUS 2006, GOMECC 2007, GasEx 2008, and AMMA 2008 cruises, J. Geophys. Res. Atmos., 117(4), 1–15, doi:10.1029/2011JD015955, 2012.

Henze, D. K. and Seinfeld, J. H.: Global secondary organic aerosol from isoprene oxidation, Geophys. Res. Lett., 33(9), 6–9, doi:10.1029/2006GL025976, 2006.

Hopkins, F. E. and Archer, S. D.: Consistent increase in dimethyl sulfide (DMS) in response to high CO2in five shipboard bioassays from contrasting NW European waters, Biogeosciences, 11(18), 4925–4940, doi:10.5194/bg-11-4925-2014, 2014.

Horowitz, L. W., Walters, S., Mauzerall, D. L., Emmons, L. K., Rasch, P. J., Granier, C., Tie, X., Lamarque, J. F., Schultz, M. G., Tyndall, G. S., Orlando, J. J. and Brasseur, G. P.: A global simulation of tropospheric ozone and related tracers: Description and evaluation of MOZART, version 2, J. Geophys. Res. Atmos., 108(24), doi:10.1029/2002jd002853, 2003.

Hu, J. H., Shi, Q., Davidovits, P., Worsnop, D. R., Zahniser, M. S. and Kolb, C. E.: Reactive uptake of Cl2(g) and Br2(g) by aqueous surfaces as a function of Br- and I- ion concentration. The effect of chemical reaction at the interface, J. Phys. Chem., 99(21), 8768–8776, doi:10.1021/j100021a050, 1995.

Huang, Z., Ito, K., Morita, I., Yokota, K., Fukushi, K., Timerbaev, A. R., Watanabe, S. and Hirokawa, T.: Sensitive monitoring of iodine species in sea water using capillary electrophoresis: Vertical profiles of dissolved iodine in the Pacific Ocean, J. Environ. Monit., 7(8), 804–808, doi:10.1039/b501398d, 2005.

Huebert, B. J., Blomquist, B. W., Yang, M., Archer, S. D., Nightingale, P. D., Yelland, M. J., Stephens, J., Pascal, R. W. and Moat, B. I.: Linearity of DMS transfer coefficient with both friction velocity and wind speed in the moderate wind speed range, Geophys. Res. Lett., 37(1), 0–4, doi:10.1029/2009GL041203, 2010.

Hyson, P., Garratt, J. R. and Francey, R. J.: Algebraic and Electronic Corrections of Measured uw Covariance in the Lower Atmosphere, J. Appl. Meteorol., 16(1), 43–47, doi:10.1175/1520-0450(1977)016<0043:AAECOM>2.0.CO;2, 1977.

IHSS: Source Materials for IHSS Samples, [online] Available from: https://humic-substances.org/source-materials-for-ihss-samples/ (Accessed 10 September 2021), 2020.

Irigoien, X., Harris, R. P., Head, R. N. and Harbour, D.: North Atlantic Oscillation and spring bloom phytoplankton composition in the English Channel, J. Plankton Res., 22(12), 2367–2371, doi:10.1093/plankt/22.12.2367, 2000.

Jacob, D. J., Field, B. D., Jin, E. M., Bey, I., Li, Q., Logan, J. A., Yantosca, R. M. and Singh, H. B.: Atmospheric budget of acetone, J. Geophys. Res. Atmos., 107(D10), doi:10.1029/2001JD000694, 2002.

Jähne, B. and Hauecker, H.: Air-water gas exchange, Annu. Rev. Fluid Mech., 30(December), 443–468, doi:10.1146/annurev.fluid.30.1.443, 1998.

Johnson, M. T.: A numerical scheme to calculate temperature and salinity dependent air-water transfer velocities for any gas, Ocean Sci., 6(4), 913–932, doi:10.5194/os-6-913-2010, 2010.

Johnson, P. N. and Davis, R. A.: Diffusivity of Ozone in Water, J. Chem. Eng. Data, 41(6), 1485–1487, doi:10.1021/je9602125, 1996.

Kahan, T. F., Kwamena, N. O. A. and Donaldson, D. J.: Heterogeneous ozonation kinetics of polycyclic aromatic hydrocarbons on organic films, Atmos. Environ., 40(19), 3448–3459, doi:10.1016/j.atmosenv.2006.02.004, 2006.

Kaimal, J., Wyngaard, J., Izumi, Y. and Cote, O.: Spectral characteristics of surface-layer turbulence, Q. J. R. Meteorol. Soc., 098(417), 563–589, doi:10.1256/smsqj.41706, 1972.

Kampa, M. and Castanas, E.: Human health effects of air pollution, Environ. Pollut., 151(2), 362–367, doi:10.1016/j.envpol.2007.06.012, 2008.

Kara, A. B., Metzger, E. J. and Bourassa, M. A.: Ocean current and wave effects on wind stress drag coefficient over the global ocean, Geophys. Res. Lett., 34(1), 2–5, doi:10.1029/2006GL027849, 2007.

Katrib, Y., Martin, S. T., Hung, H. M., Rudich, Y., Zhang, H., Slowik, J. G., Davidovits, P., Jayne, J. T. and Worsnop, D. R.: Products and mechanisms of ozone reactions with oleic acid for aerosol particles having core-shell morphologies, J. Phys. Chem. A, 108(32), 6686–6695, doi:10.1021/jp049759d, 2004.

Kawa, S. R. and Pearson, R.: Ozone budgets from the dynamics and chemistry of marine stratocumulus experiment, J. Geophys. Res., 94(D7), 9809, doi:10.1029/JD094iD07p09809, 1989.

Kazemiparkouhi, F., Eum, K. Do, Wang, B., Manjourides, J. and Suh, H. H.: Long-term ozone exposures and cause-specific mortality in a US Medicare cohort, J. Expo. Sci. Environ. Epidemiol., 30(4), 650–658, doi:10.1038/s41370-019-0135-4, 2020.

Kesselmeier, J. and Staudt, M.: Biogenic Volatile Organic Compound (VOC): An Overview on Emissions, Physiology and Ecology, J. Atmos. Chem., 33(1), 23–88, doi:10.1023/A:1006127516791, 1999.

Khan, M. A. H., Cooke, M. C., Utembe, S. R., Archibald, A. T., Maxwell, P., Morris, W. C., Xiao, P., Derwent, R. G., Jenkin, M. E., Percival, C. J., Walsh, R. C., Young, T. D. S., Simmonds, P. G., Nickless, G., O'Doherty, S. and Shallcross, D. E.: A study of global atmospheric budget and distribution of acetone using global atmospheric model STOCHEM-CRI, Atmos. Environ., 112, 269–277, doi:10.1016/j.atmosenv.2015.04.056, 2015.

Kieber, R. J., Zhou, X. and Mopper, K.: Formation of carbonyl compounds from UV-induced photodegradation of humic substances in natural waters: Fate of riverine carbon in the sea, Limnol. Oceanogr., 35(7), 1503–1515, doi:10.4319/lo.1990.35.7.1503, 1990.

Kiene, R. P., Linn, L. J. and Bruton, J. A.: New and important roles for DMSP in marine microbial communities, J. Sea Res., 43(3–4), 209–224, doi:10.1016/S1385-1101(00)00023-X, 2000.

Kim, M. J., Novak, G. A., Zoerb, M. C., Yang, M., Blomquist, B. W., Huebert, B. J., Cappa, C. D. and Bertram, T. H.: Air-Sea exchange of biogenic volatile organic compounds and the impact on aerosol particle size distributions, Geophys. Res. Lett., 44(8), 3887–3896, doi:10.1002/2017GL072975, 2017.

King, M. D., Rennie, A. R., Thompson, K. C., Fisher, F. N., Dong, C. C., Thomas, R. K., Pfrang, C. and Hughes, A. V.: Oxidation of oleic acid at the air–water interface and its potential effects on cloud critical supersaturations, Phys. Chem. Chem. Phys., 11(35), 7699, doi:10.1039/b906517b, 2009.

King, M. D., Jones, S. H., Lucas, C. O. M., Thompson, K. C., Rennie, A. R., Ward, A. D., Marks, A. A., Fisher, F. N., Pfrang, C., Hughes, A. V. and Campbell, R. A.: The reaction of oleic acid monolayers with gas-phase ozone at the air water interface: The effect of sub-phase viscosity, and inert secondary components, Phys. Chem. Chem. Phys., 22(48), 28032–28044, doi:10.1039/d0cp03934a, 2020.

Koss, A. R., Warneke, C., Yuan, B., Coggon, M. M., Veres, P. R. and De Gouw, J. A.: Evaluation of NO+ reagent ion chemistry for online measurements of atmospheric volatile organic compounds, Atmos. Meas. Tech., 9(7), 2909–2925, doi:10.5194/amt-9-2909-2016, 2016.

Kossinna, E.: Die Tiefen des Weltmeeres, Veröff. Inst. Meeresk. Univ. Berl., 9, 1–70, 1921.

Kumar, G. S., Prakash, S., Ravichandran, M. and Narayana, A. C.: Trends and relationship between chlorophyll-a and sea surface temperature in the central equatorial Indian Ocean, Remote Sens. Lett., 7(11), 1093–1101, doi:10.1080/2150704X.2016.1210835, 2016.

Lana, A., Bell, T. G., Simó, R., Vallina, S. M., Ballabrera-Poy, J., Kettle, A. J., Dachs, J., Bopp, L., Saltzman, E. S., Stefels, J., Johnson, J. E. and Liss, P. S.: An updated climatology of surface dimethlysulfide concentrations and emission fluxes in the global ocean, Global Biogeochem. Cycles, 25(1), 1–17, doi:10.1029/2010GB003850, 2011.

Langmuir, I.: THE CONSTITUTION AND FUNDAMENTAL PROPERTIES OF SOLIDS AND LIQUIDS. PART I. SOLIDS., J. Am. Chem. Soc., 38(11), 2221–2295, doi:10.1021/ja02268a002, 1916.

Langmuir, I.: Part II.—"Heterogeneous reactions". Chemical reactions on surfaces, Trans. Faraday Soc., 17(1897), 607–620, doi:10.1039/TF9221700607, 1922a.

Langmuir, I.: The mechanism of the catalytic action of platinum in the reactions 2Co + O2= 2Co2 and 2H2+ O2= 2H2O, Trans. Faraday Soc., 17(1905), 621, doi:10.1039/tf9221700621, 1922b.

Laurila, T. K., Sinclair, V. A. and Gregow, H.: Climatology, variability, and trends in near-surface wind speeds over the North Atlantic and Europe during 1979–2018 based on <scp>ERA5</scp>, Int. J. Climatol., 41(4), 2253–2278, doi:10.1002/joc.6957, 2021.

Leck, C., Larsson, U., Bågander, L. E., Johansson, S. and Hajdu, S.: Dimethyl sulfide in the Baltic Sea: Annual variability in relation to biological activity, J. Geophys. Res., 95(C3), 3353, doi:10.1029/jc095ic03p03353, 1990.

Lee, C., Wakeham, S. and Arnosti, C.: Particulate organic matter in the sea: The composition conundrum, Ambio, 33(8), 565–575, doi:10.1579/0044-7447-33.8.565, 2004.

Lee, Y. and Zhou, X.: Aqueous reaction kinetics of ozone and dimethylsulfide and its atmospheric implications order aqueous rate coefficient of O3-DMS reaction M -1 s -1 at The implications of this reaction include lifetime of DMS phase reaction with OH radicals, , 99, 3597–3605, 1994.

Lenschow, D. H. and Hicks, B. B.: Global tropospheric chemistry chemical fluxes in the global atmopshere., 1989.

Lenschow, D. H., Pearson, R. and Stankov, B. B.: Measurements of ozone vertical flux to ocean and forest ( Gulf of Mexico, Pacific Ocean (N), Gulf Coast)., J. Geophys. Res., 87(C11), 8833–8837, doi:10.1029/JC087iC11p08833, 1982.

Lewis, A. C., Carpenter, L. J. and Pilling, M. J.: Nonmethane hydrocarbons in Southern Ocean boundary layer air, J. Geophys. Res. Atmos., 106(D5), 4987–4994, doi:10.1029/2000JD900634, 2001.

Lewis, A. C., Hopkins, J. R., Carpenter, L. J., Stanton, J., Read, K. A. and Pilling, M. J.: Sources and sinks of acetone, methanol, and acetaldehyde in North Atlantic marine air, Atmos. Chem. Phys., 5(7), 1963–1974, doi:10.5194/acp-5-1963-2005, 2005.

Li, J., Deng, S., Li, G., Lu, Z., Song, H., Gao, J., Sun, Z. and Xu, K.: VOCs characteristics and their ozone and SOA formation potentials in autumn and winter at Weinan, China., Environ. Res., 203(July 2021), doi:10.1016/j.envres.2021.111821, 2022.

Li, M., Karu, E., Brenninkmeijer, C. A. M., Fischer, H., Lelieveld, J. and Williams, J.: Tropospheric OH and stratospheric OH and Cl concentrations determined from CH4, CH3Cl, and SF6 measurements, Clim. Atmos. Sci., 1(1), 29, doi:10.1038/s41612-018-0041-9, 2018.

Lincoln, B. J., Rippeth, T. P. and Simpson, J. H.: Surface mixed layer deepening through wind shear alignment in a seasonally stratified shallow sea, J. Geophys. Res. Ocean., 121(8), 6021–6034, doi:10.1002/2015JC011382, 2016.

Lindinger, W., Hansel, A. and Jordan, A.: On-line monitoring of volatile organic compounds at pptv levels by means of proton-transfer-reaction mass spectrometry (PTR-MS) medical applications, food control and environmental research, Int. J. Mass Spectrom. Ion Process., 173(3), 191–241, doi:10.1016/S0168-1176(97)00281-4, 1998.

Liss, P. S. and Merlivat, L.: The Role of Air-Sea Exchange in Geochemical Cycling, edited by P. Buat-Ménard, Springer Netherlands, Dordrecht., 1986.

Liss, P. S. and Slater, P. G.: Flux of Gases across the Air-Sea Interface, Nature, 247(5438), 181–184, doi:10.1038/247181a0, 1974.

Liss, P. S., Marandino, C. A., Dahl, E. E., Helmig, D., Hintsa, E. J., Hughes, C., Johnson, M. T., Moore, R. M., Plane, J. M. C. C., Quack, B., Singh, H. B., Stefels, J., von Glasow, R. and Williams, J.: Short-Lived Trace Gases in the Surface Ocean and the Atmosphere, in Ocean-Atmosphere Interactions of Gases and Particles, edited by P. S. Liss and M. T. Johnson, pp. 1–54, Springer Berlin Heidelberg, Berlin, Heidelberg., 2014.

Liu, Q., Schurter, L. M., Muller, C. E., Aloisio, S., Francisco, J. S. and Margerum, D. W.: Kinetics and mechanisms of aqueous ozone reactions with bromide, sulfite, hydrogen sulfite, iodide, and nitrite ions, Inorg. Chem., 40(17), 4436–4442, doi:10.1021/ic000919j, 2001.

Liu, Y.: Is the free energy change of adsorption correctly calculated?, J. Chem. Eng. Data, 54(7), 1981–1985, doi:10.1021/je800661q, 2009.

Loades, D. C., Yang, M., Bell, T. G., Vaughan, A. R., Pound, R. J., Metzger, S., Lee, J. D. and Carpenter, L. J.: Ozone deposition to a coastal sea: comparison of eddy covariance observations with reactive air–sea exchange models, Atmos. Meas. Tech., 13(12), 6915–6931, doi:10.5194/amt-13-6915-2020, 2020.

Loewen, M., Dor, M. and Skafel, M.: Laboratory Measurements of Bubble Size Distributions Beneath Breaking Waves, in Air-Water Gas Transfer, edited by B. Jähne and E. C. Monahan, pp. 337–349, AEON Verlag & Studio, Hanau. [online] Available from: https://archiv.ub.uni-heidelberg.de/volltextserver/17063/, 1995.

Longhurst, A.: Ecological Geography of the Sea, 2nd ed., Elsevier., 2007.

Longhurst, A., Sathyendranath, S., Platt, T. and Caverhill, C.: An estimate of global primary production in the ocean from satellite radiometer data, J. Plankton Res., 17(6), 1245–1271, doi:10.1093/plankt/17.6.1245, 1995.

Luhar, A. K., Woodhouse, M. T. and Galbally, I. E.: A revised global ozone dry deposition estimate based on a new two-layer parameterisation for air–sea exchange and the multi-year MACC composition reanalysis, Atmos. Chem. Phys., 18(6), 4329–4348, doi:10.5194/acp-18-4329-2018, 2018.

Macdonald, S. M., Gómez Martín, J. C., Chance, R., Warriner, S., Saiz-Lopez, A., Carpenter, L. J. and Plane, J. M. C.: A laboratory characterisation of inorganic iodine emissions from the sea surface: Dependence on oceanic variables and parameterisation for global modelling, Atmos. Chem. Phys., 14(11), 5841–5852, doi:10.5194/acp-14-5841-2014, 2014.

Mackay, D. and Yeun, A. T. K.: Mass Transfer Coefficient Correlations for Volatilization of Organic Solutes from Water, Environ. Sci. Technol., 17(4), 211–217, doi:10.1021/es00110a006, 1983.

Mackay, D., Shiu, W. Y. and Sutherl, R. P.: Determination of Air-Water Henry's Law Constants for Hydrophobic Pollutants, Environ. Sci. Technol., 13(3), 333–337, doi:10.1021/es60151a012, 1979.

Magi, L., Schweitzer, F., Pallares, C., Cherif, S., Mirabel, P. and George, C.: Investigation of the uptake rate of ozone and methyl hydroperoxide by water surfaces, J. Phys. Chem. A, 101(27), 4943–4949, doi:10.1021/jp970646m, 1997.

Malcolm, R. L.: The uniqueness of humic substances in each of soil, stream and marine environments, Anal. Chim. Acta, 232(C), 19–30, doi:10.1016/S0003-2670(00)81222-2, 1990.

Marandino, C. A., de Bruyn, W. J., Miller, S. D., Prather, M. J. and Saltzman, E. S.: Oceanic uptake and the global atmospheric acetone budget, Geophys. Res. Lett., 32(15), doi:10.1029/2005GL023285, 2005.

Martino, M., Lézé, B., Baker, A. R. and Liss, P. S.: Chemical controls on ozone deposition to water, Geophys. Res. Lett., 39(5), 39–43, doi:10.1029/2011GL050282, 2012.

McClain, C. R.: A Decade of Satellite Ocean Color Observations, Ann. Rev. Mar. Sci., 1(1), 19–42, doi:10.1146/annurev.marine.010908.163650, 2009.

McDonald, S., Bishop, A. G., Prenzler, P. D. and Robards, K.: Analytical chemistry of freshwater humic substances, Anal. Chim. Acta, 527(2), 105–124, doi:10.1016/j.aca.2004.10.011, 2004.

McKenna, S. P. and McGillis, W. R.: The role of free-surface turbulence and surfactants in air-water gas transfer, Int. J. Heat Mass Transf., 47(3), 539–553, doi:10.1016/j.ijheatmasstransfer.2003.06.001, 2004.

Meon, B. and Kirchman, D. L.: Dynamics and molecular composition of dissolved organic material during experimental phytoplankton blooms, Mar. Chem., 75(3), 185–199, doi:10.1016/S0304-4203(01)00036-6, 2001.

Millet, D. B., Guenther, A. B., Siegel, D. A., Nelson, N. B., Singh, H. B., De Gouw, J. A., Warneke, C., Williams, J., Eerdekens, G., Sinha, V., Karl, T. R., Flocke, F., Apel, E. C., Riemer, D. D., Palmer, P. I. and Barkley, M.: Global atmospheric budget of acetaldehyde: 3-

D model analysis and constraints from in-situ and satellite observations, Atmos. Chem. Phys., 10(7), 3405–3425, doi:10.5194/acp-10-3405-2010, 2010.

Milne, P. J., Riemer, D. D., Zika, R. G. and Brand, L. E.: Measurement of vertical distribution of isoprene in surface seawater, its chemical fate, and its emission from several phytoplankton monocultures, Mar. Chem., 48(3–4), 237–244, doi:10.1016/0304-4203(94)00059-M, 1995.

Mmereki, B. T., Donaldson, D. J., Gilman, J. B., Eliason, T. L. and Vaida, V.: Kinetics and products of the reaction of gas-phase ozone with anthracene adsorbed at the air-aqueous interface, Atmos. Environ., 38(36), 6091–6103, doi:10.1016/j.atmosenv.2004.08.014, 2004.

Molina, M. J., Ivanov, A. V., Trakhtenberg, S. and Molina, L. T.: Atmospheric evolution of organic aerosol, Geophys. Res. Lett., 31(22), 1–5, doi:10.1029/2004GL020910, 2004.

Momzikoff, A., Brinis, A., Dallot, S., Gondry, G., Saliot, A. and Lebaron, P.: Field study of the chemical characterization of the upper ocean surface using various samplers, Limnol. Oceanogr. Methods, 2(11), 374–386, doi:10.4319/lom.2004.2.374, 2004.

Monks, P. S.: Gas-phase radical chemistry in the troposphere, Chem. Soc. Rev., 34(5), 376, doi:10.1039/b307982c, 2005.

Monks, P. S., Archibald, A. T., Colette, A., Cooper, O., Coyle, M., Derwent, R., Fowler, D., Granier, C., Law, K. S., Mills, G. E., Stevenson, D. S., Tarasova, O., Thouret, V., von Schneidemesser, E., Sommariva, R., Wild, O. and Williams, M. L.: Tropospheric ozone and its precursors from the urban to the global scale from air quality to short-lived climate forcer, Atmos. Chem. Phys., 15(15), 8889–8973, doi:10.5194/acp-15-8889-2015, 2015.

Moore, K.: Influence of the Sea Surface Microlayer on Ozone Deposition Velocity, Honor. Theses [online] Available from: http://digitalcommons.colby.edu/honorstheses/728, 2014.

Moore, M. N.: Do airborne biogenic chemicals interact with the PI3K/Akt/mTOR cell signalling pathway to benefit human health and wellbeing in rural and coastal environments?, Environ. Res., 140, 65–75, doi:10.1016/j.envres.2015.03.015, 2015.

Moore, R. M., Oram, D. E. and Penkett, S. A.: Production of isoprene by marine phytoplankton cultures, Geophys. Res. Lett., 21(23), 2507–2510, doi:10.1029/94GL02363, 1994.

Moreno, C. G., Gálvez, O., López-Arza Moreno, V., Espildora-García, E. M. and Baeza-Romero, M. T.: A revisit of the interaction of gaseous ozone with aqueous iodide. Estimating the contributions of the surface and bulk reactions, Phys. Chem. Chem. Phys., 20(43), 27571–27584, doi:10.1039/c8cp04394a, 2018.

Morris, J.: The aqueous solubility of ozone - A review, Ozone news, 1, 14–16, 1988.

Murphy, J. J., Delucchi, M. A., McCubbin, D. R. and Kim, H. J.: The cost of crop damage caused by ozone air pollution from motor vehicles, J. Environ. Manage., 55(4), 273–289, doi:10.1006/jema.1999.0256, 1999.

Mustaffa, N. I. H., Badewien, T. H., Ribas-Ribas, M. and Wurl, O.: High-resolution observations on enrichment processes in the sea-surface microlayer, Sci. Rep., 8(1), 1–12, doi:10.1038/s41598-018-31465-8, 2018.

Myriokefalitakis, S., Vrekoussis, M., Tsigaridis, K., Wittrock, F., Richter, A., Brühl, C., Volkamer, R., Burrows, J. P. and Kanakidou, M.: The influence of natural and anthropogenic secondary sources on the glyoxal global distribution, Atmos. Chem. Phys., 8(16), 4965–4981, doi:10.5194/acp-8-4965-2008, 2008.

Nelson, N. B. and Siegel, D. A.: The global distribution and dynamics of chromophoric dissolved organic matter, Ann. Rev. Mar. Sci., 5, 447–476, doi:10.1146/annurev-marine-120710-100751, 2013.

Nightingale, P. D., Malin, G., Law, C. S., Watson, A. J., Liss, P. S., Liddicoat, M. I., Boutin, J. and Upstill-Goddard, R. C.: In situ evaluation of air-sea gas exchange parameterizations using novel conservative and volatile tracers, Global Biogeochem. Cycles, 14(1), 373–387, doi:10.1029/1999GB900091, 2000.

Nurdin, S., Mustapha, M. A. and Lihan, T.: The relationship between sea surface temperature and chlorophyll-a concentration in fisheries aggregation area in the archipelagic waters of spermonde using satellite images, AIP Conf. Proc., 1571, 466–472, doi:10.1063/1.4858699, 2013.

Ogawa, H. and Tanoue, E.: Dissolved Organic Matter in Oceanic Waters, J. Oceanogr., 59, 139–147, doi:10.1023/A:1025528919771, 2003.

Opsahl, S. and Benner, R.: Organic Matter in the Ocean, Nature, 386(April), 480–482, 1997.

Pagano, T., Bida, M. and Kenny, J. E.: Trends in levels of allochthonous dissolved organic carbon in natural water: A review of potential mechanisms under a changing climate, Water (Switzerland), 6(10), 2862–2897, doi:10.3390/w6102862, 2014.

Palmer, P. I. and Shaw, S. L.: Quantifying global marine isoprene fluxes using MODIS chlorophyll observations, Geophys. Res. Lett., 32(9), 1–5, doi:10.1029/2005GL022592, 2005.

Parrish, D. D., Millet, D. B. and Goldstein, A. H.: Increasing ozone in marine boundary layer inflow at the west coasts of North America and Europe, Atmos. Chem. Phys., 9(4), 1303–1323, doi:10.5194/acp-9-1303-2009, 2009.

Pereira, R., Schneider-Zapp, K. and Upstill-Goddard, R. C.: Surfactant control of gas transfer velocity along an offshore coastal transect: Results from a laboratory gas exchange tank, Biogeosciences, 13(13), 3981–3989, doi:10.5194/bg-13-3981-2016, 2016.

Pereira, R., Ashton, I., Sabbaghzadeh, B., Shutler, J. D. and Upstill-Goddard, R. C.: Reduced air-sea CO2 exchange in the Atlantic Ocean due to biological surfactants, Nat. Geosci., 11(7), 492–496, doi:10.1038/s41561-018-0136-2, 2018.

Phillips, D. P., Hopkins, F. E., Bell, T. G., Liss, P. S., Nightingale, P. D., Reeves, C. E., Wohl, C. and Yang, M.: Air–sea exchange of acetone, acetaldehyde, DMS and isoprene at a UK coastal site, Atmos. Chem. Phys., 21(13), 10111–10132, doi:10.5194/acp-21-10111-2021, 2021.

Pingree, R. D., Pugh, P. R., Holligan, P. M. and Forster, G. R.: Summer phytoplankton blooms and red tides along tidal fronts in the approaches to the English Channel, Nature, 258(5537), 672–677, doi:10.1038/258672a0, 1975.

Pound, R. J., Sherwen, T., Helmig, D., Carpenter, L. J. and Evans, M. J.: Influences of oceanic ozone deposition on tropospheric photochemistry, Atmos. Chem. Phys., 20(7), 4227–4239, doi:10.5194/acp-20-4227-2020, 2020.

Prins, R.: Eley–Rideal, the Other Mechanism, Top. Catal., 61(9–11), 714–721, doi:10.1007/s11244-018-0948-8, 2018.

Quinn, P. K., Bates, T. S., Coffman, D. J., Upchurch, L., Johnson, J. E., Moore, R., Ziemba, L., Bell, T. G., Saltzman, E. S., Graff, J. and Behrenfeld, M. J.: Seasonal Variations in Western North Atlantic Remote Marine Aerosol Properties, J. Geophys. Res. Atmos., 124(24), 14240–14261, doi:10.1029/2019JD031740, 2019.

Raja, S. and Valsaraj, K. T.: Heterogeneous Oxidation by Ozone of Naphthalene Adsorbed at the Air-Water Interface of Micron-Size Water Droplets, J. Air Waste Manage. Assoc., 55(9), 1345–1355, doi:10.1080/10473289.2005.10464732, 2005.

Read, K. A.: Cape Verde Atmospheric Observatory: Ozone measurements from Thermo Electron Instrument, [online] Available from: https://catalogue.ceda.ac.uk/uuid/9124046f77d8eac688fb974b8409e96a, 2019.

Reader, M. C., Plummer, D. A., Scinocca, J. F. and Shepherd, T. G.: Contributions to twentieth century total column ozone change from halocarbons, tropospheric ozone precursors, and climate change, Geophys. Res. Lett., 40(23), 6276–6281, doi:10.1002/2013GL057776, 2013.

Reeser, D. I. and Donaldson, D. J.: Influence of water surface properties on the heterogeneous reaction between O3(g) and I(aq)-, Atmos. Environ., 45(34), 6116–6120, doi:10.1016/j.atmosenv.2011.08.042, 2011.

Reeser, D. I., Jammoul, A., Clifford, D., Brigante, M., D'Anna, B., George, C. and Donaldson, D. J.: Photoenhanced reaction of ozone with chlorophyll at the seawater surface, J. Phys. Chem. C, 113(6), 2071–2077, doi:10.1021/jp805167d, 2009.

Reeves, C. E., Penkett, S. A., Bauguitte, S., Law, K. S., Evans, M. J., Bandy, B. J., Monks, P. S., Edwards, G. D., Phillips, G., Barjat, H., Kent, J., Dewey, K., Schmitgen, S. and Kley, D.: Potential for photochemical ozone formation in the troposphere over the North Atlantic as derived from aircraft observations during ACSOE, J. Geophys. Res. D Atmos., 107(23), 1–14, doi:10.1029/2002JD002415, 2002.

Rodríguez-López, L., Rincón-Fontán, M., Vecino, X., Cruz, J. M. and Moldes, A. B.: Biological surfactants vs. polysorbates: Comparison of their emulsifier and surfactant properties, Tenside, Surfactants, Deterg., 55(4), 273–280, doi:10.3139/113.110574, 2018.

Rodríguez-Ros, P., Galí, M., Cortés, P., Robinson, C. M., Antoine, D., Wohl, C., Yang, M. X. and Simó, R.: Remote Sensing Retrieval of Isoprene Concentrations in the Southern Ocean, Geophys. Res. Lett., 47(13), 1–10, doi:10.1029/2020GL087888, 2020.

Rogerson, L.: The Photochemical Production of Acetone in Natural Waters, University of Plymouth., 2016.

Rolph, G., Stein, A. and Stunder, B.: Real-time Environmental Applications and Display sYstem: READY, Environ. Model. Softw., 95, 210–228, doi:10.1016/j.envsoft.2017.06.025, 2017.

Romera-Castillo, C., Sarmento, H., Álvarez-Salgado, X. A., Gasol, J. M. and Marrasé, C.: Production of chromophoric dissolved organic matter by marine phytoplankton, Limnol. Oceanogr., 55(1), 446–454, doi:10.4319/lo.2010.55.1.0446, 2010.

Romera-Castillo, C., Letscher, R. T. and Hansell, D. A.: New nutrients exert fundamental control on dissolved organic carbon accumulation in the surface Atlantic Ocean, Proc. Natl. Acad. Sci., 113(38), 10497–10502, doi:10.1073/pnas.1605344113, 2016.

Romera-Castillo, C., Álvarez, M., Pelegrí, J. L., Hansell, D. A. and Álvarez-Salgado, X. A.: Net Additions of Recalcitrant Dissolved Organic Carbon in the Deep Atlantic Ocean, Global Biogeochem. Cycles, 33(9), 1162–1173, doi:10.1029/2018GB006162, 2019.

Royer, S. J., Galí, M., Mahajan, A. S., Ross, O. N., Pérez, G. L., Saltzman, E. S. and Simó, R.: A high-resolution time-depth view of dimethylsulphide cycling in the surface sea, Sci. Rep., 6(November 2015), 1–13, doi:10.1038/srep32325, 2016.

Rühl, S., Thompson, C. E. L., Queirós, A. M. and Widdicombe, S.: Intra-Annual Patterns in the Benthic-Pelagic Fluxes of Dissolved and Particulate Matter, Front. Mar. Sci., 7(November), doi:10.3389/fmars.2020.567193, 2020.

Sabbaghzadeh, B., Upstill-Goddard, R. C., Beale, R., Pereira, R. and Nightingale, P. D.: The Atlantic Ocean surface microlayer from 50°N to 50°S is ubiquitously enriched in surfactants at wind speeds up to 13 m s−1, Geophys. Res. Lett., 44(6), 2852–2858, doi:10.1002/2017GL072988, 2017.

Sakamoto, Y., Yabushita, A., Kawasaki, M. and Enami, S.: Direct Emission of I 2 Molecule and IO Radical from the Heterogeneous Reactions of Gaseous Ozone with Aqueous Potassium Iodide Solution, J. Phys. Chem. A, 113(27), 7707–7713, doi:10.1021/jp903486u, 2009.

Salter, M. E., Upstill-Goddard, R. C., Nightingale, P. D., Archer, S. D., Blomquist, B., Ho, D. T., Huebert, B., Schlosser, P. and Yang, M.: Impact of an artificial surfactant release on air-sea gas fluxes during Deep Ocean Gas Exchange Experiment II, J. Geophys. Res. Ocean., 116(11), 1–9, doi:10.1029/2011JC007023, 2011.

Saltzman, E. S., King, D. B., Holmen, K. and Leck, C.: Experimental determination of the diffusion coefficient of dimethylsulfide in water, J. Geophys. Res., 98(C9), 481–486, doi:10.1029/93jc01858, 1993.

Sander, R.: Compilation of Henry's law constants (version 4.0) for water as solvent, Atmos. Chem. Phys., 15(8), 4399–4981, doi:10.5194/acp-15-4399-2015, 2015.

Sarwar, G., Kang, D., Foley, K., Schwede, D., Gantt, B. and Mathur, R.: Technical note: Examining ozone deposition over seawater, Atmos. Environ., 141, 255–262, doi:10.1016/j.atmosenv.2016.06.072, 2016.

Schlundt, C., Tegtmeier, S., Lennartz, S. T., Bracher, A., Cheah, W., Krüger, K., Quack, B. and Marandino, C. A.: Oxygenated volatile organic carbon in the western Pacific convective center: Ocean cycling, air-sea gas exchange and atmospheric transport, Atmos. Chem. Phys., 17(17), 10837–10854, doi:10.5194/acp-17-10837-2017, 2017.

Schneider, S. R., Collins, D. B., Lim, C. Y., Zhu, L. and Abbatt, J. P. D.: Formation of Secondary Organic Aerosol from the Heterogeneous Oxidation by Ozone of a Phytoplankton Culture, ACS Earth Sp. Chem., 3(10), 2298–2306, doi:10.1021/acsearthspacechem.9b00201, 2019.

Schwarz, K., Filipiak, W. and Amann, A.: Determining concentration patterns of volatile compounds in exhaled breath by PTR-MS, J. Breath Res., 3(2), 027002, doi:10.1088/1752-7155/3/2/027002, 2009.

Scott, J. C.: The role of salt in whitecap persistence, Deep Sea Res. Oceanogr. Abstr., 22(10), 653–657, doi:10.1016/0011-7471(75)90002-9, 1975.

Sharp, J. H.: Size Classes of Organic Carbon in Seawater, Limnol. Oceanogr., 18(3), 441–447, doi:10.4319/lo.1973.18.3.0441, 1973.

Shaw, S. L., Chisholm, S. W. and Prinn, R. G.: Isoprene production by Prochlorococcus, a marine cyanobacterium, and other phytoplankton, Mar. Chem., 80(4), 227–245, doi:10.1016/S0304-4203(02)00101-9, 2003.

Sherwen, T., Chance, R. J., Tinel, L., Ellis, D., Evans, M. J. and Carpenter, L. J.: A machine-learning-based global sea-surface iodide distribution, Earth Syst. Sci. Data, 11(3), 1239–1262, doi:10.5194/essd-11-1239-2019, 2019.

Shimotori, K., Satou, T., Imai, A., Kawasaki, N., Komatsu, K., Kohzu, A., Tomioka, N., Shinohara, R. and Miura, S.: Quantification and characterization of coastal dissolved organic matter by high-performance size exclusion chromatography with ultraviolet absorption, fluorescence, and total organic carbon analyses, Limnol. Oceanogr. Methods, 14(10), 637–648, doi:10.1002/lom3.10118, 2016.

Shine, K. P.: Atmospheric ozone and climate change, Ozone Sci. Eng., 23(6), 429–435, doi:10.1080/01919510108962026, 2001.

Shine, K. P. and Forster, P. M. D. F.: The effect of human activity on radiative forcing of climate change: A review of recent developments, Glob. Planet. Change, 20(4), 205–225, doi:10.1016/S0921-8181(99)00017-X, 1999.

Siegel, D. A., Behrenfeld, M. J., Maritorena, S., McClain, C. R., Antoine, D., Bailey, S. W., Bontempi, P. S., Boss, E. S., Dierssen, H. M., Doney, S. C., Eplee, R. E., Evans, R. H., Feldman, G. C., Fields, E., Franz, B. A., Kuring, N. A., Mengelt, C., Nelson, N. B., Patt, F. S., Robinson, W. D., Sarmiento, J. L., Swan, C. M., Werdell, P. J., Westberry, T. K., Wilding, J. G. and Yoder, J. A.: Regional to global assessments of phytoplankton dynamics from the SeaWiFS mission, Remote Sens. Environ., 135, 77–91, doi:10.1016/j.rse.2013.03.025, 2013.

Siegenthaler, U. and Sarmiento, J. L.: Atmospheric carbon dioxide and the ocean, Nature, 365(6442), 119–125, doi:10.1038/365119a0, 1993.

Sims, R. P., Schuster, U., Watson, A. J., Yang, M., Hopkins, F. E., Stephens, J. A. and Bell, T. G.: A measurement system for vertical seawater profiles close to the air–sea interface, Ocean Sci., 13(5), 649–660, doi:10.5194/os-13-649-2017, 2017.

Singh, H. B., Kanakidou, M., Crutzen, P. J. and Jacob, D. J.: High concentrations and photochemical fate of oxygenated hydrocarbons in the global troposphere, Nature, 378(6552), 50–54, doi:10.1038/378050a0, 1995.

Sinreich, R., Coburn, S., Dix, B. and Volkamer, R.: Ship-based detection of glyoxal over the remote tropical Pacific Ocean, Atmos. Chem. Phys., 10(23), 11359–11371, doi:10.5194/acp-10-11359-2010, 2010.

Smyth, T. J.: L4 CTD data, [online] Available from: https://www.westernchannelobservatory.org.uk/l4_ctdf/index.php, 2021.

Smyth, T. J., Moore, G. F., Groom, S. B., Land, P. E. and Tyrrell, T.: Optical modeling and measurements of a coccolithophore bloom, Appl. Opt., 41(36), 7679–7688, doi:10.1364/AO.41.007679, 2002.

Smyth, T. J., Fishwick, J. R., Al-Moosawi, L., Cummings, D. G., Harris, C., Kitidis, V., Rees, A., Martinez-Vicente, V. and Woodward, E. M. S.: A broad spatio-temporal view of the Western English Channel observatory, J. Plankton Res., 32(5), 585–601, doi:10.1093/plankt/fbp128, 2010.

Spirig, C., Neftel, A., Ammann, C., Dommen, J., Grabmer, W., Thielmann, A., Schaub, A., Beauchamp, J. L., Wisthaler, A. and Hansel, A.: Eddy covariance flux measurements of biogenic VOCs during ECHO 2003 using proton transfer reaction mass spectrometry, Atmos. Chem. Phys., 5(2), 465–481, doi:10.5194/acp-5-465-2005, 2005.

Staehelin, J. and Holgné, J.: Decomposition of Ozone in Water: Rate of Initiation by Hydroxide Ions and Hydrogen Peroxide, Environ. Sci. Technol., 16(10), 676–681, doi:10.1021/es00104a009, 1982.

Stein, A. F., Draxler, R. R., Rolph, G. D., Stunder, B. J. B., Cohen, M. D. and Ngan, F.: Noaa's hysplit atmospheric transport and dispersion modeling system, Bull. Am. Meteorol. Soc., 96(12), 2059–2077, doi:10.1175/BAMS-D-14-00110.1, 2015.

Stevenson, D. S., Dentener, F. J., Schultz, M. G., Ellingsen, K., van Noije, T. P. C., Wild, O., Zeng, G., Amann, M., Atherton, C. S., Bell, N., Bergmann, D. J., Bey, I., Butler, T. M., Cofala, J., Collins, W., Derwent, R. G., Doherty, R. M., Drevet, J., Eskes, H. J., Fiore, A. M., Gauss, M., Hauglustaine, D. A., Horowitz, L. W., Isaksen, I. S. A., Krol, M. C., Lamarque, J. F., Lawrence, M. G., Montanaro, V., Müller, J. F., Pitari, G., Prather, M. J., Pyle, J. A., Rast, S., Rodriquez, J. M., Sanderson, M. G., Savage, N. H., Shindell, D. T., Strahan, S. E., Sudo, K. and Szopa, S.: Multimodel ensemble simulations of present-day and near-future tropospheric ozone, J. Geophys. Res. Atmos., 111(8), doi:10.1029/2005JD006338, 2006.

Sulzer, P., Edtbauer, A., Hartungen, E., Jürschik, S., Jordan, A., Hanel, G., Feil, S., Jaksch, S., Märk, L. and Märk, T. D.: From conventional proton-transfer-reaction mass spectrometry (PTR-MS) to universal trace gas analysis, Int. J. Mass Spectrom., 321–322, 66–70, doi:10.1016/j.ijms.2012.05.003, 2012.

Suratman, S., Weston, K., Jickells, T. and Fernand, L.: Spatial and seasonal changes of dissolved and particulate organic C in the North Sea, Hydrobiologia, 628(1), 13–25, doi:10.1007/s10750-009-9730-z, 2009.

Tanner, C. B. and Thurtell, G. W.: Anemoclinometer measurements of Reynolds stress and heat transport in the atmospheric surface layer., 1969.

Tapin, A.: L4 DOC data, 2014.

Thames, A. B., Brune, W. H., Miller, D. O., Allen, H. M., Apel, E. C., Blake, D. R., Paul Bui, T., Commane, R., Crounse, J. D., Daube, B. C., Diskin, G. S., Digangi, J. P., Elkins, J. W., Hall, S. R., Hanisco, T. F., Hannun, R. A., Hintsa, E., Hornbrook, R. S., Kim, M. J., McKain, K., Moore, F. L., Nicely, J. M., Peischl, J., Ryerson, T. B., St. Clair, J. M., Sweeney, C., Teng, A., Thompson, C. R., Ullmann, K., Wennberg, P. O. and Wolfe, G. M.: Missing OH reactivity in the global marine boundary layer, Atmos. Chem. Phys., 20(6), 4013–4029, doi:10.5194/acp-20-4013-2020, 2020.

The European Parliament and the Council of the European Union: Directive 2004/42/CE of the European Parliament and of the Council of 21 April 2004 on the limitation of emissions of volatile organic compounds due to the use of organic solvents in certain paints and varnishes and vehicle refinishing products and amendi., 2004.

Thomas, H., Bozec, Y., Elkalay, K., De Baar, H. J. W., Borges, A. V. and Schiettecatte, L. S.: Controls of the surface water partial pressure of CO2 in the North Sea, Biogeosciences, 2(4), 323–334, doi:10.5194/bg-2-323-2005, 2005.

Thompson, A. M.: The Oxidizing Capacity of the Earth's Atmosphere: Probable Past and Future Changes, Science (80-. )., 256(5060), 1157–1165, doi:10.1126/science.256.5060.1157, 1992.

Thornberry, T. and Abbatt, J. P. D.: Heterogeneous reaction of ozone with liquid unsaturated fatty acids: detailed kinetics and gas-phase product studies, Phys. Chem. Chem. Phys., 6(1), 84, doi:10.1039/b310149e, 2004.

Thurman, E. M.: Organic Geochemistry of Natural Waters, Springer Netherlands, Dordrecht., 1985.

Tian, R. C. and Nicolas, E.: Iodine speciation in the northwestern Mediterranean Sea, method and vertical profile, Mar. Chem., 48(2), 151–156, doi:10.1016/0304-4203(94)00048-I, 1995.

Tilstone, G. H.: L4 CDOM data, 2009.

Triesch, N., Van Pinxteren, M., Frka, S., Stolle, C., Spranger, T., Hans Hoffmann, E., Gong, X., Wex, H., Schulz-Bull, D., Gasparovic, B. and Herrmann, H.: Concerted measurements of lipids in seawater and on submicrometer aerosol particles at the Cabo Verde islands: Biogenic sources, selective transfer and high enrichments, Atmos. Chem. Phys., 21(6), 4267–4283, doi:10.5194/acp-21-4267-2021, 2021.

Uncles, R. J., Stephens, J. A. and Harris, C.: Physical processes in a coupled bay-estuary coastal system: Whitsand Bay and Plymouth Sound, Prog. Oceanogr., 137, 360–384, doi:10.1016/j.pocean.2015.04.019, 2015.

Upstill-Goddard, R. C.: Air-sea gas exchange in the coastal zone, Estuar. Coast. Shelf Sci., 70(3), 388–404, doi:10.1016/j.ecss.2006.05.043, 2006.

Valach, A. C.: Volatile organic compound fluxes and mixing ratios in two contrasting atmospheric environments : London and the Amazon rainforest, , (July), 2015.

Veres, P. R., Andrew Neuman, J., Bertram, T. H., Assaf, E., Wolfe, G. M., Williamson, C. J., Weinzierl, B., Tilmes, S., Thompson, C. R., Thames, A. B., Schroder, J. C., Saiz-Lopez, A., Rollins, A. W., Roberts, J. M., Price, D., Peischl, J., Nault, B. A., Møller, K. H., Miller, D. O., Meinardi, S., Li, Q., Lamarque, J. F., Kupc, A., Kjaergaard, H. G., Kinnison, D., Jimenez, J. L., Jernigan, C. M., Hornbrook, R. S., Hills, A., Dollner, M., Day, D. A., Cuevas, C. A., Campuzano-Jost, P., Burkholder, J. B., Paul Bui, T., Brune, W. H., Brown, S. S., Brock, C. A., Bourgeois, I., Blake, D. R., Apel, E. C. and Ryerson, T. B.: Global airborne sampling reveals a previously unobserved dimethyl sulfide oxidation mechanism in the marine atmosphere, Proc. Natl. Acad. Sci. U. S. A., 117(9), 4505–4510, doi:10.1073/pnas.1919344117, 2020.

Vingarzan, R.: A review of surface ozone background levels and trends, Atmos. Environ., 38(21), 3431–3442, doi:10.1016/j.atmosenv.2004.03.030, 2004.

Voss, L. F., Hadad, C. M. and Allen, H. C.: Competition between atmospherically relevant fatty acid monolayers at the air/water interface, J. Phys. Chem. B, 110(39), 19487–19490, doi:10.1021/jp062595b, 2006.

Voss, L. F., Bazerbashi, M. F., Beekman, C. P., Hadad, C. M. and Allen, H. C.: Oxidation of oleic acid at air/liquid interfaces, J. Geophys. Res. Atmos., 112(6), 1–9, doi:10.1029/2006JD007677, 2007.

Wallace, J. W. and Hobbs, P. V: Atmospheric Science: An Introductory Survey, 2nd ed., Academic Press, London., 2006.

Wang, S., Hornbrook, R. S., Hills, A., Emmons, L. K., Tilmes, S., Lamarque, J. F., Jimenez, J. L., Campuzano-Jost, P., Nault, B. A., Crounse, J. D., Wennberg, P. O., Kim, M., Allen, H. M., Ryerson, T. B., Thompson, C. R., Peischl, J., Moore, F., Nance, D., Hall, B., Elkins, J., Tanner, D., Huey, L. G., Hall, S. R., Ullmann, K., Orlando, J. J., Tyndall, G. S., Flocke, F. M., Ray, E., Hanisco, T. F., Wolfe, G. M., St. Clair, J., Commane, R., Daube, B., Barletta, B., Blake, D. R., Weinzierl, B., Dollner, M., Conley, A., Vitt, F., Wofsy, S. C., Riemer, D. D. and Apel, E. C.: Atmospheric Acetaldehyde: Importance of Air-Sea Exchange and a Missing Source in

the Remote Troposphere, Geophys. Res. Lett., 46(10), 5601–5613, doi:10.1029/2019GL082034, 2019.

Wang, S., Apel, E. C., Schwantes, R., Bates, K., Jacob, D., Fischer, E., Hornbrook, R. S., Hills, A., Emmons, L., Pan, L., Honomichl, S., Tilmes, S., Lamarque, J., Yang, M., Marandino, C., Saltzman, E., Bruyn, W., Kameyama, S., Tanimoto, H., Omori, Y., Hall, S., Ullmann, K., Ryerson, T., Thompson, C. R., Peischl, J., Daube, B., Commane, R., McKain, K., Sweeney, C., Thames, A. B., Miller, D., Brune, W. H., Diskin, G., DiGangi, J. and Wofsy, S.: Global Atmospheric Budget of Acetone: Air-Sea Exchange and the Contribution to Hydroxyl Radicals, J. Geophys. Res. Atmos., 2, 1–23, doi:10.1029/2020JD032553, 2020a.

Wang, W.-C., Liang, X.-Z., Dudek, M. P., Pollard, D. and Thompson, S. L.: Atmospheric ozone as a climate gas, Atmos. Res., 37(1–3), 247–256, doi:10.1016/0169-8095(94)00080-W, 1995.

Wang, W.-L., Song, G., Primeau, F., Saltzman, E., Bell, T. G. and Moore, J. K.: Global ocean dimethyl sulfide climatology estimated from observations and an artificial neural network, Biogeosciences Discuss., 1–26, doi:10.1002/essoar.10502127.1, 2020b.

Wanninkhof, R.: Relationship between wind speed and gas exchange over the ocean, J. Geophys. Res., 97(C5), 7373, doi:10.1029/92JC00188, 1992.

Wanninkhof, R., Asher, W. E., Ho, D. T., Sweeney, C. and McGillis, W. R.: Advances in Quantifying Air-Sea Gas Exchange and Environmental Forcing, Ann. Rev. Mar. Sci., 1(1), 213–244, doi:10.1146/annurev.marine.010908.163742, 2009.

Warneck, P. and Moortgat, G. K.: Quantum yields and photodissociation coefficients of acetaldehyde in the troposphere, Atmos. Environ., 62, 153–163, doi:10.1016/j.atmosenv.2012.08.024, 2012.

Warneke, C., De Gouw, J. A., Kuster, W. C., Goldan, P. D. and Fall, R.: Validation of atmospheric VOC measurements by proton-transfer-reaction mass spectrometry using a gas-chromatographic preseparation method, Environ. Sci. Technol., 37(11), 2494–2501, doi:10.1021/es026266i, 2003.

Watson, A. J., Upstill-Goddard, R. C. and Liss, P. S.: Air–sea gas exchange in rough and stormy seas measured by a dual-tracer technique, Nature, 349(6305), 145–147, doi:10.1038/349145a0, 1991.

Whalley, L. K., Furneaux, K. L., Goddard, A., Lee, J. D., Mahajan, A., Oetjen, H., Read, K. A., Kaaden, N., Carpenter, L. J., Lewis, A. C., C. Plane, J. M., Saltzman, E. S., Wiedensohler, A. and Heard, D. E.: The chemistry of OH and HO2 radicals in the boundary layer over the tropical Atlantic Ocean, Atmos. Chem. Phys., 10(4), 1555–1576, doi:10.5194/acp-10-1555-2010, 2010.

Widdicombe, C. E., Eloire, D., Harbour, D., Harris, R. P. and Somerfield, P. J.: Long-term phytoplankton community dynamics in the Western English Channel, J. Plankton Res., 32(5), 643–655, doi:10.1093/plankt/fbp127, 2010.

Wigley, T. M. L., Smith, S. J. and Prather, M. J.: Radiative Forcing Due to Reactive Gas Emissions, J. Clim., 15(18), 2690–2696, doi:10.1175/1520-0442(2002)015<2690:RFDTRG>2.0.CO;2, 2002.

Williams, J., Holzinger, R., Gros, V., Xu, X., Atlas, E. L. and Wallace, D. W. R.: Measurements of organic species in air and seawater from the tropical Atlantic, Geophys. Res. Lett., 31(23), 1–5, doi:10.1029/2004GL020012, 2004.

Winkler, P.: Surface ozone over the Atlantic ocean, J. Atmos. Chem., 7(1), 73–91, doi:10.1007/BF00048255, 1988.

Wofsy, S. C., Afshar, S., Allen, H. M., Apel, E. C., Asher, E. C., Barletta, B., Bent, J., Bian, H., Biggs, B. C., Blake, D. R., Blake, N., Bourgeois, I., Brock, C. A., Brune, W. H., Budney, J. W., Bui, T. P., Butler, A., Campuzano-Jost, P., Chang, C. S., Chin, M., Commane, R., Correa, G., Crounse, J. D., Cullis, P. D., Daube, B. C., Day, D. A., Dean-Day, J. M., Dibb, J. E., DiGangi, J. P., Diskin, G. S., Dollner, M., Elkins, J. W., Erdesz, F., Fiore, A. M., Flynn, C.

M., Froyd, K. D., Gesler, D. W., Hall, S. R., Hanisco, T. F., Hannun, R. A., Hills, A. J., Hintsa, E. J., Hoffman, A., Hornbrook, R. S., Huey, L. G., Hughes, S., Jimenez, J. L., Johnson, B. J., Katich, J. M., Keeling, R. F., Kim, M. J., Kupc, A., Lait, L. R., Lamarque, J.-F., Liu, J., McKain, K., Mclaughlin, R. J., Meinardi, S., Miller, D. O., Montzka, S. A., Moore, F. L., Morgan, E. J., Murphy, D. M., Murray, L. T., Nault, B. A., Neuman, J. A., Newman, P. A., Nicely, J. M., Pan, X., Paplawsky, W., Peischl, J., Prather, M. J., Price, D. J., Ray, E. A., Reeves, J. M., Richardson, M., Rollins, A. W., Rosenlof, K. H., Ryerson, T. B., Scheuer, E., Schill, G. P., Schroder, J. C., Schwarz, J. P., St.Clair, J. M., Steenrod, S. D., Stephens, B. B., Strode, S. A., Sweeney, C., Tanner, D., Teng, A. P., Thames, A. B., Thompson, C. R., Ullmann, K., Veres, P. R., Vieznor, N., Wagner, N. L., Watt, A., Weber, R., Weinzierl, B., et al.: ATom: Merged Atmospheric Chemistry, Trace Gases, and Aerosols, , doi:10.3334/ORNLDAAC/1581, 2018.

Wohl, C., Capelle, D., Jones, A., Sturges, W. T., Nightingale, P. D., Else, B. G. T. and Yang, M.: Segmented flow coil equilibrator coupled to a proton-transfer-reaction mass spectrometer for measurements of a broad range of volatile organic compounds in seawater, Ocean Sci., 15(4), 925–940, doi:10.5194/os-15-925-2019, 2019.

Wohl, C., Brown, I. J., Kitidis, V., Jones, A. E., Sturges, W. T., Nightingale, P. D. and Yang, M.: Underway seawater and atmospheric measurements of volatile organic compounds in the Southern Ocean, Biogeosciences, 17(9), 2593–2619, doi:10.5194/bg-17-2593-2020, 2020.

Wohl, C., Jones, A. E., Sturges, W. T., Nightingale, P. D., Else, B., Butterworth, B. J. and Yang, M.: Sea ice concentration impacts dissolved organic gases in the Canadian Arctic, Biogeosciences, 19(4), 1021–1045, doi:10.5194/bg-19-1021-2022, 2022.

Wolfe, G. M., Kaiser, J., Hanisco, T. F., Keutsch, F. N., De Gouw, J. A., Gilman, J. B., Graus, M., Hatch, C. D., Holloway, J., Horowitz, L. W., Lee, B. H., Lerner, B. M., Lopez-Hilifiker, F., Mao, J., Marvin, M. R., Peischl, J., Pollack, I. B., Roberts, J. M., Ryerson, T. B., Thornton, J. A., Veres, P. R. and Warneke, C.: Formaldehyde production from isoprene oxidation across NOx regimes, Atmos. Chem. Phys., 16(4), 2597–2610, doi:10.5194/acp-16-2597-2016, 2016.

Wróblewski, T., Ziemczonek, L., Alhasan, A. M. and Karwasz, G. P.: Ab initio and density functional theory calculations of proton affinities for volatile organic compounds, Eur. Phys. J. Spec. Top., 144(1), 191–195, doi:10.1140/epjst/e2007-00126-7, 2007.

Wurl, O., Wurl, E., Miller, L., Johnson, K. and Vagle, S.: Formation and global distribution of sea-surface microlayers, Biogeosciences, 8(1), 121–135, doi:10.5194/bg-8-121-2011, 2011.

Yang, M.: Penlee Point Atmospheric Observatory rain data, [online] Available from: https://www.westernchannelobservatory.org.uk/penlee/, 2021.

Yang, M. and Fleming, Z. L.: Estimation of atmospheric total organic carbon (TOC) - Paving the path towards carbon budget closure, Atmos. Chem. Phys., 19(1), 459–471, doi:10.5194/acp-19-459-2019, 2019.

Yang, M., Blomquist, B. W., Fairall, C. W., Archer, S. D. and Huebert, B. J.: Air-sea exchange of dimethylsulfide in the Southern Ocean: Measurements from so GasEx compared to temperate and tropical regions, J. Geophys. Res. Ocean., 116(8), 1–17, doi:10.1029/2010JC006526, 2011a.

Yang, M., Huebert, B. J., Blomquist, B. W., Howell, S. G., Shank, L. M., McNaughton, C. S., Clarke, A. D., Hawkins, L. N., Russell, L. M., Covert, D. S., Coffman, D. J., Bates, T. S., Quinn, P. K., Zagorac, N., Bandy, A. R., de Szoeke, S. P., Zuidema, P. D., Tucker, S. C., Brewer, W. A., Benedict, K. B. and Collett, J. L.: Atmospheric sulfur cycling in the southeastern Pacific – longitudinal distribution, vertical profile, and diel variability observed during VOCALS-REx, Atmos. Chem. Phys., 11(10), 5079–5097, doi:10.5194/acp-11-5079-2011, 2011b.

Yang, M., Nightingale, P. D., Beale, R., Liss, P. S., Blomquist, B. W. and Fairall, C. W.: Atmospheric deposition of methanol over the Atlantic Ocean, Proc. Natl. Acad. Sci., 110(50), 20034–20039, doi:10.1073/pnas.1317840110, 2013a.

Yang, M., Archer, S. D., Blomquist, B. W., Ho, D. T., Lance, V. P. and Torres, R. J.: Lagrangian evolution of DMS during the Southern Ocean gas exchange experiment: The effects of vertical mixing and biological community shift, J. Geophys. Res. Ocean., 118(12), 6774–6790, doi:10.1002/2013JC009329, 2013b.

Yang, M., Beale, R., Smyth, T. J. and Blomquist, B. W.: Measurements of OVOC fluxes by eddy covariance using a proton-transfer- reaction mass spectrometer - method development at a coastal site, Atmos. Chem. Phys., 13(13), 6165–6184, doi:10.5194/acp-13-6165-2013, 2013c.

Yang, M., Blomquist, B. W. and Nightingale, P. D.: Air-sea exchange of methanol and acetone during HiWinGS: Estimation of air phase, water phase gas transfer velocities, J. Geophys. Res. Ocean., 119(10), 7308–7323, doi:10.1002/2014JC010227, 2014a.

Yang, M., Beale, R., Liss, P. S., Johnson, M. T., Blomquist, B. W. and Nightingale, P. D.: Air–sea fluxes of oxygenated volatile organic compounds across the Atlantic Ocean, Atmos. Chem. Phys., 14(14), 7499–7517, doi:10.5194/acp-14-7499-2014, 2014b.

Yang, M., Bell, T. G., Hopkins, F. E., Kitidis, V., Cazenave, P. W., Nightingale, P. D., Yelland, M. J., Pascal, R. W., Prytherch, J., Brooks, I. M. and Smyth, T. J.: Air-sea fluxes of CO2 and CH4 from the penlee point atmospheric observatory on the south-west coast of the UK, Atmos. Chem. Phys., 16(9), 5745–5761, doi:10.5194/acp-16-5745-2016, 2016a.

Yang, M., Bell, T. G., Blomquist, B. W., Fairall, C. W., Brooks, I. M. and Nightingale, P. D.: Air-sea transfer of gas phase controlled compounds, IOP Conf. Ser. Earth Environ. Sci., 35(1), doi:10.1088/1755-1315/35/1/012011, 2016b.

Yang, M., Bell, T. G., Hopkins, F. E. and Smyth, T. J.: Attribution of atmospheric sulfur dioxide over the English Channel to dimethyl sulfide and changing ship emissions, Atmos. Chem. Phys., 16(8), 4771–4783, doi:10.5194/acp-16-4771-2016, 2016c.

Yang, M., Prytherch, J., Kozlova, E., Yelland, M. J., Parenkat Mony, D. and Bell, T. G.: Comparison of two closed-path cavity-based spectrometers for measuring air-water CO2 and CH4 fluxes by eddy covariance, Atmos. Meas. Tech., 9(11), 5509–5522, doi:10.5194/amt-9-5509-2016, 2016d.

Yang, M., Bell, T. G., Brown, I. J., Fishwick, J. R., Kitidis, V., Nightingale, P. D., Rees, A. P. and Smyth, T. J.: Insights from year-long measurements of air–water CH4 and CO2 exchange in a coastal environment, Biogeosciences, 16(5), 961–978, doi:10.5194/bg-16-961-2019, 2019a.

Yang, M., Norris, S. J., Bell, T. G. and Brooks, I. M.: Sea spray fluxes from the southwest coast of the United Kingdom-Dependence on wind speed and wave height, Atmos. Chem. Phys., 19(24), 15271–15284, doi:10.5194/acp-19-15271-2019, 2019b.

Yang, M., Smyth, T. J., Kitidis, V., Brown, I. J., Wohl, C., Yelland, M. J. and Bell, T. G.: Natural variability in air–sea gas transfer efficiency of CO2, Sci. Rep., 11(1), doi:10.1038/s41598-021-92947-w, 2021.

Yoo, J. M., Lee, Y. R., Kim, D., Jeong, M. J., Stockwell, W. R., Kundu, P. K., Oh, S. M., Shin, D. Bin and Lee, S. J.: New indices for wet scavenging of air pollutants (O3, CO, NO2, SO2, and PM10) by summertime rain, Atmos. Environ., 82(2), 226–237, doi:10.1016/j.atmosenv.2013.10.022, 2014.

Young, I. R.: Seasonal variability of the global ocean wind and wave climate, Int. J. Climatol., 19(9), 931–950, doi:10.1002/(SICI)1097-0088(199907)19:9<931::AID-JOC412>3.0.CO;2-O, 1999.

Yu, L., Zhong, S. and Sun, B.: The climatology and trend of surface wind speed over antarctica and the southern ocean and the implication to wind energy application, Atmosphere (Basel)., 11(1), doi:10.3390/atmos11010108, 2020.

Zahardis, J., LaFranchi, B. W. and Petrucci, G. A.: Photoelectron resonance capture ionization-aerosol mass spectrometry of the ozonolysis products of oleic acid particles: Direct measure

of higher molecular weight oxygenates, J. Geophys. Res. D Atmos., 110(8), 1–10, doi:10.1029/2004JD005336, 2005.

Zhao, J. and Zhang, R.: Proton transfer reaction rate constants between hydronium ion (H3O+) and volatile organic compounds, Atmos. Environ., 38(14), 2177–2185, doi:10.1016/j.atmosenv.2004.01.019, 2004.

Zhou, S., Gonzalez, L., Leithead, A., Finewax, Z., Thalman, R., Vlasenko, A., Vagle, S., Miller, L. A., Li, S. M., Bureekul, S., Furutani, H., Uematsu, M., Volkamer, R. and Abbatt, J. P. D.: Formation of gas-phase carbonyls from heterogeneous oxidation of polyunsaturated fatty acids at the air-water interface and of the sea surface microlayer, Atmos. Chem. Phys., 14(3), 1371–1384, doi:10.5194/acp-14-1371-2014, 2014.

Zhou, X. and Mopper, K.: Photochemical production of low-molecular-weight carbonyl compounds in seawater and surface microlayer and their air-sea exchange, Mar. Chem., 56(3–4), 201–213, doi:10.1016/S0304-4203(96)00076-X, 1997.

Zhu, Y. and Kieber, D. J.: Wavelength- and Temperature-Dependent Apparent Quantum Yields for Photochemical Production of Carbonyl Compounds in the North Pacific Ocean, Environ. Sci. Technol., 52(4), 1929–1939, doi:10.1021/acs.est.7b05462, 2018.